# Thermosensitive and degradable nanogels by RAFT-mediated PITSA in aqueous dispersion

Thi Nga Tran

# Thèse de doctorat de

LE MANS UNIVERSITE

ECOLE DOCTORALE N° 596
Matière, Molécules, Matériaux
Spécialité : Chimie et Physio-Chimie des Polymères

Par

**Thi Nga TRAN**

# Thermosensitive and degradable nanogels by RAFT-mediated PITSA in aqueous dispersion

**Thèse présentée et soutenue à Le Mans, le 25 Mars 2021**
**Unité de recherche : ED 3M**
**Thèse N° : 021LEMA1007**

**Rapporteurs avant soutenance** :

| | |
|---|---|
| **Muriel Lansalot** | Directeur de recherche, CNRS, France |
| **Vincent Lapinte** | Maître de Conférence, Université de Montpellier, France |

**Composition du Jury :**

| | |
|---|---|
| Examinateurs : **Jean-Luc Six** | Professor, Université de Lorraine, France |
| Dir. de thèse : **Sagrario Pascual** | Maître de Conférence HDR, Le Mans Université, France |
| Co-dir. de thèse : **Sandie Piogé** | Maître de Conférence, Le Mans Université, France |
| Co-dir. de thèse : **Laurent Fontaine** | Professor, Le Mans Université, France |

**Invité(s)**

| | |
|---|---|
| **Damien Montarnal** | Chercheur, CNRS, France |

# Acknowledgements

This work has been performed in the Institut des Molécules et Matériaux du Mans (IMMM)-UMRCNRS-6283 Laboratory in the Méthodologie et Synthèse des Polymères (MSP) team in Le Mans Université. I would like to thanks The Ministry of Higher Education, Research and Innovation (Ministère de l'Enseignement supérieur, de la Recherche et de l'Innovation, MESRI) for the financial support.

I would like to thank first to my thesis director Dr Sagrario Pascual for the interesting topic and for giving me her trust for the project. Moreover, I want to say thank to her for all the advices during my PhD, I had learned a lot from her. Every time when I went out of my way she always pull me back. Thanks for her kindness and her supports, not only in the working issues but also in my personal life especially when I had my first born in the third year of PhD, with the childcare process and the extension of doctoral contract.

I would like to thank my warmly advisor, Dr Sandie Piogé for her advices and all encouraging words during three and a half years. Thanks Sandie for her sense of humor, she lightened up the atmosphere around and brought a lot of laugh for everyone in the lab.

I would like to give many grateful thanks to my co-supervisor, Pr Laurent Fontaine for welcome me in the laboratory. I would like to thank him, for his advices and great ideas during all the discussions.

I would like to express my sincere gratitude to the Dr Muriel Lansalot and the Dr Vincent Lapinte to report my PhD work. I am honored that they accepted to do this work. It is my honor that the Pr. Jean-Luc Six accepted to preside the evaluation comitee of my work. I would like to thank him for his evaluation.

I would like to express my sincere gratitude to the Dr Damien Montarnal from CP2M laboratory-CPE Lyon. I am so lucky to have the chance to work under his supervision during 6 months for my Master internship and he had followed my PhD work as a member of the CSI committee. I would like to thank him for his advices, his evaluations during the years and his help for the SEC characterization in DMSO.

I would like to give many grateful thanks to the Pr. Véronique Montembault for her help and for her advices during the last 3 years as a member of my CSI committee.

I would like to especially thank Alexandre Bénard for the advices for the chromatography column and for numerous SEC characterizations during the years.

I would like to thank Sullivan Bricaud for NMR analyses and thank Anthony Rousseau for TEM images.

I would like to give grateful thanks to Anita Loiseau for her help and their kindness.

I would like to thank Wenhao, my office co-worker, my dear friend for his thoughtfulness, his care and his kindness. Thanking Wenhao for the lunches he had prepared, for always being my “Johnny-on-the-spot”.

I would like to thank Clémence, my labmate for all the lunches together, for her help in my very first days in the lab. Thanks Clémence for her kindness and her caring during the years.

I would like all the PhD student I met and the interns who worked on this project: Yuwen, Tharin and Corentin.

I would like to thank all my good Vietnamese friends who supported me a lot during my last three years: Thuy, Dung and Yen.

I would like to thank my family, my parents, Dam and Ha, my parents-in-law, Hanh and Xuyen, my brother Dao, my sisters Hang and Hoa, my brother-in-law, Manh who love me unconditionally and always help me to be in good mood.

My little boy, Rémi Mam, thank you for always being nice. Thank you for coming and bringing ton of happiness and funs to our family. You are my sunshine.

I would like to finish by thanking, the one who has support me the most during these years, who has listened to me, the one who give me her energy and courage. Together, we have made it work. Thank you for all honey!

# Thermosensitive and degradable nanogels by RAFT-mediated PITSA in aqueous dispersion

**Abstract:**

Stimuli-sensitive nanogels are three-dimensional hydrogel materials in the nanoscale size range formed by crosslinked polymer networks with a high capacity to swell in water. They are of interest for drug delivery, carriers for imaging probes and genetic materials, for separation processes and for heavy metals removal. The characteristics, such as size, porosity, softness, swelling ratio, surface and degradability, of stimuli-sensitive nanogels based on synthetic polymers can be tuned by finely choosing an appropriate and a versatile synthetic pathway. The reversible addition-fragmentation chain transfer (RAFT) mediated polymerization-induced thermal self-assembly (PITSA) is a powerful way to target thermosensitive nanogels thanks to the tolerance of the radical process and to the formation of self-assembled block copolymers in nano-objects in a one-pot process using aqueous dispersed medium. This work studies the synthesis and characterization of thermosensitive and pH-sensitive core-shell chemically crosslinked nanogels through RAFT-mediated PITSA in aqueous dispersion. The nanogels shell is based on a poly(oligo(ethylene glycol) acrylate) which chemical structure including chain-end has been monitored thanks to soft initiating modes (thermal and UV-light activations) for the RAFT polymerization. Dual-sensitive nanogels cores with a upper critical solution temperature (UCST) based on poly(*N*-acryloyl glycinamide) or a lower critical solution temperature (LCST) based on poly(*N*-isopropylacrylamide) combined to a pH-degradable ketal crosslinker were obtained through UV light RAFT-mediated PITSA in aqueous dispersion. By the judicious combination of monomer to RAFT precursor shell initial ratio, of the amount of crosslinker and of the solid content, the size, water content, swelling ratio, degradability and phase transition temperature of nanogels have been fine-tuned.

**Keywords** : Nanostructured hydrogel, LCST-type thermosensitive nanogel, UCST-type thermosensitive nanogel, pH-degradable nanogel, RAFT-mediated PITSA, Thermally-activated RAFT polymerization, UV light-initiated RAFT polymerization, Polymerization in aqueous dispersion

**Table of contents**

# List of Abbreviations

| | |
|---|---|
| $\overline{M_{n,NMR}}$ | Number-average molar mass determined by $^{1}$H-NMR analysis |
| $\overline{M_{n,PPEGA}}$ | Number-average molar mass of PPEGA |
| $\overline{M_{n,SEC}}$ | Experimental number-average molar mass determined by SEC analysis |
| $\overline{M_{n,theo}}$ | Theoretical number-average molar mass |
| $\overline{DP_{n,POEGMA}}$ | Number-average polymerization degree of POEGMA |
| $\overline{DP_{n,PPEGA}}$ | Number-average polymerization degree of PPEGA |
| $\overline{DP_n}$ | Number-average polymerization degree |
| $\Delta G_{mix}$ | Change in Gibbs free energy of a polymer in a solvent |
| $\Delta H_{mix}$ | Change in enthalpy of a polymer in a solvent |
| $M_{COPYDC}$ | Molar mass of COPYDC |
| $M_{NIPAm}$ | Molar mass of NIPAm |
| $M_{VDM-Am}$ | Molar mass of VDM-Am |
| $M_{VDM-Aspa}$ | Molar mass of VDM-Aspa |
| $M_{VDM-Gly}$ | Molar mass of VDM-Gly |
| $\Delta S_{mix}$ | Changes in entropy of a polymer in a solvent |
| AA | Allylamine |
| AAc | Acrylic acid |
| AC-PU | Copolymer AM-PU substituted with acetyl groups |
| ACVA | 4,4'-azobis(4-cyanovaleric acid) |
| AGET ATRP | Activator Generated by Electron Transfer Atom Transfer Radical Polymerization |
| AIBN | 2,2'-Azobis(2-methylpropionitrile) |
| Ald | Aldehyde |
| Am | Acrylamide |

| | |
|---|---|
| AM-PU | Poly(allylamine-*co*-allylurea) copolymer containing 90 mol% ureido and 10 mol% amino groups |
| AN | Acrylonitrile |
| AOT | Sodium dioctyl sulfosuccinate |
| APS | Ammonium persulfate |
| ATRP | Atom Transfer Radical Polymerization |
| BA | Butyl acrylate |
| BAm | Benzyl acrylamide |
| BSA | Bovine serum albumin |
| BZ | Benzophenone |
| CD | Cyclodextrin |
| CD | Cyclodextrin polymer |
| CHM | Cholesteryl-bearing polysaccharide mannan |
| CMA | 4-methyl-[7-(methacryloyl)oxy-ethyl-oxy]coumarin |
| CMC | Critical micellar concentration |
| COPYDC | 2-cyano-5-oxo-5-(prop-2-yn-1-ylamino)pentan-2-yl |
| CRP | Controlled Radical Polymerization |
| CTA | Chain transfer agent |
| Cys-Tat | Trans-Activator of Transcription containing a C-terminal cysteine |
| Đ | Dispersity |
| $D_2O$ | Deuterium oxide |
| DEAm | *N,N'*-diethyl acrylamide |
| Dex-*g*-PDLA | Dextran-graft-poly(D-lactide) |
| Dex-*g*-PLLA | Dextran-graft-poly(L-lactide) |
| $D_h$ | Hydrodynamic diameter |

| | |
|---|---|
| DLS | Dynamic Light Scattering |
| DMAEMA | *N,N*-dimethyl aminoethyl methacrylate |
| DMAm | *N,N*-dimethyl acrylamide |
| DMAPS | 3-dimethyl(methacryloyloxyethyl)ammonium propanesulfonate |
| DMF | *N,N*-dimethylformamide |
| DMPA | 2,2-dimethoxy-2-phenylacetophenone |
| DMSO | Dimethyl sulfoxide |
| DNA | Deoxyribonucleic acid |
| DOX | Doxorubicin |
| DSC | Differential scanning calorimetry |
| DTT | Dithiothreitol |
| ECT | 4-cyano-4-(ethylsulfanylthiocarbonyl) sulfanylpentanoic acid |
| EDA | Ethylenediamine |
| EG | Ethylene glycol |
| EGDMA | Ethylene glycol dimethacrylate |
| EO | Ethylene oxide |
| $Et_2O$ | Diethyl ether |
| FITC | Thiol-modified fluorescein isothiocyanate |
| FT-IR | Fourier-Transform Infrared Spectroscopy |
| GlyMA | Glycidyl methacrylate |
| HR-MS | High-resolution Mass Spectra |
| Hzd | Hydrazide |
| Inisolv | initiator and solvent |
| IS-BU | Poly(allylamine-*co*-allylurea) modified with isobutanoyl groups |
| IS-PU | Copolymer AM-PU substituted with isobutanoyl |

| | |
|---|---|
| IUPAC | International Union for Pure and Applied Chemistry |
| $K_2CO_3$ | Potassium carbonate |
| KB | Ketal-containing crosslinker |
| LCST | Lower critical solution temperature |
| LiBr | Lithium bromide |
| MAAc | Methacrylic acid |
| Macro-CTA | Macromolecular chain transfer agent |
| MADIX | Macromolecular Design by Interchange of Xanthates |
| MBA | *N*,*N*′-methylenebis(acrylamide) |
| MDex | Hydrophobically modified dextran |
| MEA | 2-methoxyethyl acrylate |
| MPTMS | 3-methacryloxypropyl trimethoxysilane |
| $NH_3$ | Ammonia |
| NIPAm | *N*-isopropyl acrylamide |
| NIPMAm | *N*-isopropyl methacrylamide |
| NIR | Near-infrared |
| NMP | Nitroxide-Mediated Polymerization |
| N*n*PAm | *N*-*n*-propyl acrylamide |
| N*n*PMAm | *N*-*n*-propyl methacrylamide |
| *N*-tBAm | *N*-*tert*-butyl acrylamide |
| NVCL | *N*-vinylcaprolactam |
| O/W | Oil-in-Water |
| OEG | Oligo(ethylene glycol) |
| OEGMA | Oligo(ethylene glycol) methacrylate |
| P(AAm-*co*-AN) | Poly(acrylamide-*co*-acrylonitrile) |

| | |
|---|---|
| P(Am-*co*-BA) | Poly(acrylamide-*co*-butyl acrylate) |
| P(DMAPS-*co*-MBA) | poly(3-dimethyl(methacryloyloxyethyl) ammonium propanesulfonate-*co*-*N*,*N*'-methylene bisacrylamide) |
| P(HPMA-GA) | Poly(N-(2-hydroxypropyl) methacrylamide) modified with glycolamide |
| P($MEO_2$MA-*co*-OEGMA) | Poly(2-(2-methoxyethoxy)ethyl methacrylate-*co*- oligo(ethylene glycol) methacrylate) |
| P(MMA-*co*-EG) | Poly(methyl methacrylate-*co*-ethylene glycol) |
| P(NAGA-*co*-BA) | Poly(*N*-acryloyl glycinamide-*co*-butyl acrylate) |
| P(NAGA-*co*-MAAc) | Poly(*N*-acryloyl glycinamide-*co*- methacrylic acid) |
| P(NAGA-*co*-S) | Poly(*N*-acryloyl glycinamide-*co*-styrene) |
| P(NIPAm-*co*-MBA) | Poly(*N*-isopropyl acrylamide-co-*N*,*N*'-methylene bisacrylamide) |
| P(NVCL-*co*-MEA) | Poly(*N*-vinylcaprolactam-*co*-2-methoxyethyl acrylate) |
| PAAc | Poly(acrylic acid) |
| PAm | Polyacrylamide |
| PAU | Poly( allylurea -*co*- allylamine) |
| PBS | phosphate buffer saline |
| PDA | 2,2'-[2,2-propanediylbis(oxy)]diethanamine |
| PDEAm | Poly(*N,N*-diethyl acrylamide) |
| pdi | Polydispersity in size |
| PDMAm | Poly(*N,N*-dimethyl acrylamide) |
| PDMAPS | Poly(3-dimethyl(methacryloyloxyethyl) ammonium propanesulfonate) |
| PDS-MA | Pyridyl disulfide-derived methacrylate |
| PEG | Poly(ethylene glycol) |
| PEGA | Poly(ethylene glycol) methyl ether acrylate |
| PEG-*b*-P(AAm-*co*-AN) | Block copolymer based on poly(ethylene glycol) and poly(acrylamide-*co*-acrylonitrile) |

| | |
|---|---|
| PEGDA | Poly(ethylene glycol) diacrylate |
| PEGDMA | Poly(ethylene glycol) dimethacrylate |
| PEO | Poly(ethylene oxide) |
| PEO-*b*-PNIPAm | Poly(ethylene oxide)-*b*-poly(*N*-isopropyl acrylamide) |
| PEO-*b*-PPO-*b*-PEO | Poly(ethylene oxide)-*b*-poly(propylene oxide)-*b*-poly(ethylene oxide) |
| PEO-CTA | Poly(ethylene oxide) chain transfer agent |
| PFP | Pentafluorophenyl |
| PG | Hyperbranched polyglycerol |
| PGlyMA | Poly(glycidyl methacrylate) |
| PGMA | Poly(glycerol monomethacrylate) |
| PHEA | Poly(2-hydroxyethyl acrylate) |
| photo-I | 2-hydroxy-4′-(2-hydroxyethoxy)-2-methylpropiophenone |
| PHPMA | Poly(2-hydroxypropyl methacrylate) |
| PHPMA-GA | poly(*N*-(2-hydroxypropyl) methacrylamide-glycolamide) |
| PI-PU | Copolymer AM-PU substituted with pivaloyl groups |
| PISA | Polymerization-induced self assembly |
| PITSA | Polymerization-induced thermal self-assembly |
| PLA | Polylactide |
| PMEA | Poly(2-methoxyethyl acrylate) |
| PMEDAPA | Poly(2-((2-(methacryloyloxy)ethyl)dimethylammonio)acetyl)(phenylsulfonyl)amide |
| $PMEO_2MA$ | Poly(2-(2-methoxyethoxy)ethyl methacrylate) |
| $PMEO_3MA$ | Poly(tri(ethylene glycol) methyl ether methacrylate) |
| PMMA | *Poly(methyl methacrylate)* |
| PMPC | Poly(2-(methacryloyloxy)ethyl phosphorylcholine) |

| | |
|---|---|
| PNAAAm | Poly(*N*-acryloyl asparagine amide) |
| PNAGA | Poly*(N*-acryloyl glycinamide) |
| PNAGAAm | Poly(*N*-acryloyl glutamine amide) |
| PNIPAm | Poly(*N*-isopropyl acrylamide) |
| PNIPMAm | Poly(*N*-isopropyl methacrylamide) |
| PNMAAAm | Poly(*N*-methacryloyl asparagine amide) |
| PNnPAm | Poly(*N*-n-propyl acrylamide) |
| PNnPMAm | Poly(N-n-propyl methacrylamide) |
| POA | Aldehyde-functionalized POEGmMA |
| POC | Poly(L-ornithine-*co*-L-citrulline) |
| $POEG_mMA$ | Poly[oligo(ethylene glycol) methacrylate]s |
| POEOMA | Poly(oligo(ethylene oxide) monomethyl ether methacrylate) |
| POH | Hydrazide-functionalized POEGmMA |
| PPEGA | Poly(poly(ethylene glycol) methyl ether acrylate) |
| PPEGMA | Poly(poly(ethyleneglycol) methyl ether methacrylate) |
| PR-PU | Copolymer AM-PU substituted with propionyl groups |
| PSPP | Poly(3-[*N*-(3-methacrylamidopropyl)-N,N-dimethyl]ammoniopropane sulfonate) |
| PSt | Polystyrene |
| PTX | Paclitaxel |
| PUEM | Poly(2-ureidoethyl methacrylate) |
| PVA | Poly(vinyl alcohol) |
| PVA-VEA | Acetal-linked poly(vinyl alcohol) functionalized with vinyl ether acrylate |
| RAFT | Reversible Addition-Fragmentation Chain Transfer Polymerization |
| RCC | Radical crosslinking copolymerization |

| | |
|---|---|
| RDRP | Reversible Deactivation Radical Polymerization |
| $R_g$ | Radius of gyration |
| $R_h$ | Hydrodynamic radius |
| RI | Refractive index |
| RITP | Degenerative chain transfer represented by iodine-mediated polymerization |
| SDS | Sodium dodecylsulfate |
| SEC | Size Exclusion Chromatography |
| Sono-RAFT-PISA | Sonochemically initiated Reversible Addition-Fragmentation chain Transfer Polymerization-induced self-assembly |
| St | Styrene |
| T | Temperature |
| Tc | LCST value |
| TEM | Transmission Electronic Microscopy |
| THF | Tetrahydrofuran |
| TM | Tamoxifen |
| TPMA | Tris-[(2-pyridyl)methyl]amine |
| TTC | Trithiocarbonate |
| P(U/A10) | statistical copolymer of poly(2-ureidoethyl methacrylate) and cationic poly(2-aminoethyl methacrylate) |
| UCST | Upper critical solution temperature |
| UV | Ultra-violet |
| UV-Vis | Ultra-violet visible |
| V50 | 2,2'-azobis(2-methylpropionamidine) dihydrochloride |
| VDM | 2-vinyl-4,4-dimethylazlactone |
| VDM-Am | *N*-(1-amino-2-methyl-1-oxopropan-2-yl)acrylamide |

| | |
|---|---|
| VDM-Aspa | 2-(2-acrylamido-2-methylpropanamido)succinamide |
| VDM-Gly | *N*-(1-((2-amino-2-oxoethyl)amino)-2-methyl-1-oxopropan-2-yl)acrylamide |
| VEA | vinyl ether acrylate |
| W/O | Water-in-Oil |
| WSC-PASP-PEG | Chitosan-poly(L-aspartic acid)-poly(ethylene glycol) |
| λ | Wavelength |

# General Introduction

Recent interest in stimuli-sensitive materials has promoted numerous efforts in preparing ‘‘smart’’ nanogels. Stimuli-sensitive nanogels are three-dimensional nanoscale hydrogel materials formed by crosslinked polymer networks whose characteristics, such as size, porosity, swelling ratio and degradability, may vary with external changes in environmental conditions such as temperature, pH, light and electric field. Among all of the above-mentioned stimuli, temperature and pH are the most common and they are mainly used in the field of biomedical applications.

Poly(*N*-isopropyl acrylamide) (PNIPAm) is one of the most popular thermosensitive polymer. The PNIPAm undergoes a lower critical solution temperature (LCST) reversible coil-to-globule transition at about 32°C. It is well soluble in water below the LCST and when the temperature increases above the LCST, the polymer becomes insoluble and precipitates out from its aqueous solution. According to its hydrosolubility change, LCST-type thermosensitive PNIPAm-based nanogels have been prepared for controlled drugs delivery which can be carried out in physiological conditions.

In contrast to the LCST-type thermosensitive polymers, only a few polymer materials with an upper critical solution temperature (UCST) in water are known. In most cases, the UCST phenomenon is based on either ionic interactions or hydrogen-bonding. However, the electrostatic interactions of polyelectrolytes (e.g., polysulfobetaines) are disturbed by the presence of salts which makes them unsuitable for the application under physiological conditions. For this reason, novel nonionic polymer systems showing sharp UCST-type phase transitions over a wide range of concentrations and being tolerant to electrolytes are highly desirable. Poly(*N*-acryloyl glycinamide) (PNAGA) has received increasing attention since it was firstly reported by Haas and Schuler in 1964. Owing to the tunable and reversible hydrogen-bonding UCST-type thermosensitive behavior, PNAGA and its copolymers have been expanded to manifold applications in different fields including. Compared with LCST-type thermosensitive nanogels, the UCST-type versions are much less explored, and limited examples in the literature.

The chemical structure and physico-chemical characteristics of LCST- and UCST-type thermosensitive nanogels based on synthetic polymers can be tuned by finely choosing an appropriate and a versatile synthetic pathway. Reversible deactivation radical polymerization (RDRP) techniques are particularly well suited to enable precise control over the architecture, molar mass, and dispersity of the polymers. Among different RDRP techniques, reversible addition-fragmentation

chain transfer (RAFT) polymerization has been advocated by many to be the most versatile polymerization technique. Indeed, RAFT polymerization provides opportunities for the preparation of polymers of controlled molar masses/lengths, architectures and precise location of functional groups. By modifying water-soluble natural polymers or by synthesizing rationally designed synthetic polymers using RAFT polymerization, nanogels can be prepared with a higher degree of control of the structures, properties and thus functions.

Polymerization-induced thermal self-assembly (PITSA) in aqueous dispersion employs a hydrophilic macromolecular chain transfer agent (macro-CTA) to chain extend a thermosensitive polymer block at a temperature above the LCST or under UCST in order to generate amphiphilic block copolymers that self-assemble into nanodomains due the phase transition behaviors of thermosensitive polymers. Finally, the *in-situ* crosslinking of the amphiphilic block copolymers inside nanodomains in presence of crosslinker results in the formation of nanogel. Combing together, PITSA syntheses using RAFT polymerization have become a powerful method to prepare thermosensitive nanogels.

Degradable nanogels are getting more and more attention for designing smart nanocarriers or biomedical diagnostic agents. To achieve the degradability of nanogel networks, degradable bonds (such as ester, carbonate, amide, etc.) need to be inserted either in crosslinkers or in polymeric chains. These nanogel networks follow degradation through solubilization, enzymatic and hydrolysis mechanisms. The acid-labile linkages have been widely introduced to fabricate pH-sensitive nanostructures and networks for intracellular drug delivery. For instance, acetal/ketal groups are relatively stable under physiological conditions, while rapidly hydrolyzed at a mildly acidic pH to release the loaded drug. The objective of my PhD work is to design and to elaborate both LCST- and UCST-type thermosensitive nanogels and also dual thermosensitive and pH-degradable nanogels (Figure 1). Their macromolecular, physicochemical characterizations and their thermal behaviors are particularly investigated.

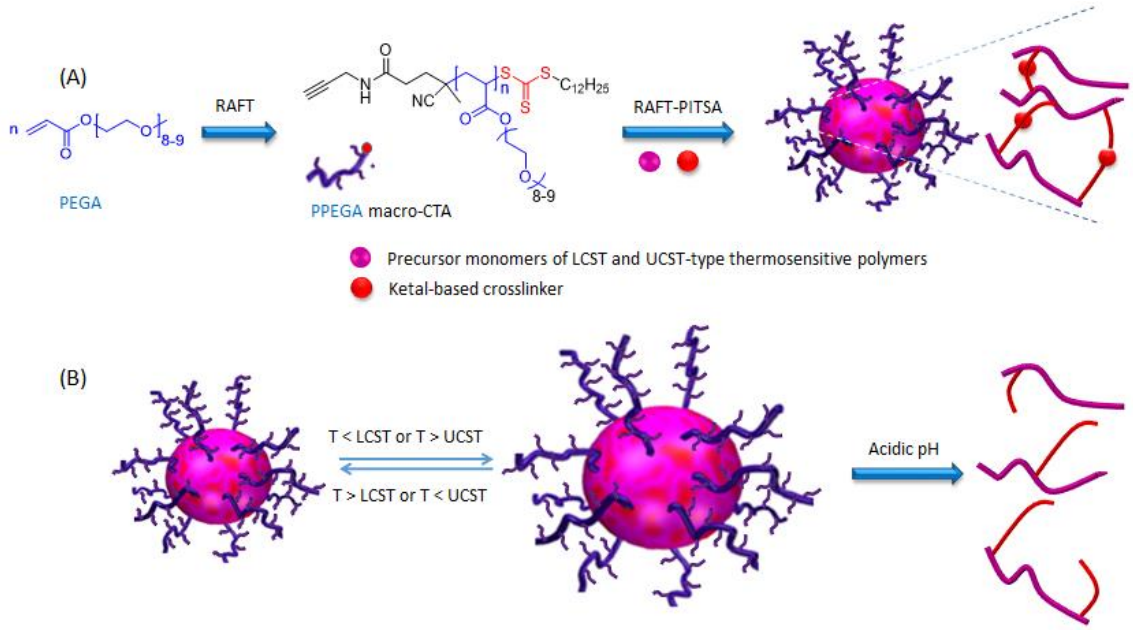


Figure 1. Synthesis strategy to target the pH-degradable and thermosensitive nanogels.

To target such goal, the strategy is, firstly, to synthesize an amphiphilic macro-CTA by RAFT polymerization of poly(ethylene glycol) methyl ether acrylate (PEGA) precursor of hydrophilic biocompatible polymer. The macro-CTA can play the role of both chain transfer agent for further elaboration of well-defined nanogel and surfactant to stabilize the nanogel. The obtained macro-CTA is employed for RAFT-PITSA of precursor monomers of LCST- or UCST-type thermosensitive polymers in aqueous dispersion in the presence of either a conventional crosslinker or a crosslinker containing a ketal group to form LCST- or UCST-type thermosensitive nanogel (Figure 1A) and dual pH-degradable and LCST- or UCST-type thermosensitive nanogels (Figure 1B), respectively.

This manuscript has been divided into four chapters with the first one dedicated to a relevant literature studies on nanogels synthesis with a focus on thermosensitive and pH-degradable ones and the other three chapters represent each step of our synthesis strategy : (*i*) well-defined PPEGAs and their ability to chain extend with monomers, NIPAm and NAGA, precursors of LCST- and UCST-type thermosensitive polymers, respectively; (*ii*) LCST-type thermosensitive nanogel based on PNIPAm and dual LCST-type thermosensitive and pH-degradable nanogels and (*iii*) UCST-type thermosensitive nanogel based on PNAGA and dual UCST-type thermosensitive and pH-degradable nanogels.

In the **Chapter I,** we concentrate primarily our attention to the relevant literature on methods used for nanogels preparation. In those sections, representative examples for each chosen method to synthesize nanogels in the literature including physical and chemical crosslinking methods will be discussed. Then, we focus on reviewing stimuli-sensitive nanogels, particularly temperature and pH-sensitive ones which are increasingly gaining attention. A summary of the chemical structures, thermal properties and several parameters impacting thermal properties of the LCST- and UCST-type

thermosensitive polymers and their synthesis methods are given. Finally, the chemistry of different pH cleavage linkers and representative examples of dual thermosensitive and pH-degradable polymer systems in the literatures will be presented.

RAFT polymerization of PEGA to prepare PPEGA macro-CTAs, their chain extension with LCST-type and UCST-type thermosensitive monomer precursors, NIPAm and NAGA, respectively, using different radical activation processes (thermal and UV-light irradiation) are described in **Chapter II**. The kinetics of polymerization, the thermosensitive phase transitions of obtained block copolymers are also studied. Moreover, an effort to search for new monomer of potential UCST-type thermosensitive polymers is discussed.

In the first part of **Chapter III**, the synthesis of LCST-type thermosensitive nanogel based on PNIPAm by RAFT-PITSA is presented. The impact of different synthesis parameters and of radical activation process (thermal and UV-light activation), $\overline{DP_{n,PPEGA}}$, $\overline{DP_{n,PNIPAM}}$ on the nanogel size, size distribution and volume swelling ratio are also studied. In the second part, by using a pH-sensitive ketal-based crosslinker, dual thermosensitive and pH-degradable nanogels are targeted through RAFT-PITSA of NIPAm using PPEGA macro-CTA. Following, the degradability of these nanogels in acidic media is investigated.

**Chapter IV** is dedicated to the synthesis and the characterization of the first hydrogen-bonding UCST-type thermosensitive nanogel and the first dual UCST-type thermosensitive and pH-degradable nanogel based on PNAGA through UV-light initiated RAFT-PITSA conducted at low temperature using PPEGA macro-CTAs, a water-soluble photo initiator and a conventional crosslinker or a crosslinker containing a ketal group, respectively.

# CHAPTER I
# LITERATURE AND BACKGROUND REVIEW

## 1.1 Introduction

Nanogels are three-dimensional nanoscale hydrogels formed through highly crosslinked polymers. At the start of the 2000s, the term ‘‘nanogel” was officially defined by the International Union for Pure and Applied Chemistry (IUPAC)[1] which mentioned nanogel is the particle of gel of any shape with an equivalent diameter of approximately 1 to 100 nm. Nanogels can be composed of a variety of natural polymers, synthetic polymers or a combination thereof, chemically crosslinked or physically crosslinked. The polymer self-assembly at the nanoscale level for nanogel elaboration was first investigated by Akiyoshi *et al.*[2], who in 1993 developed the first nanogel *via* physically crosslinked amphiphilic hydrophobized polysaccharides. Later, in 1999 the first chemically crosslinked nanogel based on poly(ethylene glycol) (PEG) was introduced by Vinogradov *et al.*[3] Compared to chemically crosslinked nanogel, nanogel conducted through physical crosslinking tends to give more fragile and more easily degradable structures than the covalently crosslinked counterparts; this is due to the weak nature of the polymer connections and their sensitivity to external parameters[4] such as dilution, ionic strength, temperature… Nanogels have the characteristics of both nanoparticles and hydrogels, they can be referred as soft materials, combining the properties of solids and fluids.[5] They possess high water content with adjustable size, extensive surface area, high loading capacity, high stability of interior network structure. The three-dimensional crosslinked structures in polymer nanogels allow water molecules to interact with hydrophilic groups of the polymer segment helping it to swell while keeping the original structure which induces nanogel softness and swelling behaviors.[6,7] Beside sol-gel transition, polymer nanogels have been designed to respond to a wide variety of stimuli such as pH[8–11], light[12,13]and temperature[14–16]by changing their physicochemical properties, such as size, swelling, water content, loading capacity, permeability, and hydrophilicity/hydrophobicity balance,[17] which make such materials unique with unprecedent

properties for potential applications. Among the applications of nanogels, the most studied are biomedical applications including delivery systems of biomacromolecules like enzymes, proteins or deoxyribonucleic acid (DNA).[18–23] Thereby, thanks to the ability to tune their final configuration according to the biological needs including biodistribution, circulation time, targeting ability and triggered response at a target site,[17,24–29] nanogels possess outstanding advantages among other types of nanomaterials for delivery systems. Moreover, nanogels loading with inorganic particles, named "nanohybrids", with optical activity, electrical conductivity and magnetic properties make them suitable for *in vivo* diagnostic and imaging applications.[30,31] Besides delivery, diagnostic and imaging applications, nanogels have been employed for analytical processes such as investigation the activity of enzymes[32] or studying the adsorption of protein,[33] and very recently for mercury removal from both produced water and hydrocarbons.[34]

In this chapter, different methods and strategies to synthesize nanogels will be reviewed. The preparation of nanogels by physical crosslinking through non-covalent interactions, by chemical crosslinking of polymer precursors or by direct crosslinking through radical polymerization of comonomers will be discussed. Finally, recent studies on stimuli-sensitive nanogels and more specifically thermosensitive and pH-degradable nanogels will be developed.

## 1.2 Nanogel synthesis

Nanogels based on synthetic or natural polymers can be mainly classified into two categories according to their crosslinked structure: physically crosslinked nanogels which form network through non-covalent bonds and chemically crosslinked nanogels which form crosslinking by covalent bonds. In the following section, few examples of different methods to prepare physically and chemically crosslinked nanogels are detailed.

### 1.2.1 Physically crosslinked nanogels

Physically crosslinked nanogels are prepared using non-covalent interactions between polymer chains, such as Van der Waals forces, hydrophobic interactions, electrostatic interactions or host-guest interactions.[5,35] Such nanogels were obtained from the self-assembly of polymers containing associating unit in solution (Figure I.1). Associating units, precursors of hydrophobic, electrostatic and host-guest interactions will be more specifically discussed in the following part.

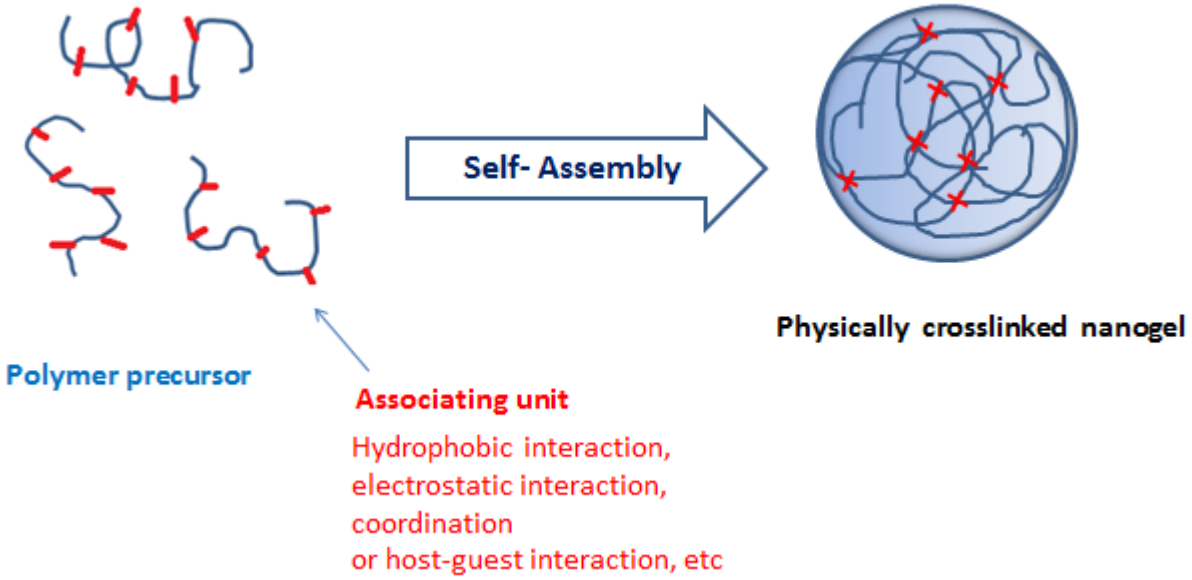


Figure I.1. Physically crosslinked nanogels formed with polymer precursors in solution.

#### 1.2.1.1 Hydrophobic interactions

Based on hydrophobic interactions, Akiyama and coworkers[36] have prepared physically crosslinked nanogels by the self-assembly of cholesterol-bearing polysaccharide mannan (CHM) (Figure I.2). Crosslinking points are formed *via* the association of hydrophobic cholesteryl groups. In the dilute regime, CHM containing 1 cholesteryl group per 100 mannopyranose units formed nanogels with a hydrodynamic radius ($R_h$) of 40 nm containing ~8 macromolecules held together *via* hydrophobic nanodomains consisting of ~9 cholesteryl groups. CHM nanogels formed a macrogel network for concentrations higher than 12.5 w/w %.

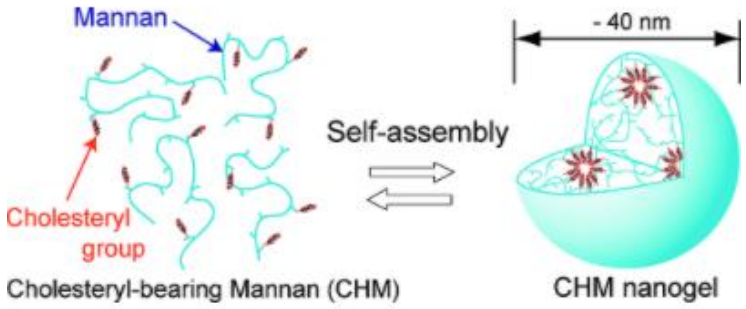


Figure I.2. Formation of cholesteryl-bearing polysaccharide mannans (CHM) nanogels. Reproduced from ref. 36.

In another example, by grafting polylactide (PLA) hydrophobic polymer chains onto hydrophilic dextran, stable nanogels with relatively large hydrophobic domains have been obtained.[37] Nanogels were obtained through the self-assembly of an equimolar mixture of dextran-*graft*-poly(L-lactide) (Dex-*g*-PLLA) and dextran-*graft*-poly(D-lactide) (Dex-*g*-PDLA) amphiphilic copolymers in a dilute aqueous solution. They possessed partially crystallized cores of hydrophobic PLA and the hydrophilic dextran skeleton by intra- and/or intermolecular self-assembly between PLLA and PDLA chains (Figure I.3). The mean diameter of resulting nanogels was 70 nm with narrow size distribution.

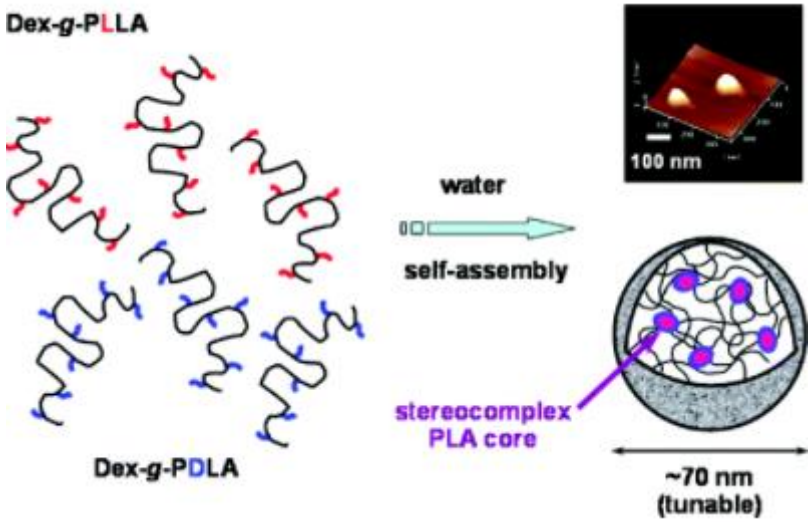


Figure I.3. Formation of nanogels through the self-assembly of Dex-*g*-PLLA and Dex-*g*-PDLA amphiphilic copolymers. Reproduced from ref. 37

### 1.2.1.2 Electrostatic interactions

Other intermolecular forces have been used as driving forces in the preparation of physically crosslinked nanogels. For example, a nanogel of water-soluble chitosan-poly(L-aspartic acid)-poly(ethylene glycol) (WSC-PASP-PEG) was prepared under relatively mild conditions using the complexation between polyelectrolytes through electrostatic interactions.[38] Inter- and intramolecular electrostatic attractions occur between the anionic carboxyl group from PASP and the cationic amino groups of WSC. PEG was incorporated as a third polymer in the system in order to make interpolymer interactions stronger due to further interactions between the carboxyl group in PASP acting as good proton donor and the ether group of PEG acting as a proton acceptor. The nanogel was prepared by mixing negatively charged PASP and positively charged WSC and PEG by a dropping method. A schematic representation of the nanogel formation is shown in Figure I.4. The

spherical nanogel with a tunable size in the range of 99 to 200 nm with different employed initial molar ratios of WSC and PASP.

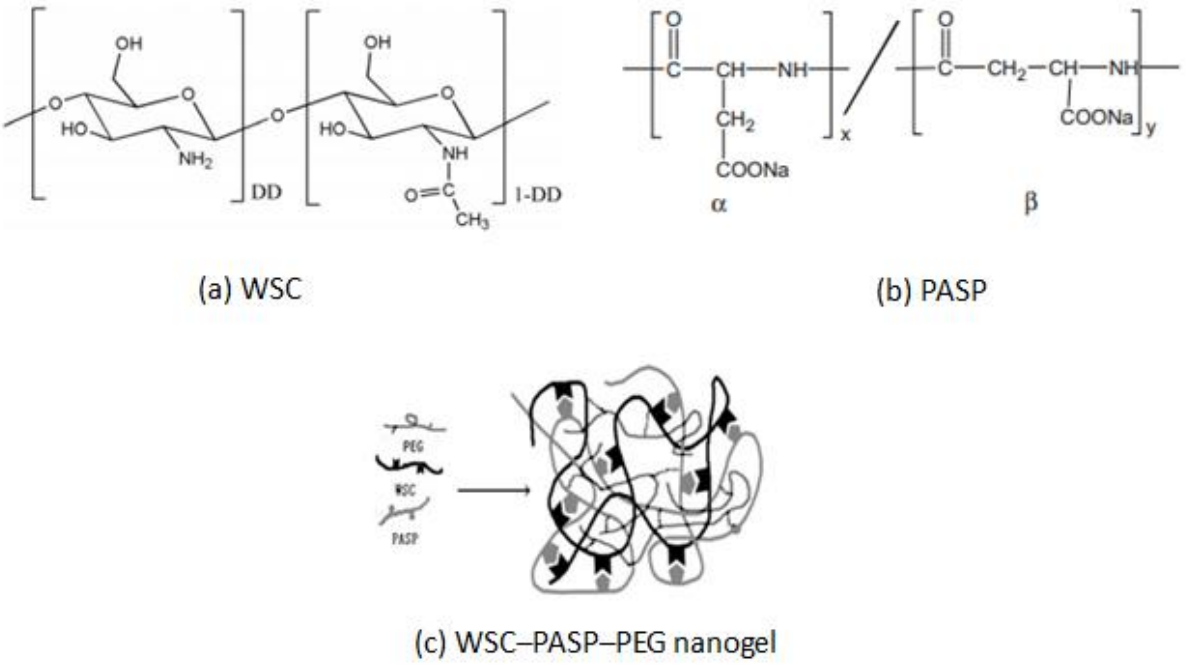


Figure I.4. (a) Chemical structure of WSC (DD is the degree of deacetylation), (b) chemical structure of PASP, (c) formation of WSC-PASP-PEG nanogels. Reproduced from ref. 38

### 1.2.1.3 Host-guest interactions

Host-guest interactions with cyclodextrin (CD) have also been employed to prepare nanogels using the association of a hydrophobically modified dextran (MDex) and a cyclodextrin polymer (Figure I.5).[39] The entrapment of two hydrophobic molecules, benzophenone (BZ) and tamoxifen (TM), into self-assembling cyclodextrin-based nanogels has been studied. With TM entrapment, drug loadings of about 0.5% (w/w) of the dried polymer mixture were achieved in nanogels of about 200 nm in diameter. Unfortunately, the suspensions were very unstable: in the first five minutes after their formation, the nanogels fused together and finally formed a gel deposit. With BZ, nanogels sizing 100-200 nm were obtained whatever the polymer concentration and the polymer ratio used. In the case of the 1 $g.L^{-1}$ preparations, these nanogels were stable, with a mean diameter lower than 200 nm.

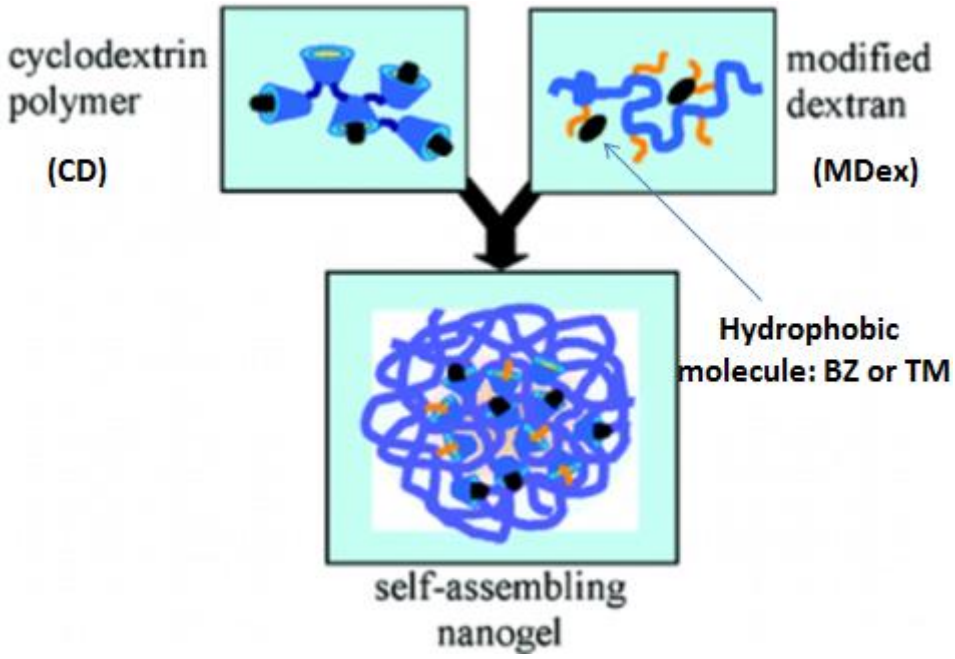


Figure I.5. Spontaneous formation of nanogels upon the association of host-guest interactions from cyclodextrin polymer (CD) and hydrophobically modified dextran (MDex) with hydrophobic molecules, benzophenone (BZ) or tamoxifen (TM). Reproduced from ref. 39

## 1.2.2 Chemically crosslinked nanogels

A variety of methods have been developed to synthesize chemically crosslinked nanogels including the crosslinking of polymer precursors, the direct crosslinking through radical polymerization of co-monomers and through polymerization-induced self-assembly (PISA) process.

### 1.2.2.1 Nanogels preparation from crosslinking of polymer precursors

By employing crosslinking reactions *via* post-modification of preformed reactive polymer precursors, a wide range of nanogels with precise control of the chemical functionality could be obtained. This technique has evolved from polymer synthesis, where post-polymerization functionalization enables the introduction of active groups into polymer chains which can be further crosslinked (Figure I.6).

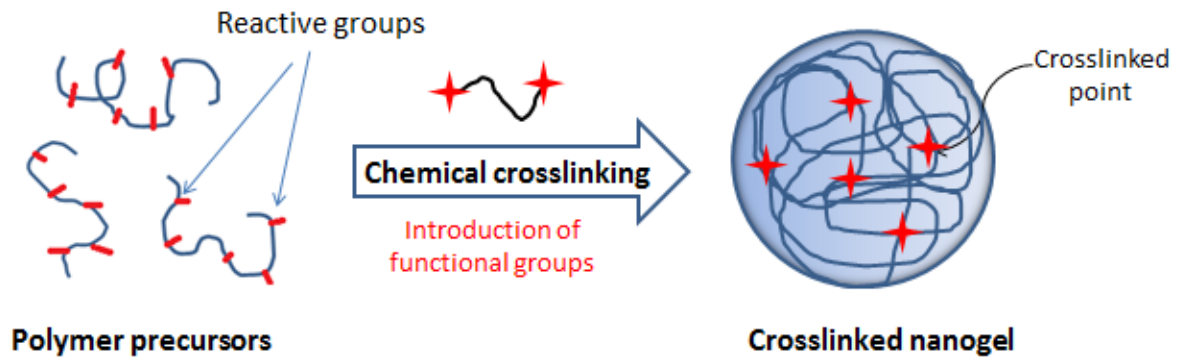


Figure I.6. Preparation of nanogels obtained by chemical crosslinking of polymer precursors.

Chemical crosslinking methods including the crosslinking reactions through reactive groups present in polymer precursors were developed to synthesize nanogels. Examples of crosslinking reactions are discussed in this paragraph.

#### 1.2.2.1.1 Thiol-disulfide exchange reaction

Thayumanavan and coworkers[40] prepared the nanogels system based on reversible addition-fragmentation chain transfer RAFT-synthesized copolymers of oligo(ethylene glycol) methacrylate (OEGMA) and pyridyl disulfide (PDS)-derived methacrylate of different compositions and molar masses. The addition of dithiothreitol (DTT) reduces a controlled percentage of PDS groups to thiols, which subsequently reacted with an equivalent amount of the remaining PDS groups to generate disulfide crosslinks, and nanogels were formed (Figure I.7). Dynamic light scattering (DLS) studies reveal that the structures obtained are approximately 190 nm in size with a single size distribution for initial polymer concentration of 10 $mg.mL^{-1}$. Different nanogel sizes can be easily obtained by varying copolymer concentration. The authors encapsulated a hydrophobic dye, Nile red, into the nanogels to test its encapsulation. They demonstrated the possibility of further functionalization of the nanogels with thiol-modified fluorescein isothiocyanate (FITC) and a thiol-based cell-penetrating peptide, Cys-Tat, containing a C-terminal cysteine. They thus showed that the multifunctional nanogels are indeed interesting materials for drug delivery applications.

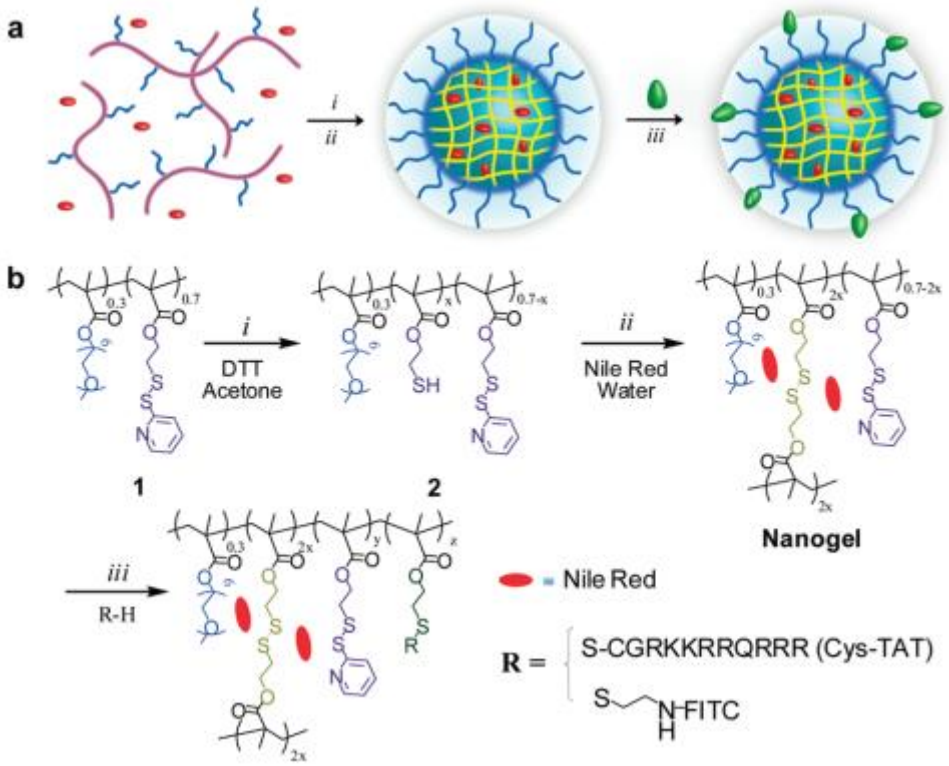


Figure I.7. Design and synthesis of the nanogels through thiol-disulfide exchange reaction of OEGMA/PDS-methacrylate copolymer precursors. (a) Schematic representation of the preparation of nanogels and their surface modification. (b) Chemical structures of the copolymer and nanogel. (i) Cleavage of specific amount of PDS groups by DTT. (ii) Nanogel formation by inter/intrachain crosslinking by thiol-disulfide exchange reaction. (iii) Surface modification of nanogels with thiol-modified FITC and a thiol-based cell-penetrating peptide, Cys-Tat. Reproduced from ref. 40

#### 1.2.2.1.2 Amidation reaction

The amidation reaction could generate nanogels from either polymer precursors containing carboxylic acid, activated ester or amine groups and crosslinkers containing amine or carboxylic acid, activated ester groups, respectively. Zhuang *et al*.[41] have developed an approach to synthesize nanogels through the amidation of a PEG-based polymer precursor P1 containing pentafluorophenyl (PFP)-activated hydrophobic esters and diamine crosslinkers. The hydrodynamic diameter ($D_h$) of obtained nanogels are in the range of 100-200 nm depending on the initial concentration of P1. As shown in Figure I.8, amphiphilic assembly can accommodate lipophilic guest molecules, these will be incorporated in the assembly during the crosslinking in aqueous solution. This causes the lipophilic molecules to be encapsulated within the crosslinked interiors of the nanogel.

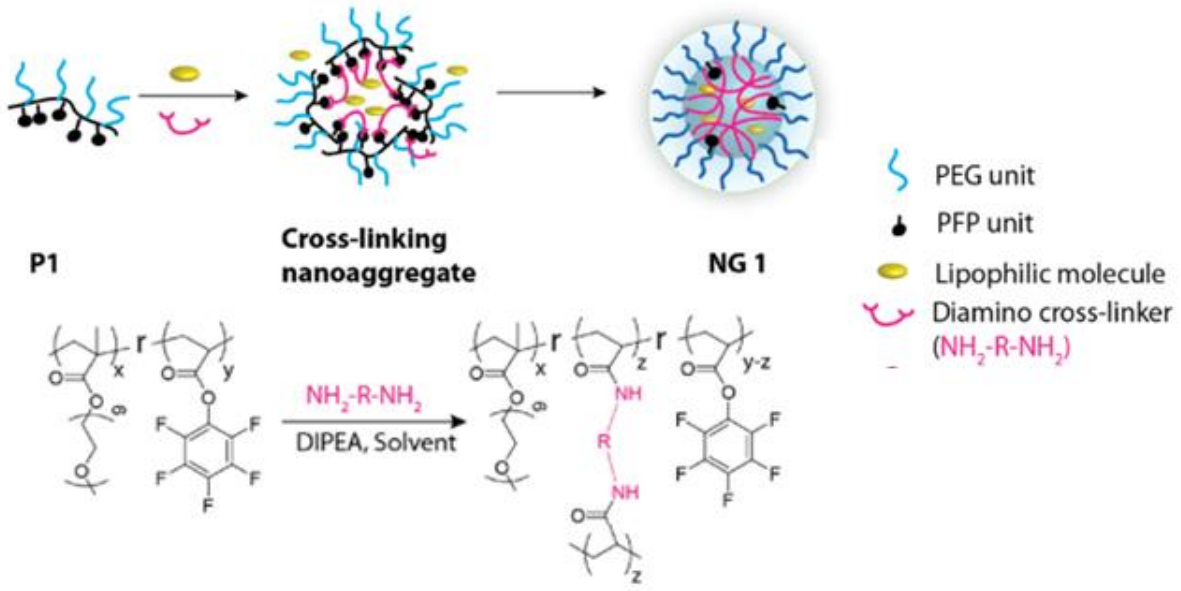


Figure I.8. Design and synthesis of the crosslinked polymer nanogels by amidation reaction of PEG-derivated copolymer precursors containing PFP side groups and the ability of nanogel to encapsulate lipophilic molecules. Reproduced from ref. 41

#### 1.2.2.1.3 Schiff base reaction

The Schiff-base reaction occurs between aldehydes and amines or hydrazide containing compounds to form an imine bond. It has been often employed to generate nanogels for biomedical applications due to its mild reaction conditions. Also, the formation of imine bonds, stable under physiological conditions and labile at acidic pH, makes these nanogels promising candidates for the intracellular delivery of proteins. Jackson *et* al.[42] prepare spherical crosslinked nanogels through imine bond formation from aldehyde and amine functional styrenic- and methyl methacrylate based copolymers at room temperature (Figure I.9). The aldehyde-functionalized (P5) and amine-functionalized (P7) copolymers were prepared then mixed in tetrahydrofuran (THF). The nanogels formed at lower concentrations (< 0.25 wt %) of total copolymers with a $R_h$ in the rage of 13-16 nm.

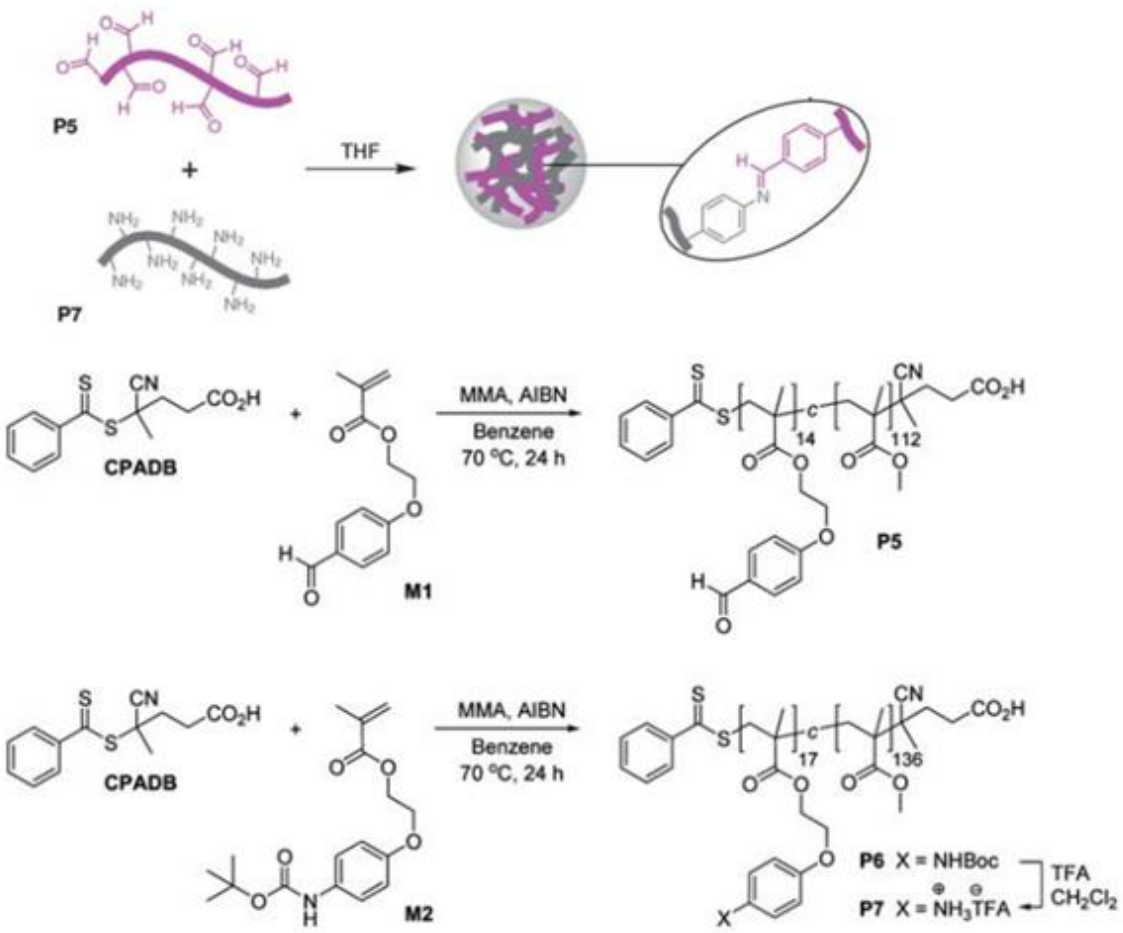


Figure I.9. The formation of nanogel facilitated by the crosslinking of polymer chains through the formation of imine bonds from aldehyde and amine functionalized copolymers P5–P7. Reproduced from ref. 42.

#### 1.2.2.1.4 Photodimerization of coumarin entities

By using the photodimerization of coumarin groups, He *et al*.[43] prepared a well-defined nanogel, based on copolymer composed of *N,N*-dimethylaminoethyl methacrylate (DMAEMA) and 4-methyl-[7-(methacryloyl)oxy-ethyl-oxy]coumarin (CMA), under UV-light irradiation with λ > 310 nm in a dilute copolymer solution in THF (Figure I.11). Photoinduced size change of nanogel was observed upon the reverse photocleavage of coumarin dimers under UV-light λ < 260 nm. The average size of core- and shell-crosslinked nanogels could be changed between ~58 and ~47 nm by optically controlling the dimerization degree between ~28% and ~80%.

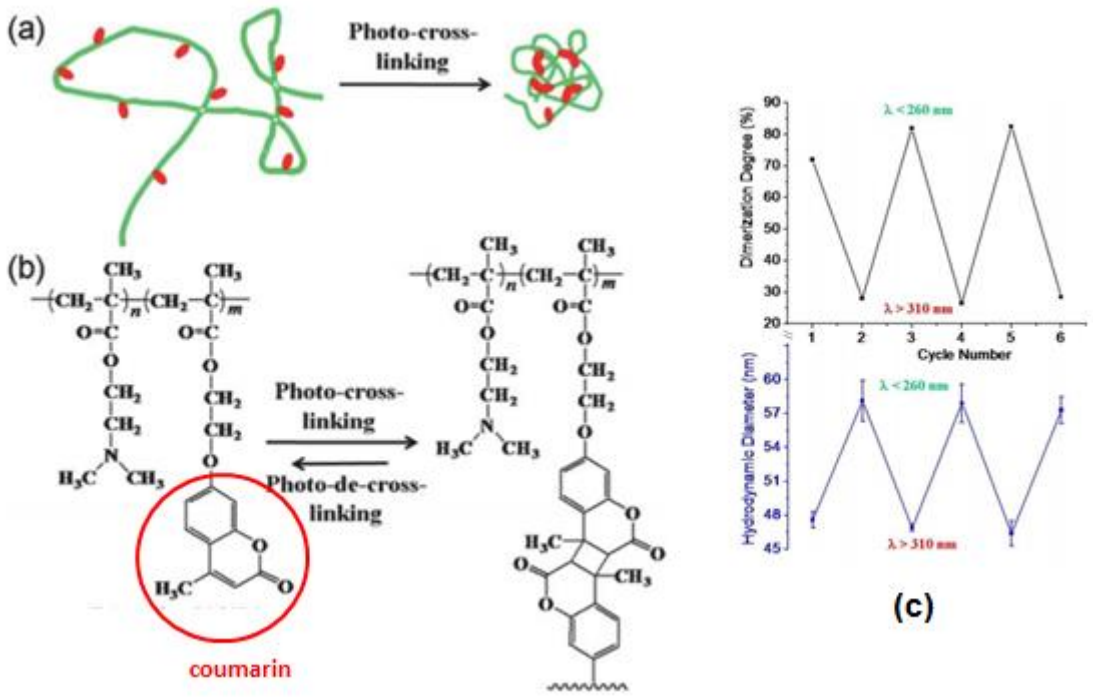


Figure I.10. (a) Schematic illustration of preparation of nanogels through photodimerization. (b) Chemical structures of coumarin-containing random copolymers based on DMAEMA and CMA and the reversible photodimerization reaction activated by UV-light. (c) The reversibility of photo-controlled size change of nanogels. Top figure: the reversible change of dimerization degree of coumarin upon the alternating irradiation by UV-light >310 nm and <260 nm. Bottom: the hydrodynamic diameter at 15°C reversibly switched between ~58 and ~47 nm by photo-crosslinking and photo-de-crosslinking reaction of coumarin. Reproduced from ref. 43

#### 1.2.2.2 Nanogels preparation by direct crosslinking through radical polymerization of comonomers

In this method, the nanogel was created by direct copolymerization of monomers. The polymerization and the crosslinking reaction occur at the same time. There are different polymerization processes and synthetic strategies based on conventional, controlled radical polymerizations and PISA process to prepare nanogels.

##### 1.2.2.2.1 Synthesis of nanogels by free radical crosslinking copolymerization (RCC)

RCC was considered as a simple and popular process to product nanogels. As nanogels are colloidal networks limited in size, the main challenge relies on identifying strategies that allow avoiding the formation of long-range networks. Several strategies have thus been developed in order to reach nanometric gels instead of macroscopic networks, i.e. macroscopic gelation. They generally rely on the control of the distance between growing polymer chains.[44] The first strategy is based on

RCC performed in highly diluted solution. Decreasing the monomer concentration increases the distance between propagating chains, limits thus intermolecular crosslinking and increases the probability of intramolecular crosslinking, consequently macroscopic gelation can be prevented. There is another efficient strategy to target the nanogel synthesis by application of heterogeneous polymerization processes, where the polymerization is performed in a confined nanometric space. In such strategy, the size of the gels will be limited by confining the crosslinking to intraparticle rather than interparticle crosslinking. Whereas the first approach, RCC in highly diluted homogeneous conditions, leads to soluble branched polymers, this second strategy may lead to denser nanoparticles possessing an internal structure comparable to that of macroscopic networks. It includes inverse (mini)emulsion and (inverse) microemulsion polymerization processes which allow for the preparation of crosslinked nanogels with narrow size distribution.

#### 1.2.2.2.2 Inverse (mini)emulsion polymerization

Inverse (mini)emulsion polymerization is a water-in-oil (W/O) polymerization process that contains aqueous droplets (including water-soluble monomers) stably dispersed with the aid of oil-soluble surfactants in a continuous organic medium. One main difference between inverse miniemulsion and inverse emulsion processes is the initial size of the dispersed phase. In the case of inverse emulsion polymerizations, monomer droplets are formed by mechanical stirring, the size of droplets are measured 1 to 20 μm. In contrast, for inverse miniemulsion, stable droplets smaller than 500 nm are formed by applying high shear stress as ultrasonication or high-pressure homogenizer. Upon addition of radical initiators, polymerization occurs within the aqueous droplets producing colloidal particles.

For instance, stable, crosslinked nanogels based on diacrylate macromonomer (M) constituted of a–poly(ethylene oxide)-*b*-poly(propylene oxide)-*b*-poly(ethylene oxide) (PEO-*b*-PPO-*b*-PEO) triblock copolymer were prepared by inverse emulsion photopolymerization.[45] The aqueous phase, containing triethanolamine (photo initiator), and diacrylate macromonomer, was dispersed in hexane by sonication with the help of Span65 as surfactant.The aqueous macromonomer nanodroplets in the inverse emulsion are stabilized by subsequent polymerization by photopolymerization of diacrylate macromonomer. After the photopolymerization, the resulting nanogels were purified by removal of the emulsifier through extensive washing with *n*-hexane (Figure I.11). The resulting nanogels had a diameter of 50 and 500 nm, which are capable of absorbing large amounts of hydrophobic drugs, here demonstrated with the anticancer drug doxorubicin (DOX).

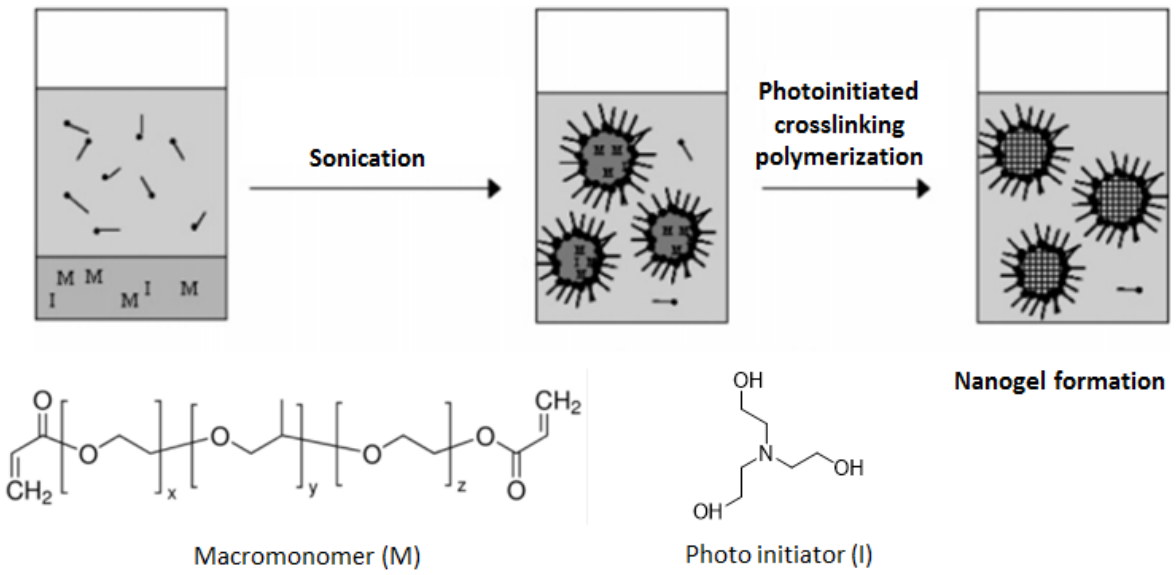


Figure I.11. Nanogel preparation *via* inverse emulsion photopolymerization of diacrylate macromonomer (M). Reproduced from ref. 45

In another example, Gao *et al.*[46] prepared poly(*N*-vinylcaprolactam-*co*-2-methoxyethyl acrylate) P(NVCL-*co*-MEA) nanogels through inverse miniemulsion polymerization using a macromolecular crosslinker poly(ethylene glycol) dimethacrylate (PEGDMA) (Figure I.12).

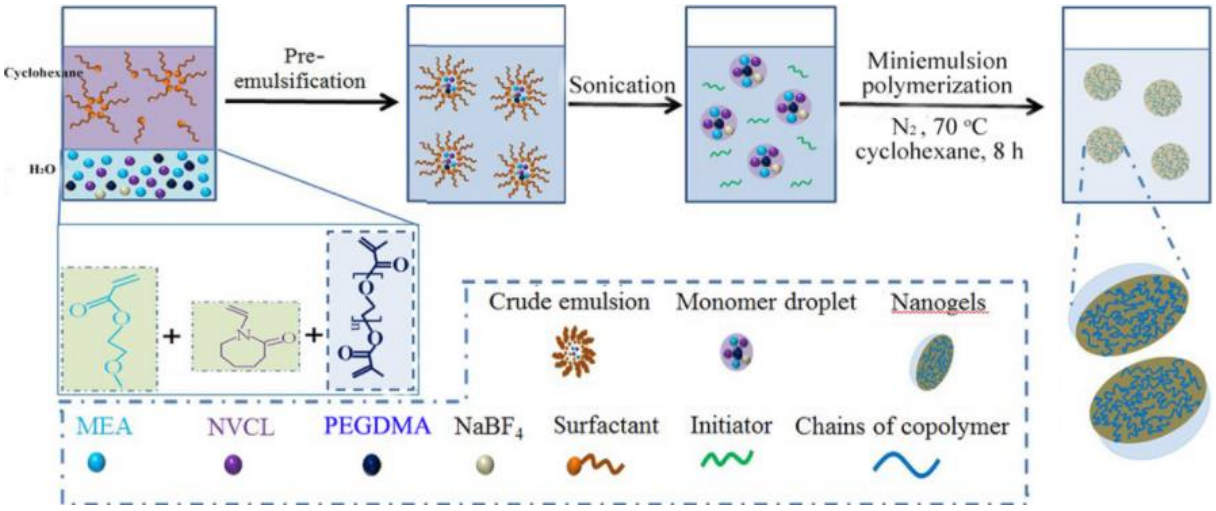


Figure I.12. Synthesis of P(NVCL-*co*-MEA)-based nanogels *via* inverse miniemulsion polymerization. Reproduced from ref. 46

Different variables including Span 80, Tween 60 surfactants and PEGDMA crosslinker contents have a significant impact on the properties of resulting nanogels. The particle size of P(NVCL-*co*-MEA) nanogels decreased with the increase of the surfactant amount compared to NVCL monomer content. For instance, when the content of surfactant was 4.8 wt.%, the $D_h$ and polydispersity in size (pdi) of P(NVCL-*co*-MEA) nanogels in the inverse emulsion were 201 nm and 0.201, respectively. The $D_h$ of nanogels decreased to 131 nm when 12.0 wt. % of surfactant was used. With the increase of PEGDMA crosslinker content, the crosslinking extent of polymer network increased, leading to the decrease of particle size of P(NVCL-*co*-MEA) nanogels. In contrast, the variation of monomer NVCL composition did not markedly influence $D_h$ and pdi value of nanogels. $D_h$ was 140 nm for 10 wt.% NVCL monomer. When the NVCL content in monomers increased to 50 wt.%, the $D_h$ of nanogels was slightly increased to 152 nm. $D_h$ of P(NVCL-*co*-MEA) nanogels did not obviously change with the further increase of NVCL content.

#### 1.2.2.2.3 Inverse microemulsion polymerization

While inverse miniemulsion polymerization forms kinetically stable macroemulsions at, below, or around the critical micelle concentration (CMC), inverse microemulsion polymerization produces thermodynamically stable microemulsions upon further addition of surfactant above the critical threshold. This process also involves aqueous droplets, stably dispersed with the aid of a large amount of oil-soluble surfactants in a continuous organic medium. Polymerization occurs within the aqueous droplets, producing stable hydrophilic and water-soluble colloidal nanoparticles. Hydrophilic submicron magnetic polymer particles based on polyacrylamide (PAm) were prepared using inverse microemulsion polymerization process in the presence of ***N,N'***-methylene bisacrylamide (MBA) as a crosslinker.[47] The aqueous phase containing the monomer (Am), crosslinker (MBA) and iron oxide nanoparticles are dispersed in a sodium dioctyl sulfosuccinate (AOT)-toluene solution to form a W/O microemulsion. The polymerization of comonomers was carried out with 2,2'-azobis(2-methylpropionitrile) (AIBN) or 2,2'-azobis(2-methylpropionamidine) dihydrochloride (V50). After polymerization, the magnetic polymeric particles were dispersed in water by two methods: (i) precipitation-redispersion, where the particles were recovered by precipitation with an excess of methanol and thoroughly washed and vacuum dried before redispersion in water using ultrasonic bath, and (ii) phase inversion, which is based on phase inversion. The polymerized W/O dispersion is inverted to O/W structure by adding an excess of water, the toluene and the AOT surfactant were removed by magnetic separation-washing process. When the phase reversion method is applied, the $D_h$ values of magnetic polymer nanogels obtained range from 70 to 120 nm, depending on the AOT/water ratio and irrespective of the MBA concentration. When the ratio of AOT/water increases, the water core size of the droplets in W/O microemulsion decreases, and this leads to smaller

particles with a $D_h$ of 74 nm. When the concentration of MBA increases, the crosslinking density of the polymer particles also increases and consequently, the particles are more difficult to be swollen by water. However, when the precipitation-redispersion method is applied, the particle size of the magnetic polymeric nanoparticles ranging from 140 to 300 nm, which is much larger than those prepared *via* phase inversion process, was found to be unrelated to AOT/water ratio and the concentration of MBA. The observed behavior may be attributed to the influence of precipitation-redispersion and dryness on irreversible aggregated particles formation which induces uncertain particle size measurement. In addition to hydrophobic initiator AIBN, the water-soluble initiator (V50) was also used in such W/O microemulsion polymerization. Using V50, $D_h$ value of the particles is about 260 nm which is much larger than the size of the sample with AIBN as initiator. Such a size difference between the two swelled magnetic polymeric particles is due to the fact that V50 is a charged initiator. The distribution of the positive charges in the polyacrylamide matrix may enhance the swelling ability of the magnetic particles *via* intra-electrostatic repulsion and hydration process, and consequently large hydrodynamic size was obtained after phase inversion.

#### 1.2.2.2.4 Synthesis of nanogels by controlled RCC

The development of controlled radical polymerization (CRP) techniques since the mid-1990 can be considered as a breakthrough towards the easy synthesis of complex macromolecular structures with high degree of functionality and compositional variety. The CRP techniques that have been employed so far are nitroxide-mediated polymerization (NMP)[48] atom transfer radical polymerization (ATRP)[49,50] degenerative chain transfer polymerizations represented by iodine-mediated polymerization (RITP)[51,52] and RAFT[53,54] polymerization. Each technique has its pros and cons such as, the synthetic ease of NMP, however, requiring high temperatures. ATRP process is compatible with multitude of reaction conditions compatible but presenting purification issues due to the use of metal catalysts.[55] RAFT is a powerful versatile process in terms of monomers and reaction conditions and compatibility to functional groups, but generally lead to colored or odorous polymers.[56] When CRP techniques are applied, the kinetics is considerably slower than in conventional radical polymerization, hence, dormant polymer chains have time to diffuse and relax before being reactivated to propagate. Consequently, crosslinking points are more homogeneously distributed within the networks (assuming equivalent reactivity of the monomer and crosslinker). Therefore, CRP techniques have successfully been applied to the controlled synthesis of nanogels.

For example, a versatile approach to functional nanogels based on poly(oligo(ethylene oxide) monomethyl ether methacrylate) (POEOMA) using an inverse miniemulsion activator generated by electron transfer (AGET) ATRP in the presence of an added disulfide-functionalized crosslinker was

described by Oh *et al.*[57] (Figure I.13). Since polymerization occurs in the aqueous monomer droplets dispersed in an organic medium, all AGET ATRP ingredients including catalyst, ligand, and initiator must be soluble in water. This requires preferential partitioning of the copper complex and initiator into the aqueous phase. A water-soluble, PEO functionalized at the chain-end with a bromoisobutyrate (PEO5000-Br) was synthesized and used as the initiator for the preparation of PEO-*b*-POEOMA copolymers. As an additional requirement, the ATRP activator and deactivator must be stable in water. This requirement was ensure by using tris-[(2-pyridyl)methyl]amine (TPMA) as the ligand. TPMA is known to provide an active water-soluble complex, which has low tendency for disproportionation. The AGET ATRP process involves the use of an oxidatively stable Cu(II) precursor that can generate the active Cu(I) catalyst by reaction with nonradical-forming reducing agents. Consequently, the concentration of the Cu(II) complex can be controlled throughout the reaction, leading to improved control over initiation and propagation. Water-soluble ascorbic acid was used as the reducing agent. The preservation of bromine functionality in the ATRP nanogels was demonstrated by successful chain extension of the active terminal functionality present throughout the nanogels by the ATRP of styrene, resulting in the formation of POEOMA nanogels chain extended with polystyrene (PS) (nanogels named POEOMA-*ce*-PS in which ce is the abbreviation for “Chain Extended”).

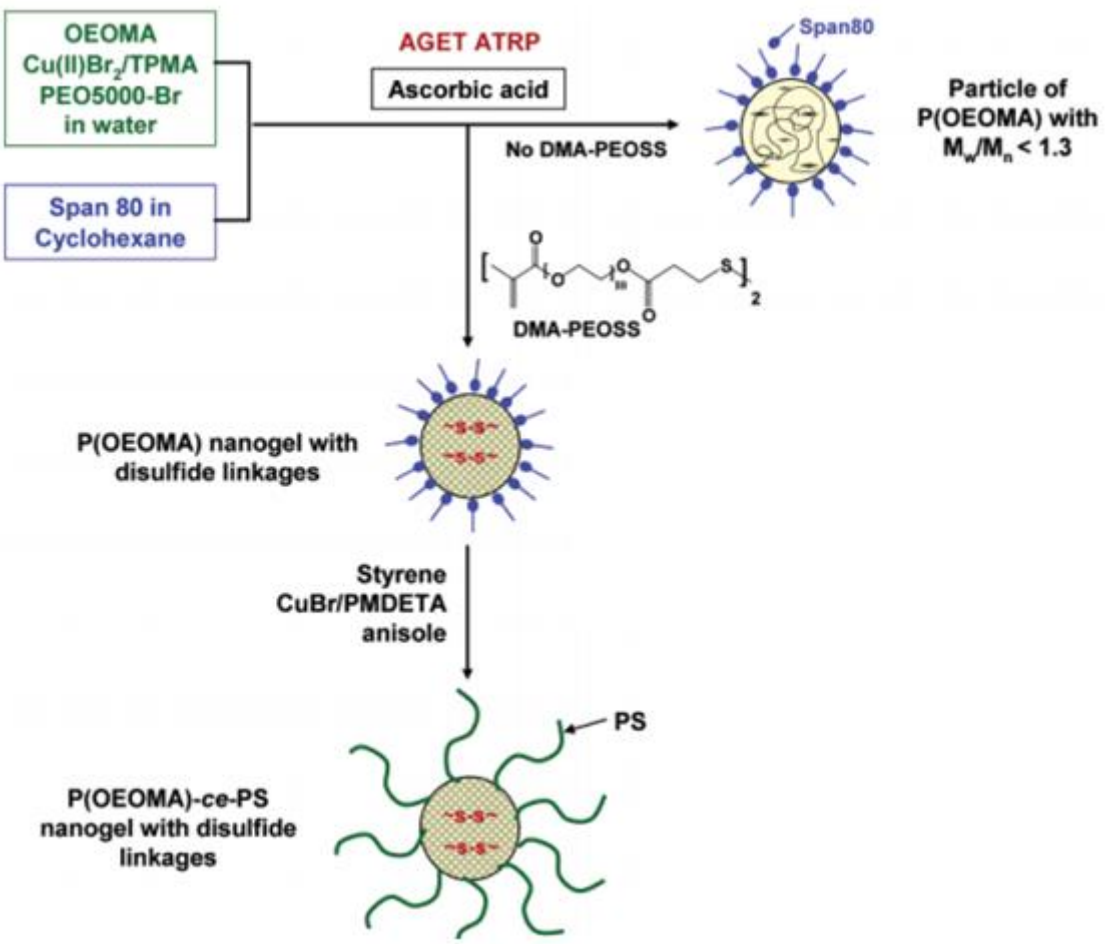


Figure I.13. Synthesis and functionalization of nanogels based on well-controlled hydro-soluble PEO-*b*-POEOMA copolymers obtained by AGET ATRP. Reproduced from ref. 57

As the RAFT-PISA process has been applied during my PhD work to target stimuli-sensitive nanogels, a particular attention will be paid on the elaboration of nanogels using RAFT-PISA process.

### 1.2.2.3 Preparation of nanogels by RAFT-PISA process

In the PISA process, typically, a soluble homopolymer (A) is chain-extended using a second monomer in a suitable solvent such that the growing second block (B) gradually becomes insoluble, which drives *in situ* self-assembly to form AB diblock copolymer nano-objects. The A block is usually prepared *via* solution polymerization and acts as a surfactant, while the insoluble B block is prepared *via* either dispersion or emulsion polymerization (depending on the monomer solubility in the continuous phase) as shown in Figure I.14.

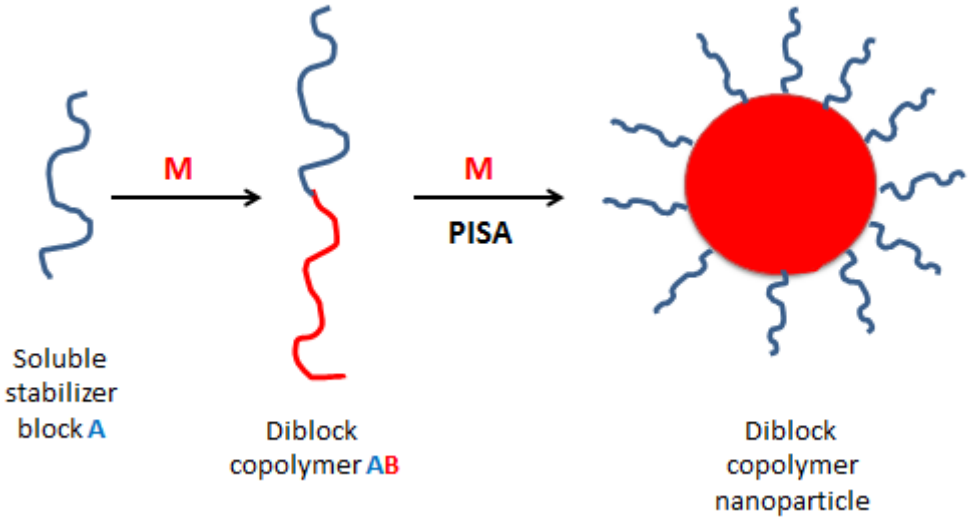


Figure I.14. Synthesis of diblock copolymer nano-objects *via* PISA process.

In principle, PISA syntheses can be conducted using any type of controlled radical polymerizations,[58–63] but in practice, the majority of literature examples are based on RAFT polymerization.[64–72] *In situ* core crosslinking of nanogel prepared by RAFT-PISA can be achieved by either (a) the post-polymerization addition of a suitable crosslinking agent (one-pot/two-step) or (b) addition of a divinyl comonomer during the latter stages of the polymerization (one-pot/one-step) (Figure I.15).

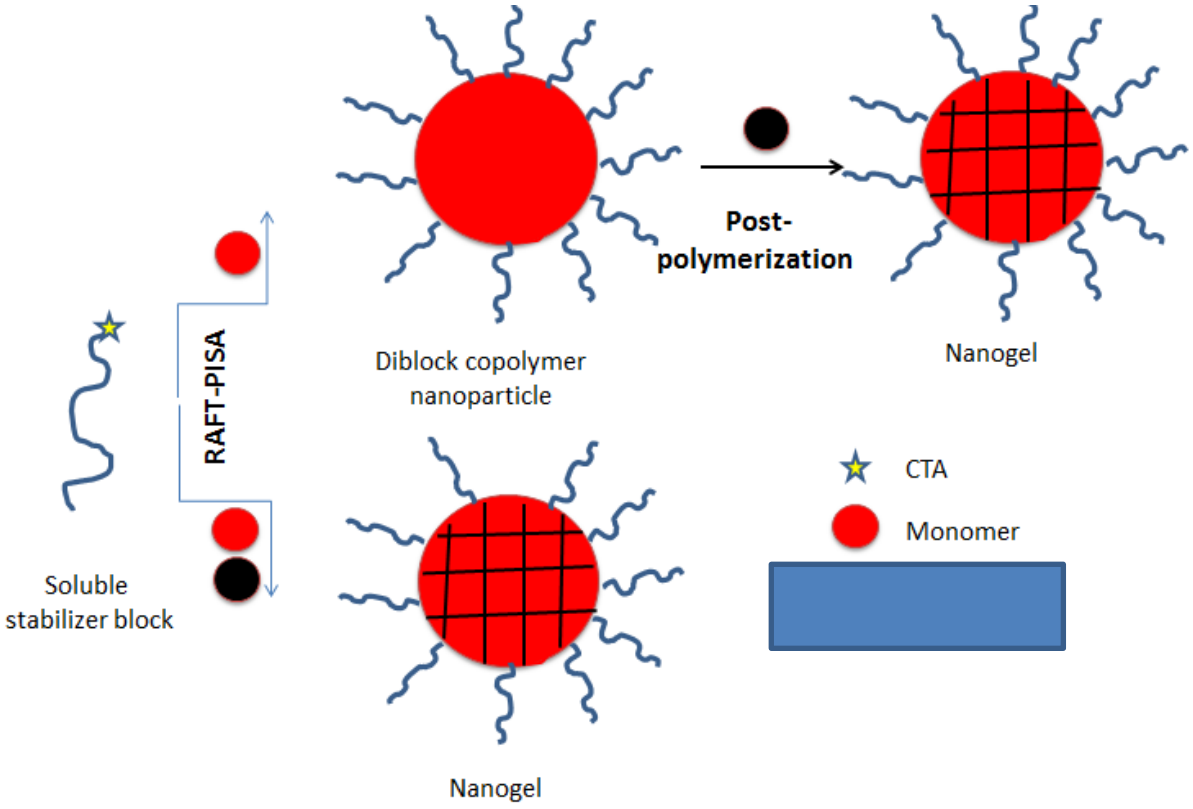


Figure I.15. Synthesis of nanogels via PISA process: (A) in two steps with post-polymerization addition of a crosslinking agent and (B) in one step using divinyl comonomer as crosslinker.

#### 1.2.2.3.1 Nanogel crosslinking by post-polymerization addition of a crosslinking agent

Well-defined epoxy-functional diblock copolymer nanogels were conveniently prepared *via* RAFT-PISA aqueous emulsion polymerization of glycidyl methacrylate (GlyMA) by Hatton *et al.*[73] Poly(glycerol monomethacrylate) (PGMA) was employed as a surfactant and a macromolecular chain transfer agent (macro-CTA) (Figure I.16). The epoxy groups were reacted with either sodium azide or model diamines to form crosslinked nanogels. The latter reagents produced highly crosslinked primary amine based nanogels.

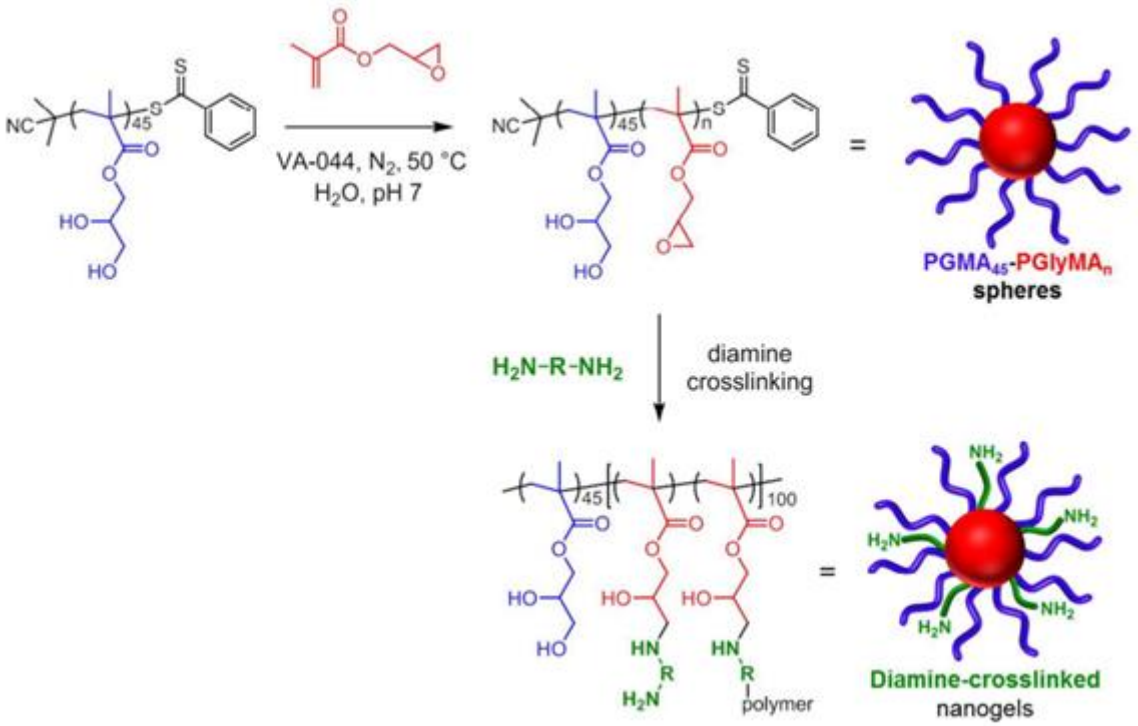


Figure I.16. Chain extension of a PGMA macro-CTA *via* RAFT-PISA aqueous emulsion polymerization of GlyMA and post-polymerization crosslinking. Reproduced from ref. 73

Two water-soluble diamines were investigated in this study: ethylenediamine (EDA) and bis(3-aminopropyl)-terminated poly(ethylene oxide) (PEGDA). When 10 w/w.% of EDA crosslinking was used, nanogels of around 37 nm diameter in water and 42-44 nm diameter in *N,N*-dimethylformamide (DMF) were obtained, respectively. Similarly, PEGDA crosslinked nanogel diameters ranged from 50 to 59 nm when dispersed in DMF but were only approximately 38-42 nm of diameter for aqueous nanogel dispersions.

#### 1.2.2.3.2 Nanogel crosslinking by addition of a divinyl comonomer during the polymerization

Sugihara *et al.*[74] prepared crosslinked diblock copolymer nanogels based on poly(2-(methacryloyloxy)ethyl phosphorylcholine) (PMPC) stabilizing chains and a highly crosslinked poly(2-hydroxypropyl methacrylate) (PHPMA) core-forming block using ethylene glycol dimethacrylate EGDMA as crosslinker. The nanogel based on PMPC-*b*-P(HPMA-*stat*-EGDMA) formed with 0.5 mol.% EGDMA crosslinker leads to spheres with $D_h$ of nanogel varied from 12 to 58 nm for PHPMA block length up to 100. The increase of PHPMA block length from 100 to 200, 300 and 400 leads to the increase of the $D_h$ of nanogel. At relatively low levels of EGDMA crosslinker (< 1 mol.%), only spherical morphologies are observed. However, higher levels of EGDMA lead to increasing particle anisotropy, with both worm-like morphologies and a novel “lumpy rod” morphology being observed (Figure I.17).

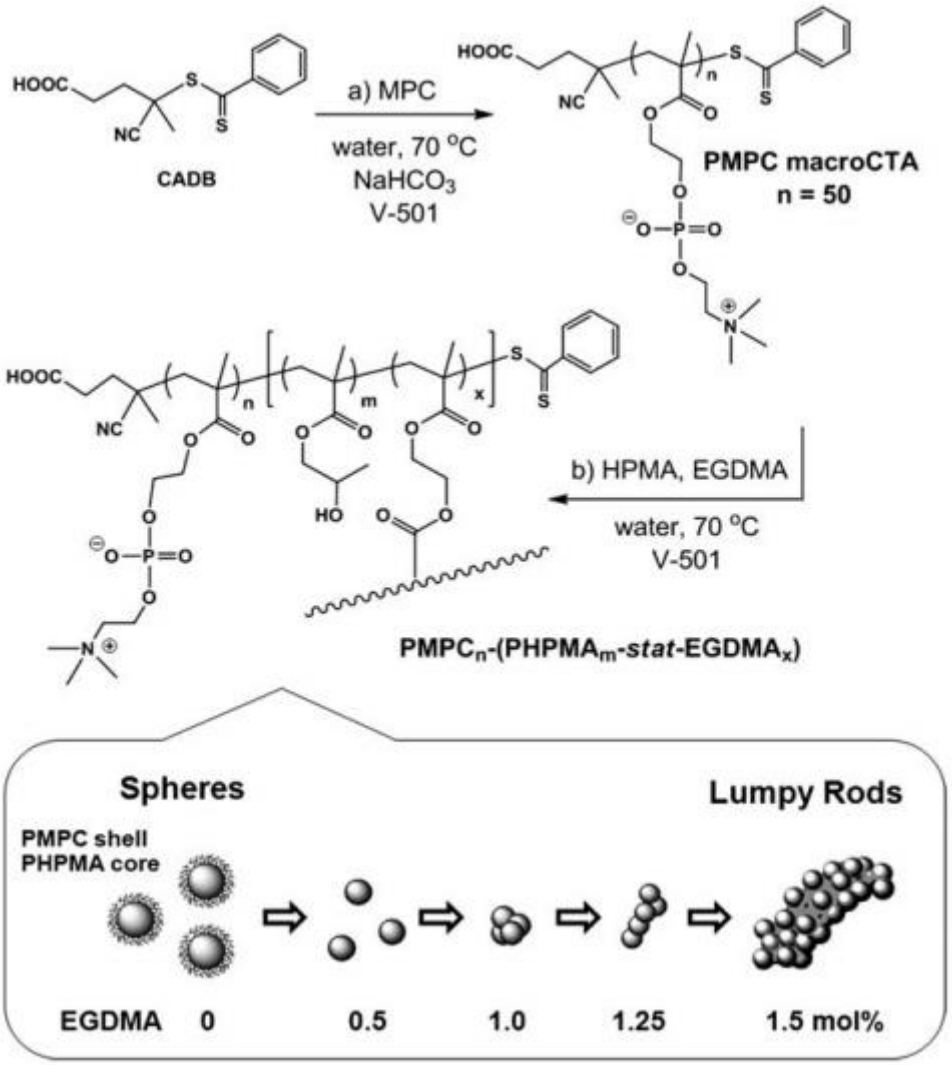


Figure I.17. Synthesis of PMPC-*b*-P(HPMA-*stat*-EGDMA) nanogels with spherical, worm-like or "lumpy rod" morphologies by RAFT-PISA aqueous dispersion polymerization at 70° C. Reproduced from ref. 74

In another example, the synthesis of well-defined PAm-based nanogels *via* RAFT dispersion polymerization, based on water-soluble polymers was reported.[75] PAm-based nanogels employing the co-non-solvency property of PAm in solvent mixtures of water and *tert*-butanol were prepared *via* RAFT dispersion polymerization of Am, in the presence of a MBA used as crosslinker, V-50 as the thermal radical initiator and poly(*N,N*-dimethyl acrylamide) PDMAm as a macro-CTA and surfactant (Figure I.18 ). Nanogels composed of either PAm or copolymer poly(acrylamide-*co*-butyl acrylate) (P(Am-*co*-BA)) with $D_h$ of 60 nm have been efficiently synthesized with uniform nanogel size and excellent colloidal stability.

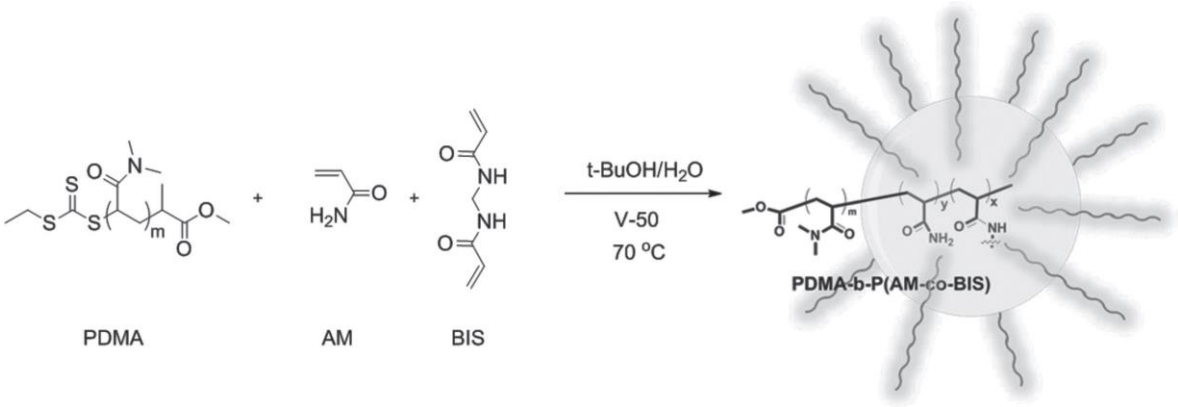


Figure I.18. RAFT dispersion polymerization of Am for the synthesis of nanogels from macro-CTA based of PDMAm. Reproduced from ref. 75

## 1.3 Stimuli-sensitive nanogels

Stimuli-sensitive nanogels are crosslinked nanoparticles based on polymers which are capable of responding to external stimuli by changing their physicochemical properties, such as size, volume, water content, degradability, and hydrophilicity/hydrophobicity balance. They are often referred to as “intelligent/smart” materials. The environmental stimuli include temperature, pH, light, redox reactions, etc. Among stimuli-sensitive nanogels, those based on temperature and pH-sensitive polymers are by far the most studied and are obtained significant attention.[76–82] In the following sections, the main studies on thermal- and pH-sensitive nanogels particularly reversible thermal-responsive and irreversible pH-responsive nanogels based on acid cleavable groups will be discussed (Figure I.19). The strategy to prepare such nanogels and their responsiveness properties will be reviewed.

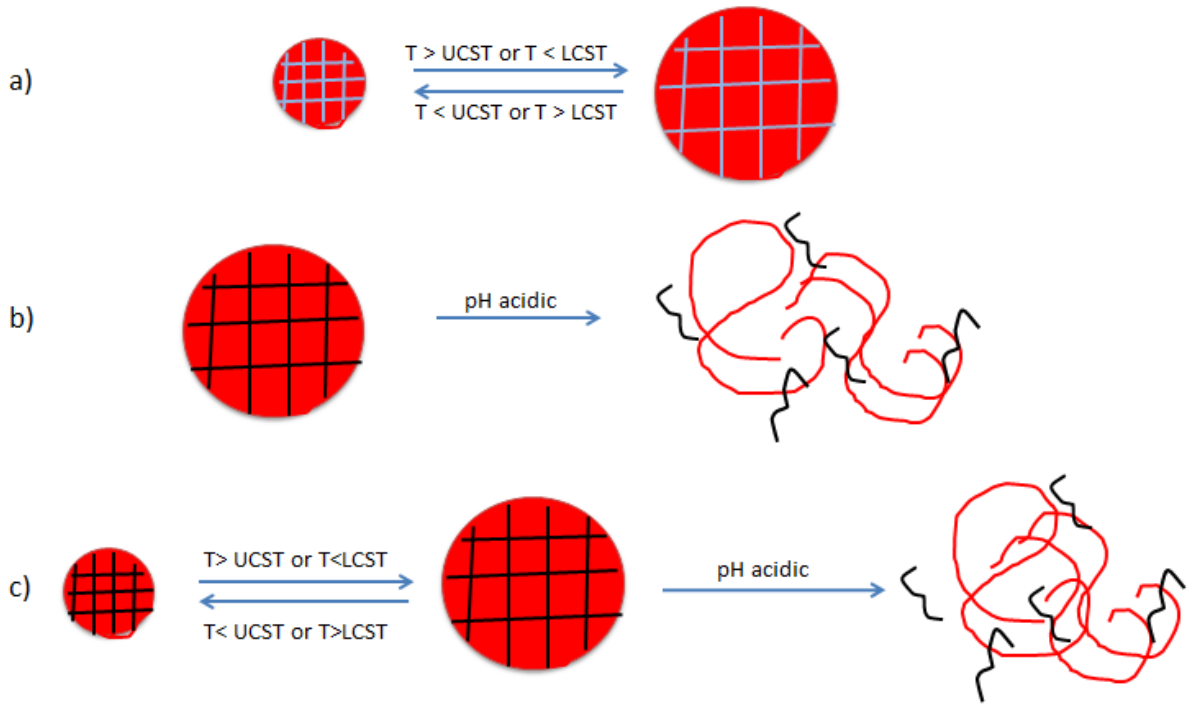


Figure I.19. a) Reversible thermal-responsive properties of thermosensitive nanogel; b) Irreversible responsive properties of pH-sensitive nanogel; c) Reversible thermal-responsive and irreversible pH-degradable properties of dual temperature/pH-sensitive nanogel.

## 1.3.1 Thermosensitive nanogels

The temperature is a stimulus that can be applied externally and reversibly in a non-invasive manner. In this context, many nanogels based on thermosensitive polymers have been reported.[83-86] The chemical structures, the critical temperature values of thermosensitive polymers with lower critical solution temperature (LCST) and with upper critical solution temperature (UCST), and the impact of different parameters including polymer concentration, molar mass, pH, addition of salts and copolymerization with a hydrophobic or hydrophilic co-monomer on their thermal behavior will be reviewed.

### 1.3.1.1 Chemical structures, critical temperature values and different parameters impacting the thermal behavior of thermosensitive polymers

Thermosensitive polymers have been subjected to extensive research in academic and applied polymer science over the last decade because of their unique property of phase separation at a critical solution temperature.[87–89] This phase separation results from the change of hydrophilicity of polymer at a specific temperature. The thermosensitive polymers are divided into two classes based on their response to change in temperature: polymers that can phase separate from solution upon

heating (polymers with a LCST) and those that can phase separate upon cooling (polymers with a UCST).

#### 1.3.1.1.1 Generalities on LCST and UCST phenomena

The solubility of LCST-type thermosensitive polymers decreases with the increase of temperature and the phase separation occurs above a critical value (named LCST value). By contrast, the solubility of UCST-type thermosensitive polymers decreases with the decrease of temperature and the phase separation occurs below a critical value (named UCST value). The LCST and UCST values are defined as the temperatures of the minimum and maximum of the bimodal of the phase diagram, respectively (Figure I.20).

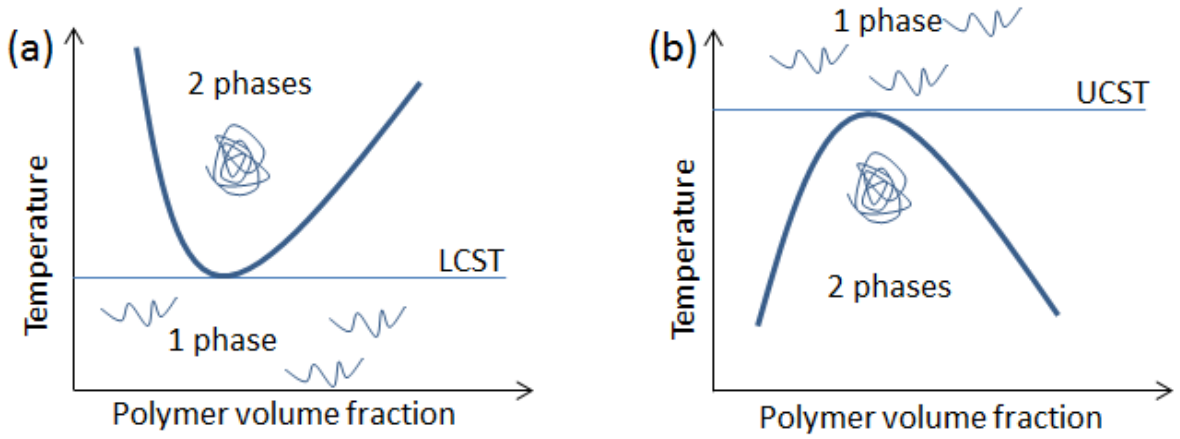


Figure I.20. Phase diagrams showing (a) the lower and (b) upper critical solution temperature, LCST and UCST behaviors, respectively, of thermosensitive polymers in solution. Reproduced from ref. 86

When temperature varies, the solvent quality changes from a good to a bad solvent at the bimodal resulting in the conformation change of the polymer chains from the open coil state to the collapsed globule state, respectively leading to the polymer aggregation (Figure I.21).

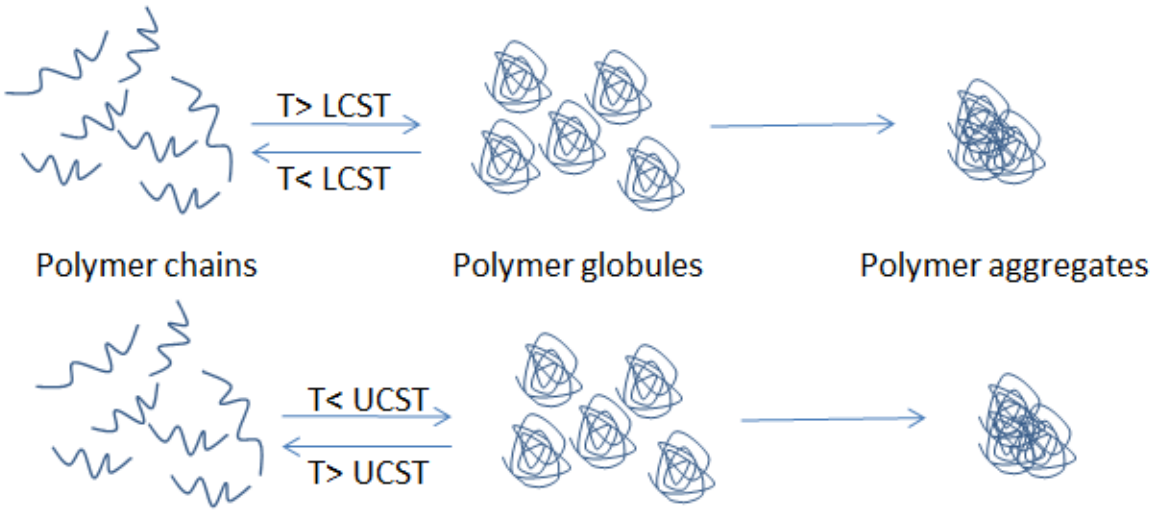


Figure I.21. Conformation changes of the polymer chains induced by the temperature.

From the thermodynamic point of view, thermosensitive polymers present a balance between hydrophobic, hydrophilic moieties and hydrogen bond (H-bond). To understand the dissolution of a polymer in a given solvent, the Gibbs free energy equation 1 is used:

$$\Delta G_{mix} = \Delta H_{mix} - T\,\Delta S_{mix} \qquad \text{(eq.1)}$$

where $\Delta G_{mix}$, $\Delta H_{mix}$ and $\Delta S_{mix}$ are the changes in Gibbs free energy, enthalpy and entropy of mixing between the polymer and solvent, respectively, at a certain temperature (T). The mixing between the polymer and solvent occurs when the $\Delta G_{mix}$ is negative. The enthalpic effect ($\Delta H_{mix}$) is due to the balance between intra- and intermolecular forces (*e.g.*, H-bond and hydrophobic interactions). The entropic effect ($\Delta S_{mix}$) is related to the dissolution process itself and due to the ordered state of water molecules in the vicinity of the polymer.

For UCST-type thermosensitive polymers, at low temperature, the strong supramolecular associative interactions strength between themselves implies a $\Delta H_{mix}$ greater than the $T\,\Delta S_{mix}$ term, leading to a positive $\Delta G_{mix}$ and thus insoluble polymer. With increasing temperature, the supramolecular associative interactions between polymer chains decreases, the $T\,\Delta S_{mix}$ term overweighs $\Delta H_{mix}$, thus $\Delta G_{mix}$ becomes negative and the polymer dissolves spontaneously. The phase transition temperature of UCST-type thermosensitive polymers is directly correlated to the strength of the inter- and intra-molecular interactions. By contrast, in the case of LCST phase transition, the $\Delta G_{mix}$ becomes positive with increasing temperature, meaning that the mixing is not favorable. The negative value of $-T\,\Delta S_{mix}$ becomes larger with increasing the temperature while the

positive value $\Delta H_{mix}$ becomes smaller, leading to a negative $\Delta G_{mix}$ at low temperature as the system is miscible.

There are several methods which can be used to characterize the phase transition temperature of thermosensitive polymers including UV-Vis spectrophotometry,[90] dynamic light scattering (DLS),[91] differential scanning calorimetry (DSC)[92,93] or $^{1}$H-NMR spectroscopy.[94] Among these techniques, UV-Vis spectrophotometry is the most common way to follow phase separation. Indeed, the phase separation is highlighted by turbidity measurements: the solution transmittance of the polymer solution at 500-700 nm is measured as a function of temperature (Figure I.22). The high transmittance means that the polymer is soluble and solution is transparent. In contrast, if the polymer is insoluble, the solution appears cloudy resulting in low transmittance. The cloud point is the temperature at which the change in transmittance is observed. The definition of the cloud point varies in the literature. Some authors take the temperature at the transmittance drops from 100% to 90%; others define the temperature at 50% or inflection point of the transmittance curve. The cloud point of a given polymer solution can also be different on heating and cooling due to kinetic hindrance and aging in the collapsed state even with the same heating/cooling rates. The difference between the cloud point upon cooling and heating is noted as thermal hysteresis.

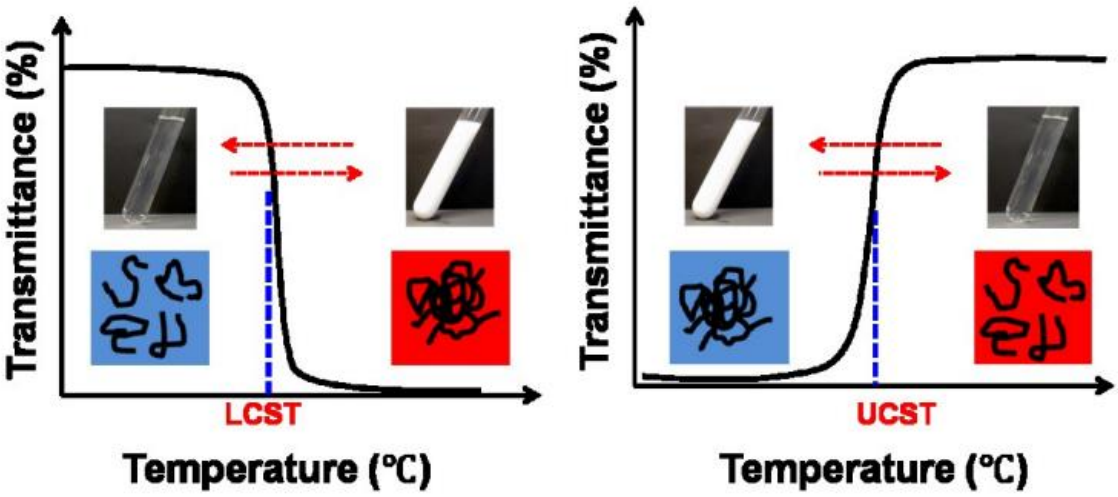


Figure I.22. Characterization of phase transition of a thermosensitive polymer solution by transmittance changes as a function of temperature. Reproduced from ref. 90

#### 1.3.1.1.2 LCST-type thermosensitive polymers

LCST-type thermosensitive polymers containing both hydrophilic and hydrophobic moieties in the pendant group of the repeating unit show phase transition temperature between 0°C and 100°C.[95] For example, amides and ethers are hydrophilic moieties while hydrophobic moieties are short

aliphatic groups such as isopropyl. The most studied LCST-type thermosensitive polymers will be selectively addressed in this section (Figure I.23).

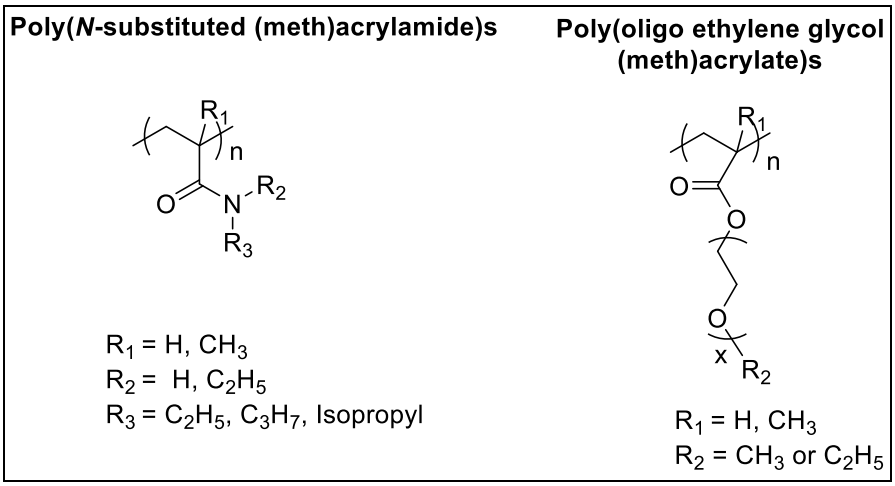


Figure I.23. Chemical structures of selected representative LCST-type thermosensitive polymers.

#### 1.3.1.1.2.1 LCST-type thermosensitive polymer based on *N*-substituted alkyl (meth)acrylamide

The most common LCST-type thermosensitive polymers are prepared from *N*-substituted alkyl (meth)acrylamide monomers.

##### *1.3.1.1.2.1.1 Poly(N-isopropyl acrylamide)*

The poly(*N*-isopropyl acrylamide) (PNIPAm) ($R_1$ = $R_2$ = H, $R_3$ = isopropyl, Figure I.23) has received most attention due to its LCST value of 32°C (between room and body temperature) in water, making it very interesting for biomedical applications.[96–98] The thermosensitive behavior of PNIPAm benefits from the contribution of the chemical structure of its repeating unit as they are composed of hydrophilic amide group and hydrophobic isopropyl groups. When the environmental temperature is below LCST, the H-bond between water molecules and amide groups urges polymer chains to form a stable hydrated structure surrounding isopropyl groups leading to PNIPAm chains in the random-coil state with high flexibility. When the temperature goes up, the hydrated structure breaks down and the hydrophobic interactions between amide groups and the hydrophobic interactions derived from isopropyl groups play predominant roles, which force the water molecules initially bound to PNIPAm to spread outwards leading to the transition of polymer chains from coil state to globular conformation and finally inducing the macroscopically phase separation of the polymer in water (Figure I.24).

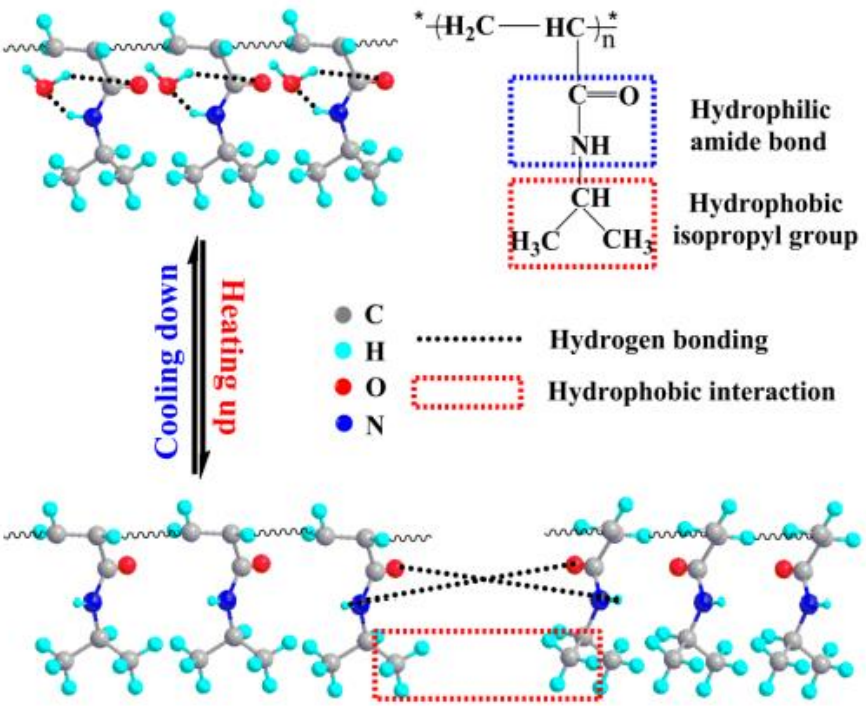


Figure I.24. Molecular structure and thermosensitive mechanism of PNIPAm in water. Reproduced from ref. 99

PNIPAm exhibits a very sharp transition when heated, but a relatively broad thermal hysteresis of 3 to 4°C can be observed during cooling.[99,100] The existence of a thermal hysteresis in the coil-to-globule-to-coil transition of PNIPAm chains in water was attributed to additional intrachain or interchain H-bonds in the collapsed state. These intersegmental H-bonds act as "the crosslinking" points among different chains so that each chain aggregate swells like a gel and the chain dissociation is delayed, which results in the observed thermal hysteresis.[101,102]

The phase transition temperature of PNIPAm is relatively insensitive to slight changes of polymer concentration, polymer chain length and pH.[99] Therefore, tuning the LCST of PNIPAm is done by different strategies. First of all, the statistical copolymerization of NIPAm with either hydrophilic or hydrophoblic monomers can impact significantly the LCST value. Indeed, it has been shown that if the NIPAm monomer is copolymerized with more hydrophilic monomers such as acrylamide (Am), the LCST increases and may even disappear.[103] If NIPAm monomer is copolymerized with more hydrophobic monomer such as *N*-*tert*-butyl acrylamide (*N*-tBAm),[104] the LCST decreases.

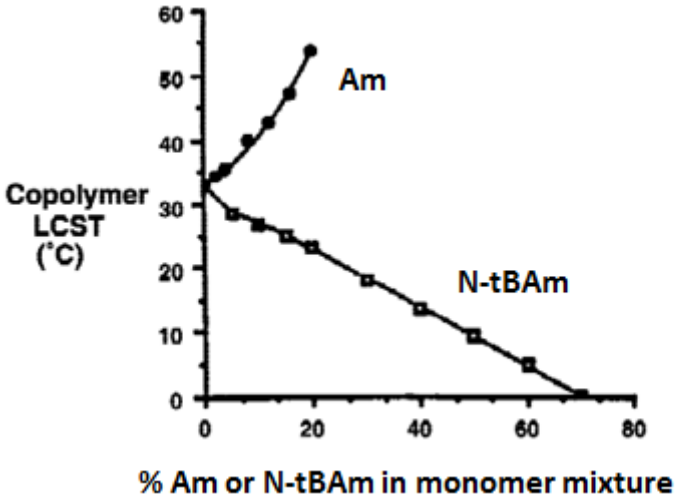


Figure I.25. Impact of the statistical copolymerization of a NIPAm monomer with a hydrophilic acrymalide (Am) or hydrophobic *N*-*tert*-butyl acrylamide (*N*-tBAm) comonomer on the copolymer LCST value. Reproduced from ref. 104

It is known that LCST value of a PNIPAm can be changed significantly through statistical copolymerization of NIPAm with an ionic comonomer such as acrylic acid (AAc). Indeed the higher ionic composition, the higher the LCST of the copolymer solution.[105,106] Under acidic condition (pH = 2.2), the LCST value of the P(NIPAm-*co*-AAc) copolymer is lower than that of PNIPAm homopolymer. The reason for this phenomenon is that AAc unit does not dissociate under acidic conditions, which effectively result in a nonionic polymer. Moreover, the intramolecular H-bonds formed between NIPAm units and AAc units, in which the acrylamide group acts as a proton acceptor and the carboxylic group acts as a proton donor lead to the further decrease of the LCST of the copolymer.[107]

Zhao *et al*.[108] synthesized poly(ethylene oxide)-*b*-poly(*N*-isopropyl acrylamide) (PEO-*b*-PNIPAm) block copolymers *via* RAFT polymerization, using a PEO-based macro-CTA (PEO-CTA). The thermosensitive properties of PEO-*b*-PNIPAm copolymers were investigated with PEO blocks of varying length. In fact, no difference between the copolymers having different length of PEO blocks was observed; their LCST was approximately 33 °C.

Beside the statistical copolymerization and block copolymerization, the phase transition temperature of PNIPAm also can be changed by adding different salts.[91] In the case of a 1% (w/w) solution of PNIPAm, the LCST value is 15°C in the presence of 1.0 M NaCl, while a 0.2 M concentration of $(NH_4)_2SO_4$ results in a lowering of the LCST value by 8°C , such LCST values are much lower than the LCST of PNIPAm in water. This effect is usually explained by mentioning that the presence of salt modifies the quality of the aqueous medium for PNIPAm compared with pure water due to the “salt-out” effect. On one hand, the addition of NaCl or $(NH_4)_2SO_4$ increases the H-bond between water molecules therefore decreases the ones between water and polymer chains.

Subsequently the H-bond between the PNIPAm chains becomes dominant, which results in a stronger tendency for the polymers to associate and decrease their LCST.

Another external parameter, the addition of metal ions, which is investigated recently, have dramatic impact on thermosensitive properties of PNIPAm. LaFrenerie *et al.*[109] investigated the changes in PNIPAm's LCST behavior in the presence of applied voltage using copper tape electrodes. In the absence of applied voltage, PNIPAm exhibits a reversible, hysteretic phase transition with a LCST value of 29 °C using the heating curve. In the presence of 1 V electric field, polymer aggregation and agglomeration begin at a lower temperature (~25 °C), consistent with a decrease in LCST value. Furthermore, the process is irreversible, as the polymer does not re-solubilize upon cooling below the LCST. These results support the hypothesis that electrochemical dissolution of copper in the sample contributes to the change of thermosensitive property of polymer systems.

#### *1.3.1.1.2.1.2 Poly(*N-n-*propyl acrylamide), Poly(*N-*n-propyl methacrylamide), poly(*N-*isopropyl methacrylamide)*

Other *N*-monosubstituted alkyl (meth)acrylamide monomers, *N-n*-propyl acrylamide (N*n*PAm) ($R_1$ = $R_2$ = H, $R_3$ = $C_3H_7$, Figure I.22), *N-n*-propyl methacrylamide (N*n*PMAm) ($R_1$ = $CH_3$, $R_2$ = H, $R_3$ = $C_3H_7$, Figure I.4) and *N*-isopropyl methacrylamide (NIPMAm) ($R_1$ = $CH_3$, $R_2$ = H, $R_3$ = isopropyl, Figure I.23) have been known to provide LCST-type thermosensitive polymers. They show the LCST behavior in water in the temperature range of 0 to 100 °C.

A difference in $R_1$ within the polymer backbone draws a slightly different behavior in the phase separation. The LCST value becomes higher in the order of PN*n*PAm (23°) < PN*n*PMAm (27°C) from one side and of PNIPAm (32°C) < PNIPMAm (36°C) on the other side.[110,111] This difference in the phase transition behavior is considered to arise from small differences in the hydrations of nonpolar alkyl backbone. Similar as the phase transition behavior of PNIPAm, the phase transition temperatures of PN*n*PAm and PN*n*PMAm are independent of the concentration and polymer chain length.[110,112,113] However, the phase transition temperature of PNIPMAm is significantly influenced by polymer concentration and chain length. With increase of molar mass from 3 to 11 $kg.mol^{-1}$, the LCST value of PNIPMAm dropped dramatically from 61 to 48°C.[114] For aqueous PNIPMAm solution with concentration of 1 and 2 wt.%, the reported LCST values are 43 and 48°C, respectively.[115] PNIPMAm exhibits a very broad transition in a wide range of temperature comparing to PNIPAm, with a significant retardation of 10°C for the cooling.

#### *1.3.1.1.2.1.3 Poly(N,N-diethyl acrylamide)*

Poly(*N,N*-diethyl acrylamide) (PDEAm) ($R_1$ = H, $R_2$ = $R_3$ = $C_2H_5$, Figure I.23) is another reported LCST-type thermosensitive polymer with similar structure and LCST value (33 °C) as PNIPAm leading

to the comparison between them. PNIPAm contains a secondary amide side group which is able to act as H-bond donor as well as H-bond acceptor, therefore the polymer can form intra- or interchain H-bonds. By contrast, PDEAm has a tertiary amide side group and thus only act as H-bond acceptor, making it unable to formH- bonds between polymer chains and to perform different phase behaviors.[101] Firstly, PNIPAm shows the thermal hysteresis of its phase transition due to the formed intra- or interchain H-bonds between polymer chains (Figure I.26.A), while PDEAm does not exhibit thermal hysteresis due to the absence of any intra- and interchain H-bonds at temperatures higher than LCST (Figure I.26.B).[116]

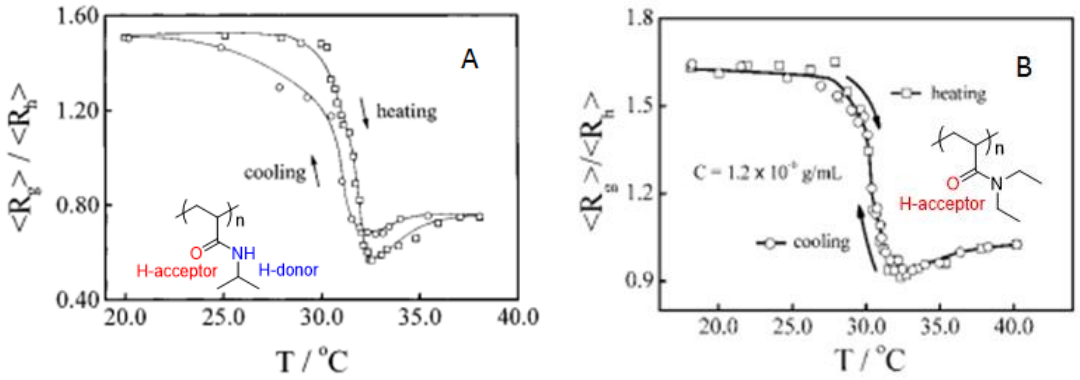


Figure I.26. (A) Temperature dependence of the ratio of radius of gyration to hydrodynamic radius ($R_g/R_h$) of the PNIPAm chains in the coil-to-globule (heating) and the globule-to-coil (cooling) transitions, respectively. (B) Temperature dependence of $R_g/R_h$ of PDEAm chains in water in one heating/cooling cycle. Reproduced from ref. 101 and ref. 116

Second, while the phase transition temperature of PNIPAm is nearly independent of polymer concentration or polymer chain length, the decrease in concentration and the increase in molar mass of PDEAm lead to the decrease in phase transition temperature of PDEAm.[117] As for PNIPAm, the addition of salts to the PDEAm solution resulted in a lowering of the LCST. Salt ions disrupt H-bond, break up the ordered water structure, and promote hydrophobic polymer-polymer interactions. In overall, like PNIPAm, the LCST of PDEAm can be modified easily by statistical copolymerization with other monomers. An increase in the hydrophobicity of the copolymer by statistical copolymerization with N-*t*BAm can rise the LCST, leading in some cases to an insoluble polymer in water. Likewise, an increase in the hydrophilicity by statistical copolymerization with Am lowers the LCST and may result in a hydrophilic polymer freely soluble at all temperatures.[105]

#### 1.3.1.1.2.2 LCST-type thermosensitive polymer based on oligo ethylene glycol (meth)acrylate

Poly[oligo(ethylene glycol) (meth)acrylate]s possessing oligo(ethylene glycol) (OEG) side chains were found to be an interesting class of poly(*N*-substituted alkyl (meth)acrylamide)s alternatives.[118–121] The thermosensitive behavior of poly[oligo(ethylene glycol) (meth)acrylate]s benefits from the contribution of its repeat unit composed of hydrophilic ethyl ethers and hydrophobic backbones. When the environmental temperature is below LCST, stable hydrated structure is formed. When the temperature goes up, the hydrated structure breaks down and the hydrophobic interactions derived from hydrophobic backbones play predominant roles, which force the water molecules initially bound to the hydrophilic ethyl ether groups to spread outwards leading to the collapse of polymer chains and finally inducing phase separation of the polymer in water. As shown in Figure I.27, the phase transition temperature of poly[oligo(ethylene glycol) methacrylate]s ($POEG_mMA$) can be tuned by varying the number of OEG repeat units (m) and the chain-end functionality (R), resulting in hydrophilicity change with similar chemical nature.[118] For instance, $POEG_2MA$ and $POEG_3MA$ have phase transition temperatures around 26 and 52°C, respectively. $POEG_mMA$s with even longer side chains can exhibit much higher LCST values in water (typically between 60°C and 90°C with m between 4 and 9).[119,120,122] The LCST values of $POEG_mMA$s with ethyl chain ends (R = $-CH_2-CH_3$) were around 22-26 °C lower in comparison with methyl chain ends (R = $CH_3$).[118] The reason why the hydrophobic ethyl chain-end induces lower LCST values than the methyl counterparts is not given by the authors.

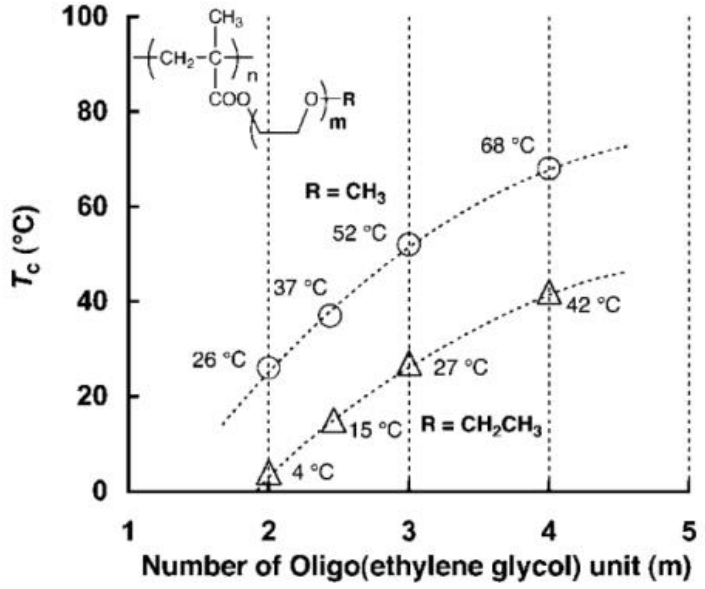


Figure I.27. Relationship between the number of OEG units (m) of $POEG_mMA$s with methyl (○) or ethyl (△) chain-end functionality and the LCST value ($T_c$). Reproduced from ref. 118

Copolymers based on 2-(2-methoxyethoxy)ethyl methacrylate and oligo(ethylene glycol) methacrylate P($MEO_2$MA-*co*-OEGMA) was found to exhibit extremely interesting solution properties in water. The phase transition temperature of the random copolymer P($MEO_2$MA-*co*-OEGMA) copolymers can be accurately tuned between 28 and 90°C by adjusting the fraction of hydrophilic OEGMA units in the copolymer chains. For example, LCST values of 32 or 37°C could be precisely obtained by using either 5 or 8 % mol of OEGMA in the initial comonomer feed. Lutz *et al.*[119] have shown that the thermal behavior of P($MEO_2$MA-*co*-OEGMA) in water is not impacted by the concentration and the chain length of copolymers. P($MEO_2$MA-*co*-OEGMA) copolymers perform an uniform thermal profile with heating/cooling cycles (no significant thermal hysteresis), probably due to the fact that OEGMA-based polymers cannot form intra- and intermolecular H-bond between polymer chains.

#### 1.3.1.1.3 UCST-type thermosensitive polymers

In contrast to LCST, the UCST-type thermosensitive polymers are dissolved in water at high temperature and undergo phase separation at low temperature. UCST-type are less studied than LCST-type thermosensitive polymers probably due to the low availability of commercial monomers leading to UCST polymers and the lack of UCST behavior stability, which is affected by pH, molar mass, ionic strength, presence of electrolytes, and polymer concentration in solution. Examples of UCST-type thermosensitive polymers are shown in Figure I.28 and they will be addressed in this section. They are classified in two categories depending on the origin of the UCST behavior, either from electrostatic interactions or either from H-bond between polymer chains.[123,124]

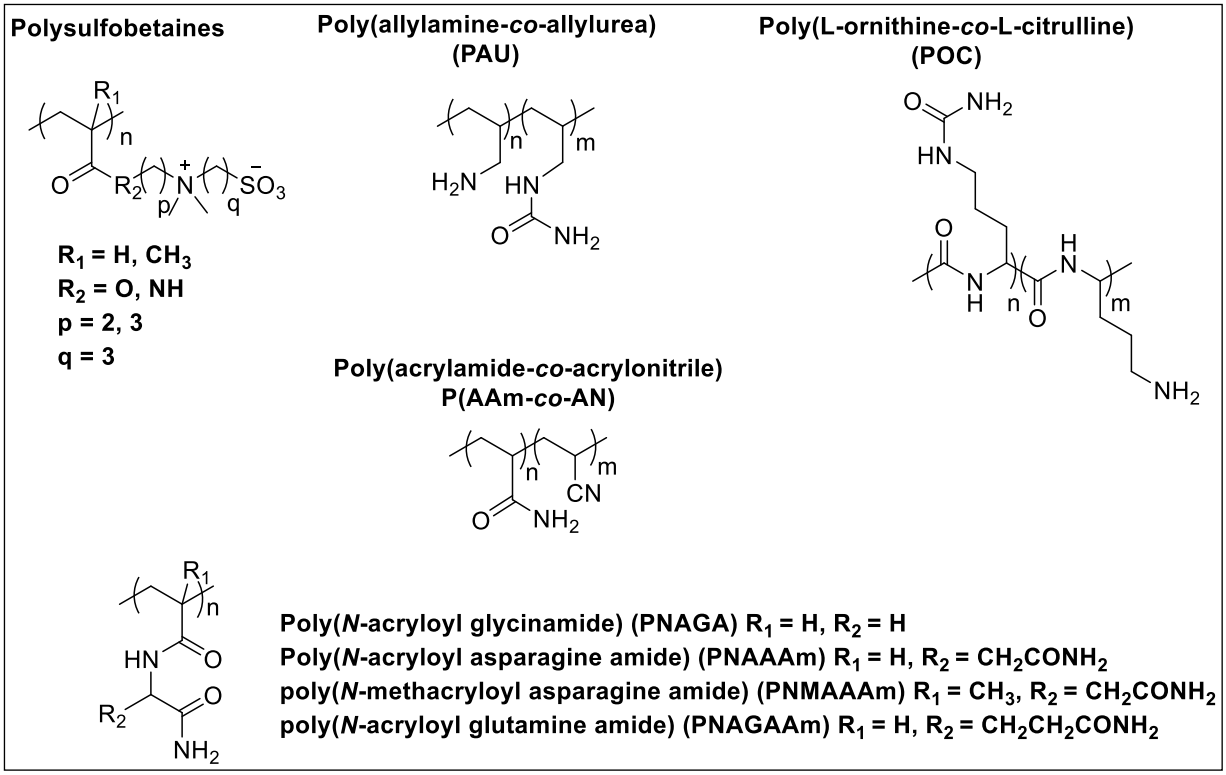


Figure I.28. Examples of UCST-type thermosensitive polymers.

#### 1.3.1.1.3.1 *Zwitterionic UCST-type thermosensitive polymers*

Among the studied zwitterionic polymers, polysulfobetaines (Figure I.28) have received growing attention.[125–127] They have both positively and negatively charged moieties located at the pendant groups of the monomer unit. At low temperature, strong interactions based on intra- and intermolecular electrostatic interactions lead to collapsed structures (Figure I.29). When temperature increases, the electrostatic interactions of zwitterionic charges are broken due to thermally enhanced molecular motions resulting in dissolution of the polymer.

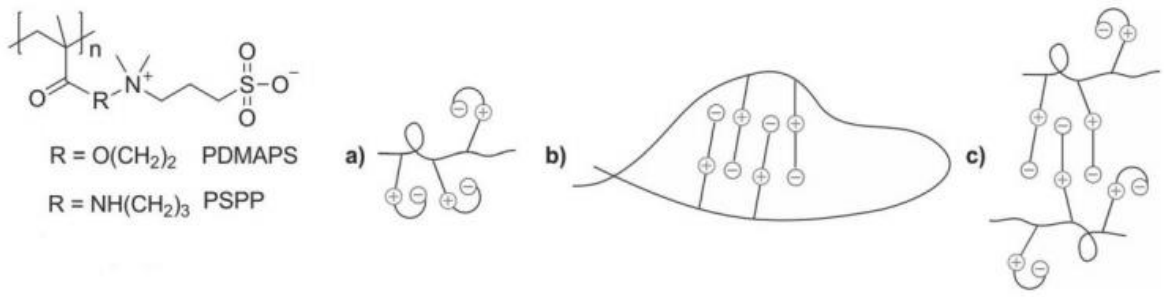


Figure I.29. Representation of intra- and intermolecular electrostatic interactions (a: intragroup; b: intrachain; c: interchain) involved in the UCST behavior of zwitterionic polymers. Reproduced from ref.[125]

Among polysulfobetaines, the poly(3-[*N*-(3-methacrylamidopropyl)-*N,N*-dimethyl]ammonio -propane sulfonate) (PSPP, Figure I.29) and the poly(3-dimethyl(methacryloyloxyethyl) ammonium propanesulfonate) (PDMAPS, Figure I.29) have received particular attention.[125] Their UCST behavior depends strongly on the molar mass of polymers. For example, PDMAPS with molar masses of 258 or 448 kg.mol$^{-1}$ present a UCST value of 26 or 43°C, respectively; while there is no cloud point observed in the case of a sample with a molar mass of 29 kg.mol$^{-1}$. Also, the thermal hysteresis phenomenon wasn't observed in the cloud point of PDMAPS upon cooling and heating.[128] As zwitterionic polymers display UCST behavior *via* electrostatic interaction in aqueous medium, their UCST value largely depends on salt concentration. In fact, adding a salt into the polymer solution enhance the solubility of zwitterionic polymers and lowers the UCST value. For example, a 0.1 wt.% solution of PDMAPS (710 kg.mol$^{-1}$) in pure water showed a cloud point upon cooling of 55°C, but the LCST value dropped to 45, 39 and 18°C with the increase of NaCl concentration from 0 to 0.05, 0.1 and 0.3 wt.%, respectively.[126] Some studies showed an increase in UCST value of zwitterionic polymers by the random incorporation of hydrophobic moieties. For example, Woodfield *et al.*[129] reported that the increase of the molar content of the hydrophobic benzyl acrylamide (BAm) within a poly(3-((3-aminopropyl)dimethylammonio)- propane-1-sulfonate) P(ADPS-*co*-BAm) random copolymer increases the UCST value from 6 to 82°C. The phase transition was also sharp, fully reversible and reproducible in low salt solutions (15 mM and 46 mM of NaCl) (Figure I.230).

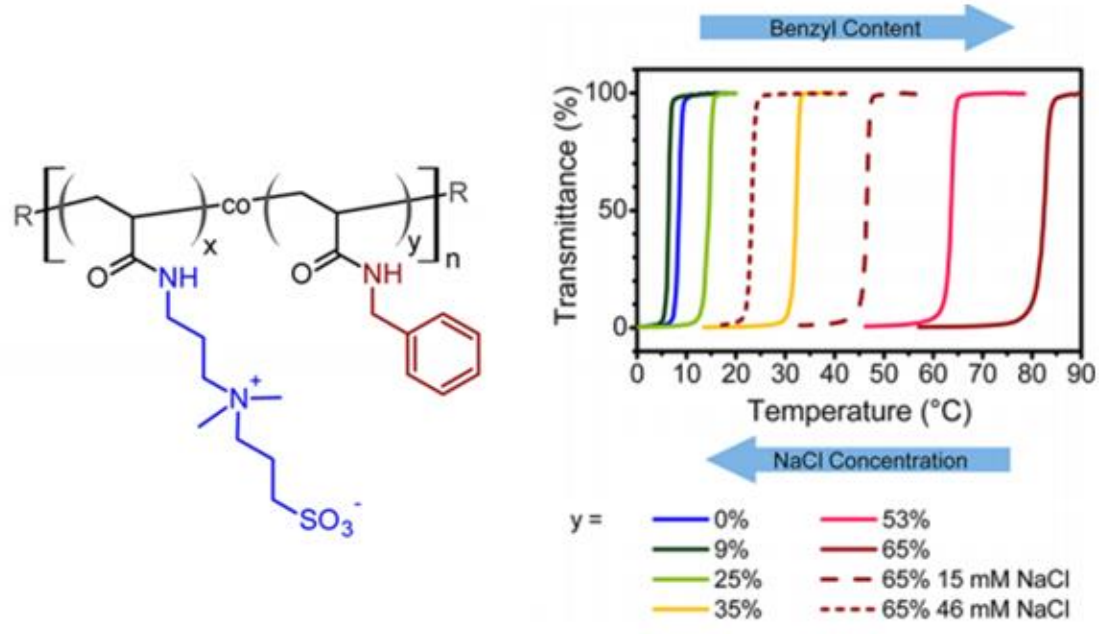


Figure I.30. Tunable UCST value of hydrophobically modified copolymers based on PADPS in aqueous solution and in NaCl solution. Reproduced from ref.[129]

An increment in UCST value of poly(sulfobetaine methacrylate)s ($R_1$ = $CH_3$, $R_2$ = O, Figure I.27) was also reported by increasing the spacer length (q, Figure I.28) separating the ammonium and the sulfonate groups.[130] For example, with p = 2, q = 3 the UCST value was reported to be 41°C and that value increased to more than 100°C for poly(sulfobetaine methacrylate) with p = 2 and q = 4.

In contrast to zwitterionic polymers, the behavior of UCST-type thermosensitive polymers based on H-bond, is less sensitive to the salt concentration in water since H-bonds are more stable against ions than the electrostatic interactions. The polymers displaying UCST behavior based on H-bond in aqueous solution are mainly based on pendant primary amide or ureido groups.

#### 1.3.1.1.3.2 H-bond based UCST-type thermosensitive polymers

##### *1.3.1.1.3.2.1 Poly(N-acryloyl glycinamide)*

Poly(*N*-acryloyl glycinamide) (PNAGA, Figure I.28) is a non-ionic polyacrylamide bearing a terminal primary amide group showing UCST behavior. Although PNAGA has been known since 1964,[131] its UCST behavior was firstly reported by Seuring and Agarwal in 2010. A 1 wt.% aqueous solution of PNAGA of 13.2 kg.mol$^{-1}$ displayed a UCST value of 22°C upon heating and 12°C upon cooling.[132] Similar as PNIPAm, the thermal hysteresis phenomenon of PNAGA is correlated to the capability to form additional intra- and interchain H-bonds upon aging in the collapsed state.[123] A UCST value of PNAGA is not affected by low polymer concentrations (Figure I.30). However, at high concentrations (greater than 2 wt.% in water), PNAGA can form reversible physical gels whatever the temperature. The gel melting temperature increases with the PNAGA concentration: from 55°C to about 81°C on changing the concentration from 5.4 to 14 wt.% (Figure I.31).[132]

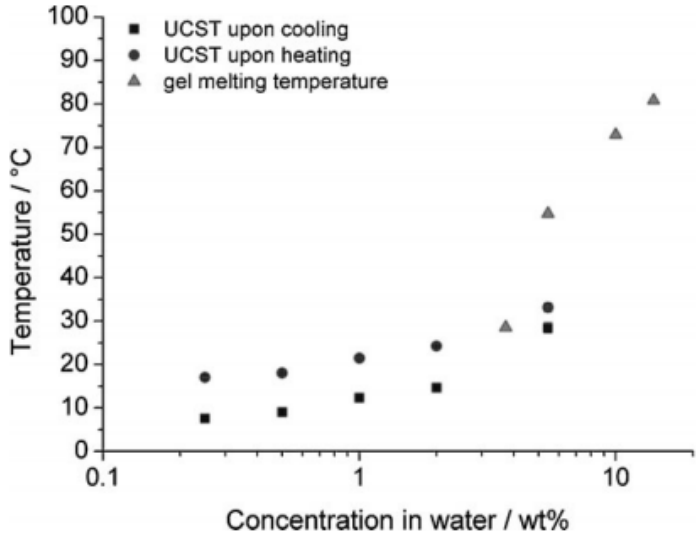

Figure I.31. UCST value upon heating and cooling, and gel melting temperature as a function of concentration for PNAGA solution in water. Reproduced from ref.[132]

In order to investigate the effect of the molar mass on the UCST behavior of PNAGA, Liu *et al*.[133] have studied the RAFT polymerization of NAGA. The UCST values of PNAGA were independent of molar mass from 15 to 35 kg.mol$^{-1}$ (Figure I.32). Below 15 kg.mol$^{-1}$, the UCST value increases due to the hydrophobic dodecyl chain end derived from the CTA. Below 8 kg.mol$^{-1}$, the UCST behavior becomes strongly dependent on molar mass. The UCST value on cooling increased steadily from 9°C at 15.7 kg.mol$^{-1}$ to 22°C at 3.7 kg.mol$^{-1}$.

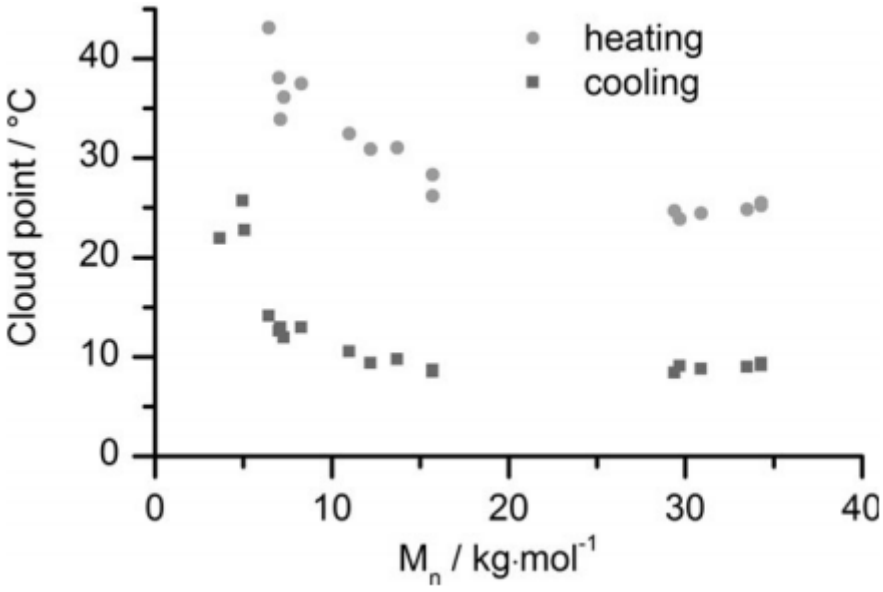


Figure I.32. Evolution of UCST value with the molar mass of PNAGA in water upon heating and cooling. Reproduced from ref.[133]

It was demonstrated that the phase transition of PNAGA could be suppressed by ionic species which can be introduced intentionally or unintentionally in a multitude of ways (Figure I.33), from impurities present in the monomer, or ionic initiators or CTAs, or hydrolysis of amide group in PNAGA caused by high polymerization temperature.

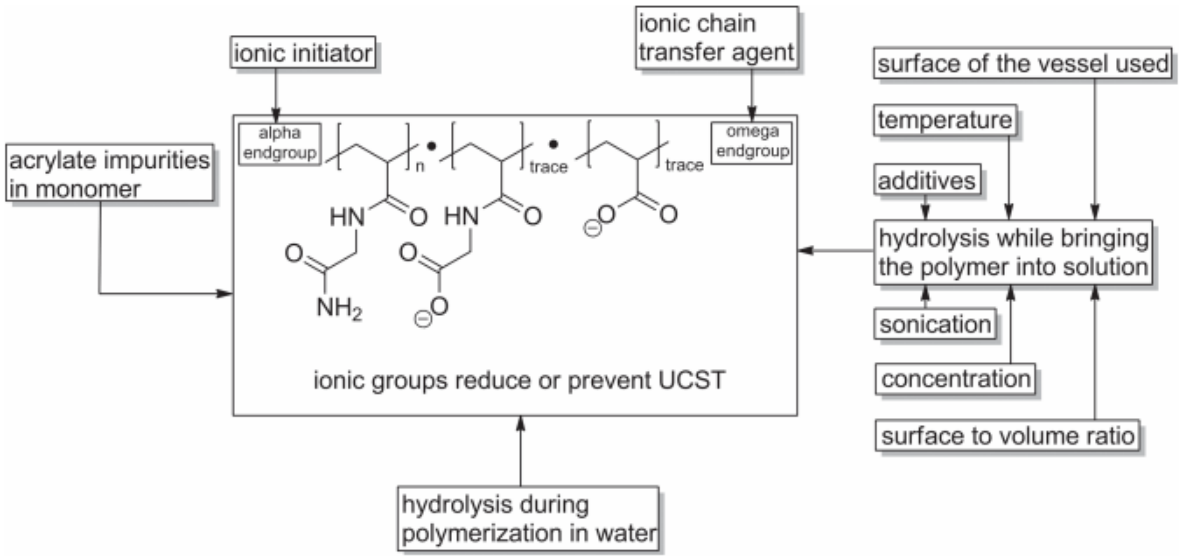


Figure I.33. Pathways of (unintentional) introduction of ionic species into PNAGA. Reproduced from ref.[90]

In particular, different PNAGAs were synthesized by the RAFT polymerization in presence of non-ionic radical initiators and two different CTAs, one with non-ionic and one with ionic chain end.[133] In pure water, the nonionic PNAGA with dodecyl omega end group showed a cloud point on cooling of 17.4°C. For the ionic PNAGA with a sulfonate omega end group, no cloud point could be detected in pure water. Such results confirmed that the ionic chain end prevents phase separation of resulting PNAGA in pure water. However, the UCST suppressing effect can be counteracted by the addition of electrolytes as NaCl or $Na_2SO_4$ (Figure I.34).

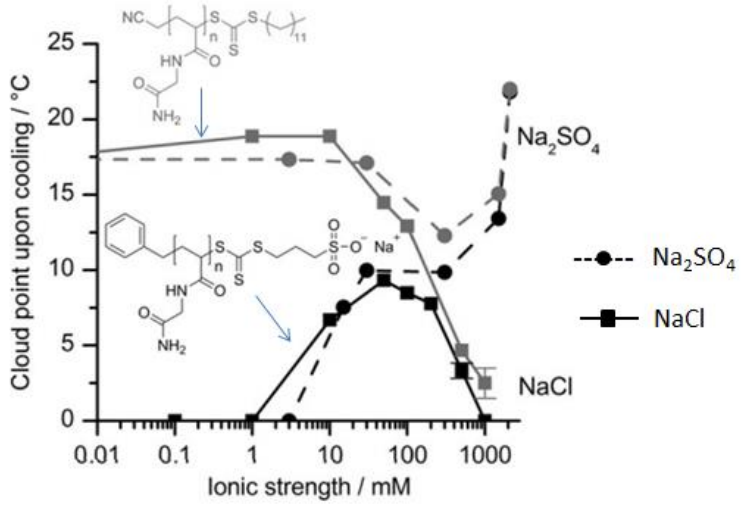


Figure I.34. Cloud point upon cooling of 0.2 wt.% aqueous solutions of PNAGA with different chain ends as a function of ionic strength for different types of salt. Reproduced from ref.[133]

The statistical copolymerization of NAGA with hydrophobic monomer such as acrylonitrile (AN)[134], butyl acrylate (BA), styrene (St)[135] provided UCST copolymers showing highly stable and sharp phase transitions without any significant thermal hysteresis between heating and cooling processes. In addition, the cloud points were independent on the copolymer concentration in water and can be tuned easily by changing the ratio of the two comonomers. The Seuring's study showed that the incorporation of hydrophobic comonomers within PNAGA increases the UCST value in a controlled manner.[135] For example, the increment of BA content in P(NAGA-*co*-BA) copolymer from 10 to 20 mol.% results in the rise of the UCST value from 8.2°C to 57°C upon cooling. However, the phase transition temperature of P(NAGA-*co*-BA) was found to decrease after each heating/cooling cycle due to increased hydrophilicity resulting from acrylic acid groups formed from the hydrolysis of BA units above 50°C. By contrast, the UCST of P(NAGA-*co*-St) was found to be stable over nine consecutive heating/cooling cycles, because the styrene does not undergo the hydrolysis reaction.

The statistical copolymerization of NAGA with hydrophilic comonomers such as methacrylic acid (MAAc) leads to the increase of phase transition temperature. For example, copolymerization of NAGA with MAAc was performed to tune the UCST value of copolymers near to human body temperature. The copolymer P(NAGA-*co*-MAAc) showed UCST values between 17 to 37°C with MAAc molar fractions ranging from 30 mol.% to 60 mol.%. However, the UCST value of P(NAGA-*co*-MAAc) is dependent on pH, ionic strength and polymer concentration, thus limiting its biomedical applicability.[136]

Further studies showed that derivatives of PNAGA (Figure I.28) can exhibit UCST behavior in water. Nagaoka and coworkers first synthesized poly(*N*-acryloyl asparagine amide) (PNAAAm), poly(*N*-methacryloyl asparagine amide) (PNMAAAm) and poly(*N*-acryloyl glutamine amide) (PNAGAAm) by free radical polymerization and examined their phase transitions at a concentration of 0.2 w/v.% in water.[137] PNAAAm with molar mass of 16 kg.mol$^{-1}$ showed UCST values of 22 and 25°C in pure water and in 20 × 10$^{-3}$M Tris-HCl buffer solution, respectively. The introduction of a methyl group to the polymer backbone led to a decrease of the UCST-type cloud point to 13°C in Tris-HCl buffer for PNMAAAm (molar mass of 17 kg.mol$^{-1}$) and the appearance of dual phase transition temperatures with UCST of 15°C and LCST of 30°C in water for PNAGAAm. It was also reported that the cloud points of both PNAAAm and PNMAAAm are not dependent on salt concentration. This behavior is probably due to two reasons.[123] First, comparing to PNAGA, PNAAAm, and PNMAAAm may exhibit stronger interpolymer H-bond due to the second primary amide group. It was theoretically believed that the increase of interpolymer H-bond can reduce the negative impact of ionic groups. Second, free-radical polymerization used by Nagaoka *et al.* leads to a broad high molar

mass distribution polymers containing a high molar mass fraction polymers which are less affected by the ionic species.

#### *1.3.1.1.3.2.2 Statistical copolymers based on acrylamide and acrylonitrile*

Agarwal's group showed that statistical copolymers based on two commercially available monomers, acrylamide (Am) and acrylonitrile (AN) (Figure I.28), can exhibit UCST behavior in water and phosphate buffer saline (PBS) solution.[135] The phase transition temperature of P(Am-*co*-AN) can easily be tuned by simply varying the comonomer feed ratio: it increases with increasing the acrylonitrile content. Asadujjaman *et al*.[138] pointed out that P(Am-*co*-AN) with increasing AN molar fraction from 0.086 to 0.221 show UCST behavior with cloud point ranging from 5.5 to 56.5°C at 1 $mg.mL^{-1}$ concentration in water. By increasing amount of acrylonitrile, the hydrophobicity of copolymer increases, interfering with the H- bond between water molecules and copolymer chains disrupting the regular hydration shell around the temperature sensitive polymer chains. In this case, the H-bond between polymer chains can be enhanced. Thus, higher temperatures are needed to reduce these polymer-polymer interactions, resulted in higher UCST value. Moreover, the thermal hysteresis phenomenon of P(Am-*co*-AN) is very small, with only 1-2°C in most cases, and UCST value remains constant over several repeated cycles due to the hydrolytic stability of the repeat units in water. Beside adjusting AN content in the copolymer, the phase transition temperature can be controlled by varying the polymer chain length of the copolymer and salt concentrations. The effect of the copolymer chain length on the UCST value of P(Am-*co*-AN) was studied at a fixed AN molar fraction (0.144) using a copolymer concentration 5 $mg.mL^{-1}$ in water. The phase transition temperature increased around 10°C by increasing molar mass from 11.4 to 28.3 $kg.mol^{-1}$. The phase transition of P(Am-*co*-AN) solution also depends on the nature and the concentration of electrolytes (Figure I.35). In pure water, the phase transition temperature of copolymer is 30°C and then decreased to 20°C and 12°C by the addition of 300 mM NaCl and 300 mM NaSCN, respectively. The decrease of the phase transition temperature by addition of NaSCN and NaCl can occur due to polarization effects, surface tension, as well as direct ion binding. The $Na_2SO_4$ salt showed the most interesting effect on the phase transition temperature of P(Am-*co*-AN). The phase transition temperature of the copolymer increased to 56 °C by addition of 300 mM $Na_2SO_4$ to the solution. This effect was expected as when more ions are present in the solution they interfere with the H-bond between water molecules and copolymer chains disrupting the regular hydration shell around the temperature sensitive polymer chains. Therefore, interchain and intrachain hydrophobic effects

among the polymer chains are favored, which increases the phase transition temperature of the P(Am-*co*-AN).

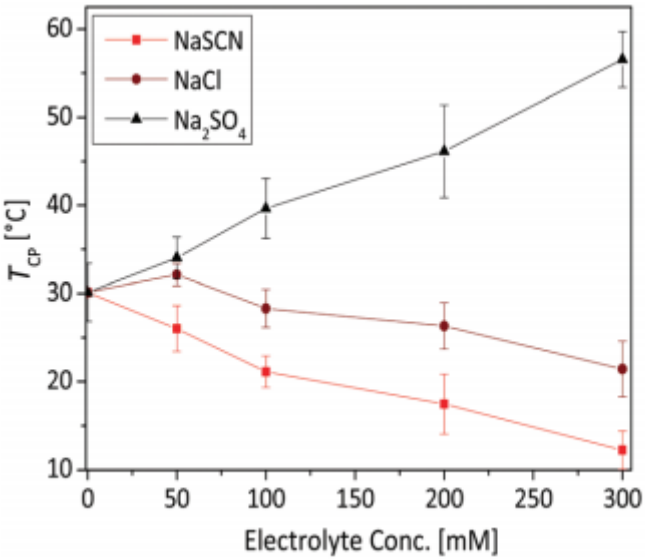


Figure I.35. The phase transition temperature of P(Am-*co*-AN) as a function of different electrolytes concentration. The data were taken during the cooling of the measurements. Reproduced from ref.[138]

Käfer *et al.*[139] reported the synthesis of a diblock copolymer based on a P(Am-*co*-AN) block and poly(ethylene glycol) (PEG) (PEG-*b*-P(Am-*co*-AN)), with double thermosensitive behavior (LCST and UCST behavior). The presence of the PEG block led to a drastic change in the thermosensitive behavior of P(Am-*co*-AN) from UCST type to multiphase-type (LCST at low temperature and UCST at higher temperature). The reason of this phenomenon is probably due to the temperature dependent close-loop solubility behavior of poly(ethylene glycol) in water.[140] For a particular molar mass (0.4-5 $kg.mol^{-1}$), PEG can display both LCST and UCST phase separations at very high temperature (80-200°C). The PEG-*b*-P(Am-*co*-AN) block copolymer with 9 mol.% of AN shows both a LCST value at ~30°C and a UCST value at about 50°C in water. The phase transition of the PEG-*b*-P(Am-*co*-AN) diblock copolymer was found to be dependent on the PEG block length. Diblock copolymer with PEG block of 2 $kg.mol^{-1}$ (12% mol AN) shows a LCST and UCST of 50 and 68°C, respectively. The increase of PEG block length to 6 $kg.mol^{-1}$ results in a solube diblock copolymer. In addition, block copolymer based on P(Am-*co*-AN) and hydrophobic polystyrene (PSt) or hydrophilic poly(*N,N*-dimethyl acrylamide) (PDMAm) or with LCST-type thermosensitive PDEAm has been also reported with the objective to obtain tunable UCST.[141] A $P(Am_{231}\text{-}co\text{-}AN_{78})$ in water showed a UCST value of 25°C meanwhile the UCST value for $P(Am_{231}\text{-}co\text{-}AN_{78})\text{-}b\text{-}PS_{42}$ increased to 50°C with the same polymer concentration (1 wt%). It is noticeable that as compared to $P(Am_{231}\text{-}co\text{-}AN_{78})\text{-}b\text{-}PS_{42}$, the UCST value of $P(Am_{231}\text{-}co\text{-}AN_{78})\text{-}b\text{-}PDMAm_{319}$ appears at lower temperature of 20 °C, understandably due to the

influence of the water-soluble PDMAm block. The diblock copolymer of P($Am_{231}$-*co*-$AN_{78}$)-*b*-$PDEAm_{319}$ displayed both UCST and LCST behavior at 22 and 41 °C, respectively.

#### *1.3.1.1.3.2.3 Statistical copolymers based on acrylic acid and acrylonitrile*

Poly(acrylic acid) (PAAc) carries both H-donor (-OH) and H-acceptor (-CO) in its repeating unit, able to form strong intra- and interchain polymer-polymer H bonds. Due to the ionization of -COOH groups and the ion-dipole interactions with water molecules, PAAc chains can be easily solvated in aqueous solutions, and the hypothetic UCST is far below 0°C. By introducing a hydrophobic comonomer AN into PAAc, the UCST value of PAAc can be driven into the ambient temperature range.[142]

The copolymers with higher AN content exhibit lower water solubility and higher UCST cloud points. A P(AAc-*co*-AN) containing 2.0 mol.% of AN content is freely soluble in water at pH 2.0. When the AN content in the copolymer is raised above 4.5 mol.%, it becomes UCST-type thermosensitive. The UCST cloud point changes from 7.2 to 37.9°C when the AN content rises from 4.5 to 22 mol %.

The UCST of the copolymer P(AAc-*co*-AN) depends on the polymer concentration. At pH 2.0, UCST value of P(AAc-co-AN) with a AN molar content of 22.0 mol.% increases from 29.7 to 40.7°C when the copolymer concentration increases from 0.1 to 1.0 wt.% and remains almost unchanged at about 41.0°C when the polymer concentration reaches 2.0 wt.%.

The UCST of the hydrophobically modified PAAc is also related to the pH of the solution. A 0.5 wt.% solution of P(AAc-*co*-AN) with a AN molar content of 22.0 mol.% in deionized water has a pH at 3.5 and shows no signs of phase separation in the measured temperature range. However, on gradual lowering of its pH by adding HCl, the polymer solution shows a UCST behavior. The UCST of P(AAc-*co*-AN) with a AN molar content of 22.0 mol.% increases from 17.2 to 37.9°C with the pH lowered from 2.7 to 2.0 and reaches a plateau at pH ≤ 2.0. The UCST becomes a constant at pH ≤ 2.0 upon the complete protonation of all carboxylate groups.

Like many other thermosensitive polymers, the transmittance curves of P(AAc-*co*-AN) show a thermal hysteresis. The width of the hysteresis does not change significantly with polymer composition or concentration but becomes larger with increasing pH. For the 0.5 wt.% aqueous solutions of P(AAc-*co*-AN) with a AN molar content of 22.0 mol.%, the gap between the two cloud points measured during cooling and heating changed from 6.9 to 2.6°C when the pH was lowered from 2.7 to 2.0 and remained constant thereafter. For P(AAc-co-AN), Zhao et *al.*[142] speculated that the main reason for the thermal hysteresis is due to the desynchrony of inter- and intramicellar H-bond during the cooling process(Figure I.35). When the temperature is lowered close to the UCST, intramicellar H-bonds can form easily, whereas the formation of intermicellar H-bonds is limited by diffusion. This causes a metastate of collapsed micelles, as shown in Figure I.36, and delayed

macroscopic phase separation of the polymer solution. In contrast, during the heating process, both intra- and intermicellar H-bonds are disassociated at the same temperature, since there is no difference in the disassociation kinetics of the two types of H-bonds. With increasing pH, the stronger electrostatic repulsion between micelles provides a higher energy barrier for the micellar aggregation, leading to a broader hysteresis.

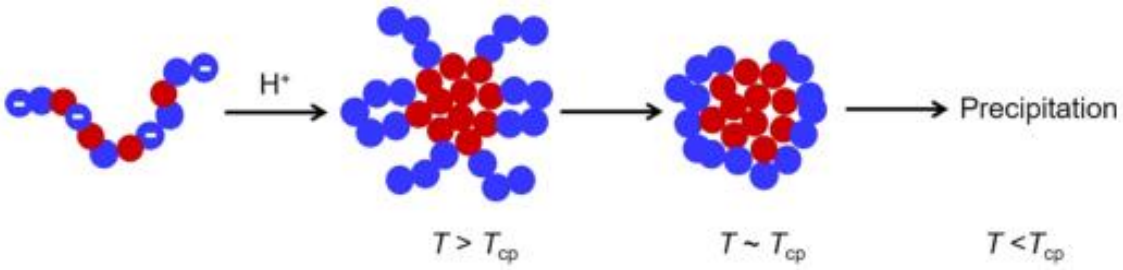


Figure I.36. Schematic illustration of the self-assembled structure of P(AAc-*co*-AN) during the cooling process. The negative charges come from the ionized AAc groups and can be neutralized by the addition of an acid. Blue and red spheres represent the AAc and AN monomers, respectively, in the polymer chain. Molecular unimers become protonated and form micelles that shrink close to Tcp (UCST) and eventually phase-separate and precipitate below UCST. Reproduced from ref.[142]

The impact of the salt has also been shown on P(AAc-*co*-AN) with a AN molar content of 22.0 mol.%. When the salt concentration reached 0.15 M in the P(AAc-*co*-AN) with a AN molar content of 22.0 mol.%, at pH 2.0 (adjusted by the addition of HCl), the UCST increased by 5.2°C with $Na_2SO_4$ and 2.2°C with NaCl and decreased by 11.6°C with NaSCN. It is interesting to note that NaSCN has a salting-in effect for the polymer in the protonated state here at pH 2 whereas the same salt shows a salting-out effect for the deprotonated polymer. This behavior is different from the effects of added salts for nonionizable copolymers as in the case of P(Am-*co*-AN).

#### *1.3.1.1.3.2.4Polymer based on ureido group*

In 2011, Shimada *et al.*[143] reported a series of ureido-derivatized polymers able to form inter- and/or intramolecularH- bond among ureido groups and their UCST behavior under physiological buffer conditions (Figure I.37). The PAU copolymers demonstrate UCST phase transition with high stability in solution and the UCST value was found to increase linearly with the increase of the molar ratio of ureido groups in the feed (from 80 to 95 mol.%), and to be tunable between 8 to 65°C under physiological salt and pH conditions. The UCST-type thermosensitive behavior of poly((L-ornithine)-*co*-(L-citrulline)) (POC) copolymers containing ureido groups also demonstrated UCST behavior under physiological conditions, which was dependent on both ureido content and molar mass of copolymer. In fact, with 85 mol.% ureido in the copolymer, the increase of molar mass from 5 kg.mol$^{-}$

[1] to 15 and 150 kg.mol$^{-1}$ results in the rise of UCST from 8 to 25 and 30°C, respectively. The thermal hysteresis phenomenon was not observed for UCST phase transition of all copolymers containing ureido groups.

Besides ureido content and molar mass, the UCST of PAU is also dependent on pH. In the case of PAU with a molar mass of 15 kg.mol$^{-1}$ and 85 mol.% ureido content, UCST value was unchanged in the pH range from 5.5 to 8.5 and increased at pH above 9.5. Since the pKa of the polyallylamine homopolymer is near 9.7, deprotonation of the amino groups around pH 9.5 presumably resulted in the increase of UCST above pH 9.5. The deprotonation reduces the electrostatic repulsions among the charged amino groups and reduces the osmotic pressure, resulting in an increase of UCST by facilitating inter- and/or intramolecular interactions of PAU polymers. The pH dependency decreased with increasing ureido content, and no pH dependency was observed for a PAU with a molar mass of 15 kg.mol$^{-1}$ and 94 mol.% of ureido content. These results confirmed a major contribution of ureido groups to generate UCST behavior and the unsubstituted amino groups to provide the pH dependency.

Shimada *et al*.[144] developed hydrophobically modified PAUs by acylation of amino groups of polyallylamine block in order to rationally obtain UCST-ureido polymers with desired UCST values. UCST value of modified PAUs can be regulated in a wide temperature ranging from about 20 to 80°C or even higher by 20 mol.% acylation with acetyl, propionyl, isobutanoyl or pivaloyl groups. This study showed the considerable impact of hydrophobic groups on UCST phase separation of polymers containing ureido groups. The acetylation of the PAU copolymers have been done through acetyl (AC-PU), propionyl (PR-PU), isobutanoyl (IS-PU), and pivaloyl (PI-PU) groups (Figure I.37). While pH strongly affected UCST of unsubstituted AM-PU copolymer in the pH range from 6.5 to 10.5, no significant change in UCST of acylated PR-PU copolymer was observed in the same pH range, indicating that thermal responses of PR-PU were not influenced by pH condition.

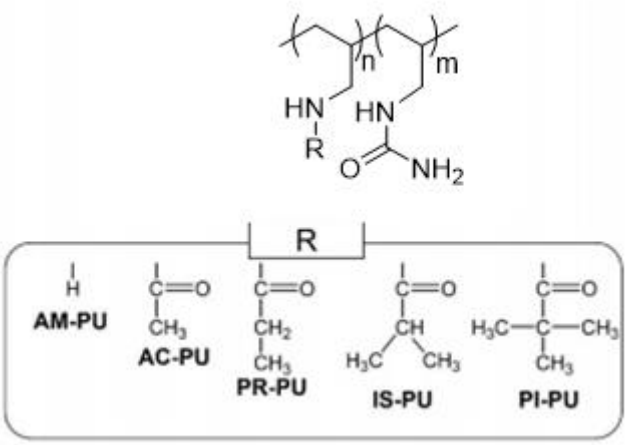


FigureI.I.37. Structural formula of hydrophobically modified poly(allylamine-*co*-allylurea)s.

After reviewing on thermosensitive behaviors and different parameters that can impact the phase transition temperatures of several LCST- and UCST-type thermosensitive polymers, the strategies to target the LCST- and UCST-thermosensitive nanogels based on previously described polymers, and their thermal properties will be discussed.

#### 1.3.1.2 Thermosensitive nanogels

Recently, thermosensitive nanogels, particularly LCST-type, are mainly prepared via polymerization-induced thermal self-assembly (PITSA) in aqueous dispersion.[66,71,72,145–149] PITSA syntheses using RAFT polymerization have become a powerful method to prepare thermosensitive nanogels.[150–154] RAFT-PITSA in aqueous dispersion employs an hydrophilic macro-CTA to chain extend a thermosensitive polymer block in order to generate amphiphilic diblock copolymers that self-assemble into nanodomains; the *in situ* crosslinking of the diblock copolymers in presence of crosslinker results in the formation of nanogel (Figure I.38).

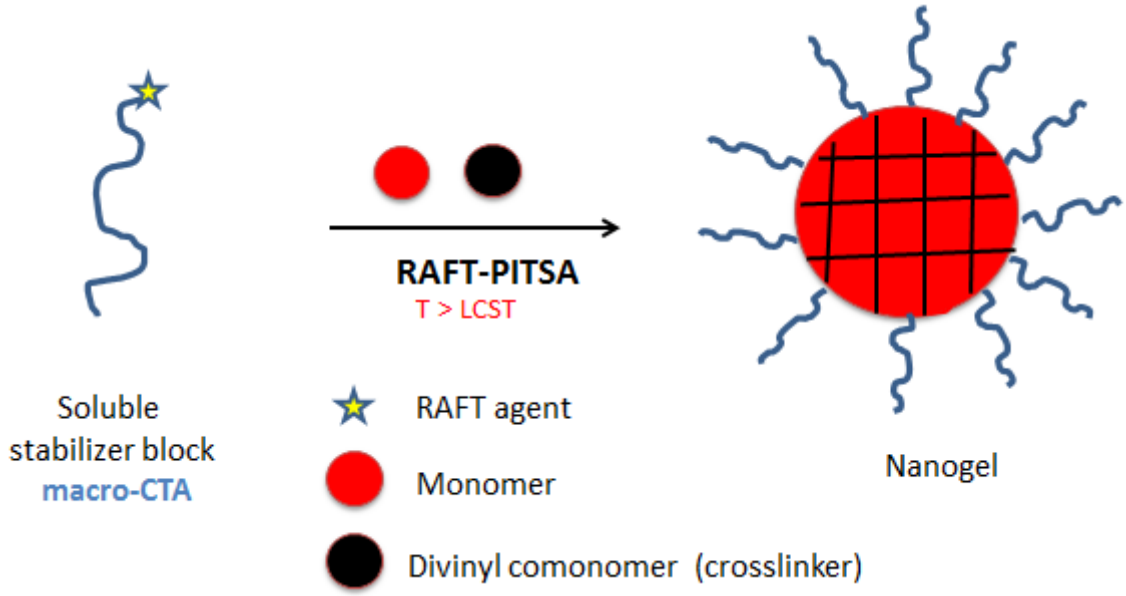


Figure I.38. Preparation of nanogel by RAFT-PITSA process.

The synthesis of thermosensitive nanogels takes advantage of the precipitation of the thermosensitive polymer from the reaction medium during polymerization at a temperature higher (LCST-type thermosensitive nanogel) or lower (UCST-type thermosensitive nanogel) than phase transition temperature.

##### 1.3.1.2.1 LCST-type thermosensitive nanogels

The area of thermosensitive nanogels is largely dominated by LCST systems.[155–157] The first report of RAFT-PITSA in aqueous dispersion was published by An et al.[158] in 2007 to synthesize LCST-type

thermosensitive nanogel based on PDMAm-*b*-PNIPAm diblock copolymers (Figure I.39). The polymerization was initiated by microwave irradiation at 70°C and the presence of MBA as crosslinker during RAFT-PITSA allowed the elaboration of well-defined nanogels. PDMAm macro-CTAs with different structural characteristics were examined: Macro-CTA1 with hydrophobic dodecyl tails and the fully hydrophilic Macro-CTA2. In both cases, the size of the nanogels decreases with increasing concentration of macro-CTA. The authors also demonstrated a strong dependence of the nanoparticles size with the molar mass of the macro-CTA. As the molar mass of Macro-CTA1 decreased from 8.3 to 5.9 kg.mol$^{-1}$, $D_h$ of the nanogels increased from 129 to 168 nm for a fixed NIPAm concentration of 0.15 M and for an initial molar ratio of $[NIPAm]_0/[Macro\text{-}CTA]_0/[V\text{-}50]_0$ of 333/1/2 with $[MBA]_0$ = 3.0 mM. Further decreasing the molar mass to 4.3 kg.mol$^{-1}$ resulted in the formation of agglomerates. A similar trend was also observed for Macro-CTA2. Nanogels consisting of crosslinked PDMAm-PNIPAm chains were used as particle seeds for further polymerization with NIPAm. When nanoparticles prepared with Macro-CTA2 (66 nm) were used as the "seeds", reaction with different amounts of NIPAm (31 wt.% and 57 wt.% relative to NIPAm in the seed nanoparticle) in the presence of 2 mol % MBA gave nanoparticles with increased diameter (77 and 84 nm, respectively). Therefore, original core-shell nanogel structures with a phase transition temperature of 32-33°C similar to that of the original seed nanoparticles were obtained.

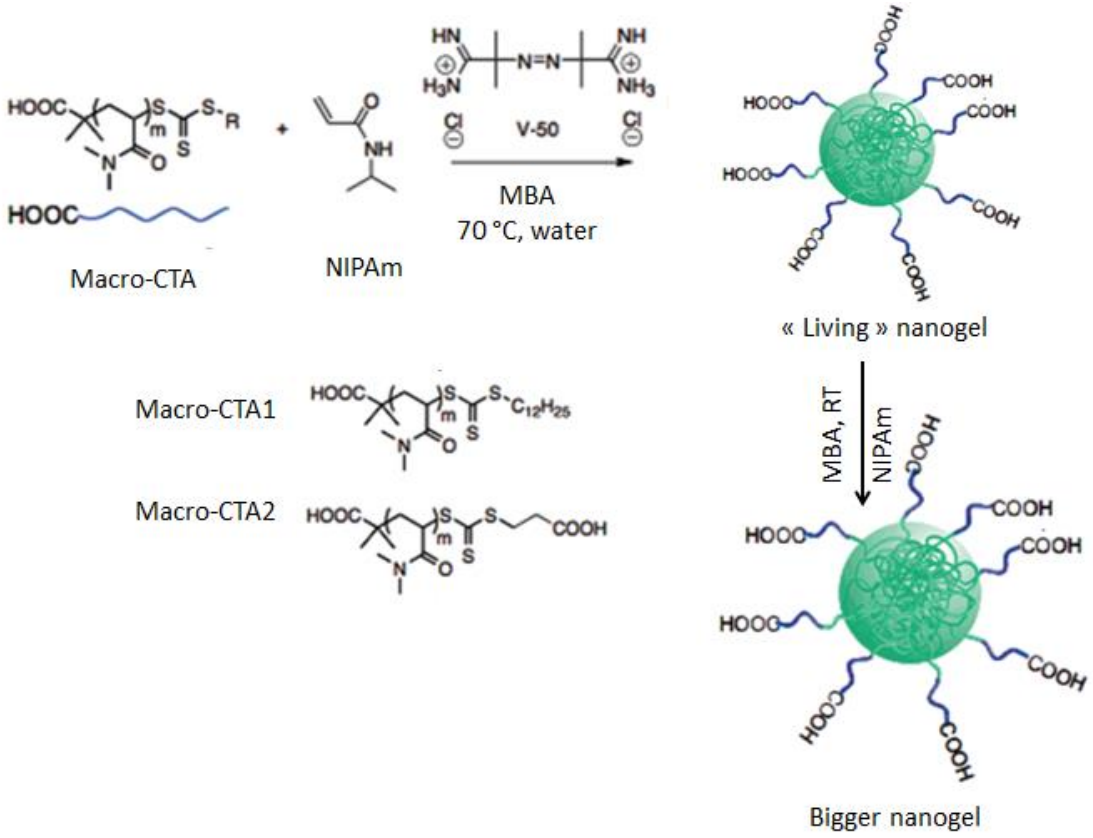

Figure I.39. Synthesis of LCST-type thermosensitive nanogel based on PDMAm-*b*-P(NIPAm-*co*-MBA) diblock copolymers *via* RAFT-PITSA at 70°C in water. Reproduced from ref. 158

LCST-type thermosensitive nanogels were also prepared by Rieger *et al*.[159] In this case, double-hydrophilic PEO-*b*-PDMAm macro-CTAs were chain-extended with a mixture of DEAm and MBA *via* RAFT-PITSA aqueous dispersion at 70 °C (Figure I.40). When DEAm was copolymerized with 3 mol.% of MBA, nanogel particles with a $D_h$ of 68 nm at 15°C were obtained. Upon heating to 50 °C, the $D_h$ of the particles shrank to 47 nm. This behavior was reversible and reproducible. The LCST reported for PDEAm nanogels is about 30°C after heating or cooling, and no hysteresis could be observed. The authors demonstrated that a critical minimum length of the PDMAm segment was necessary to obtain nanometric particles, whose size decreased with increasing length of this soluble polymer block. In fact, when macro-CTA composed of a slightly shorter PDMAm segment of 1.2 kg.mol$^{-1}$ is employed, heterogeneous dispersions were obtained containing aggregates. At 15 °C, with increasing length of the stabilizing PDMAm block from 5 to 10.3 kg.mol$^{-1}$, $D_h$ of the nanogels decreased from 110 to 63 nm. The polydispersity in size (pdi) was not affected significantly. The influence of the initial monomer and crosslinker concentrations in the reaction medium was also studied. All RAFT-PITSA were performed with the PEO-*b*-PDMAm macro-CTA with a $\overline{M_{n,PDMAm}}$ of 6.8 kg.mol$^{-1}$ at constant initial $[DEAm+MBA]_0/[Macro\text{-}CTA]_0$ molar ratio of 200 and in the presence of 3 mol.% MBA. The $D_h$ of the particles at 15°C increases from 68 to 91nm and similar trend for the pdi (from 0.13 to 0.17) with increasing monomer and macro-CTA concentrations from 3 to 12 wt%.

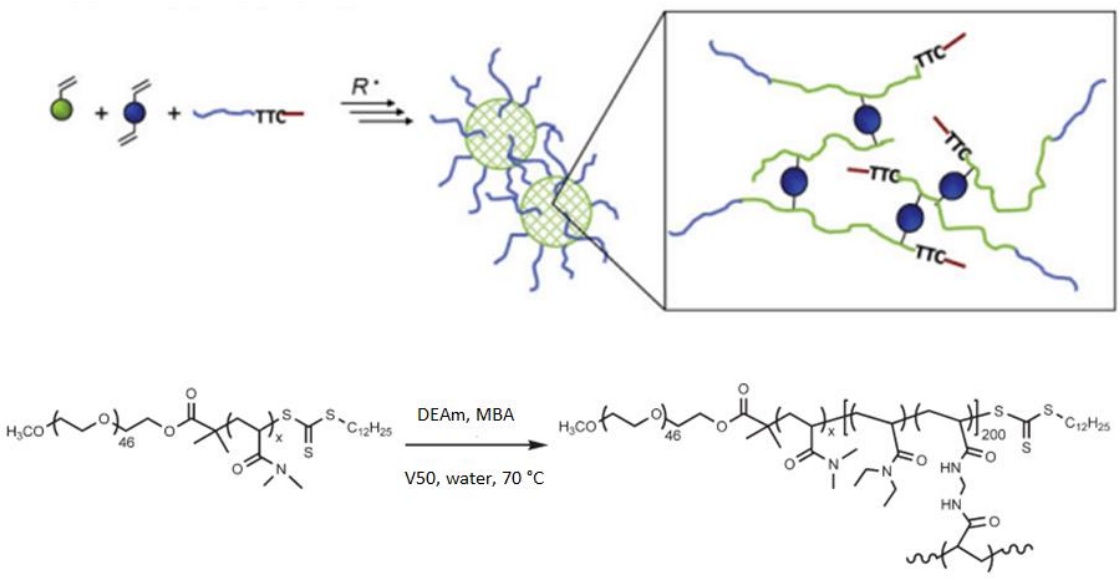


Figure I.40. Synthesis of LCST-type thermosensitive nanogels by RAFT-PITSA of DEAm in water and at 70°C in presence of PEO-*b*-PDMAm macro-CTA containing trithiocarbonate group (TTC).Reproduced from ref.[159]

Although poly(2-methoxyethyl acrylate) (PMEA) is not water-soluble, copolymers containing MEA units with more hydrophilic units are water-soluble and can exhibit thermosensitive properties depending on their relative composition.[160,161]

Shen *et* al.[162] reported on a novel type of core-shell LCST-type thermosensitive nanogel consisting of linear poly(ethylene glycol) (linear-PEG) and/or their nonlinear analogues such as polymers derived from oligo(ethylene glycol) (meth)acrylates (grafted-PEGs) via RAFT-PITSA of $MEO_2MA$ or statistical copolymerization of $MEO_2MA$ with PEGA (Figure I.41). The impact of architecture of different macro-CTAs of linear-PEG (PEG-TTC) and grafted-PEG ($POEGMA_x$-TTC and $POEGMA_x$-DT, where x represents the $\overline{DP_{n,POEGMA}}$, TTC stands for trithiocarbonate and DT stands for dithioester) was studied on physico-chemical properties of nanogels. Nanogels prepared using linear PEG were obtained with a single size distribution and $D_h$ in the range of 50 to 80 nm and those obtained using grafted PEG are with tunable size. The molar masses of grafted PEGs can be easily controlled by the number-average degree of polymerization of OEGMA. With increasing $\overline{DP_{n,POEGMA}}$, the $D_h$ of nanogels becomes smaller. However, no well-defined nanogels could be obtained using $POEGMA_{10}$-TTC and $POEGMA_{10}$-DT with a $\overline{DP_{n,POEGMA}}$ of 10. The size of nanogels can also be tuned by varying the molar ratio of macro-CTA/monomer. For example, the nanogel size is tuned from 52 to 82 nm when the molar ratio of $POEGMA_{32}$-DT/$MEO_2MA$ is increased from 1/150 to 1/250. Increasing the solid content leads to an increase in the nanogel size, but further increase in concentration results in the formation of macrogels. RAFT-PITSA of statistical copolymerization of $MEO_2MA$ with PEGA with adjustable molar ratios leads to nanogels with tunable thermo-sensitivity. The molar ratio of the monomers also affects the size of nanogels. When the incorporation of PEGA is high, no nanogels are formed possibly due to the significantly increased hydrophilicity of the resulting polymers which could not collapse to form nanogels.

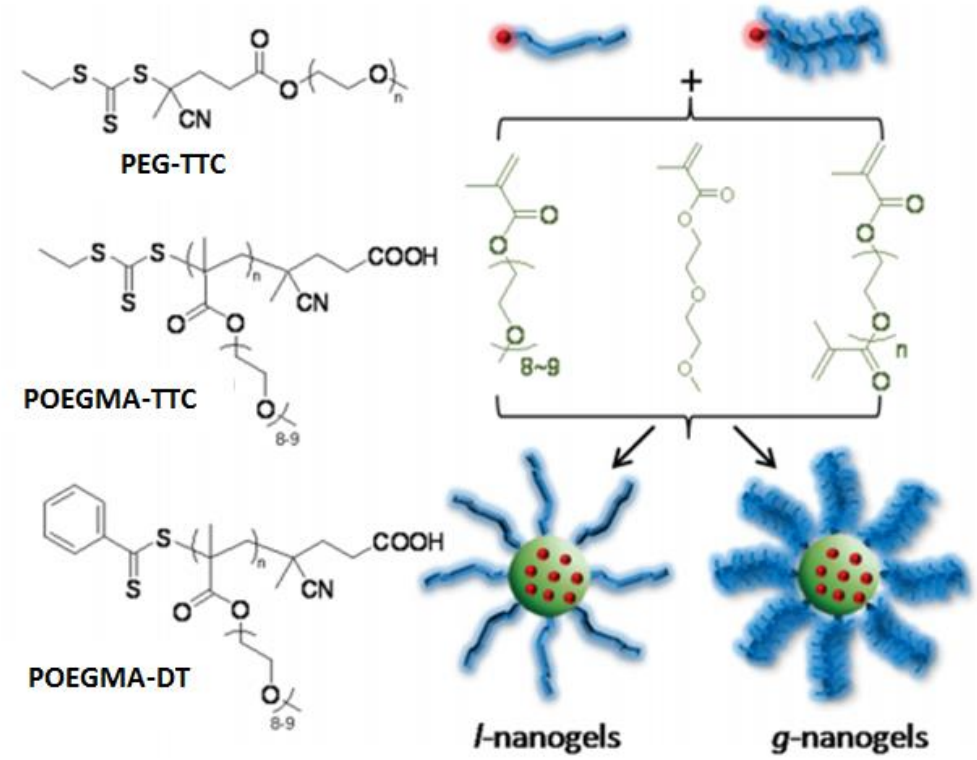


Figure I.41. Elaboration of LCST-type thermosensitive nanogels consisting of linear poly(ethylene glycol) (linear-PEG) and/or their nonlinear analogues such as polymers derived from oligo(ethylene glycol) (meth)acrylates (grafted-PEGs) via RAFT-PITSA of statistical copolymerization of $MEO_2MA$ with PEGA in aqueous dispersion at 70 °C . Reproduced from ref.[162]

The double thermosensitive nanogels with multi-domains were prepared in water-ethanol mixtures by RAFT-PITSA by Li and co-workers.[163] These nanogels consisted of a crosslinked thermosensitive P(NIPAm-*co*-MBA) core with a LCST of 32°C, a hydrophilic PDMAm midblock, and a thermosensitive $POEG_3MA$ shell with a LCST of 15°C. The unique location of these two thermosensitive blocks with different phase transition temperatures in the $POEG_3MA$-*b*-PDMAm-*b*-P(NIPAm-*co*-MBA) nanogels was expected to facilitate thermo-induced gelation and provided mechanical enhancement in comparison with PNIPAm-*b*-PDMAm-*b*–P($OEG_3MA$-*co*-MBA) nanogel and $POEG_3MA$-*b*-PDMAm-*b*-PNIPAm triblock polymer. By a simple inverted vial test, the thermo-induced solution/gelation transition was visually determined. As shown in Figure I.42, when temperature increased up to the phase transition temperature of the shell thermosensitive $POEG_3MA$, the hydrophobic association of $POEG_3MA$ block would lead to physically crosslink of nanogels and thus thermally induced gelation, while the hydrophilic PDMAm mid-block acted as the interconnected bridge. The gelation ability, sensitivity, and mechanical properties could be tuned by changing the polymerization parameters, such as the block ratios and the crosslinking density.

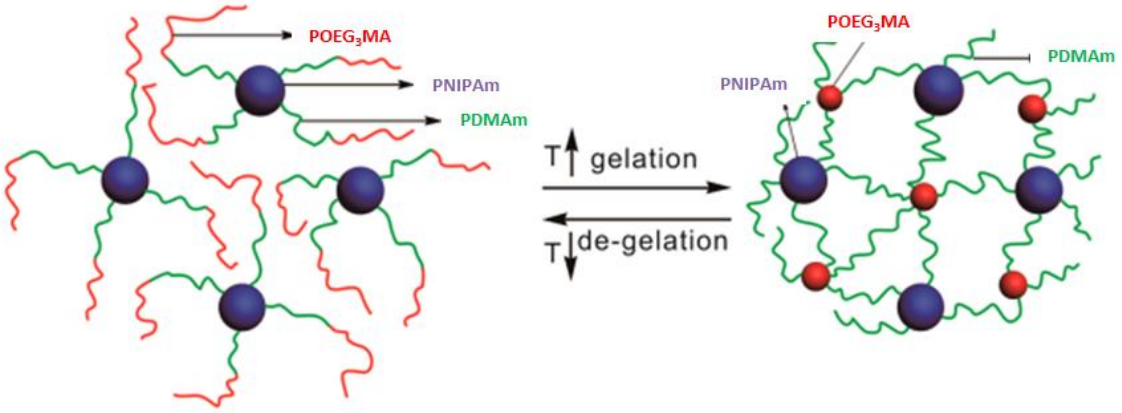


Figure I.42. Schematic representation of reversible thermally induced solution/gelation transition of $POEG_3MA$-*b*-PDMAm-*b*-P(NIPAm-*co*-MBA) nanogel, which was physically crosslinked by hydrophobic association of thermosensitive $POEG_3MA$ block when temperature increase up to LCST and de-crosslinked when temperature decrease below LCST of $POEG_3MA$.Reproduced from ref. 163

In our group, we target LCST-type thermosensitive nanogels based on P(NIPAm-*co*-MBA) core and PPEGA shell by sonochemically induced RAFT-PITSA process (Sono-RAFT-PITSA).[148] High frequency ultrasound (490 kHz) at moderate temperature (45°C) in the absence of organic initiator was applied for the controlled copolymerization of NIPAm and MBA from PPEGA macro-CTA and using water as *inisolv* (initiator and solvent) (Figure I.43).

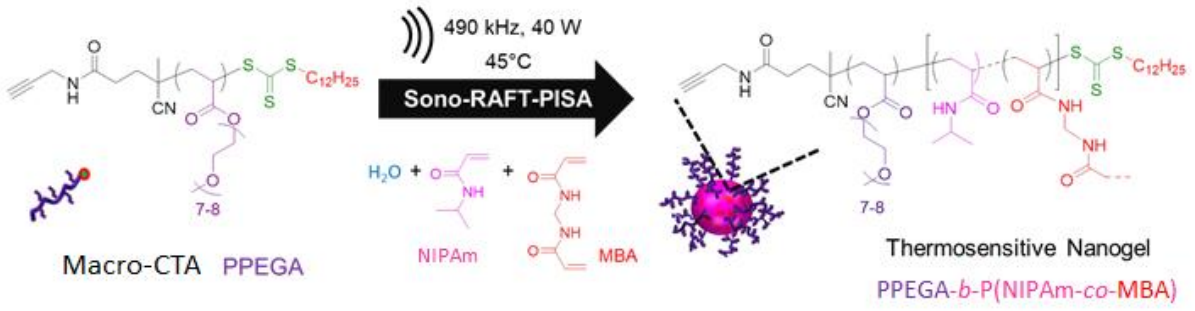


Figure I.43. Synthesis of LCST-type thermosensitive nanogels based on PPEGA-*b*-P(NIPAm-*co*-MBA) via Sono-RAFT-PITSA process. Reproduced from ref.148

Different synthetic parameters including PPEGA macro-CTA chain length and NIPAm molar content affected the size, dispersity, swelling, and stability of nanogels. A minimum $\overline{DP_n}$ of the PPEGA macro-CTA is necessary to reach effective stabilization of the nano-objects formed *in situ* during the PITSA process. An heterogenous dispersion was obtained containing aggregates from a PPEGA macro-CTA with $\overline{DP_{n,PPEGA}}$ of 7. By contrast, higher $\overline{DP_{n,PPEGA}}$ (11, 20, 26, 33, and 49) produced stable thermosensitive nanogels. With increasing $\overline{DP_{n,PPEGA}}$ from 11 to 49, $D_h$ of nanogels

decreased from 272 to 33 nm. The pdi and the volume swelling ratio were not affected significantly by the $\overline{DP_{n,PPEGA}}$. The impact of $\overline{DP_{n,PNIPAm}}$ was further investigated. With increasing $\overline{DP_{n,PNIPAm}}$ block from 204 to 500, $D_h$ of the particles at increased from 42 to 222 nm and the volume swelling ratio upon heating from 25 to 45°C increased from 3 to 11, respectively. TEM images also confirmed the formation of spherical object with a size consistent with the DLS study of the shrinked nanogel as the sonochemical activation process process did not impact spherical morphology of resulting nanogels.

#### 1.3.1.2.2 UCST-type thermosensitive nanogels

First UCST-type thermosensitive nanogels based on a POEGMA shell and a crosslinked thermosensitive P(DMAPS-*co*-MBA) core were reported on 2017 by Fu *et al.*[164] The UCST-type zwitterionic block copolymer nanogels were synthesized by RAFT-PITSA of DMAPS using POEGMA as a macro-CTA in water-organic mixture at 70 °C and through *in-situ* crosslinking strategy (Figure I.44).

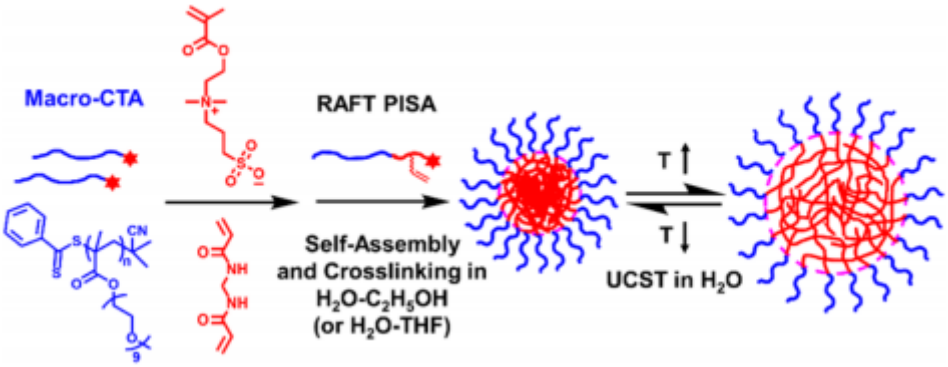


Figure I.44. Synthesis of UCST-thermosensitive nanogels by RAFT PITSA in water/ethanol mixture and schematic illustration of thermally induced reversible swelling/shrinking of nanogels in water. Reproduced from ref.[164]

The critical requirement for the synthesis of nano-objects by PITSA is that the second block must precipitate out from the reaction media and self-assemble into nanodomains, which are stabilized by the macro-CTA during the polymerization. As UCST-type thermosensitive polymers show a better solubility in water at higher temperatures, the authors change the solubility of a PDMAPS in water by adding ethanol or THF, leading to the aggregation of polymer even at high temperature (higher than its UCST in water). Spherical nanogels with a single size distribution were obtained. At 70°C, the $D_h$ was 278 nm, and the pdi was 0.083. The $D_h$ decreased upon cooling, reaching 226 nm at 10°C. This corresponds to a volume shrinkage of 46%. The UCST value upon cooling was 46.6 C (Figure I.45.A) and the phase transition temperature upon heating was 40°C (Figure I.45.B). The thermal induced swelling/shrinking was reversible (Figure I.45.C).

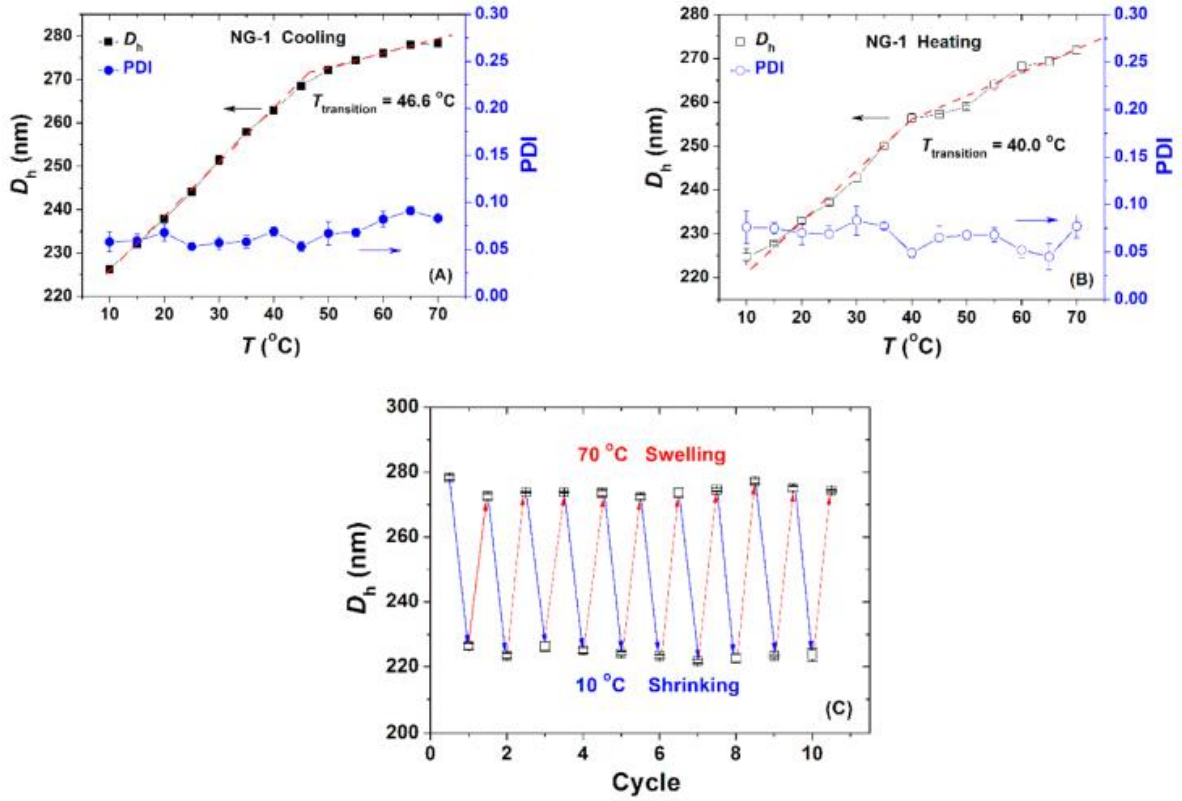


Figure I.45. Plots of $D_h$ and pdi of POEGMA-*b*-PDMAPS-based nanogels in water at a concentration of 0.05 mg.g$^{-1}$, obtained from a DLS study, *versus* temperature upon cooling (A) and heating (B) in the temperature range of 70 to 10°C. (C) The $D_h$ values of nanogel at 70 and 10°C in water at a concentration of 0.05 mg.g$^{-1}$ from repeated heating and cooling experiments. Reproduced from ref.[164]

The authors shows that the $D_h$, volume swelling ratio, and UCST value of nanogels based on PDMAPS can be tuned in the range of 40 to 50°C by changing the polymerization parameters as nature and $\overline{DP_n}$ of PDMAm macro-CTA, ethanol content in water/ethanol mixture or monomers-to-macro-CTA molar ratio. Firstly, two PDMAm macro-CTAs with $\overline{DP_n}$ of 38 and 116 were employed to target PDMAPS-based nanogels under similar conditions than for the synthesis of nanogels obtained from $POEG_9MA$ with a $\overline{DP_n}$ of 40 (called $POEG_9MA_{40}$) but both were unsuccessful; precipitation was observed during the polymerization. Although the reason was unclear, $POEG_9MA_{40}$ appeared to have a better ability to stabilize the insoluble PDMAPS block in the reaction mixture. Secondly, with decreasing ethanol content from 60 to 40 wt.% in water/ethanol mixture, the nanogel's $D_h$ at 10 °C decreased from 226 to 125 nm and the volume swelling ratio upon heating from 10 to 70°C increased from 1.86 to 2.78. These are likely because a higher water content in the medium increased the solubility of PDMAPS. The water content was increased to 80% and resulted in two size distributions. Although there was still a very poor medium for PDMAPS, the self-assemblies during the RAFT polymerization may be irregular, and the nanodomains may not be well stabilized, likely because the

mobility of PDMAPS chains increased with increasing water content. Thirdly, with increasing initial molar ratio of DMAPS, the nanogel's $D_h$ increased. The phase transition temperatures and the volume swelling ratio upon heating from 10 to 70°C were in the same order of increasing DMAPS amount in the synthesis of nanogels. Finally, with decreasing amount of MBA crosslinker, the volume swelling ratio of nanogel increased. Further decreasing amount of MBA crosslinker, multiple size distributions were observed due to the insufficient crosslinking.

The nanogels based on poly(2-((2-(methacryloyloxy)ethyl)dimethylammonio)acetyl)-(phenyl-sulfonyl)amide (PMEDAPA) with different degrees of crosslinking were prepared via free radical precipitation polymerization in water using sodium dodecyl sulfonate (SDS), MBA as surfactant to stabilize nanogels and crosslinker, potassium peroxodisulfate as initiator (Figure I.46).[165]

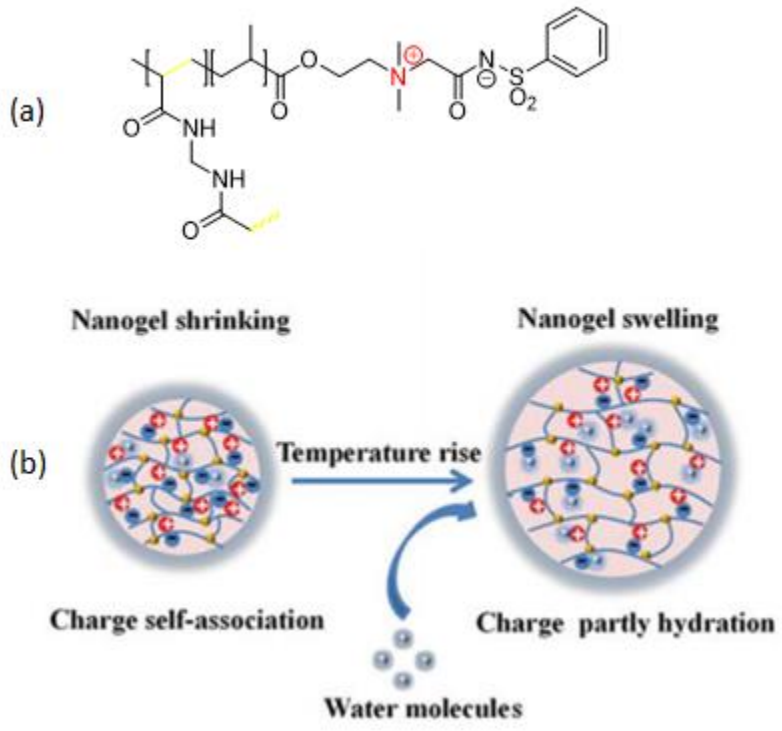


Figure I.46. (a) Structure of nanogel based on P(MEDAPA-*co*-MBA). (b) The illustration of the $D_h$ change of nanogels with temperature. Reproduced from ref.[166]

The resulting nanogels showed reversible thermal induced swelling/shrinking transition, demonstrating UCST behavior with phase transition temperature in the range of 44 to 54°C. The $D_h$ of P(MEDAPA-*co*-MBA) nanogel containing 5 wt.% of MBA crosslinker was 155 nm at 10°C and increased to 191 nm at 70°C, and the swelling ratio was calculated to be 1.86. The $D_h$ of nanogels increased from 155 nm to 234 nm with the increasing degree of crosslinking from 5 to 20 wt.%. In contrast, the UCST value and volume swelling ratio of P(MEDAPA-*co*-MBA) nanogels decreased when the degree of crosslinking increased, the reason is probably due to the more compact structure of

P(MEDAPA-*co*-MBA) nanogels with a higher degree of crosslinking which impaired the swelling ability of the nanogels. The pdi of nanogels remained low and nearly constant (≤ 0.1). In addition, the P(MEDAPA-*co*-MBA) nanogels exhibited a NaCl-induced swelling behavior. The $D_h$ of P(MEDAPA-*co*-MBA) nanogels containing 5 wt.% of MBA crosslinker was 166 nm in water at 25°C and increased to 370 nm in 0.9 wt.% NaCl solution and the swelling ratio was as high as 11. Meanwhile, the pdi of the P(MEDAPA-*co*-MBA) nanogel also increased from 0.065 to 0.231 when the NaCl concentration increased from 0 wt.% to 0.9 wt.%, may be owing to the significant volume expansion in this process. As in pure water, the volume swelling ratio of P(MEDAPA-*co*-MBA) nanogels also decreased when the degree of crosslinking increased. The water-induced shrinking and NaCl-induced swelling was reversible without significant difference in different cycles. The addition of cations ($Na^+$, $K^+$, $Mg^{2+}$ or $Ca^{2+}$) increased the $D_h$ of all P(MEDAPA-*co*-MBA) nanogels, which were significantly prominent in the samples with a low degree of crosslinking. Furthermore, it appeared that divalent cations ($Ca^{2+}$ and $Mg^{2+}$) led to larger $D_h$ in all nanogels than did monovalent cations ($Na^+$ and $K^+$), demonstrating that the divalent cations bind more strongly with sulfamide groups compared to monovalent cations. With regard to anions, nanogels showed the largest $D_h$ in salt solutions with $NO_3^-$ and the smallest $D_h$ in salt solutions with $SO_4^{2-}$, which agreed well with the hydration ability order of the Hofmeister effect.[167]

H-bond UCST-type thermosensitive nanogel based on ureido polymers was prepared through 2 steps by Ohshio *et al*.[168] Firstly, a diblock copolymer composed of a water-soluble poly(2-methacryloyloxyethyl phosphorylcholine) (PMPC) first block and a second block based on a statistical copolymer of poly(2-ureidoethyl methacrylate) and cationic poly(2-aminoethyl methacrylate) (named P(U/A10 in Figure I.46) was synthesized *via* RAFT polymerization using $PMPC_{20}$ macro-CTA in water. Below the UCST-phase transition temperature (24°C), the block copolymer forms micelles composed of UCST-type thermosensitive $(U/A10)_{165}$ core and hydrophilic $PMPC_{20}$ shell in water The nanogel was prepared by physical crosslinking of pendent primary amines within the micelle core using tetrakis(hydroxymethyl)phosphonium chloride as crosslinker at 20°C (Figure I.47). The nanogel with an UCST value of 26°C shows a $D_h$ of 30 nm at 10°C. With increasing temperature, the nanogel swells 1.2 times upon hydration while retaining its core-shell structure. The nanogel is capable of reversibly swelling and shrinking with temperature change. The UCST value of micelle increases with increasing concentration of diblock copolymer solution, whereas the UCST value of the nanogel is independent of concentration. Below UCST, the nanogel core being hydrophobic, a fluorescence-labeled bovine serum albumin (BSA) was encapsulated then released to the aqueous phase at 40°C.

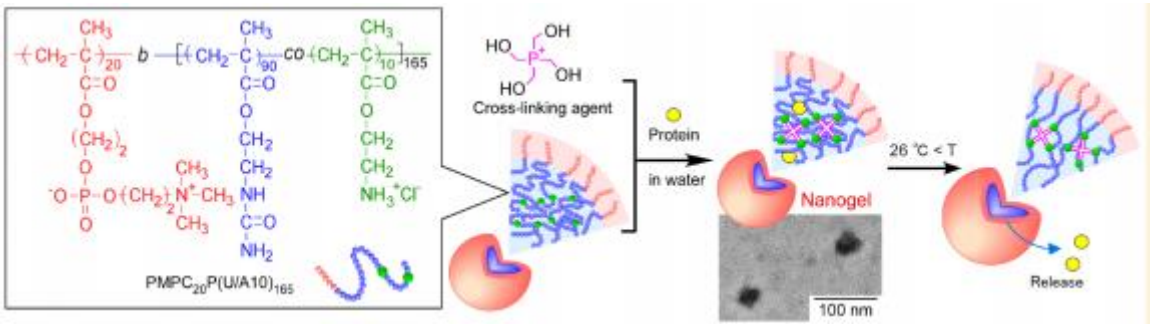


Figure I.47. Chemical structure of UCST-type thermosensitive diblock copolymer based on $PMPC_{20}$ and $P(U/A10)_{165}$ and the thermo-responsive behavior of the resulting nanogel in water. Reproduced from ref. 168

More recently, Auge *et al.*[169] reported the synthesis of light-sensitive and UCST-thermosensitive nanogels based on PDMAm shell and P(Am-*co*-AN) core covalently crosslinked with both MBA and a photo-thermally active nickel-bis(dithiolene) complex (Figure I.48).

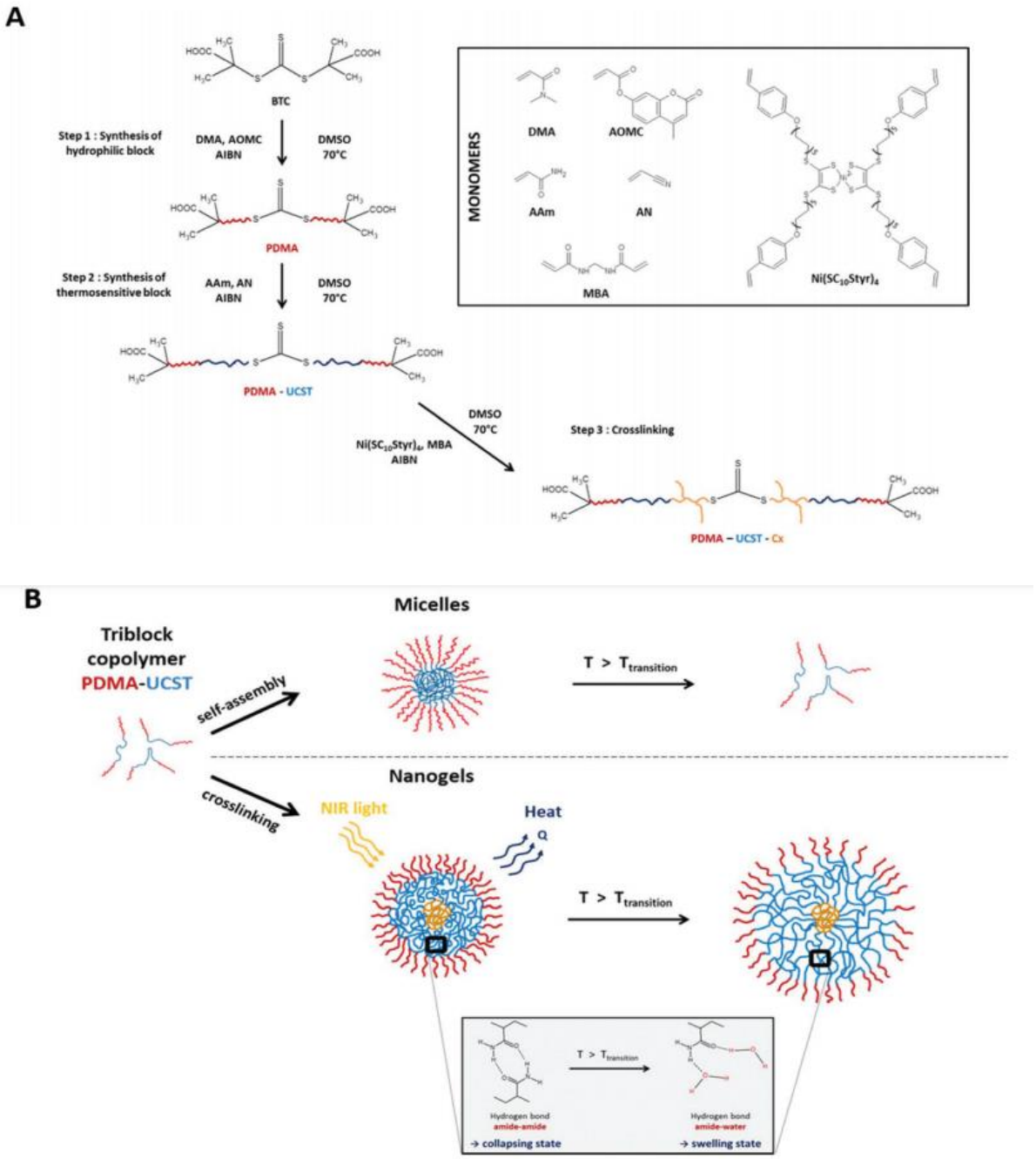


Figure I.48. (A) Synthetic steps to obtain the triblock copolymer PDMAm-*b*-P(Am-*co*-AN) and chemical structures of the monomers used. (B) Schematic showing the principle of conversion of light into heat by the crosslinked core based on the nickel-bis(dithiolene) complex, leading to phase transition of the near-infrared (NIR) light-responsive and thermosensitive copolymer nanogel. Reproduced from ref.[169]

Resulting nanogels shows UCST-type thermosensitive properties as the $D_h$ increases gradually from 100 nm at 10°C to 210 nm at 40°C. The crosslinking did not affect much the phase transition temperature since the nanoparticles, before and after crosslinking possess nearly the same UCST value of around 40-45°C. The volume of the nanogel above the phase transition temperature is about

2.1 times larger than that at 10°C. The UCST-type thermosensitive behavior for nanogels was reversible for different heating/cooling cycles. The efficiency of light-to-heat conversion of nanogel can reach 64%, placing the nickel-bis(dithiolene) complex among the most efficient photo-thermal agents in the NIR region around 1000 nm.

## 1.3.2 Dual temperature/pH-sensitive nanogels

To date, the intelligent biomaterials that can generate a cooperative response under multiple stimuli, such as pH and temperature, have shown advantages over those systems sensitive to a single stimulus. In this section, the chemistry of different pH-degradable entities, dual pH-sensitive and thermosensitive nanogels were discussed.

### 1.3.2.1 Chemistry of pH-degradable entities

A range of chemical bonds are known to be unstable in strong acid or basic solution. This is the case for the various protective groups commonly used in organic synthesis. However, only a few of them show an enhanced degradation or hydrolysis in the presence of slightly acidic media, while being stable at neutral pH. This unique property, determined by the chemical structure of the bond, makes them candidates of choice for the preparation of acid-degradable polymers. The acid-sensitive linkers most commonly employed in the literature include orthoester, acetal, hydrazone and imine.[170–172] The mechanism of the hydrolysis of each moiety was illustrated in the following parts.

#### 1.3.2.1.1 Acetal and ketal linker

The acetal and ketal are functional groups with the connectivity $R_1CH(OR_2)_2$ and $R_3R_2C(OR_1)_2$, respectively. In an acidic solution, one oxygen of the acetal group is protonated, which activates the neighboring carbon. This facilitates the attack of water, resulting in the cleavage of the acetal to the appropriate aldehyde and alcohol. The mechanism of the hydrolysis of the acetals and ketals is shown in Scheme I.1. In the hydrolysis process, formation of the intermediate of resonance-stabilized carboxonium ion (shown within the red color square bracket in Scheme I.1) has been suggested to be the rate determining step. Therefore, the stability of this carboxonium ion would dictate the hydrolysis rate of the corresponding acetal or ketal; *i.e.,* if the intermediate carboxonium ion is more stabilized, then the hydrolysis rate would be faster. Due to the cationic character of the intermediate, electron-donating group substituents are generally expected to stabilize the intermediate and thus accelerate hydrolysis.

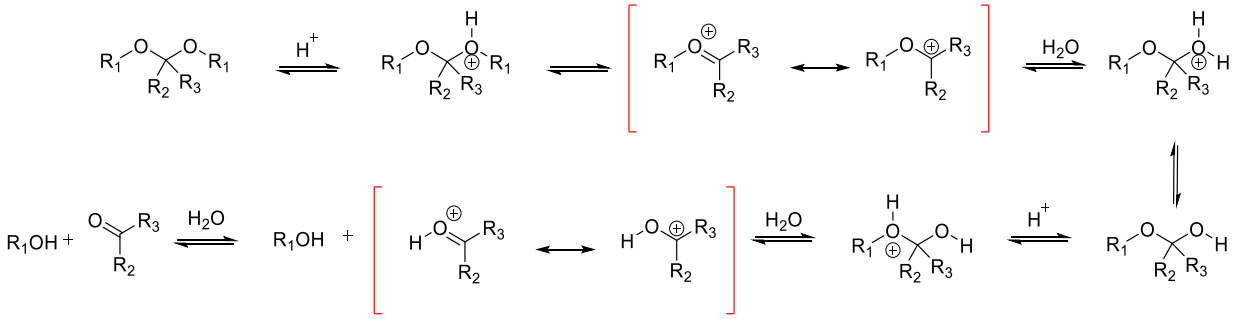

Scheme I.1. The mechanism of the hydrolysis of acetals and ketals.

#### 1.3.2.1.2 Orthoester linker

The orthoester is a functional group containing three alkoxy groups attached to one carbon atom ($R_1C(OR_2)_3$) that can be prepared by the reaction of nitriles with alcohols under acid catalysis. They are readily hydrolyzed in mild aqueous acid to form esters, and therefore usually used as protecting groups for esters. The mechanism for the acid-catalyzed hydrolysis of orthoesters consists of three separate reaction steps: generation of a dialkoxy carbonium ion, hydration of this ion to a hydrogen orthoester, and breakdown of the latter to alcohol and carboxylic acid or ester products (Scheme I.2).[173]

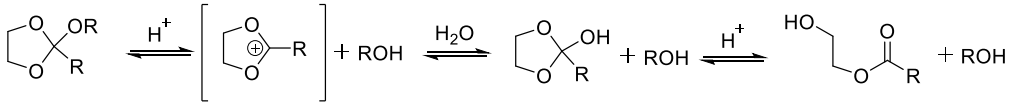

Scheme I.2. The three-steps mechanism for the acid-catalyzed hydrolysis of a cyclic orthoester.

#### 1.3.2.1.3 Imine linker

An imine is a functional group containing a carbon-nitrogen double bond, with the nitrogen attached to a hydrogen atom or an alkyl group ($R_1R_2C=NR_3$ with $R_3$ = H or an alkyl group). If this group is an alkyl group, then the compound is more stable and defined as a Schiff base. They are obtained by reaction of an aldehyde or ketone with a primary amine. The mechanism of the hydrolysis of the imines is shown in Scheme I.3. It starts by protonation of the nitrogen converting the imine into iminium ion which is very electrophilic and is attacked by water in the next step. After a proton transfer from the oxygen to the nitrogen (likely an intermolecular process), the ammonium ion is kicked out as a neutral amine. This step forms an oxonium ion which, after a deprotonation, gives the desired ketone.[174]

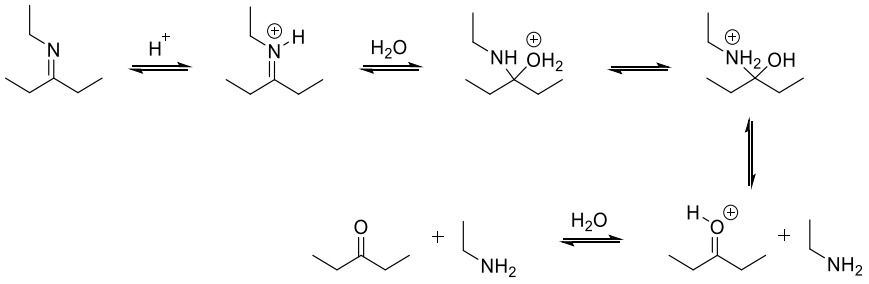

Scheme I.3. The mechanism of the hydrolysis of imine.

#### 1.3.2.1.4 Hydrazone linker

Hydrazones ($R_1HC=NNR_2R_3$) are a class of organic compound, usually formed by the reaction of hydrazine on ketones or aldehydes. Under acidic conditions, the hydrolysis reaction of hydrazone starts with the protonation of nitrogen, followed by the formation of carbinolamine intermediate (Scheme I.4). In the following step, a proton is lost from positively charged oxygen to yield intermediate which decomposes into corresponding hydrazine and aldehyde/ketone species.[175]

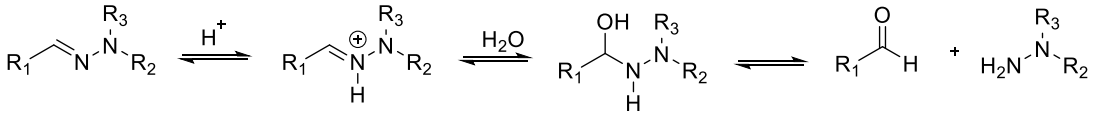

Scheme I.4. Mechanism proposed for the hydrolysis of hydrazone.

### 1.3.2.2 Dual pH-sensitive and LCST-type thermosensitive nanogels

To the best of our knowledge, several LCST-thermosensitive nanogels containing acetal/ketal and imine groups have been reported. For instance, in the study of Chen *et al.*,[176] thermosensitive and pH-degradable nanogels, with defined shape and size for encapsulation of Paclitaxel (PTX, a chemotherapy medication used to treat a number of types of cancer) and intracellular release were prepared by photo-crosslinking. A pre-polymer based on acetal-linked poly(vinyl alcohol) functionalized with vinyl ether acrylate (PVA-VEA) was first synthesized by acetalization between vinyl ether groups and hydroxyl groups and then crosslinked under UV-light using a water-soluble photo-initiator (Figure I.49). The nanogel PVA-VEA with 6 mol.% VEA showed a $D_h$ of 180 nm with a particularly narrow size distribution of 0.05 and LCST value of 16°C. Such resulting nanogel showed rapid degradation (the half-life of acetal hydrolysis at pH = 5 was about 6h) and a pH-triggered drug release in a controlled manner under intracellular acidic conditions at 37°C.

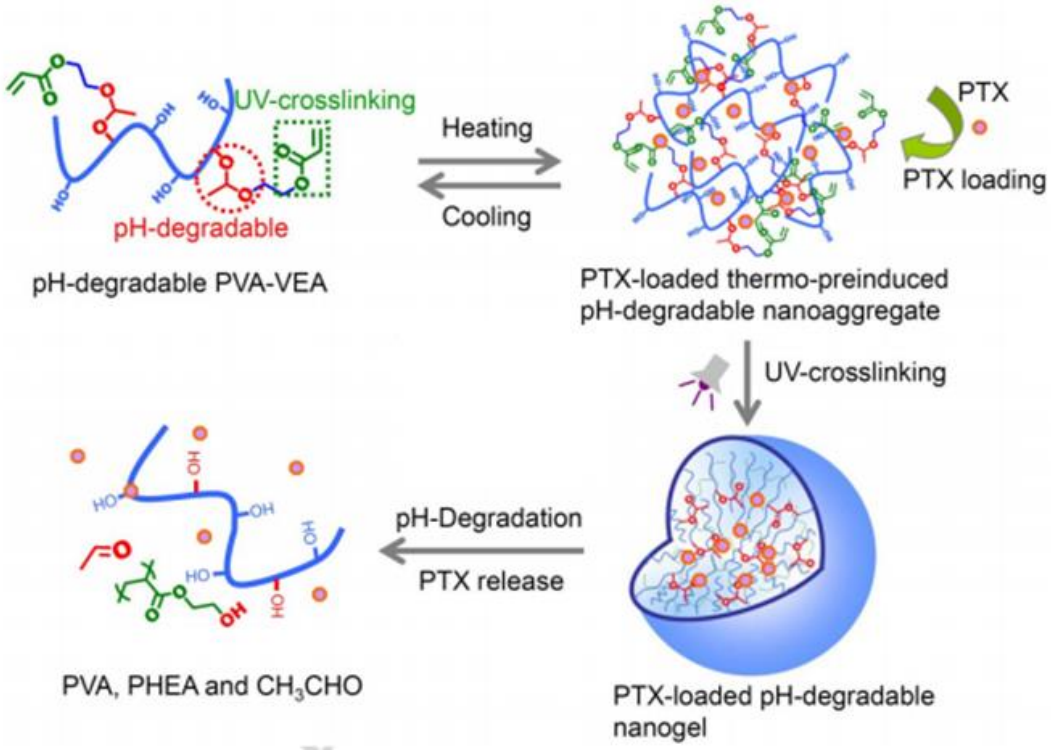


Figure I.49. Synthesis of thermosensitive and pH-degradable nanogels loading PTX based on PVA-VEA and their degradation under acidic pH. Reproduced from ref.[176]

Banejiee *et al*. [177] also reported the use of acetal linkage to form crosslinking which undergo decrosslinking at lysosomal pH of cancer cells (~5.0). The diol groups of PEG-*b*-PNIPAm-*b*-PGMA poly(glycidyl methacrylate) diol functionalized triblock copolymer were used to form the core crosslinked nanogel by reaction with aldehyde functionalized crosslinkers through formation of acetal linkages. Resulting nanogels show a single size distribution with $D_h$ in the range of 80-110 nm. The nanogels indicated a nearly complete breakage after incubation for 48h at pH 5.0. The nanogel showed efficient loading of doxorubicin with the loading capacity of 29.6% at pH ~ 7.4 at 20°C and more than 80% of the loaded drug molecules were freed from the acetal functionalized crosslinked networks after incubation for about 20h in pH ~ 5.0 medium at 37°C, a temperature higher than LCST of PNIPAm (32 °C) (Figure I.50).

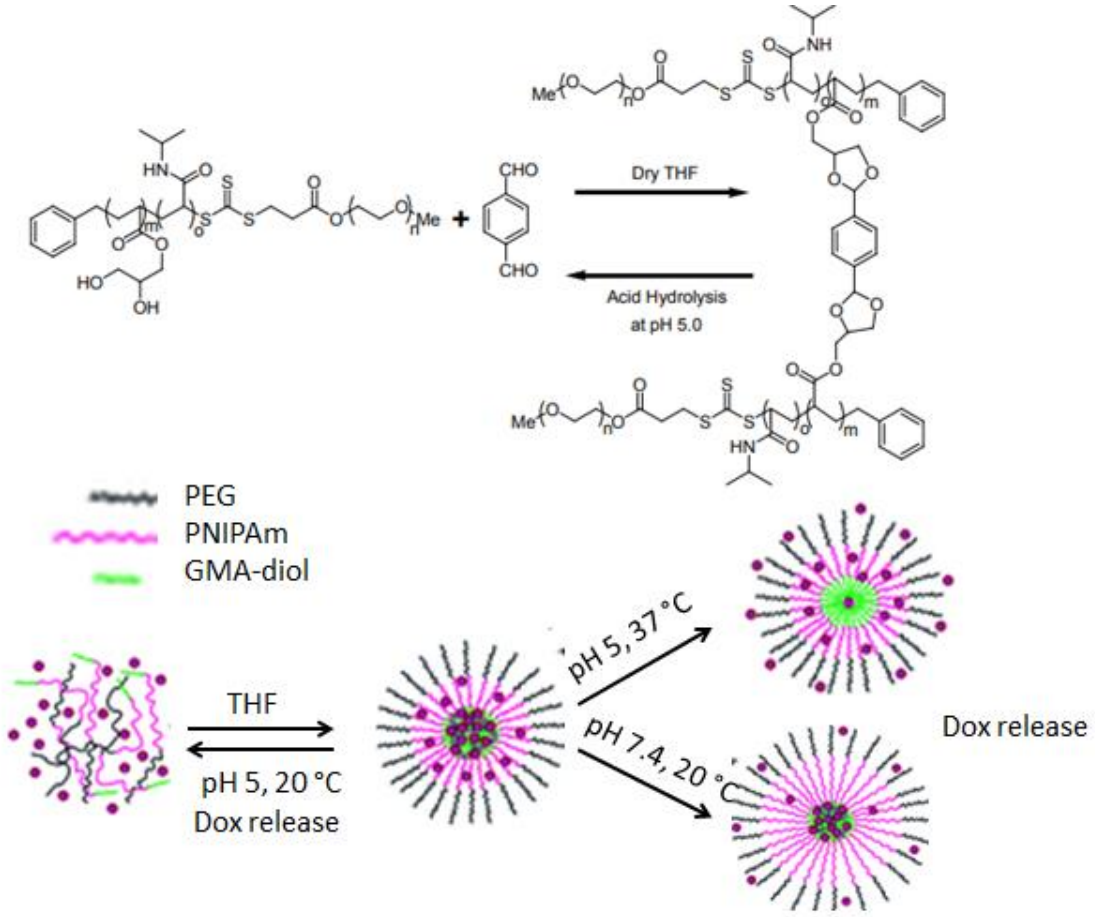


Figure I.50. The preparation of core crosslinked dual thermo- and pH-sensitive PEG-*b*-PNIPAm-*b*-PGMA -based nanogels *via* acetal formation and the acid hydrolysis of the nanogels gives back the reactants. Reproduced from ref.[177]

Beside acetal and ketal groups, degradability of nanogels based on imine bond are also reported. Fulton *et al*.[42,178] have synthesized a wide range of LCST-type thermosensitive and pH-degradable shell and core crosslinked polymer assemblies respectively using thermosensitive PNIPAm and acid cleavable imine bond. For example, core crosslinked polymers possessing responsiveness to pH and temperature stimuli have been prepared from aldehyde-functionalized diblock copolymer (P1) based on poly(*N*-ethylacrylamide-2-(4-formylbenzamide)) and amine-functionalized diblock copolymers based on poly(*N*-*(tert*-butoxycarbonyl)-propylaminoacrylamide).[42] Dual pH- and thermo-sensitive nanogels can be used to trigger the release and uptake of a hydrophobic dye molecule. Nile Red can be encapsulated within the hydrophobic core of nanogel at 45°C and be released at 5 °C. In addition, at pH 5.5, the release of Nile Red can be triggered by pH-induced disassembly and the encapsulation occurred at pH 11. Both of these processes are reversible, and the Nile Red can be re-encapsulated upon removal of the pH or temperature stimuli.

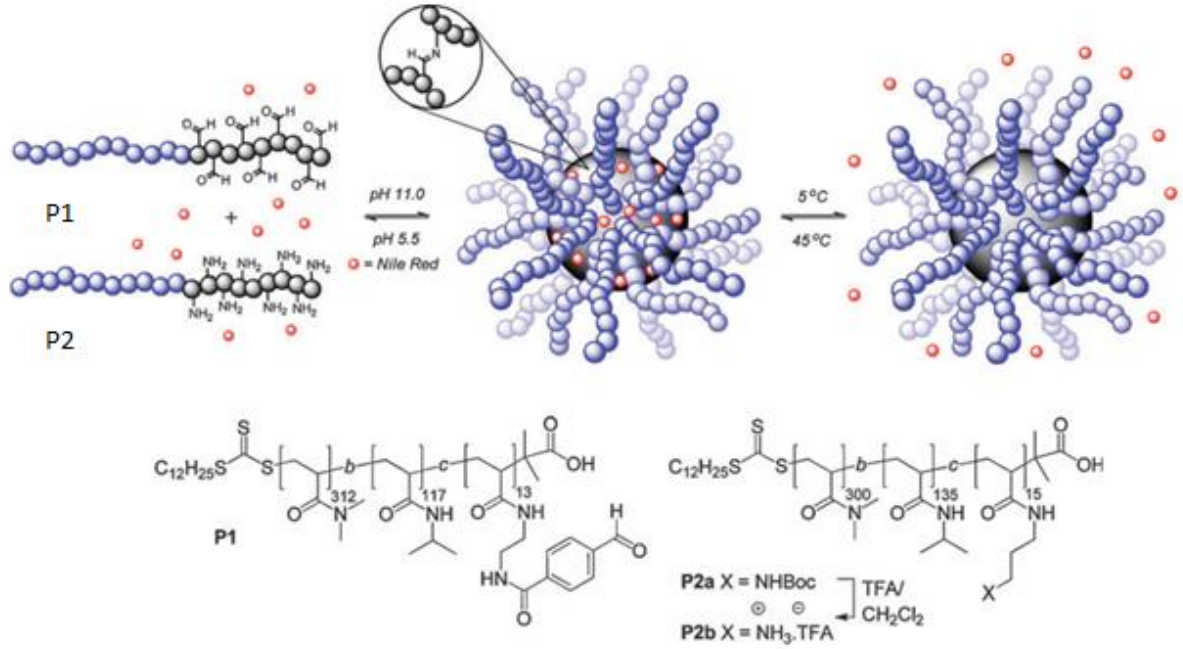


Figure I.51. The preparation of core crosslinked dual thermal and pH-sensitive nanogel based on aldehyde-functionalized diblock copolymer from poly(*N*-ethylacrylamide-2-(4-formylbenzamide) and amine-functionalized diblock copolymers from poly(*N-(tert*-butoxycarbonyl)-propylaminoacrylamide). *via* imine bond formation. The reversible encapsulation and release cycles of Nile Red when temperature and pH change. Reproduced from ref.[42]

### 1.3.2.3 Dual pH-sensitive and UCST-type thermosensitive nanogels

From our knowledge, there is no pH-degradable and UCST-type thermosensitive nanogel in the literature up to now. Moreover, the pH-dependent synthetic UCST-type thermosensitive polymers that operate within a physiological window are also extremely rare and only a few examples have been reported. Sponchioni *et al*.[179] developed a new class of degradable zwitterionic UCST-type thermosensitive polymer nanoparticles by synthesizing poly(sulfobetaine-*co*-sulfabetaine)-*g*-poly(ε-caprolactone) copolymers via RAFT polymerization. They showed that the degradation rate of the nanoparticles at pH 14 is dependent on the length of the oligoester grafts. Roth *et al*.[180] described the synthesis of thioester-based statistical UCST-type thermoensitive copolymers based on the radical copolymerization of the dibenzo[c,e]oxepane-5-thione with either the zwitterionic sulfobutyl betaine or either AN and Am comonomers. They studied the degradation of such UCST-type thermosenstive polymers through aminolysis. More recently, Zhang *et al* [181] reported the preparation of a pH-degradable and UCST thermosensitive polymer based on poly(*N*-(2-hydroxypropyl) methacrylamide-glycolamide) (P(HPMA-GA)). N-(2-hydroxypropyl) methacrylamide was firstly modified on the hydroxyl-position with glycolamide to form the HMPA-GA monomer with a degradable carbonate ester linkage and a primary amid pendant group to potential H- bond

formation. The P(HPMA-GA) was obtained by RAFT polymerization of modified monomer HPMA-GA The obtained modified PHPMA-GA shows both UCST-thermosensitive and pH-degradable properties. An aqueous solutions of the polymer with $\overline{DP_n}$ of 50 displays UCST of 22°C upon heating at a concentration of 5 mg.mL$^{-1}$. In addition, there was a gradual decrease of the cloud point temperature upon hydrolysis at pH 7.4 of the polymer side chains until it becomes lower than 37°C leading to solubilization of the polymer. This is an interesting finding as it indicates that despite the relatively slow degradation (10 h) of the polymer, a rather rapid phase transition takes place at physiological temperature (37°C) and pH (7.4).

## 1.4 Conclusions

We mainly focused our attention to the relevant literature regarding available methods used for general preparation of nanogel including physical crosslinking and chemical crosslinking methods. Physically crosslinked nanogels are prepared using non-covalent interactions between polymer chains as hydrophobic interactions, electrostatic interactions or host-guest interactions. Compare to physically crosslinked type, the chemically crosslinked nanogels are much more stable and well-defined. A variety of methods have been developed to synthesize chemically crosslinked nanogels including the crosslinking of polymer precursors, the direct crosslinking through radical polymerization of co-monomers and through polymerization-induced self-assembly (PISA) process. By employing crosslinking reactions *via* post-modification of preformed reactive polymer precursors like thiol-disulfide exchange reaction, amidation reaction, Schiff base reaction or photodimerization of coumarin entities, a wide range of nanogels with precise control of the chemical functionality could be obtained. This technique has evolved from polymer synthesis, where post-polymerization functionalization enables the introduction of active groups into polymer chains which can be further crosslinking. In the direct crosslinking through radical polymerization of co-monomers, the polymerization and the crosslinking reaction occur at the same time. There are different polymerization processes and synthetic strategies based on conventional (Inverse (mini)emulsion polymerization, Inverse microemulsion polymerization) or controlled radical polymerizations (NMP, ATRP, RITP, RAFT) to prepare nanogels. In the PISA process, typically, a soluble homopolymer (A) is chain-extended using a second monomer in a suitable solvent such that the growing second block (B) gradually becomes insoluble, which drives *in situ* self-assembly to form AB diblock copolymer nano-objects. The A block is usually prepared *via* solution polymerization and acts as a surfactant, while the insoluble B block is prepared *via* either dispersion or emulsion polymerization. Among the various chemical crosslink processes, RAFT-PITSA is a powerful method to prepare LCST-type thermosensitive nanogels in a one-pot process. Up to now, there are only few reports on the

synthesis procedure of UCST-type thermosensitive nanogels, which all have disadvantage as purification requirement, post-polymerization for crosslinking or involving unfriendly environment organic solvent. The dual pH-sensitive and UCST-type thermosensitive systems are also rare in the literatures and no dual pH-sensitive and UCST-type thermosensitive nanogel was reported.

## 1.5 References


(1) Alemán, J. V.; Chadwick, A. V.; He, J.; Hess, M.; Horie, K.; Jones, R. G.; Kratochvíl, P.; Meisel, I.; Mita, I.; Moad, G.; Penczek, S.; Stepto, R. F. T. Definitions of Terms Relating to the Structure and Processing of Sols, Gels, Networks, and Inorganic-Organic Hybrid Materials (IUPAC Recommendations 2007). *Pure Appl. Chem.* **2007**, *79* (10), 1801–1829. https://doi.org/10.1351/pac200779101801.

(2) Akiyoshi, K.; Deguchi, S.; Moriguchi, N.; Yamaguchi, S.; Sunamoto, J. Self-Aggregates of Hydrophobized Polysaccharides in Water. Formation and Characteristics of Nanoparticles. *Macromolecules* **1993**, *26* (12), 3062–3068. https://doi.org/10.1021/ma00064a011.

(3) Vinogradov, S.; Batrakova, E.; Kabanov, A. Poly(Ethylene Glycol)–Polyethyleneimine NanoGel™ Particles: Novel Drug Delivery Systems for Antisense Oligonucleotides. *Colloids Surf. B: Biointerfaces* **1999**, *16* (1–4), 291–304. https://doi.org/10.1016/S0927-7765(99)00080-6.

(4) Sasaki, Y.; Akiyoshi, K. Nanogel Engineering for New Nanobiomaterials: From Chaperoning Engineering to Biomedical Applications. *Chem Record* **2010**, n/a-n/a. https://doi.org/10.1002/tcr.201000008.

(5) Neamtu, I.; Rusu, A. G.; Diaconu, A.; Nita, L. E.; Chiriac, A. P. Basic Concepts and Recent Advances in Nanogels as Carriers for Medical Applications. *Drug Delivery* **2017**, *24* (1), 539–557. https://doi.org/10.1080/10717544.2016.1276232.

(6) Satarkar, N.; Hilt, J. Magnetic Hydrogel Nanocomposites for Remote Controlled Pulsatile Drug Release. *JCR* **2008**, *130* (3), 246–251. https://doi.org/10.1016/j.jconrel.2008.06.008.

(7) Demirel, G.; Rzaev, Z.; Patir, S.; Pişkin, E. Poly(<I>N</I>-Isopropylacrylamide) Layers on Silicon Wafers as Smart DNA-Sensor Platforms. *J. Nanosci. Nanotech.* **2009**, *9* (3), 1865–1871. https://doi.org/10.1166/jnn.2009.388.

(8) Cao, L.; Li, X.; Wang, S.; Li, S.; Li, Y.; Yang, G. A Novel Nanogel-Based Fluorescent Probe for Ratiometric Detection of Intracellular PH Values. *Chem. Commun.* **2014**, *50* (63), 8787–8790. https://doi.org/10.1039/C4CC03716B.

(9) Hayashi, H.; Iijima, M.; Kataoka, K.; Nagasaki, Y. PH-Sensitive Nanogel Possessing Reactive PEG Tethered Chains on the Surface. *Macromolecules* **2004**, *37* (14), 5389–5396. https://doi.org/10.1021/ma049199g.

(10) Morimoto, N.; Hirano, S.; Takahashi, H.; Loethen, S.; Thompson, D. H.; Akiyoshi, K. Self-Assembled PH-Sensitive Cholesteryl Pullulan Nanogel As a Protein Delivery Vehicle. *Biomacromolecules* **2013**, *14* (1), 56–63. https://doi.org/10.1021/bm301286h.

(11) Park, C. W.; Yang, H.-M.; Lee, H. J.; Kim, J.-D. Core–Shell Nanogel of PEG–Poly(Aspartic Acid) and Its PH-Responsive Release of Rh-Insulin. *Soft Matter* **2013**, *9* (6), 1781–1788. https://doi.org/10.1039/C2SM26865E.

(12) He, J.; Tong, X.; Zhao, Y. Photoresponsive Nanogels Based on Photocontrollable Cross-Links. *Macromolecules* **2009**, *42* (13), 4845–4852. https://doi.org/10.1021/ma900665v.

(13) Khatun, Z.; Nurunnabi, M.; Nafiujjaman, M.; Reeck, G. R.; Khan, H. A.; Cho, K. J.; Lee, Y. A Hyaluronic Acid Nanogel for Photo–Chemo Theranostics of Lung Cancer with Simultaneous Light-Responsive Controlled Release of Doxorubicin. *Nanoscale* **2015**, *7* (24), 10680–10689. https://doi.org/10.1039/C5NR01075F.

(14) Morimoto, N.; Ohki, T.; Kurita, K.; Akiyoshi, K. Thermo-Responsive Hydrogels with Nanodomains: Rapid Shrinking of a Nanogel-Crosslinking Hydrogel of Poly(N-Isopropyl Acrylamide). *Macromol. Rapid Commun.* **2008**, *29* (8), 672–676. https://doi.org/10.1002/marc.200700864.

(15) Werz, P. D. L.; Kainz, J.; Rieger, B. Thermo- and PH-Responsive Nanogel Particles Bearing Secondary Amine Functionalities for Reversible Carbon Dioxide Capture and Release. *Macromolecules* **2015**, *48* (18), 6433–6439. https://doi.org/10.1021/acs.macromol.5b01367.

(16) Zhuang, J.; Gordon, M. R.; Ventura, J.; Li, L.; Thayumanavan, S. Multi-Stimuli Responsive Macromolecules and Their Assemblies. *Chem. Soc. Rev.* **2013**, *42* (17), 7421. https://doi.org/10.1039/c3cs60094g.

(17) Zha, L.; Banik, B.; Alexis, F. Stimulus Responsive Nanogels for Drug Delivery. *Soft Matter* **2011**, *7* (13), 5908. https://doi.org/10.1039/c0sm01307b.

(18) Ayame, H.; Morimoto, N.; Akiyoshi, K. Self-Assembled Cationic Nanogels for Intracellular Protein Delivery. *Bioconjugate Chem.* **2008**, *19* (4), 882–890. https://doi.org/10.1021/bc700422s.

(19) Qiao, Z.-Y.; Zhang, R.; Du, F.-S.; Liang, D.-H.; Li, Z.-C. Multi-Responsive Nanogels Containing Motifs of Ortho Ester, Oligo(Ethylene Glycol) and Disulfide Linkage as Carriers of Hydrophobic Anti-Cancer Drugs. *JCR* **2011**, *152* (1), 57–66. https://doi.org/10.1016/j.jconrel.2011.02.029.

(20) Oh, J. K.; Lee, D. I.; Park, J. M. Biopolymer-Based Microgels/Nanogels for Drug Delivery Applications. *Prog. Polym. Sci.* **2009**, *34* (12), 1261–1282. https://doi.org/10.1016/j.progpolymsci.2009.08.001.

(21) Nochi, T.; Yuki, Y.; Takahashi, H.; Sawada, S.; Mejima, M.; Kohda, T.; Harada, N.; Kong, I. G.; Sato, A.; Kataoka, N.; Tokuhara, D.; Kurokawa, S.; Takahashi, Y.; Tsukada, H.; Kozaki, S.; Akiyoshi, K.; Kiyono, H. Nanogel Antigenic Protein-Delivery System for Adjuvant-Free Intranasal Vaccines. *Nature Mater* **2010**, *9* (7), 572–578. https://doi.org/10.1038/nmat2784.

(22) Chacko, R. T.; Ventura, J.; Zhuang, J.; Thayumanavan, S. Polymer Nanogels: A Versatile Nanoscopic Drug Delivery Platform. *Adv. Drug Deliv. Rev.* **2012**, *64* (9), 836–851. https://doi.org/10.1016/j.addr.2012.02.002.

(23) McAllister, K.; Sazani, P.; Adam, M.; Cho, M. J.; Rubinstein, M.; Samulski, R. J.; DeSimone, J. M. Polymeric Nanogels Produced via Inverse Microemulsion Polymerization as Potential Gene and

Antisense Delivery Agents. *J. Am. Chem. Soc.* **2002**, *124* (51), 15198–15207. https://doi.org/10.1021/ja027759q.

(24) Kabanov, A. V.; Vinogradov, S. V. Nanogels as Pharmaceutical Carriers: Finite Networks of Infinite Capabilities. *Angew. Chem. Int. Ed.* **2009**, *48* (30), 5418–5429. https://doi.org/10.1002/anie.200900441.

(25) Torchilin, V. P. Multifunctional, Stimuli-Sensitive Nanoparticulate Systems for Drug Delivery. *Nat Rev Drug Discov* **2014**, *13* (11), 813–827. https://doi.org/10.1038/nrd4333.

(26) Mura, S.; Nicolas, J.; Couvreur, P. Stimuli-Responsive Nanocarriers for Drug Delivery. *Nature Mater* **2013**, *12* (11), 991–1003. https://doi.org/10.1038/nmat3776.

(27) Motornov, M.; Roiter, Y.; Tokarev, I.; Minko, S. Stimuli-Responsive Nanoparticles, Nanogels and Capsules for Integrated Multifunctional Intelligent Systems. *Prog. Polym. Sci.***2010**, *35* (1–2), 174–211. https://doi.org/10.1016/j.progpolymsci.2009.10.004.

(28) Stuart, M. A. C.; Huck, W. T. S.; Genzer, J.; Müller, M.; Ober, C.; Stamm, M.; Sukhorukov, G. B.; Szleifer, I.; Tsukruk, V. V.; Urban, M.; Winnik, F.; Zauscher, S.; Luzinov, I.; Minko, S. Emerging Applications of Stimuli-Responsive Polymer Materials. *Nature Mater* **2010**, *9* (2), 101–113. https://doi.org/10.1038/nmat2614.

(29) Oh, J. K.; Drumright, R.; Siegwart, D. J.; Matyjaszewski, K. The Development of Microgels/Nanogels for Drug Delivery Applications. *Prog. Polym. Sci.* **2008**, *33* (4), 448–477. https://doi.org/10.1016/j.progpolymsci.2008.01.002.

(30) Beija, M.; Marty, J.-D.; Destarac, M. RAFT/MADIX Polymers for the Preparation of Polymer/Inorganic Nanohybrids. *Prog. Polym. Sci.***2011**, *36* (7), 845–886. https://doi.org/10.1016/j.progpolymsci.2011.01.002.

(31) Siegwart, D. J.; Oh, J. K.; Matyjaszewski, K. ATRP in the Design of Functional Materials for Biomedical Applications. *Prog. Polym. Sci.* **2012**, *37* (1), 18–37. https://doi.org/10.1016/j.progpolymsci.2011.08.001.

(32) Shiroya, T.; Tamura, N.; Yasui, M.; Fujimoto, K.; Kawaguchi, H. Enzyme Immobilization on Thermosensitive Hydrogel Microspheres. *Colloids Surf. B: Biointerfaces* **1995**, *4* (5), 267–274. https://doi.org/10.1016/0927-7765(94)01177-7.

(33) Duracher, D.; Elaïssari, A.; Mallet, F.; Pichot, C. Adsorption of Modified HIV-1 Capsid P24 Protein onto Thermosensitive and Cationic Core−Shell Poly(Styrene)−Poly( *N* -Isopropylacrylamide) Particles †. *Langmuir* **2000**, *16* (23), 9002–9008. https://doi.org/10.1021/la0004045.

(34) Zhang, Y.; Bland, G. D.; Yan, J.; Avellan, A.; Xu, J.; Wang, Z.; Hoelen, T. P.; Lopez-Linares, F.; Hatakeyama, E. S.; Matyjaszewski, K.; Tilton, R. D.; Lowry, G. V. Amphiphilic Thiol Polymer Nanogel Removes Environmentally Relevant Mercury Species from Both Produced Water and Hydrocarbons. *Environ. Sci. Technol.* **2021**, *55* (2), 1231–1241. https://doi.org/10.1021/acs.est.0c05470.

(35) Sasaki, Y.; Akiyoshi, K. Nanogel Engineering for New Nanobiomaterials: From Chaperoning Engineering to Biomedical Applications. *Chem Record* **2010**, n/a-n/a. https://doi.org/10.1002/tcr.201000008.

(36) Akiyama, E.; Morimoto, N.; Kujawa, P.; Ozawa, Y.; Winnik, F. M.; Akiyoshi, K. Self-Assembled Nanogels of Cholesteryl-Modified Polysaccharides: Effect of the Polysaccharide Structure on Their Association Characteristics in the Dilute and Semidilute Regimes. *Biomacromolecules* **2007**, *8* (8), 2366–2373. https://doi.org/10.1021/bm070136q.

(37) Nagahama, K.; Mori, Y.; Ohya, Y.; Ouchi, T. Biodegradable Nanogel Formation of Polylactide-Grafted Dextran Copolymer in Dilute Aqueous Solution and Enhancement of Its Stability by Stereocomplexation. *Biomacromolecules* **2007**, *8* (7), 2135–2141. https://doi.org/10.1021/bm070206t.

(38) Shu, S.; Zhang, X.; Teng, D.; Wang, Z.; Li, C. Polyelectrolyte Nanoparticles Based on Water-Soluble Chitosan–Poly(l-Aspartic Acid)–Polyethylene Glycol for Controlled Protein Release. *Carbohydr. Res* **2009**, *344* (10), 1197–1204. https://doi.org/10.1016/j.carres.2009.04.018.

(39) Daoud-Mahammed, S.; Couvreur, P.; Bouchemal, K.; Chéron, M.; Lebas, G.; Amiel, C.; Gref, R. Cyclodextrin and Polysaccharide-Based Nanogels: Entrapment of Two Hydrophobic Molecules, Benzophenone and Tamoxifen. *Biomacromolecules* **2009**, *10* (3), 547–554. https://doi.org/10.1021/bm801206f.

(40) Ryu, J.-H.; Jiwpanich, S.; Chacko, R.; Bickerton, S.; Thayumanavan, S. Surface-Functionalizable Polymer Nanogels with Facile Hydrophobic Guest Encapsulation Capabilities. *J. Am. Chem. Soc.* **2010**, *132* (24), 8246–8247. https://doi.org/10.1021/ja102316a.

(41) Zhuang, J.; Jiwpanich, S.; Deepak, V. D.; Thayumanavan, S. Facile Preparation of Nanogels Using Activated Ester Containing Polymers. *ACS Macro Lett.* **2012**, *1* (1), 175–179. https://doi.org/10.1021/mz200123f.

(42) Jackson, A. W.; Fulton, D. A. PH Triggered Self-Assembly of Core Cross-Linked Star Polymers Possessing Thermoresponsive Cores. *Chem. Commun.* **2011**, *47* (24), 6807. https://doi.org/10.1039/c1cc11785h.

(43) He, J.; Yan, B.; Tremblay, L.; Zhao, Y. Both Core- and Shell-Cross-Linked Nanogels: Photoinduced Size Change, Intraparticle LCST, and Interparticle UCST Thermal Behaviors. *Langmuir* **2011**, *27* (1), 436–444. https://doi.org/10.1021/la1040322.

(44) Gao, H.; Matyjaszewski, K. Synthesis of Functional Polymers with Controlled Architecture by CRP of Monomers in the Presence of Cross-Linkers: From Stars to Gels. *Prog. Polym. Sci.***2009**, *34* (4), 317–350. https://doi.org/10.1016/j.progpolymsci.2009.01.001.

(45) Missirlis, D.; Tirelli, N.; Hubbell, J. A. Amphiphilic Hydrogel Nanoparticles. Preparation, Characterization, and Preliminary Assessment as New Colloidal Drug Carriers. *Langmuir* **2005**, *21* (6), 2605–2613. https://doi.org/10.1021/la047367s.

(46) Gao, F.; Mi, Y.; Wu, X.; Yao, J.; Qi, Q.; Cao, Z. Preparation of Thermoresponsive Poly( *N* -vinylcaprolactam- *Co*- 2-methoxyethyl Acrylate) Nanogels via Inverse Miniemulsion Polymerization. *J Appl Polym Sci* **2019**, *136* (46), 48237. https://doi.org/10.1002/app.48237.

(47) Deng, Y.; Wang, L.; Yang, W.; Fu, S.; Elaïssari, A. Preparation of Magnetic Polymeric Particles via Inverse Microemulsion Polymerization Process. *J. Magn. Magn. Mater.* **2003**, *257* (1), 69–78. https://doi.org/10.1016/S0304-8853(02)00987-3.

(48) Nicolas, J.; Guillaneuf, Y.; Lefay, C.; Bertin, D.; Gigmes, D.; Charleux, B. Nitroxide-Mediated Polymerization. *Prog. Polym. Sci.* **2013**, *38* (1), 63–235. https://doi.org/10.1016/j.progpolymsci.2012.06.002.

(49) Ouchi, M.; Terashima, T.; Sawamoto, M. Transition Metal-Catalyzed Living Radical Polymerization: Toward Perfection in Catalysis and Precision Polymer Synthesis. *Chem. Rev.* **2009**, *109* (11), 4963–5050. https://doi.org/10.1021/cr900234b.

(50) Braunecker, W. A.; Matyjaszewski, K. Controlled/Living Radical Polymerization: Features, Developments, and Perspectives. *Prog. Polym. Sci.* **2007**, *32* (1), 93–146. https://doi.org/10.1016/j.progpolymsci.2006.11.002.

(51) Matyjaszewski, K.; Gaynor, S.; Wang, J.-S. Controlled Radical Polymerizations: The Use of Alkyl Iodides in Degenerative Transfer. *Macromolecules* **1995**, *28* (6), 2093–2095. https://doi.org/10.1021/ma00110a050.

(52) Lacroix-Desmazes, P.; Severac, R.; Boutevin, B. Reverse Iodine Transfer Polymerization of Methyl Acrylate and *n* -Butyl Acrylate. *Macromolecules* **2005**, *38* (15), 6299–6309. https://doi.org/10.1021/ma050056j.

(53) Chiefari, J.; Chong, Y. K. (Bill); Ercole, F.; Krstina, J.; Jeffery, J.; Le, T. P. T.; Mayadunne, R. T. A.; Meijs, G. F.; Moad, C. L.; Moad, G.; Rizzardo, E.; Thang, S. H. Living Free-Radical Polymerization by Reversible Addition−Fragmentation Chain Transfer: The RAFT Process. *Macromolecules* **1998**, *31* (16), 5559–5562. https://doi.org/10.1021/ma9804951.

(54) *Handbook of RAFT Polymerization*; Barner-Kowollik, C., Ed.; Wiley-VCH: Weinheim, 2008.

(55) Bannister, I.; Billingham, N. C.; Armes, S. P. Monte Carlo Modelling of Living Branching Copolymerisation of Monovinyl and Divinyl Monomers: Comparison of Simulated and Experimental Data for ATRP Copolymerisation of Methacrylic Monomers. *Soft Matter* **2009**, *5* (18), 3495. https://doi.org/10.1039/b901892a.

(56) Favier, A.; Charreyre, M.-T. Experimental Requirements for an Efficient Control of Free-Radical Polymerizations via the Reversible Addition-Fragmentation Chain Transfer (RAFT) Process. *Macromol. Rapid Commun.* **2006**, *27* (9), 653–692. https://doi.org/10.1002/marc.200500839.

(57) Oh, J. K.; Tang, C.; Gao, H.; Tsarevsky, N. V.; Matyjaszewski, K. Inverse Miniemulsion ATRP: A New Method for Synthesis and Functionalization of Well-Defined Water-Soluble/Cross-Linked Polymeric Particles. *J. Am. Chem. Soc.* **2006**, *128* (16), 5578–5584. https://doi.org/10.1021/ja060586a.

(58) Delaittre, G.; Nicolas, J.; Lefay, C.; Save, M.; Charleux, B. Surfactant-Free Synthesis of Amphiphilic Diblock Copolymer Nanoparticles via Nitroxide-Mediated Emulsion Polymerization. *Chem. Commun.* **2005**, No. 5, 614. https://doi.org/10.1039/b415959d.

(59) Brusseau, S.; D'Agosto, F.; Magnet, S.; Couvreur, L.; Chamignon, C.; Charleux, B. Nitroxide-Mediated Copolymerization of Methacrylic Acid and Sodium 4-Styrenesulfonate in Water Solution and One-Pot Synthesis of Amphiphilic Block Copolymer Nanoparticles. *Macromolecules* **2011**, *44* (14), 5590–5598. https://doi.org/10.1021/ma2008282.

(60) Groison, E.; Brusseau, S.; D'Agosto, F.; Magnet, S.; Inoubli, R.; Couvreur, L.; Charleux, B. Well-Defined Amphiphilic Block Copolymer Nanoobjects via Nitroxide-Mediated Emulsion Polymerization. *ACS Macro Lett.* **2012**, *1* (1), 47–51. https://doi.org/10.1021/mz200035b.

(61) Kim, K. H.; Kim, J.; Jo, W. H. Preparation of Hydrogel Nanoparticles by Atom Transfer Radical Polymerization of N-Isopropylacrylamide in Aqueous Media Using PEG Macro-Initiator. *Polymer* **2005**, *46* (9), 2836–2840. https://doi.org/10.1016/j.polymer.2005.02.009.

(62) Sugihara, S.; Armes, S. P.; Lewis, A. L. One-Pot Synthesis of Biomimetic Shell Cross-Linked Micelles and Nanocages by ATRP in Alcohol/Water Mixtures. *Angew. Chem. Int. Ed.***2010**, *49* (20), 3500–3503. https://doi.org/10.1002/anie.201000095.

(63) Sugihara, S.; Sugihara (nee Nishikawa), K.; Armes, S. P.; Ahmad, H.; Lewis, A. L. Synthesis of Biomimetic Poly(2-(Methacryloyloxy)Ethyl Phosphorylcholine) Nanolatexes via Atom Transfer Radical Dispersion Polymerization in Alcohol/Water Mixtures. *Macromolecules* **2010**, *43* (15), 6321–6329. https://doi.org/10.1021/ma101136v.

(64) Moad, G.; Rizzardo, E.; Thang, S. H. Living Radical Polymerization by the RAFT Process—A First Update. *Aust. J. Chem.* **2006**, *59* (10), 669. https://doi.org/10.1071/CH06250.

(65) Rieger, J. Guidelines for the Synthesis of Block Copolymer Particles of Various Morphologies by RAFT Dispersion Polymerization. *Macromol. Rapid Commun.* **2015**, *36* (16), 1458–1471. https://doi.org/10.1002/marc.201500028.

(66) Charleux, B.; Delaittre, G.; Rieger, J.; D'Agosto, F. Polymerization-Induced Self-Assembly: From Soluble Macromolecules to Block Copolymer Nano-Objects in One Step. *Macromolecules* **2012**, *45* (17), 6753–6765. https://doi.org/10.1021/ma300713f.

(67) Sun, J.-T.; Hong, C.-Y.; Pan, C.-Y. Recent Advances in RAFT Dispersion Polymerization for Preparation of Block Copolymer Aggregates. *Polym. Chem.* **2013**, *4* (4), 873–881. https://doi.org/10.1039/C2PY20612A.

(68) Derry, M. J.; Fielding, L. A.; Armes, S. P. Polymerization-Induced Self-Assembly of Block Copolymer Nanoparticles via RAFT Non-Aqueous Dispersion Polymerization. *Prog. Polym. Sci.* **2016**, *52*, 1–18. https://doi.org/10.1016/j.progpolymsci.2015.10.002.

(69) Chong, ) Y. K.; Le, T. P. T.; Moad, G.; Rizzardo, E.; Thang, S. H. A More Versatile Route to Block Copolymers and Other Polymers of Complex Architecture by Living Radical Polymerization: The RAFT Process. *Macromolecules* **1999**, *32* (6), 2071–2074. https://doi.org/10.1021/ma981472p.

(70) Hill, M. R.; Carmean, R. N.; Sumerlin, B. S. Expanding the Scope of RAFT Polymerization: Recent Advances and New Horizons. *Macromolecules* **2015**, *48* (16), 5459–5469. https://doi.org/10.1021/acs.macromol.5b00342.

(71) Le, D.; Keller, D.; Delaittre, G. Reactive and Functional Nanoobjects by Polymerization-Induced Self-Assembly. *Macromol. Rapid Commun.* **2019**, *40* (2), 1800551. https://doi.org/10.1002/marc.201800551.

(72) D'Agosto, F.; Rieger, J.; Lansalot, M. RAFT-Mediated Polymerization-Induced Self-Assembly. *Angew. Chem. Int. Ed.* **2020**, *59* (22), 8368–8392. https://doi.org/10.1002/anie.201911758.

(73) Hatton, F. L.; Lovett, J. R.; Armes, S. P. Synthesis of Well-Defined Epoxy-Functional Spherical Nanoparticles by RAFT Aqueous Emulsion Polymerization. *Polym. Chem.* **2017**, *8* (33), 4856–4868. https://doi.org/10.1039/C7PY01107E.

(74) Sugihara, S.; Blanazs, A.; Armes, S. P.; Ryan, A. J.; Lewis, A. L. Aqueous Dispersion Polymerization: A New Paradigm for in Situ Block Copolymer Self-Assembly in Concentrated Solution. *J. Am. Chem. Soc*. **2011**, *133* (39), 15707–15713. https://doi.org/10.1021/ja205887v.

(75) Ma, K.; Xu, Y.; An, Z. Templateless Synthesis of Polyacrylamide-Based Nanogels via RAFT Dispersion Polymerization. *Macromol. Rapid Commun.* **2015**, *36* (6), 566–570. https://doi.org/10.1002/marc.201400730.

(76) Qu, T.; Wang, A.; Yuan, J.; Gao, Q. Preparation of an Amphiphilic Triblock Copolymer with PH- and Thermo-Responsiveness and Self-Assembled Micelles Applied to Drug Release. *J. Colloid Interface Sci.* **2009**, *336* (2), 865–871. https://doi.org/10.1016/j.jcis.2009.04.001.

(77) Zhao, C.; Zhuang, X.; He, P.; Xiao, C.; He, C.; Sun, J.; Chen, X.; Jing, X. Synthesis of Biodegradable Thermo- and PH-Responsive Hydrogels for Controlled Drug Release. *Polymer* **2009**, *50* (18), 4308–4316. https://doi.org/10.1016/j.polymer.2009.07.010.

(78) Huo, D.; Li, Y.; Qian, Q.; Kobayashi, T. Temperature–PH Sensitivity of Bovine Serum Albumin Protein-Microgels Based on Cross-Linked Poly(N-Isopropylacrylamide-Co-Acrylic Acid). *Colloids Surf. B: Biointerfaces* **2006**, *50* (1), 36–42. https://doi.org/10.1016/j.colsurfb.2006.03.020.

(79) Schmaljohann, D. Thermo- and PH-Responsive Polymers in Drug Delivery☆. *Advanced Drug Delivery Reviews* **2006**, *58* (15), 1655–1670. https://doi.org/10.1016/j.addr.2006.09.020.

(80) Hajebi, S.; Rabiee, N.; Bagherzadeh, M.; Ahmadi, S.; Rabiee, M.; Roghani-Mamaqani, H.; Tahriri, M.; Tayebi, L.; Hamblin, M. R. Stimulus-Responsive Polymeric Nanogels as Smart Drug Delivery Systems. *Acta Biomaterialia* **2019**, *92*, 1–18. https://doi.org/10.1016/j.actbio.2019.05.018.

(81) Ekkelenkamp, A. E.; Elzes, M. R.; Engbersen, J. F. J.; Paulusse, J. M. J. Responsive Crosslinked Polymer Nanogels for Imaging and Therapeutics Delivery. *J. Mater. Chem. B* **2018**, *6* (2), 210–235. https://doi.org/10.1039/C7TB02239E.

(82) Soni, G.; Yadav, K. S. Nanogels as Potential Nanomedicine Carrier for Treatment of Cancer: A Mini Review of the State of the Art. *Saudi Pharm J* **2016**, *24* (2), 133–139. https://doi.org/10.1016/j.jsps.2014.04.001.

(83) Roy, D.; Brooks, W. L. A.; Sumerlin, B. S. New Directions in Thermoresponsive Polymers. *Chem. Soc. Rev.* **2013**, *42* (17), 7214. https://doi.org/10.1039/c3cs35499g.

(84) Gandhi, A.; Paul, A.; Sen, S. O.; Sen, K. K. Studies on Thermoresponsive Polymers: Phase Behaviour, Drug Delivery and Biomedical Applications. *Asian J. Pharm. Sci.* **2015**, *10* (2), 99–107. https://doi.org/10.1016/j.ajps.2014.08.010.

(85) Ward, M. A.; Georgiou, T. K. Thermoresponsive Polymers for Biomedical Applications. *Polymers* **2011**, *3* (3), 1215–1242. https://doi.org/10.3390/polym3031215.

(86) Gibson, M. I.; O'Reilly, R. K. To Aggregate, or Not to Aggregate? Considerations in the Design and Application of Polymeric Thermally-Responsive Nanoparticles. *Chem. Soc. Rev.* **2013**, *42* (17), 7204–7213. https://doi.org/10.1039/C3CS60035A.

(87) Zarrintaj, P.; Jouyandeh, M.; Ganjali, M. R.; Hadavand, B. S.; Mozafari, M.; Sheiko, S. S.; Vatankhah-Varnoosfaderani, M.; Gutiérrez, T. J.; Saeb, M. R. Thermo-Sensitive Polymers in Medicine: A Review. *Eur. Polym. J.* **2019**, *117*, 402–423. https://doi.org/10.1016/j.eurpolymj.2019.05.024.

(88) Nadeem, N.; Sohail, M.; Hassan Bin Asad, M. H.; Minhas, M. U.; Mudassir; Shah, S. A. Thermosensitive Hydrogels:From Bench to Market. *Current Science* **2018**, *114* (11), 2256. https://doi.org/10.18520/cs/v114/i11/2256-2266.

(89) Talelli, M.; Hennink, W. E. Thermosensitive Polymeric Micelles for Targeted Drug Delivery. *Nanomedicine* **2011**, *6* (7), 1245–1255. https://doi.org/10.2217/nnm.11.91.

(90) Seuring, J.; Bayer, F. M.; Huber, K.; Agarwal, S. Upper Critical Solution Temperature of Poly( *N* -Acryloyl Glycinamide) in Water: A Concealed Property. *Macromolecules* **2012**, *45* (1), 374–384. https://doi.org/10.1021/ma202059t.

(91) Liu, X. The Effect of Salt and PH on the Phase-Transition Behaviors of Temperature-Sensitive Copolymers Based on N-Isopropylacrylamide. *Biomaterials* **2004**, *25* (25), 5659–5666. https://doi.org/10.1016/j.biomaterials.2004.01.019.

(92) Wanka, G.; Hoffmann, H.; Ulbricht, W. The Aggregation Behavior of Poly-(Oxyethylene)-Poly-(Oxypropylene)-Poly-(Oxyethylene)-Block-Copolymers in Aqueous Solution. *Colloid & Polymer Sci* **1990**, *268* (2), 101–117. https://doi.org/10.1007/BF01513189.

(93) Jeong, B.; Kim, S. W.; Bae, Y. H. Thermosensitive Sol–Gel Reversible Hydrogels. *Adv. Drug Deliv. Rev.* **2012**, *64*, 154–162. https://doi.org/10.1016/j.addr.2012.09.012.

(94) Deng, J.; Shi, Y.; Jiang, W.; Peng, Y.; Lu, L.; Cai, Y. Facile Synthesis and Thermoresponsive Behaviors of a Well-Defined Pyrrolidone Based Hydrophilic Polymer. *Macromolecules* **2008**, *41* (9), 3007–3014. https://doi.org/10.1021/ma800145s.

(95) Aseyev, V.; Tenhu, H.; Winnik, F. M. Non-Ionic Thermoresponsive Polymers in Water. *Self Organized Nanostructures of Amphiphilic Block Copolymers II*, **2011**, 29–89.

(96) Aoshima, S.; Kanaoka, S. Synthesis of Stimuli-Responsive Polymers by Living Polymerization: Poly(N-Isopropylacrylamide) and Poly(Vinyl Ether)s. In *Wax Crystal Control · Nanocomposites · Stimuli-Responsive Polymers*; Advances in Polymer Science; Springer Berlin Heidelberg: Berlin, Heidelberg, 2007; Vol. 210, pp 169–208. https://doi.org/10.1007/12_2007_120.

(97) Aseyev, V. O.; Tenhu, H.; Winnik, F. M. Temperature Dependence of the Colloidal Stability of Neutral AmphiphilicPolymers in Water. *Conformation-Dependent Design of Sequences in Copolymers II*, 2006, 1–85.

(98) Dimitrov, I.; Trzebicka, B.; Müller, A. H. E.; Dworak, A.; Tsvetanov, C. B. Thermosensitive Water-Soluble Copolymers with Doubly Responsive Reversibly Interacting Entities. *Prog. Polym. Sci.***2007**, *32* (11), 1275–1343. https://doi.org/10.1016/j.progpolymsci.2007.07.001.

(99) Wang, X.; Qiu, X.; Wu, C. Comparison of the Coil-to-Globule and the Globule-to-Coil Transitions of a Single Poly( *N* -Isopropylacrylamide) Homopolymer Chain in Water. *Macromolecules* **1998**, *31* (9), 2972–2976. https://doi.org/10.1021/ma971873p.

(100) Wu, C.; Wang, X. Globule-to-Coil Transition of a Single Homopolymer Chain in Solution. *Phys. Rev. Lett.* **1998**, *80* (18), 4092–4094. https://doi.org/10.1103/PhysRevLett.80.4092.

(101) Lu, Y.; Zhou, K.; Ding, Y.; Zhang, G.; Wu, C. Origin of Hysteresis Observed in Association and Dissociation of Polymer Chains in Water. *Phys. Chem. Chem. Phys.* **2010**, *12* (13), 3188. https://doi.org/10.1039/b918969f.

(102) Cheng, H.; Shen, L.; Wu, C. LLS and FTIR Studies on the Hysteresis in Association and Dissociation of Poly( *N*- Isopropylacrylamide) Chains in Water. *Macromolecules* **2006**, *39* (6), 2325–2329. https://doi.org/10.1021/ma052561m.

(103) Brazel, C. S.; Peppas, N. A. Synthesis and Characterization of Thermo- and Chemomechanically Responsive Poly(N-Isopropylacrylamide-Co-Methacrylic Acid) Hydrogels. *Macromolecules* **1995**, *28* (24), 8016–8020. https://doi.org/10.1021/ma00128a007.

(104) Allan S. Hoffman; Patrick S. Stayton; Volga Bulmus. Really Smart Bioconjugates of Smart Polymers and Receptor Proteins. *J Biomed Mater Res* **2000**, *52* (4), 577–586. https://doi.org/10.1002/1097-4636(20001215)52:4<577::AID-JBM1>3.0.CO;2-5.

(105) Liu, H. Y.; Zhu, X. X. Lower Critical Solution Temperatures of N -Substituted Acrylamide Copolymers in Aqueous Solutions. *Polymer* **1999**, *40* (25), 6985–6990. https://doi.org/10.1016/S0032-3861(98)00858-1.

(106) Chen, G.; Hoffman, A. S. Temperature-Induced Phase Transition Behaviors of Random vs. Graft Copolymers of N-Isopropylacrylamide and Acrylic Acid. *Macromol. Rapid Commun.* **1995**, *16* (3), 175–182. https://doi.org/10.1002/marc.1995.030160304.

(107) Bokias, G.; Staikos, G.; Iliopoulos, I. Solution Properties and Phase Behaviour of Copolymers of Acrylic Acid with N -Isopropylacrylamide: The Importance of the Intrachain Hydrogen Bonding. *Polymer* **2000**, *41* (20), 7399–7405. https://doi.org/10.1016/S0032-3861(00)00090-2.

(108) Zhao, J.; Zhang, G.; Pispas, S. Morphological Transitions in Aggregates of Thermosensitive Poly(Ethylene Oxide)- *b* -Poly( *N* -Isopropylacrylamide) Block Copolymers Prepared via RAFT Polymerization: Morphological Transitions in PEO- *b* -PNIPAM. *J. Polym. Sci. A Polym. Chem.* **2009**, *47* (16), 4099–4110. https://doi.org/10.1002/pola.23470.

(109) LaFreniere, J.; Roberge, E.; Ren, T.; Seitz, W. R.; Balog, E. R. M.; Halpern, J. M. Insights on the Lower Critical Solution Temperature Behavior of PNIPAM in an Applied Electric Field. *ECS Trans.* **2020**, *97* (7), 709–715. https://doi.org/10.1149/09707.0709ecst.

(110) Kano, M.; Kokufuta, E. On the Temperature-Responsive Polymers and Gels Based on *N* -Propylacrylamides and *N* -Propylmethacrylamides †. *Langmuir* **2009**, *25* (15), 8649–8655. https://doi.org/10.1021/la804286j.

(111) Maeda, Y.; Nakamura, T.; Ikeda, I. Changes in the Hydration States of Poly( *N* -Alkylacrylamide)s during Their Phase Transitions in Water Observed by FTIR Spectroscopy †. *Macromolecules* **2001**, *34* (5), 1391–1399. https://doi.org/10.1021/ma001306t.

(112) Ito, D.; Kubota, K. Solution Properties and Thermal Behavior of Poly( *N* - *n* -Propylacrylamide) in Water. *Macromolecules* **1997**, *30* (25), 7828–7834. https://doi.org/10.1021/ma971005s.

(113) Ito, D.; Kubota, K. Thermal Response of Poly(N-n-Propylacrylamide). *Polym J* **1999**, *31* (3), 254–257. https://doi.org/10.1295/polymj.31.254.

(114) Schild, H. G.; Tirrell, D. A. Microcalorimetric Detection of Lower Critical Solution Temperatures in Aqueous Polymer Solutions. *J. Phys. Chem.* **1990**, *94* (10), 4352–4356. https://doi.org/10.1021/j100373a088.

(115) Netopilík, M.; Bohdanecký, M.; Chytrý, V.; Ulbrich, K. Cloud Point of Poly(N-Isopropylmethacrylamide) Solutions in Water: Is It Really a Point? *Macromol. Rapid Commun.* **1997**, *18* (2), 107–111. https://doi.org/10.1002/marc.1997.030180206.

(116) Zhou, K.; Lu, Y.; Li, J.; Shen, L.; Zhang, G.; Xie, Z.; Wu, C. The Coil-to-Globule-to-Coil Transition of Linear Polymer Chains in Dilute Aqueous Solutions: Effect of Intrachain Hydrogen Bonding. *Macromolecules* **2008**, *41* (22), 8927–8931. https://doi.org/10.1021/ma8019128.

(117) Tong, Z.; Zeng, F.; Zheng, X.; Sato, T. Inverse Molecular Weight Dependence of Cloud Points for Aqueous Poly( *N* -Isopropylacrylamide) Solutions. *Macromolecules* **1999**, *32* (13), 4488–4490. https://doi.org/10.1021/ma990062d.

(118) Ishizone, T.; Seki, A.; Hagiwara, M.; Han, S.; Yokoyama, H.; Oyane, A.; Deffieux, A.; Carlotti, S. Anionic Polymerizations of Oligo(Ethylene Glycol) Alkyl Ether Methacrylates: Effect of Side Chain Length and ω-Alkyl Group of Side Chain on Cloud Point in Water. *Macromolecules* **2008**, *41* (8), 2963–2967. https://doi.org/10.1021/ma702828n.

(119) Lutz, J.-F.; Akdemir, Ö.; Hoth, A. Point by Point Comparison of Two Thermosensitive Polymers Exhibiting a Similar LCST: Is the Age of Poly(NIPAM) Over? *J. Am. Chem. Soc.* **2006**, *128* (40), 13046–13047. https://doi.org/10.1021/ja065324n.

(120) Lutz, J.-F. Polymerization of Oligo(Ethylene Glycol) (Meth)Acrylates: Toward New Generations of Smart Biocompatible Materials. *J. Polym. Sci. A Polym. Chem.* **2008**, *46* (11), 3459–3470. https://doi.org/10.1002/pola.22706.

(121) Lutz, J.-F.; Hoth, A. Preparation of Ideal PEG Analogues with a Tunable Thermosensitivity by Controlled Radical Copolymerization of 2-(2-Methoxyethoxy)Ethyl Methacrylate and Oligo(Ethylene Glycol) Methacrylate. *Macromolecules* **2006**, *39* (2), 893–896. https://doi.org/10.1021/ma0517042.

(122) Mertoglu, M.; Garnier, S.; Laschewsky, A.; Skrabania, K.; Storsberg, J. Stimuli Responsive Amphiphilic Block Copolymers for Aqueous Media Synthesised via Reversible Addition Fragmentation Chain Transfer Polymerisation (RAFT). *Polymer* **2005**, *46* (18), 7726–7740. https://doi.org/10.1016/j.polymer.2005.03.101.

(123) Seuring, J.; Agarwal, S. Polymers with Upper Critical Solution Temperature in Aqueous Solution. *Macromol. Rapid Commun.* **2012**, *33* (22), 1898–1920. https://doi.org/10.1002/marc.201200433.

(124) Fu, W.; Zhao, B. Thermoreversible Physically Crosslinked Hydrogels from UCST-Type Thermosensitive ABA Linear Triblock Copolymers. *Polym. Chem.* **2016**, *7* (45), 6980–6991. https://doi.org/10.1039/C6PY01517D.

(125) Mary, P.; Bendejacq, D. D.; Labeau, M.-P.; Dupuis, P. Reconciling Low- and High-Salt Solution Behavior of Sulfobetaine Polyzwitterions. *J. Phys. Chem. B* **2007**, *111* (27), 7767–7777. https://doi.org/10.1021/jp071995b.

(126) Schulz, D. N.; Peiffer, D. G.; Agarwal, P. K.; Larabee, J.; Kaladas, J. J.; Soni, L.; Handwerker, B.; Garner, R. T. Phase Behaviour and Solution Properties of Sulphobetaine Polymers. *Polymer* **1986**, *27* (11), 1734–1742. https://doi.org/10.1016/0032-3861(86)90269-7.

(127) Huglin, M. B.; Radwan, M. A. Unperturbed Dimensions of a Zwitterionic Polymethacrylate. *Polym. Int.* **1991**, *26* (2), 97–104. https://doi.org/10.1002/pi.4990260208.

(128) Willcock, H.; Lu, A.; Hansell, C. F.; Chapman, E.; Collins, I. R.; O'Reilly, R. K. One-Pot Synthesis of Responsive Sulfobetaine Nanoparticles by RAFT Polymerisation: The Effect of Branching on the UCST Cloud Point. *Polym. Chem.* **2014**, *5* (3), 1023–1030. https://doi.org/10.1039/C3PY00998J.

(129) Woodfield, P. A.; Zhu, Y.; Pei, Y.; Roth, P. J. Hydrophobically Modified Sulfobetaine Copolymers with Tunable Aqueous UCST through Postpolymerization Modification of Poly(Pentafluorophenyl Acrylate). *Macromolecules* **2014**, *47* (2), 750–762. https://doi.org/10.1021/ma402391a.

(130) Hildebrand, V.; Laschewsky, A.; Päch, M.; Müller-Buschbaum, P.; Papadakis, C. M. Effect of the Zwitterion Structure on the Thermo-Responsive Behaviour of Poly(Sulfobetaine Methacrylates). *Polym. Chem.* **2017**, *8* (1), 310–322. https://doi.org/10.1039/C6PY01220E.

(131) Haas, H. C.; Schuler, N. W. Thermally Reversible Homopolymer Gel Systems. *J. Polym. Sci. B Polym. Lett.* **1964**, *2* (12), 1095–1096. https://doi.org/10.1002/pol.1964.110021203.

(132) Seuring, J.; Agarwal, S. Non-Ionic Homo- and Copolymers with H-Donor and H-Acceptor Units with an UCST in Water. *Macromol. Chem. Phys.* **2010**, *211* (19), 2109–2117. https://doi.org/10.1002/macp.201000147.

(133) Liu, F.; Seuring, J.; Agarwal, S. Controlled Radical Polymerization of *N* -Acryloylglycinamide and UCST-Type Phase Transition of the Polymers. *J. Polym. Sci. A Polym. Chem.* **2012**, *50* (23), 4920–4928. https://doi.org/10.1002/pola.26322.

(134) Käfer, F.; Lerch, A.; Agarwal, S. Tunable, Concentration-Independent, Sharp, Hysteresis-Free UCST Phase Transition from Poly( *N* -Acryloyl Glycinamide-Acrylonitrile) System. *J. Polym. Sci. Part A: Polym. Chem.* **2017**, *55* (2), 274–279. https://doi.org/10.1002/pola.28374.

(135) Seuring, J.; Agarwal, S. First Example of a Universal and Cost-Effective Approach: Polymers with Tunable Upper Critical Solution Temperature in Water and Electrolyte Solution. *Macromolecules* **2012**, *45* (9), 3910–3918. https://doi.org/10.1021/ma300355k.

(136) Sun, W.; An, Z.; Wu, P. Hydrogen Bonding Reinforcement as a Strategy to Improve Upper Critical Solution Temperature of Poly( *N* -Acryloylglycinamide- *Co* -Methacrylic Acid). *Polym. Chem.* **2018**, *9* (26), 3667–3673. https://doi.org/10.1039/C8PY00733K.

(137) Hirokazu NAGAOKA; Noriyuki OHNSHI; Masaru EGUCHI. THERMORESPONSIVE POLYMER AND PRODUCTION METHOD THEREOF. US 2007/0203313 A1.

(138) Asadujjaman, A.; Kent, B.; Bertin, A. Phase Transition and Aggregation Behaviour of an UCST-Type Copolymer Poly(Acrylamide-Co-Acrylonitrile) in Water: Effect of Acrylonitrile Content, Concentration in Solution, Copolymer Chain Length and Presence of Electrolyte. *Soft Matter* **2017**, *13* (3), 658–669. https://doi.org/10.1039/C6SM02262F.

(139) Käfer, F.; Liu, F.; Stahlschmidt, U.; Jérôme, V.; Freitag, R.; Karg, M.; Agarwal, S. LCST and UCST in One: Double Thermoresponsive Behavior of Block Copolymers of Poly(Ethylene Glycol) and Poly(Acrylamide -*Co*- Acrylonitrile). *Langmuir* **2015**, *31* (32), 8940–8946. https://doi.org/10.1021/acs.langmuir.5b02006.

(140) Saeki, S.; Kuwahara, N.; Nakata, M.; Kaneko, M. Upper and Lower Critical Solution Temperatures in Poly (Ethylene Glycol) Solutions. *Polymer* **1976**, *17* (8), 685–689. https://doi.org/10.1016/0032-3861(76)90208-1.

(141) Zhang, H.; Tong, X.; Zhao, Y. Diverse Thermoresponsive Behaviors of Uncharged UCST Block Copolymer Micelles in Physiological Medium. *Langmuir* **2014**, *30* (38), 11433–11441. https://doi.org/10.1021/la5026334.

(142) Zhao, C.; Dolmans, L.; Zhu, X. X. Thermoresponsive Behavior of Poly(Acrylic Acid- *Co* -Acrylonitrile) with a UCST. *Macromolecules* **2019**, *52* (12), 4441–4446. https://doi.org/10.1021/acs.macromol.9b00794.

(143) Shimada, N.; Ino, H.; Maie, K.; Nakayama, M.; Kano, A.; Maruyama, A. Ureido-Derivatized Polymers Based on Both Poly(Allylurea) and Poly( L -Citrulline) Exhibit UCST-Type Phase Transition Behavior under Physiologically Relevant Conditions. *Biomacromolecules* **2011**, *12* (10), 3418–3422. https://doi.org/10.1021/bm2010752.

(144) Shimada, N.; Sasaki, T.; Kawano, T.; Maruyama, A. Rational Design of UCST-Type Ureido Copolymers Based on a Hydrophobic Parameter. *Biomacromolecules* **2018**, *19* (10), 4133–4138. https://doi.org/10.1021/acs.biomac.8b01152.

(145) Canning, S. L.; Smith, G. N.; Armes, S. P. A Critical Appraisal of RAFT-Mediated Polymerization-Induced Self-Assembly. *Macromolecules* **2016**, *49* (6), 1985–2001. https://doi.org/10.1021/acs.macromol.5b02602.

(146) Warren, N. J.; Armes, S. P. Polymerization-Induced Self-Assembly of Block Copolymer Nano-Objects via RAFT Aqueous Dispersion Polymerization. *J. Am. Chem. Soc*. **2014**, *136* (29), 10174–10185. https://doi.org/10.1021/ja502843f.

(147) Xu, Y.; Li, Y.; Cao, X.; Chen, Q.; An, Z. Versatile RAFT Dispersion Polymerization in Cononsolvents for the Synthesis of Thermoresponsive Nanogels with Controlled Composition, Functionality and Architecture. *Polym. Chem.* **2014**, *5* (21), 6244–6255. https://doi.org/10.1039/C4PY00867G.

(148) Piogé, S.; Tran, T. N.; McKenzie, T. G.; Pascual, S.; Ashokkumar, M.; Fontaine, L.; Qiao, G. Sono-RAFT Polymerization-Induced Self-Assembly in Aqueous Dispersion: Synthesis of LCST-Type Thermosensitive Nanogels. *Macromolecules* **2018**, *51* (21), 8862–8869. https://doi.org/10.1021/acs.macromol.8b01606.

(149) Figg, C. A.; Simula, A.; Gebre, K. A.; Tucker, B. S.; Haddleton, D. M.; Sumerlin, B. S. Polymerization-Induced Thermal Self-Assembly (PITSA). *Chem. Sci.* **2015**, *6* (2), 1230–1236. https://doi.org/10.1039/C4SC03334E.

(150) Truong, N. P.; Whittaker, M. R.; Anastasaki, A.; Haddleton, D. M.; Quinn, J. F.; Davis, T. P. Facile Production of Nanoaggregates with Tuneable Morphologies from Thermoresponsive P(DEGMA-Co-HPMA). *Polym. Chem.* **2016**, *7* (2), 430–440. https://doi.org/10.1039/C5PY01467K.

(151) Truong, N. P.; Quinn, J. F.; Anastasaki, A.; Haddleton, D. M.; Whittaker, M. R.; Davis, T. P. Facile Access to Thermoresponsive Filomicelles with Tuneable Cores. *Chem.Commun.* **2016**, *52* (24), 4497–4500. https://doi.org/10.1039/C6CC00900J.

(152) Canning, S. L.; Smith, G. N.; Armes, S. P. A Critical Appraisal of RAFT-Mediated Polymerization-Induced Self-Assembly. *Macromolecules* **2016**, *49* (6), 1985–2001. https://doi.org/10.1021/acs.macromol.5b02602.

(153) Wang, X.; An, Z. New Insights into RAFT Dispersion Polymerization-Induced Self-Assembly: From Monomer Library, Morphological Control, and Stability to Driving Forces. *Macromol. Rapid Commun.* **2019**, *40* (2), 1800325. https://doi.org/10.1002/marc.201800325.

(154) Penfold, N. J. W.; Yeow, J.; Boyer, C.; Armes, S. P. Emerging Trends in Polymerization-Induced Self-Assembly. *ACS Macro Lett.* **2019**, *8* (8), 1029–1054. https://doi.org/10.1021/acsmacrolett.9b00464.

(155) Delaittre, G.; Save, M.; Charleux, B. Nitroxide-Mediated Aqueous Dispersion Polymerization: From Water-Soluble Macroalkoxyamine to Thermosensitive Nanogels. *Macromol. Rapid Commun.* **2007**, *28* (15), 1528–1533. https://doi.org/10.1002/marc.200700230.

(156) Lu, Y.; Wittemann, A.; Ballauff, M.; Drechsler, M. Preparation of Polystyrene-Poly(N-Isopropylacrylamide) (PS-PNIPA) Core-Shell Particles by Photoemulsion Polymerization. *Macromol. Rapid Commun.* **2006**, *27* (14), 1137–1141. https://doi.org/10.1002/marc.200600190.

(157) Rajan, R.; Matsumura, K. Tunable Dual-Thermoresponsive Core-Shell Nanogels Exhibiting UCST and LCST Behavior. *Macromol. Rapid Commun.* **2017**, *38* (22), 1700478. https://doi.org/10.1002/marc.201700478.

(158) An, Z.; Shi, Q.; Tang, W.; Tsung, C.-K.; Hawker, C. J.; Stucky, G. D. Facile RAFT Precipitation Polymerization for the Microwave-Assisted Synthesis of Well-Defined, Double Hydrophilic Block Copolymers and Nanostructured Hydrogels. *J. Am. Chem. Soc.* **2007**, *129* (46), 14493–14499. https://doi.org/10.1021/ja0756974.

(159) Rieger, J.; Grazon, C.; Charleux, B.; Alaimo, D.; Jérôme, C. Pegylated Thermally Responsive Block Copolymer Micelles and Nanogels via *in Situ* RAFT Aqueous Dispersion Polymerization. *Journal of Polymer Science Part A: Polym. Chem.* **2009**, *47* (9), 2373–2390. https://doi.org/10.1002/pola.23329.

(160) Steinhauer, W.; Hoogenboom, R.; Keul, H.; Moeller, M. Copolymerization of 2-Hydroxyethyl Acrylate and 2-Methoxyethyl Acrylate via RAFT: Kinetics and Thermoresponsive Properties. *Macromolecules* **2010**, *43* (17), 7041–7047. https://doi.org/10.1021/ma101122b.

(161) Lavigueur, C.; García, J. G.; Hendriks, L.; Hoogenboom, R.; Cornelissen, J. J. L. M.; Nolte, R. J. M. Thermoresponsive Giant Biohybrid Amphiphiles. *Polym. Chem.* **2011**, *2* (2), 333–340. https://doi.org/10.1039/C0PY00229A.

(162) Shen, W.; Chang, Y.; Liu, G.; Wang, H.; Cao, A.; An, Z. Biocompatible, Antifouling, and Thermosensitive Core−Shell Nanogels Synthesized by RAFT Aqueous Dispersion Polymerization. *Macromolecules* **2011**, *44* (8), 2524–2530. https://doi.org/10.1021/ma200074n.

(163) Li, Y.; Ye, Z.; Shen, L.; Xu, Y.; Zhu, A.; Wu, P.; An, Z. Formation of Multidomain Hydrogels via Thermally Induced Assembly of PISA-Generated Triblock Terpolymer Nanogels. *Macromolecules* **2016**, *49* (8), 3038–3048. https://doi.org/10.1021/acs.macromol.5b02538.

(164) Fu, W.; Luo, C.; Morin, E. A.; He, W.; Li, Z.; Zhao, B. UCST-Type Thermosensitive Hairy Nanogels Synthesized by RAFT Polymerization-Induced Self-Assembly. *ACS Macro Letters* **2017**, *6* (2), 127–133. https://doi.org/10.1021/acsmacrolett.6b00888.

(165) Yu, X.; Liu, J.; Xin, Y.; Zhan, M.; Xiao, J.; Lu, L.; Peng, S. Temperature and Salt Responsive Zwitterionic Polysulfamide-Based Nanogels with Surface Regeneration Ability and Controlled Drug Release. *Polym. Chem.* **2019**, *10* (47), 6423–6431. https://doi.org/10.1039/C9PY01548E.

(166) Yu, L.; Zhang, Y.; Dai, X.; Zhang, L.; Tan, J. Monodisperse Poly(Methyl Methacrylate) Microspheres with Tunable Carboxyl Groups on the Surface Obtained by Photoinitiated RAFT Dispersion Polymerization. *Chem. Commun.* **2019**, *55* (54), 7848–7851. https://doi.org/10.1039/C9CC03452H.

(167) Zhang, Y.; Cremer, P. Interactions between Macromolecules and Ions: The Hofmeister Series. *Curr Opin Chem Biol* **2006**, *10* (6), 658–663. https://doi.org/10.1016/j.cbpa.2006.09.020.

(168) Ohshio, M.; Ishihara, K.; Maruyama, A.; Shimada, N.; Yusa, S. Synthesis and Properties of Upper Critical Solution Temperature Responsive Nanogels. *Langmuir* **2019**, *35* (22), 7261–7267. https://doi.org/10.1021/acs.langmuir.9b00849.

(169) Augé, A.; Camerel, F.; Benoist, A.; Zhao, Y. Near-Infrared Light-Responsive UCST-Nanogels Using an Efficient Nickel-Bis(Dithiolene) Photothermal Crosslinker. *Polym. Chem.* **2020**, *11* (23), 3863–3875. https://doi.org/10.1039/D0PY00567C.

(170) Binauld, S.; Stenzel, M. H. Acid-Degradable Polymers for Drug Delivery: A Decade of Innovation. *Chem. Commun.* **2013**, *49* (21), 2082. https://doi.org/10.1039/c2cc36589h.

(171) Gao, W.; Chan, J. M.; Farokhzad, O. C. PH-Responsive Nanoparticles for Drug Delivery. *Mol. Pharmaceutics* **2010**, *7* (6), 1913–1920. https://doi.org/10.1021/mp100253e.

(172) Kamaly, N.; Yameen, B.; Wu, J.; Farokhzad, O. C. Degradable Controlled-Release Polymers and Polymeric Nanoparticles: Mechanisms of Controlling Drug Release. *Chem. Rev.* **2016**, *116* (4), 2602–2663. https://doi.org/10.1021/acs.chemrev.5b00346.

(173) Cordes, E. H.; Bull, H. G. Mechanism and Catalysis for Hydrolysis of Acetals, Ketals, and Ortho Esters. *Chem. Rev.* **1974**, *74* (5), 581–603. https://doi.org/10.1021/cr60291a004.

(174) Cordes, E. H.; Jencks, W. P. On the Mechanism of Schiff Base Formation and Hydrolysis. *J. Am. Chem. Soc.* **1962**, *84* (5), 832–837. https://doi.org/10.1021/ja00864a031.

(175) Yildiz, I. A DFT Approach to the Mechanistic Study of Hydrozone Hydrolysis. *J. Phys. Chem. A* **2016**, *120* (20), 3683–3692. https://doi.org/10.1021/acs.jpca.6b02882.

(176) Chen, W.; Hou, Y.; Tu, Z.; Gao, L.; Haag, R. PH-Degradable PVA-Based Nanogels via Photo-Crosslinking of Thermo-Preinduced Nanoaggregates for Controlled Drug Delivery. *JCR* **2017**, *259*, 160–167. https://doi.org/10.1016/j.jconrel.2016.10.032.

(177) Banerjee, R.; Parida, S.; Maiti, C.; Mandal, M.; Dhara, D. PH-Degradable and Thermoresponsive Water-Soluble Core Cross-Linked Polymeric Nanoparticles as Potential Drug Delivery Vehicle for Doxorubicin. *RSC Adv.* **2015**, *5* (102), 83565–83575. https://doi.org/10.1039/C5RA17158J.

(178) Jackson, A. W.; Fulton, D. A. Triggering Polymeric Nanoparticle Disassembly through the Simultaneous Application of Two Different Stimuli. *Macromolecules* **2012**, *45* (6), 2699–2708. https://doi.org/10.1021/ma202721s.

(179) Sponchioni, M.; Rodrigues Bassam, P.; Moscatelli, D.; Arosio, P.; Capasso Palmiero, U. Biodegradable Zwitterionic Nanoparticles with Tunable UCST-Type Phase Separation under Physiological Conditions. *Nanoscale* **2019**, *11* (35), 16582–16591. https://doi.org/10.1039/C9NR04311J.

(180) Bingham, N. M.; Nisa, Q. un; Chua, S. H. L.; Fontugne, L.; Spick, M. P.; Roth, P. J. Thioester-Functional Polyacrylamides: Rapid Selective Backbone Degradation Triggers Solubility Switch Based on Aqueous Lower Critical Solution Temperature/Upper Critical Solution Temperature. *ACS Appl. Polym. Mater.* **2020**, *2* (8), 3440–3449. https://doi.org/10.1021/acsapm.0c00503.

(181) Zhang, Z.; Li, H.; Kasmi, S.; Van Herck, S.; Deswarte, K.; Lambrecht, B. N.; Hoogenboom, R.; Nuhn, L.; De Geest, B. G. A Synthetic, Transiently Thermoresponsive Homopolymer with UCST Behaviour within a Physiologically Relevant Window. *Angew. Chem. Int. Ed.* **2019**, *58* (23), 7866–7872. https://doi.org/10.1002/anie.201900224.

# CHAPTER II

# SYNTHESIS AND CHAIN EXTENSION OF PPEGA MACROMOLECULAR CHAIN TRANSFER AGENTS

## 2.1 Introduction

Poly(ethylene glycol) (PEG) is a hydrophilic, biocompatible polymer widely used in the biopharmaceutical and biomedical fields to increase the stealth of bioactive molecules such as proteins, peptides and biopolymers. Covalent conjugation of PEG to a therapeutic agent, *i.e.* PEGylation, helps prolong blood circulation lifetimes, improve passive targeting, and decrease proteolysis and renal excretion of the agent, thereby allowing a reduced therapeutic dosing frequency[1]. Resulting bioconjugates show changes in their physical characteristics depending on the PEG architecture (linear, branched, comb-like, cyclic, multi-arm and dendronized PEGs).[2]

Reversible deactivation radical polymerization (RDRP) techniques are particularly well suited to enable precise control over the architecture, molar mass, and dispersity of PEG polymers. RAFT polymerization has been employed to induce PEGylation through the polymerization of PEG macromomers, such as oligo(ethylene glycol) methyl ether acrylate, also called poly(ethylene glycol) methyl ether acrylate (PEGA).[3–10] The relevance of RAFT in the elaboration of well-defined polymers for PEGylation is due to both the absence of cytotoxic metal catalysts and the functionality that can be introduced into the CTA to allow various coupling chemistries at the R or Z moieties for subsequent conjugation.[6,11–13] A precise control over the end-group functionality of the PPEGA polymer is nontrivial due to the fact that the radical polymerization of acrylate monomers is strongly affected by radical transfer events, where the presence of mid-chain radicals caused by backbiting or intermolecular radical transfer leads to branching of the polymer chain.[14–16] Additionally, intermolecular chain transfer and termination through combination can result in chains of high molar mass and broadening of molar mass distributions.[16] The undesirable branching phenomenon is exacerbated by high polymerization temperatures, low monomer concentrations (<3 wt.%) and/or

high conversions,[16] and has been previously observed in the literature for the PPEGA polymer. Zhao *et al.* optimized the synthesis of PPEGA employing water as the predominant co-solvent with dioxane to induce acceleration of the polymerization kinetics in order to offset the retardation effects associated with lowering the temperature (44 °C) and initiator loading.[17] Under these polymerization conditions, a very high percentage of theoretical living chains was observed; moreover, the high molar mass shoulder ascribed to chain transfer side reactions (exhibited at higher temperatures) could be minimized, especially if the reaction is stopped at moderate monomer conversion (67%). In general, PEGA polymerizations are usually stopped at low-to-moderate monomer conversion to preserve a high proportion of living chain ends and low dispersity, despite the associated waste of the monomeric product which necessitates dialysis.[3,4,13,18] Motivated by the wide utility of brush PPEGA and the relative synthetic strategies reported in the literature, we sought to expand the arsenal of RAFT polymerization techniques to synthesize this high-value hydrophilic material. In this chapter, the RAFT polymerization of the PEGA will be conducted using various initiating radical sources: thermal activation and UV-light irradiation to target well-defined PPEGAs with high chain-end fidelity at high monomer conversion. The optimized conditions will then be used to synthesize a wide range of PPEGA with different number-average polymerization degrees ($\overline{DP_n}$) which will be used for the subsequent elaboration of nanogels in Chapters 3 and 4.

## 2.2 Synthesis of PPEGA macromolecular chain transfer by RAFT polymerization*

A chain transfer agent, namely 2-cyano-5-oxo-5-(prop-2-yn-1-ylamino)pentan-2-yl dodecyltrithiocarbonate (COPYDC) was employed, which is synthesized as described in the literature.[10] This compound contains an alkyne R-group and a trithiocarbonate Z-group. The alkyne group is linked *via* an amide functionality. The stability of the alkyne bond could avoid side reactions during the polymerization, and the amide group is a robust functionality that can resist to hydrolysis in view of further (biological) applications in aqueous media. The alkyne group can react with a thiol by thiol-yne coupling reaction to functionalize the $\alpha$-position and the trithiocarbonate group can be removed thanks to a radical process to functionalize the $\omega$-position of the RAFT-synthesized polymer.[10]

* A part of this study has been published in *Polymer Chemistry* (A.R. Mazo *et al. Polym. Chem.* **2020**, **11**, 5238-5248).

## 2.2.1 PPEGA obtained by thermally-initiated RAFT polymerization (named Thermal-PPEGA)[†]

A lot of literature works report the synthesis of PPEGA by thermally-initiated RAFT polymerization[3–10] in organic or aqueous media, through the use of initiators which decomposition temperatures varied from 40 °C to 70 °C. In the present work, given the hydrophobicity of the COPYDC, the PEGA polymerization was performed in *N,N*-dimethylformamide (DMF) at 70 °C with the use of 4,4'-azobis(4-cyanovaleric acid) (ACVA) as an initiator. Our aim was to optimize the thermally-initiated RAFT polymerization of PEGA by investigating the impact of $[PEGA]_0/[COPYDC]_0$ initial molar ratio on the control of polymerization.

### 2.2.1.1 Impact of the $[PEGA]_0/[COPYDC]_0$ initial molar ratio

Scheme II.1 shows thermally-initiated RAFT polymerization of PEGA using COPYDC as CTA, ACVA as initiator in DMF at 70°C. During the course of the RAFT polymerizations, aliquots were taken to monitor the PEGA conversion by $^1$H-NMR spectroscopy by comparing the integration values of the formamide proton of DMF at 8.02 ppm and of the alkene protons of PEGA between 5.7 and 6.5 ppm. The number-average molar mass ($\overline{M_{n,\,SEC}}$) and dispersity (Đ) values are obtained by size exclusion chromatography (SEC) in THF using polystyrene (PSt) standards.

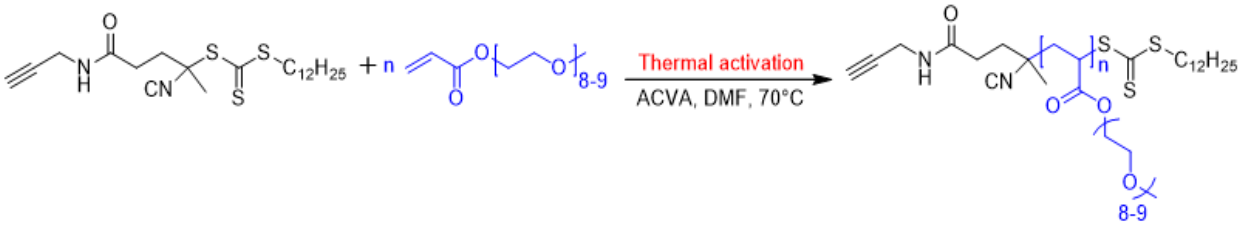


Scheme II.1**.** Thermally-initiated RAFT polymerization of PEGA using COPYDC as CTA, ACVA as initiator in DMF at 70°C.

Different $[PEGA]_0/[COPYDC]_0$ initial molar ratios were studied for the RAFT polymerization using a constant initial concentration of PEGA ($[PEGA]_0$ = 1.45 M), a constant $[COPYDC]_0/[ACVA]_0$ initial molar ratio of 1/0.1 and changing the $[PEGA]_0/[COPYDC]_0$ initial molar ratio (50/1, 60/1 and 80/1). The influence of the $[PEGA]_0/[COPYDC]_0$ initial molar ratio on the polymerization kinetics, the $\overline{M_{n,\,SEC}}$ and *Đ* evolutions with PEGA conversion were studied. The Figure II.1 shows the comparison of the evolution of $\ln([M]_0/[M]_t)$ and conversion *vs.* time of three RAFT polymerizations of PEGA with

[†] Thermal-PPEGA: PPEGA was synthesized through thermally-initiated RAFT polymerization. Wenhao Zhang is thanked for his contribution about the kinetic study of PEGA polymerization with $[PEGA]_0/[COPYDC]_0$ initial molar ratio of 80/1.

$[PEGA]_0/[COPYDC]_0$ initial molar ratio of 50/1, 60/1 and 80/1. An inhibition period has been observed whatever the $[PEGA]_0/[COPYDC]_0$ initial molar ratio and is shorter for the higher $[PEGA]_0/[COPYC]_0$ initial molar ratio: this result is consistent with a RAFT polymerization process.[19] The possible explanations are based on slow fragmentation, slow re-initiation by the expelled radical, and the ability of the propagating radical to add to the CTA rather than to monomer. Monteiro *et al.*[20] also postulate an additional and overriding mechanism to explain the retardation in rate, namely intermediate radical termination of the radicals. In our experiments, after the inhibition period, a constant slope of $\ln([M]_0/[M]_t)$ *vs.* time, in agreement with a constant concentration of propagating radicals, was observed up to 74%, 64% and 53% PEGA conversions for $[PEGA]_0/[COPYDC]_0$ equal to 50/1, 60/1 and 80/1, respectively.

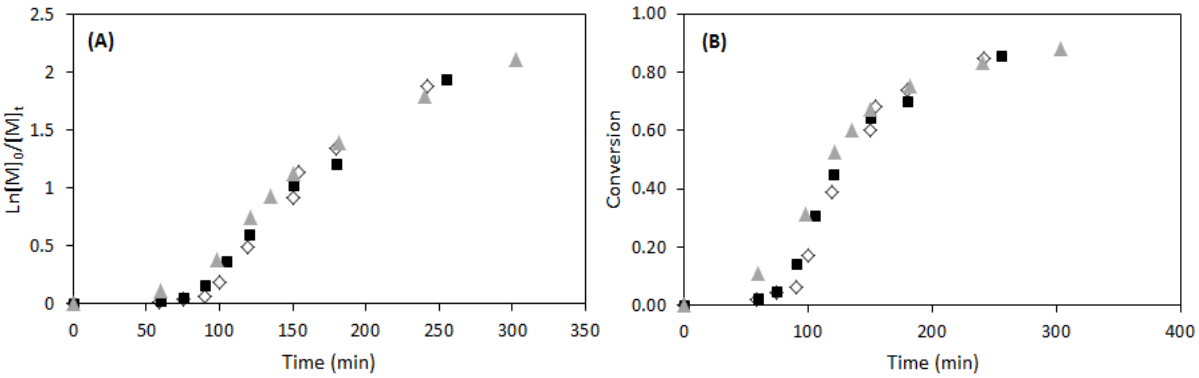


Figure II.1**.** Evolution of $\ln([M]_0/[M]_t)$ (A) and conversion (B) *versus* time during the RAFT polymerization of PEGA mediated through ACVA and COPYDC in DMF at 70°C, $[PEGA]_0/[COPYDC]_0/[ACVA]_0$ = 50/1/0.1 (◇), $[PEGA]_0/[COPYDC]_0/[ACVA]_0$ = 60/1/0.1 (■) and $[PEGA]_0/[COPYDC]_0/[ACVA]_0$ = 80/1/0.1 (▲).

The influence of the $[PEGA]_0/[COPYDC]_0$ initial molar ratio on the evolution of $\overline{M_{n,SEC}}$ and *Đ* with PEGA conversion was studied. Figure II.2 illustrates the evolution of $\overline{M_{n,SEC}}$ and *Đ versus* PEGA conversion and highlights an increase of $\overline{M_{n,SEC}}$ with PEGA conversion. The increase of the initial molar ratio of $[PEGA]_0/[COPYDC]_0$ led to the loss of control of the polymerization as shown by the kinetic study (Figure II.1) and by the discrepancy between $\overline{M_{n,SEC}}$ and $\overline{M_{n,theo}}$ ($\overline{M_{n,theo}} = \frac{[PEGA]_0}{[COPYDC]_0} \times conv \times \overline{M_{n,PEGA}} + M_{COPYDC}$ where conv is the PEGA conversion) and higher *Đ* values (Figure II.2). Therefore, the polymerization of PEGA for $[PEGA]_0/[COPYDC]_0$ = 50/1 is no longer controlled beyond 180 min (at 74% PEGA conversion). However, this critical time for $[PEGA]_0/[COPYDC]_0$ = 60/1 is 150 min, at 64% PEGA conversion and decrease to 120 min for $[PEGA]_0/[COPYDC]_0$ = 80/1 at PEGA conversion of 53%. Whatever the initial molar ratio of $[PEGA]_0/[COPYDC]_0$ studied, at higher PEGA conversions, the $\overline{M_{n,SEC}}$ of resulting PPEGAs seem to remain stable, which is expected due to side reactions such as irreversible terminations or irreversible transfer reactions. Additionally, the

discrepancy between $\overline{M_{n,SEC}}$ and $\overline{M_{n,theo}}$ is also due to the SEC calibration as the hydrodynamic volume of PS, used for SEC calibration, is different from the hydrodynamic volume of branched PPEGA in THF. A decrease of the apparent propagation rate constant was also observed (Figure II.1A) with a sharp increase in *Đ* values (Figure II.2B). This is probably due to side reactions coming from irreversible bimolecular termination by coupling. However, low dispersity values (*Đ* < 1.2) for PPEGA can be obtained for PEGA conversion up to 74% using a $[PEGA]_0/[COPYDC]_0/[ACVA]_0$ initial ratio of 50/1/0.1.

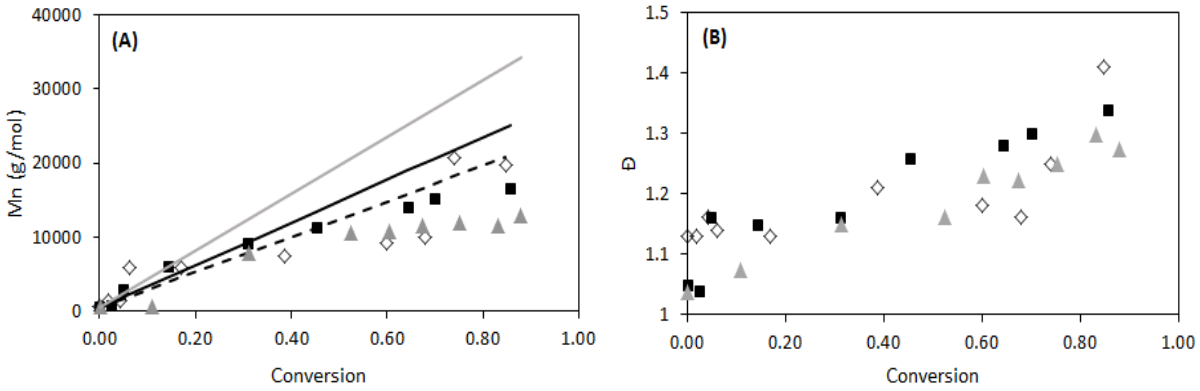


Figure II.2. Evolution of (A) $\overline{M_{n,SEC}}$ (symbol) and $\overline{M_{n,theo}}$ (line) and, (B) *Đ versus* PEGA conversion of thermally-initiated RAFT polymerizations of PEGA mediated through ACVA and COPYDC in DMF at 70°C, $[PEGA]_0/[COPYDC]_0/[ACVA]_0$ = 50/1/0.1 (◇), $[PEGA]_0/[COPYDC]_0/[ACVA]_0$ = 60/1/0.1 (■) and $[PEGA]_0/[COPYDC]_0/[ACVA]_0$ = 80/1/0.1 (▲).

The SEC traces of crude polymerization media (Figure II.3) show a decrease in the intensity of the PEGA signal as the reaction proceeds. However, at the higher conversions tested, asymmetric chromatograms were observed where the emergence of a high molar mass shoulder could be evidenced at lower elution times. Again bimolecular coupling terminations or intramolecular and intermolecular transfer events known for radical polymerization of acrylates operate.[19] The Perrier's group[17] showed that a reduction in the ratio of the initiator to CTA employed in the PEGA polymerization, as well as a careful choice of the initiator with longer radical half-life (*i.e.*, lower decomposition rate), led to a lower extent of bimolecular termination. Nonetheless, these formulation steps failed to eliminate the high molar mass shoulder observed in PPEGA.[13] The authors showed that only by targeting a much lower temperature (from 70 to 44 °C) and stopping the reaction at 67% conversion could suppress polymer branching and/or bimolecular coupling terminations.[13] These actions are in line with the literature on acrylate polymerizations, where it has been noted that chain transfer to the polymer is vastly decreased upon decreasing temperature, or by targeting high monomer concentrations and low conversions. Very low monomer concentrations

cause an increase in the concentration of mid-chain radicals, and the probability of β-scission is also greater under these conditions.[16]

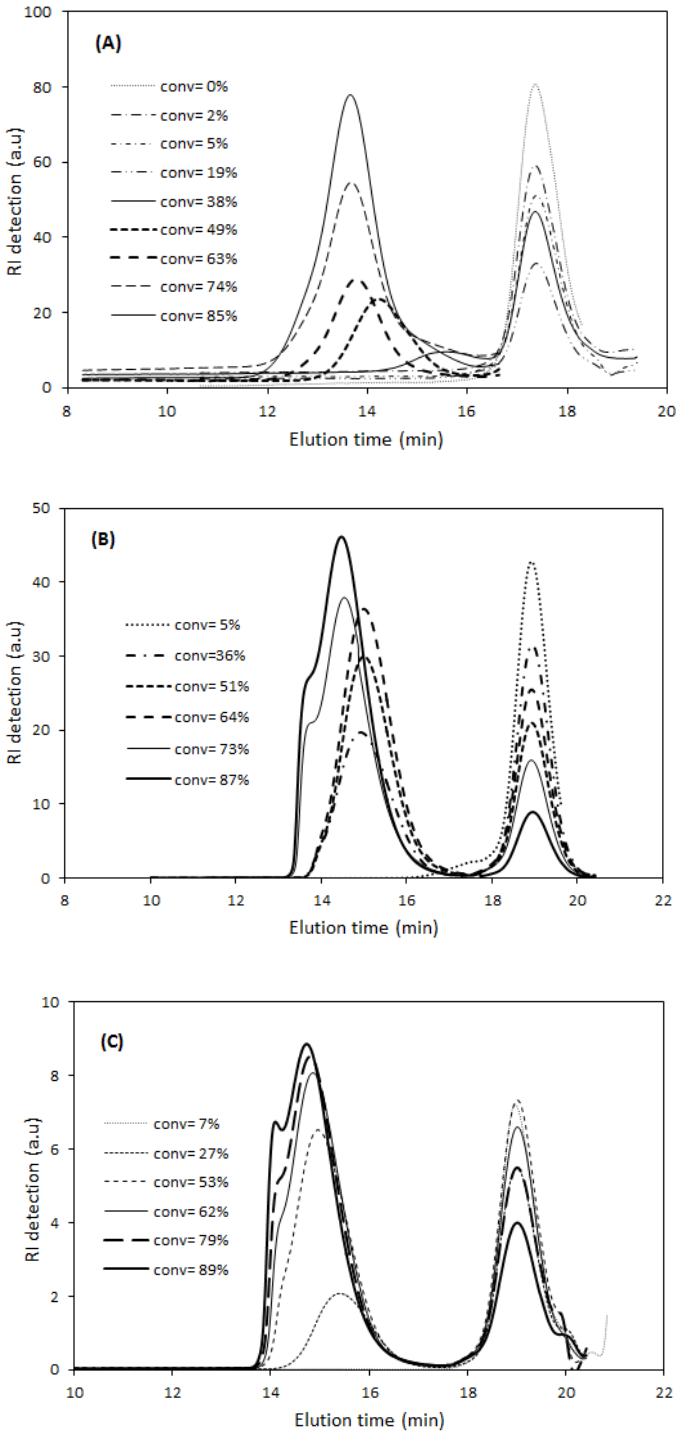


Figure II.3. Overlaid SEC traces of crude polymerization media using RI detection obtained at different PEGA conversions of thermally-initiated RAFT polymerization of PEGA mediated through ACVA and COPYDC in DMF ($[PEGA]_0$ = 1.45 M) at 70°C at various initial molar ratios $[PEGA]_0/[COPYDC]_0$ = 50/1 (A), 60/1 (B) and 80/1 (C).

To conclude on this part, the optimized synthesis conditions to target well-defined Thermal-PPEGA through thermally-initiated RAFT polymerization of PEGA is an initial $[PEGA]_0/[COPYDC]_0/[ACVA]_0$ ratio of 50/1/0.1, a monomer concentration of 1.45 M in DMF at 70°C and stopping the reaction at PEGA conversions below 74%. These conditions were used in the following part in order to synthesize a range of Thermal-PPEGA with variable $\overline{DP_{n,PPEGA}}$.

### 2.2.1.2 Synthesis of Thermal-PPEGA with different $\overline{DP_n}$

Well-defined Thermal-PPEGAs with different $\overline{DP_n}$ were targeted using the optimized experimental conditions defined in previous §II.1.a. RAFT polymerizations of PEGA were performed using the $[PEGA]_0/[COPYDC]_0/[AVCA]_0$ initial molar ratio of 50/1/0.1 with the monomer concentration of 1.45 M in DMF at 70°C and stopping the reaction at PEGA conversions below 74%. The PEGA conversion was determined by $^1$H-NMR analysis of the crude reaction mixture. Final crude reaction mixtures were purified by dialysis in pure water during 3 days and freeze-dried. The pure Thermal-PPEGAs obtained were analyzed by $^1$H-NMR spectroscopy to determine experimental $\overline{DP_{n,PPEGA}}$ and by SEC in THF to determine $\overline{M_{n,SEC}}$ and dispersity. One purified Thermal-PPEGA is employed as an example to show the detailed calculation to determine the experimental $\overline{DP_{n,PPEGA}}$ by $^1$H-HMR spectroscopy. The $^1$H NMR spectrum (Figure II.4) shows the characteristic signals of the $CH_2CH_2O$ of the EO repeating unit at 3.65 ppm (labeled e and f in Figure II.4) of Thermal-PPEGA. The singlet at 3.38 ppm corresponds to the methyl protons $(CH_2CH_2O)_8CH_3$ of the repeating units of PPEGA (labeled g in Figure II.4). The triplet at 0.88 ppm is characteristic of the methyl protons of the dodecyl chain (labeled a in Figure II.4). The $\overline{DP_{n,PPEGA}}$ was calculated by comparing the integration values of the methyl protons of the dodecyl chains (3 protons, labeled a in Figure II.4) with the integration values of the methylene protons $C(=O)OCH_2CH_2O(CH_2CH_2O)_8$ and $HC{\equiv}CCH_2NH$ (2n+2 protons, labeled d and h in Figure II.4, respectively). The $\overline{DP_{n,PPEGA}}$ is equal to 20.

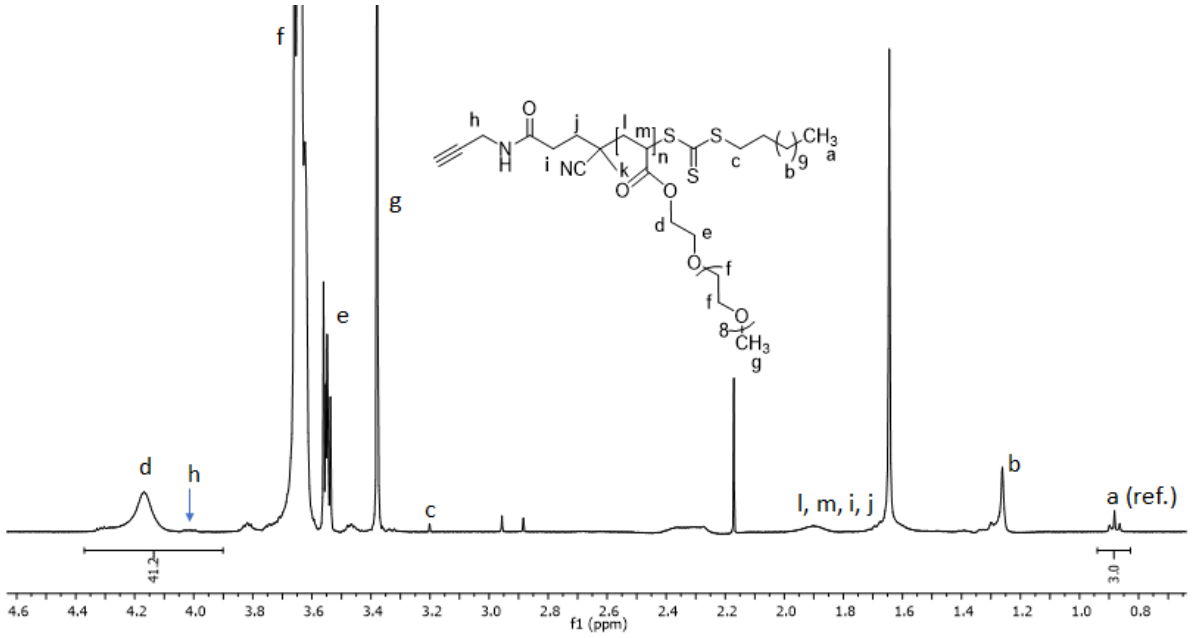


Figure II.4. $^{1}$H-NMR spectrum (400 MHz, $CDCl_3$) of a purified Thermal-PPEGA synthesized by thermally-initiated RAFT polymerization of PEGA using ACVA and COPYDC ($[PEGA]_0/[COPYDC]_0/[ACVA]_0$ = 50/1/0.1, $[PEGA]_0$ = 1.45 M) in DMF at 70°C after 2h of reaction.

The SEC trace of the above purified Thermal-PPEGA of $\overline{DP_{n,PPEGA}}$ equal to 20 using the RI detection shows an unimodal and narrow signal with $\overline{M_{n,SEC}}$ = 10 400 g.mol$^{-1}$ (PS equivalents) and $Đ$ = 1.18 (Figure II.5). As shown on SEC analysis using UV-vis detection (Figure II.5), the Thermal-$PPEGA_{20}$ absorbs at 309 nm which is the characteristic wavelength of the trithiocarbonate end-group associated with the n–π* transition of C=S bond.

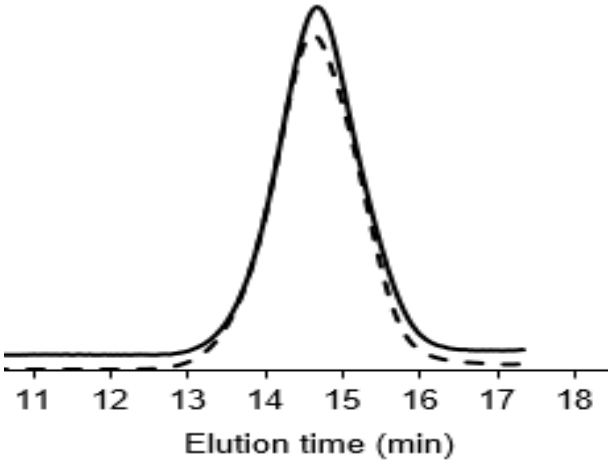


Figure II.5. Overlaid SEC traces of purified Thermal-$PPEGA_{20}$ using RI detection (line) and UV-vis detection (dash line) at 309 nm obtained by thermally-initiated RAFT polymerization of PEGA using ACVA and COPYDC ($[PEGA]_0/[COPYDC]_0/[ACVA]_0$ = 50/1/0.1, $[PEGA]_0$ = 1.45 M) in DMF at 70°C after 2h of reaction.

The macromolecular characteristics of Thermal-PPEGAs with different $\overline{DP_{n,PPEGA}}$ obtained through thermally-initiated RAFT polymerizations of PEGA are summarized in Table II.1.

Table II.1. Macromolecular characteristics of Thermal-PPEGAs synthesized through thermally-initiated RAFT polymerization in DMF at 70°C with $[PEGA]_0/[COPYDC]_0/[AVCA]_0$ = 50/1/0.1 with $[PEGA]_0$ = 1.45 M.

| Run | Time (h) | Conv. (%)[a] | $\overline{DP_{n,PPEGA}}$[b] | $\overline{M_{n,theo}}$[c] (g.mol$^{-1}$) | $\overline{M_{n,SEC}}$[d] (g.mol$^{-1}$) | $Đ$[d] |
|---|---|---|---|---|---|---|
| 1 | 1.5 | 17 | 7 | 3800 | 4000 | 1.13 |
| 2 | 1.67 | 40 | 15 | 7640 | 7500 | 1.13 |
| 3 | 2 | 42 | 20 | 10840 | 10400 | 1.18 |
| 4 | 2.4 | 60 | 24 | 11960 | 9300 | 1.23 |
| 5 | 2.5 | 62 | 30 | 14840 | 10600 | 1.22 |

[a] Determined by $^1$H NMR spectroscopy (200 MHz, $CDCl_3$) by comparing the integration values of the formamide proton of DMF at 8.02 ppm and of the alkene protons of PEGA between 5.7 and 6.5 ppm. [b] Determined by $^1$H-NMR spectroscopy (400 MHz, $CDCl_3$). [c] $\overline{M_{n,theo}} = \frac{[\mathrm{PEGA}]_0}{[\mathrm{COPYDC}]_0} \times \mathrm{conv} \times \overline{M_{n,PEGA}} + M_{COPYDC}$ where conv is the PEGA conversion, $\overline{M_{n,PEGA}}$ is the number-average molar mass of PEGA ($\overline{M_{PEGA}}$ = 480 g.mol$^{-1}$) and $M_{COPYDC}$ = 440 g.mol$^{-1}$. [d] Determined by SEC in THF using PSt equivalents.

The results in Table II.1 show the increase of $\overline{DP_{n,PPEGA}}$ and $\overline{M_{n,SEC}}$ with time and monomer conversion. The dispersity is also lower at lower PEGA conversions. Generally, the RAFT polymerization of PEGA with initial molar ratio $[PEGA]_0/[COPYDC]_0$ = 50/1 shows a good control at low PEGA conversion (<74%). Desiring to target well-defined PPEGAs at near-total PEGA conversion and knowing that at low temperatures side reactions including irreversible transfer reactions are reduced, RAFT polymerizations of PEGA were then studied at room temperature. Therefore, the activation mode was switch to UV-light initiation mode.

## 2.2.2 PPEGA obtained by UV-light initiated RAFT polymerization (named UV-PPEGA)[‡]

Interestingly, the UV-light initiated polymerization of butyl acrylate has been found to yield polymers with a very low degree of branching, five-fold lower than that with comparable thermally-initiated polymerization.[21] For this reason, we switched to this method of initiation in order to carry out the reaction at room temperature, to verify whether a low reaction temperature could improve polymerization control. In addition to reaction temperature, monomer concentration plays an important role to limit side reactions during the RAFT polymerization of acrylates.[19] Particularly, in solution polymerization of acrylic monomer, where monomer concentration is lower (< 3 wt.%), the relative rate of backbiting is higher and thus a higher amount of mid-chain radicals is produced.[16] Hence, in this part, we conducted the RAFT polymerization with different PEGA initial concentrations to investigate how the monomer concentration can impact the formation of PPEGA through UV-light initiated RAFT polymerization at room temperature (25°C).

### 2.2.2.1 Impact of the PEGA initial concentration

The UV-light initiated polymerization of PEGA was carried out in the presence of COPYDC in DMF with various initial concentrations of monomer ($[PEGA]_0$ = 0.39 M, 1.42 M and 5 M) using an initial molar ratio $[PEGA]_0/[COPYDC]_0/[Initiator]_0$ of 50/1/0.1 and a UV lamp source (λ = 365 nm, P = 34 mW/cm$^2$). 2-hydroxy-4'-(2-hydroxyethoxy)-2-methylpropiophenone (photo-I) was used as a water-soluble photoinitiator and the polymerizations were conducted at 25 °C. Kinetic plots for UV-light initiated RAFT polymerizations were obtained by withdrawn samples at different time intervals. As shown in Figure II.6, a fast initial rate of polymerization was observed: approximately 80% conversion are reached after 100 min under UV irradiation (in comparison, 250 min for thermally-initiated RAFT polymerization) for the polymerization with PEGA initial concentration of 1.42 M. The inhibition period is longer for lower PEGA initial concentration. For example, the inhibition time changes from 30 min to 60 min when initial concentration of PEGA changes from 5 M to 0.39 M. A constant slope of $\ln([M]_0/[M]_t)$ *vs.* reaction time, relevant with a constant concentration of propagating radicals, is observed till 54 %, 68 % and 72 % PEGA conversion for the polymerization with PEGA initial concentration of 0.39 M, 1.42 M and 5 M, respectively. However, as in thermally-initiated RAFT polymerization, a decrease of the apparent propagation rate constant was observed at higher PEGA conversions.

[‡] UV-PPEGA: PPEGA was obtained via UV-light initiated RAFT polymerization. Yuwen MENG is thanked for her contribution to this work.

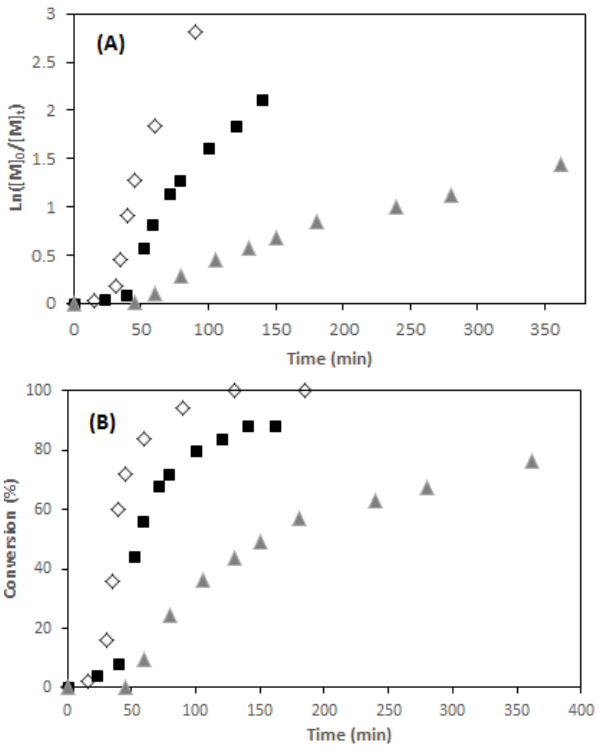


Figure II.6. Evolution of $\ln([M]_0/[M]_t)$ (A) and conversion (B) *versus* time during the UV-light initiated RAFT polymerization of PEGA using photo-I and COPYDC in DMF at 25 °C, $[PEGA]_0$ = 5 M (◇), $[PEGA]_0$ = 1.42 M (■) and $[PEGA]_0$ = 0.39M (▲).

As shown in Figure II.7, an increase of $\overline{M_{n,SEC}}$ and *Đ* with PEGA conversion whatever the initial PEGA concentration. Dispersity values of the obtained UV-PPEGA were relatively low (*Đ* ≤ 1.3) for PEGA conversion below 80%. Moreover, for a similar PEGA conversion, such values were generally lower using $[PEGA]_0$ = 5 M in comparison with $[PEGA]_0$ = 0.39 M and 1.42 M. This is consistent with previously reported studies by Ballard *et al.*: lower monomer concentration leads to higher relative rate of irreversible transfer reaction (backbiting) and thus a greater fraction of mid-chain radicals is produced.[16]

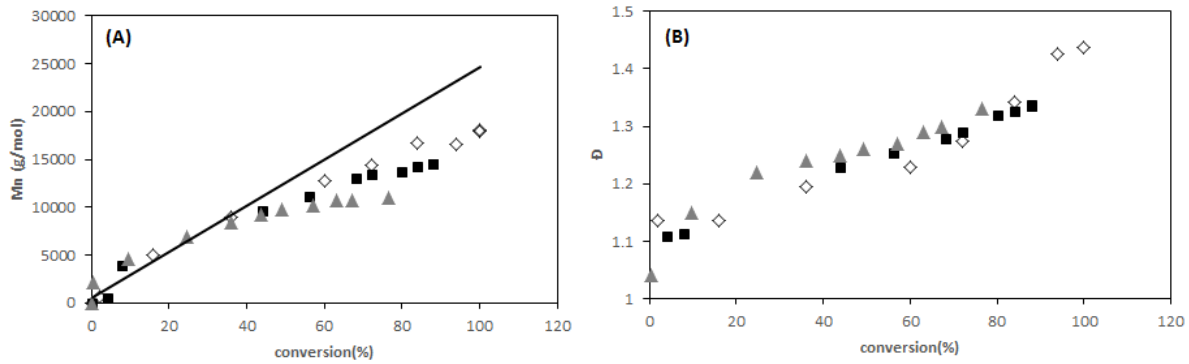

Figure II.7. Evolution of $\overline{M_{n,SEC}}$ (symbol) and $\overline{M_{n,theo}}$ (line) (A) and $Đ$ (B) obtained by SEC (THF) *versus* PEGA conversion of RAFT polymerizations of PEGA using photo-I and COPYDC in DMF at 25 °C, $[PEGA]_0$ = 5 M (◇), $[PEGA]_0$ = 1.42 M (■) and $[PEGA]_0$ = 0.39M (▲).

Figure II.8 shows the evolution of SEC traces of crude polymerization mixtures with PEGA conversion for different $[PEGA]_0$. A decrease in the intensity of the PEGA signal is observed as the reaction proceeds. Moreover, SEC traces of resulting PPEGAs showed symmetrical monomodal peaks that shift to higher molar mass with increasing PEGA conversion up to 60, 68, and 76 % at $[PEGA]_0$ = 5 M, 1.42 M, and 0.39 M, respectively (Figure II.8A, B and C). At higher PEGA conversions, the presence of shoulders at high molecular weights was observed (Figure II.8 A and B) due to irreversible termination reactions and/or irreversible chain transfer reaction during PEGA polymerization.

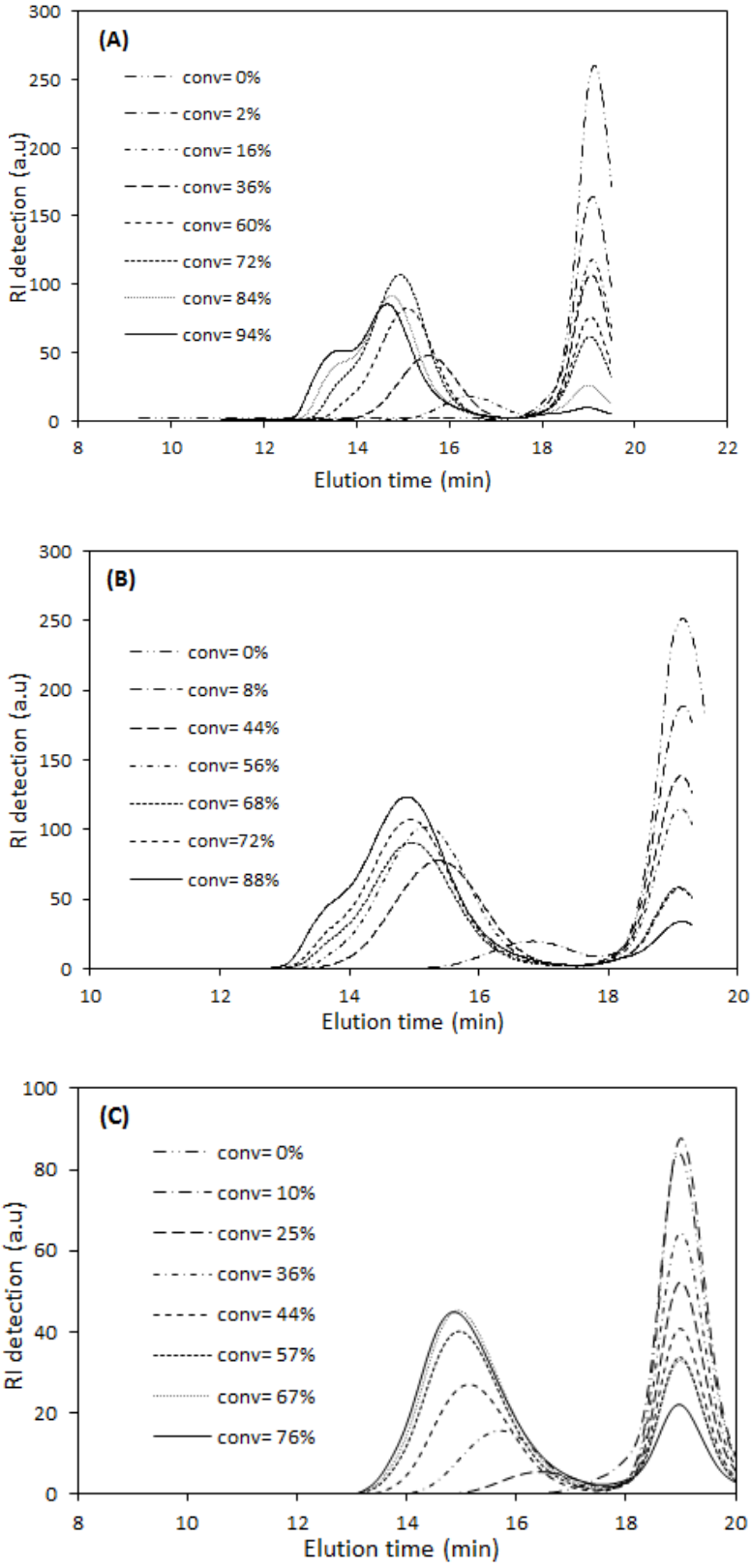


Figure II.8. Overlaid SEC (THF) traces of crude polymerizations mixtures using RI detection obtained by UV-light initiated RAFT polymerization of PEGA using photo-I and COPYDC ($[PEGA]_0/[COPYDC]_0/[Photo\text{-}I]_0$ = 50/1/0.1) in DMF at 25 °C at various initial PEGA concentrations, (A) $[PEGA]_0$ = 5 M, (B) $[PEGA]_0$ = 1.42 M and (C) $[PEGA]_0$ = 0.39 M.

Despite a low temperature reaction, UV-light initiated RAFT polymerization did not afford an improved control compared to the thermally-initiated RAFT polymerization with the same PEGA initial concentration of 1.42 M for a PPEGA conversion above 60%. An explanation could be the existence of premature termination reactions due to an undesired photolysis-derived fate of the CTA (*i.e.*, decomposition of the thiyl radical species under UV and subsequent side reactions).[22–24] These concerns were partially allayed by the examination of the UV response of the polymers at 310 nm, characteristic of the presence of a trithiocarbonate chain-end (Figure II.9). An alternative hypothesis that we considered to a lesser extent is the photodegradation of the PEG side chains to produce additional radicals and subsequent branching. This photodegradation could be possible based on reports of PEG-based polymers undergoing photodegradation when irradiated with UV light, albeit at higher light intensities.[25–27]

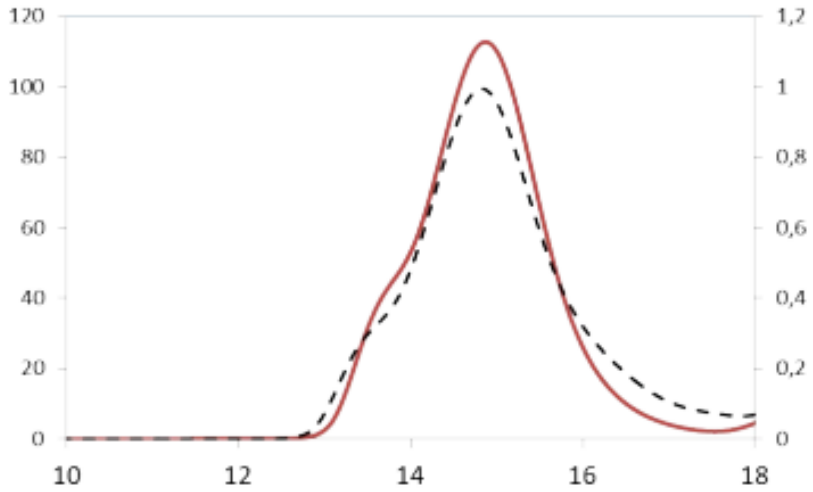


Figure II.9. Overlaid SEC (THF) traces of UV-PPEGA using RI detection (—) and UV detection at 310 nm (---) obtained by UV-light initiated RAFT polymerization of PEGA using photo-I and COPYDC at final time (150 min; conv. = 88 %) ($[PEGA]_0/[COPYDC]_0/[Photo\text{-}I]_0$ = 50/1/0.1) in DMF at 25 °C and at $[PEGA]_0$ = 1.42 M.

In conclusion, the optimized synthesis conditions for UV-PPEGA prepared through UV-light initiated polymerization at ambient temperature is: an initial molar ratio $[PEGA]_0/[COPYDC]_0$ = 50/1. Results show lower dispersity values and better control of polymerization for PEGA initial concentration of 5 M when the polymerization is stopped at low PEGA conversions (< 60%). At higher PEGA conversion (70%) the polymerization with $[PEGA]_0$ = 5 M leads to the presence of a shoulder of high molar mass which is not observed using $[PEGA]_0$ = 0.39 M.

### 2.2.2.2 Synthesis of UV-PPEGA with different $\overline{DP_n}$

Different UV-PPEGAs were synthesized keeping the $[PEGA]_0/[COPYDC]_0/[Photo\text{-}I]_0$ initial molar ratio to 50/1/0.1 and the initial PEGA concentration of 0.39 M. The same purification protocol and characterizations used for Thermal-PPEGAs were applied to UV-PPEGAs. The macromolecular characteristics of the so-obtained UV-PPEGAs are reported in Table II.2.

Table II.2. Macromolecular characteristics of UV-PPEGAs synthesized by UV-light initiated RAFT polymerization in DMF at 25 °C with $[PEGA]_0/[COPYDC]_0/[Photo\text{-}I]_0$ = 50/1/0.1 and $[PEGA]_0$ = 0.39 M.

| Run | Time (h) | Conv. (%)[a] | $\overline{DP_{n,PPEGA}}$ [b] | $\overline{M_{theo}}$ (g.mol$^{-1}$)[c] | $\overline{M_{n,SEC}}$ (g.mol$^{-1}$)[d] | $Đ$ [d] |
|---|---|---|---|---|---|---|
| 1 | 1.45 | 35 | 18 | 9080 | 8500 | 1.27 |
| 2 | 3 | 60 | 24 | 11960 | 11200 | 1.22 |
| 3 | 4 | 62 | 30 | 14840 | 11700 | 1.25 |

[a] Determined by $^1$H-NMR spectroscopy (200 MHz, $CDCl_3$) by comparing the integration values of the formamide proton of DMF at 8.02 ppm and of the alkene protons of PEGA between 5.7 and 6.5 ppm. [b] Determined by $^1$H-NMR spectroscopy (400 MHz, $CDCl_3$). [c] $\overline{M_{n,theo}} = \frac{[PEGA]_0}{[COPYDC]_0} \times conv \times \overline{M_{PEGA}} + M_{COPYDC}$ where conv is the PEGA conversion, $\overline{M_{n,PEGA}}$ is the number-average molar mass of PEGA ($\overline{M_{PEGA}}$ = 480 g.mol$^{-1}$) and $M_{COPYDC}$ = 440g.mol$^{-1}$. [d] Determined by SEC in THF using PSt equivalents.

The Table II.2 shows the increase of the $\overline{DP_{n,PPEGA}}$ and the $\overline{M_{n,SEC}}$ with time and monomer conversion. Compared to Thermal-PPEGA in Table II.1 having the same $\overline{DP_{n,PPEGA}}$ (= 24), $\overline{M_{n,SEC}}$ of UV-PPEGAs are closer to $\overline{M_{n,theo}}$ with lower dispersity values, showing a better control of PEGA polymerization (run 4, Table II.1 *versus* run 2, Table II.2).

As the trithiocaronate group is sensitive to UV-light[28], additional SEC analysis using UV detection was performed on a purified UV-$PPEGA_{18}$ (run 1, Table II.2) used as an example to check the end-group fidelity. The SEC trace using RI detection shows a unimodal and narrow signal giving $\overline{M_{n,SEC}}$ = 8500 g.mol$^{-1}$ (in THF, PSt equivalents) and $Đ$ = 1.27 (Figure II.10). Overlaying RI and UV traces confirmed the chain-end fidelity of the polymer by a trithiocarbonate group.

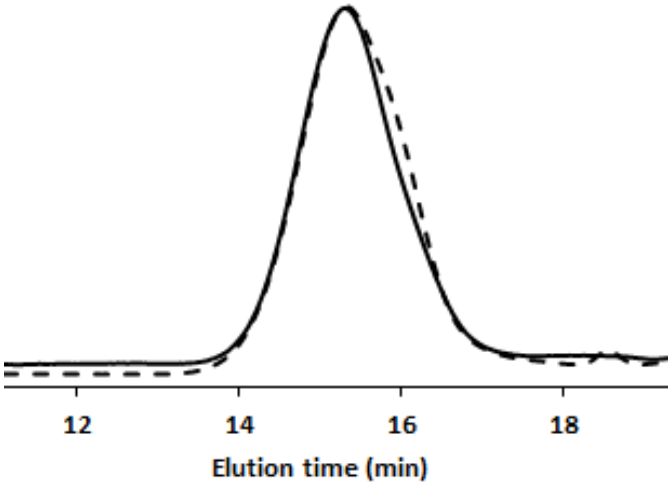


Figure II.10. Overlaid SEC (THF) traces using RI detection (line) and UV-Vis detection (dash line) at 310 nm of purified UV-PPEGA$_{18}$ (Table II.2, run 1) obtained by UV-light initiated RAFT polymerization of PEGA using Photo-I and COPYDC ([PEGA]$_0$/[COPYDC]$_0$/[Photo-I]$_0$ = 50/1/0.1, [PEGA]$_0$ = 0.39 M) in DMF at 25 °C after 1h45 of reaction.

In conclusion, PPEGAs could be obtained by RAFT polymerization using either thermal activation or UV-light activation with a sufficient molar mass control and narrow molar masses distributions for low PEGA conversions. Employing a lower monomer concentration and stopping the reaction at low conversion results in a better control of PEGA polymerization. Such well-defined PPEGAs can be used as macro-CTAs for further synthesis of thermosensitive diblock copolymers by RAFT polymerization in water.

## 2.3 Chain extension of PPEGA macromolecular chain transfer agents through RAFT polymerization in water

Having evidenced the high $\omega$-end group retention of PPEGAs obtained by thermal activation and UV-light irradiation in the previous section, we then wish to further demonstrate the level of $\omega$-group chain-end fidelity by doing chain extension of these PPEGAs with thermosensitive (LCST and UCST) polymers *via* thermal activation and UV-light irradiation RAFT polymerization in aqueous medium.

### 2.3.1 Extension with monomers precursors to LCST-type thermosensitive polymer

Chain extension experiments were carried out with NIPAm as the corresponding polymer (PNIPAm) has received considerable attention due to its LCST value of 32°C (between room and body

temperature) in water making it very interesting for biomedical applications.[29–31] In line with several other studies where PPEGAs between 10 and 22 kg.mol$^{-1}$ were synthesized,[3,12,32] the chain extension of Thermal-PPEGA$_{20}$ and UV-PPEGA$_{18}$ were herein realized by thermally- and UV-light initiated RAFT polymerizations of NIPAm in water at different temperatures in the presence of water-soluble initiators 2,2'-azobis(2-methylpropionamidine) dihydrochloride (V50) or photo-I (Scheme II.2).

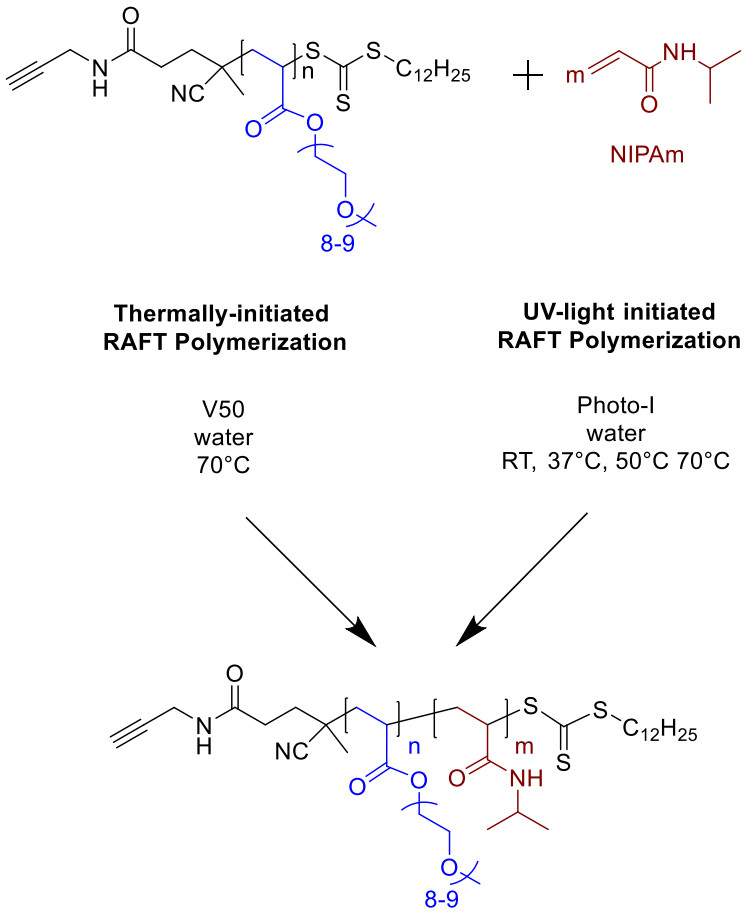


Scheme II.2. RAFT polymerization of NIPAm using PPEGA as macro-CTA in water at different temperatures with various initiating radical sources (thermal, UV-light irradiation).

### 2.3.1.1 Synthesis of Thermal-PPEGA-b-Thermal-PNIPAm[§] diblock copolymers by thermally-initiated RAFT-PITSA of NIPAm in aqueous dispersion from Thermal-PPEGA

The thermally-initiated RAFT polymerization-induced thermal self-assembly (PITSA) [33–35] of NIPAm was studied in aqueous dispersion, at a low solid content (2.4 wt.%) in the presence of Thermal-

[§] *Thermal-PPEGA-b-Thermal-PNIPAm*: *diblock copolymers by thermally-initiated RAFT of NIPAm in aqueous dispersion from Thermal-PPEGA macro-CTA.*

$PPEGA_{20}$ as macro-CTA (run3, Table II.1) and at 70°C (T°C > LCST of PNIPAm).The term PITSA is used here as the RAFT polymerization of NIPAm in water involves the chain extension of a hydrophillic PPEGA acting both as macro-CTA and stabilizer with a hydrophobic polymer to generate self-assembled nanodomains at T > LCST of PNIPAm). Thermally-initiated RAFT-PITSA of NIPAm was conducted in presence of V50 as hydrosoluble initiator with an initial molar ratio of $[NIPAm]_0/[Thermal\text{-}PPEGA_{20}]_0/[V50]_0$ = 204/1/0.3 at 70 °C. A kinetic plot for the thermally-initiated RAFT-PITSA of NIPAm was obtained by withdrawing samples at different time intervals (Figure II.11A).

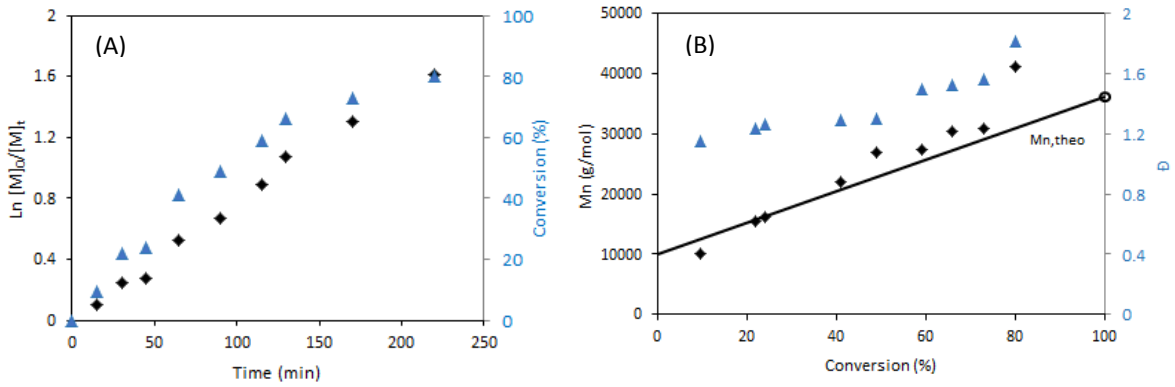


Figure II.11. Evolution of (A) $\ln([M]_0/[M]_t)$ and conversion *vs.* time and (B) evolution of $\overline{M_{n,SEC}}$ and *Đ vs.* NIPAm conversion during the thermally-initiated RAFT PITSA of NIPAm using V50 and Thermal-$PPEGA_{20}$ in aqueous dispersion at 70°C.

Figure II.11A shows that the conversion of NIPAm increases with the increase of polymerization time and a constant slope of $\ln([M]_0/[M]_t)$ *vs.* reaction time, relevant with a constant concentration of propagating radicals observed until NIPAm conversion of 66 %. At higher NIPAm conversions, a decrease of the apparent propagation rate constant was observed, with sharp increases in both $\overline{M_{n,SEC}}$ and *Đ* (Figure II.11B). A decrease in the radical concentration would be expected due to irreversible bimolecular termination by coupling, which would entail an increase in dispersity as the percentage of dead chains becomes significant and also higher $\overline{M_{n,SEC}}$ than $\overline{M_{n,theo}}$. Moreover, the SEC traces of crude polymerizations mixtures (Figure II.12) showed the appearance of high molar mass shoulders relevant with the loss of polymerization control from 41% NIPAm conversion, due to a moderate proportion of dead chains.

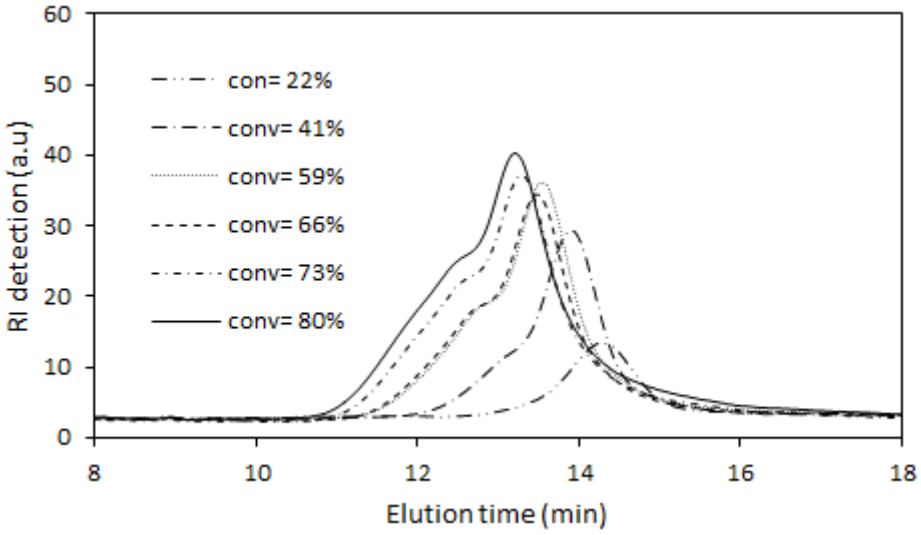


Figure II.12. Overlaid SEC (DMF, LiBr) traces of crude polymerization mixtures using RI detection obtained during the thermally-initiated RAFT-PITSA of NIPAm using V50 and Thermal-PPEGA$_{20}$ in aqueous dispersion at 70°C.

To target the Thermal-PPEGA$_{20}$-*b*-Thermal-PNIPAm block copolymers with a $\overline{DP_{n,\,PNIPAM}}$ = 200, the initial molar ratio between Thermal-PPEGA$_{20}$, NIPAm and V50 ([NIPAM]$_0$/[Thermal-PPEGA$_{20}$]$_0$/[V50]$_0$) of 204/1/0.3 was employed with the solid content of 2.4 wt.%. The reaction was stopped after 6h of polymerization and a total NIPAm conversion was observed by $^1$H-NMR spectroscopy with the disappearance of vinyl protons between 5.52 and 6.25 ppm (Figure II.13).

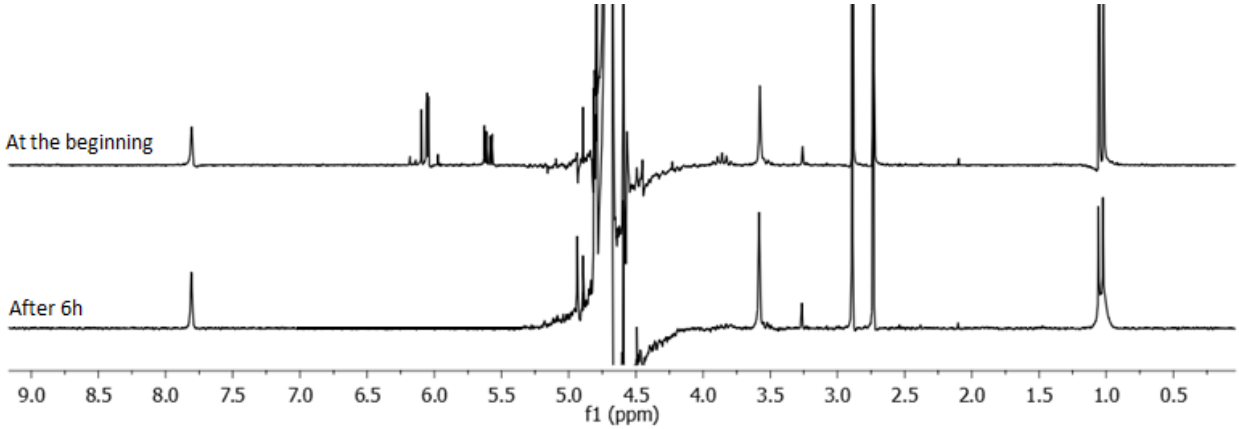


Figure II.13. $^{1}$H-NMR spectrum (200 MHz in $D_2O$) showing the complete conversion of NIPAm after 6h of thermally-initiated RAFT-PITSA of NIPAm using V50 and Thermal-PPEGA$_{20}$ in aqueous dispersion at 70°C.

The $^{1}$H-NMR spectrum (Figure II.14) of the resultingThermal-PPEGA$_{20}$-*b*-Thermal-PNIPAm shows signals at 3.35 ppm ((CH$_2$CH$_2$O)$_8$C*H$_3$*, labeled b) and 4.15 ppm (C(=O)OC*H$_2$CH$_2$*O-(CH$_2$CH$_2$O)$_8$, labeled a and e, respectively) characteristic of the PPEGA block and a signal at 3.95 ppm (-NH-C*H*(CH$_3$)$_2$, labeled c) characteristic of the PNIPAm block. These signals were used to determine the molar composition of the resulting copolymer: $\overline{DP_{n,\,PPEGA}}$ = 20 and $\overline{DP_{n,\,PNIPAM}}$ = 200.

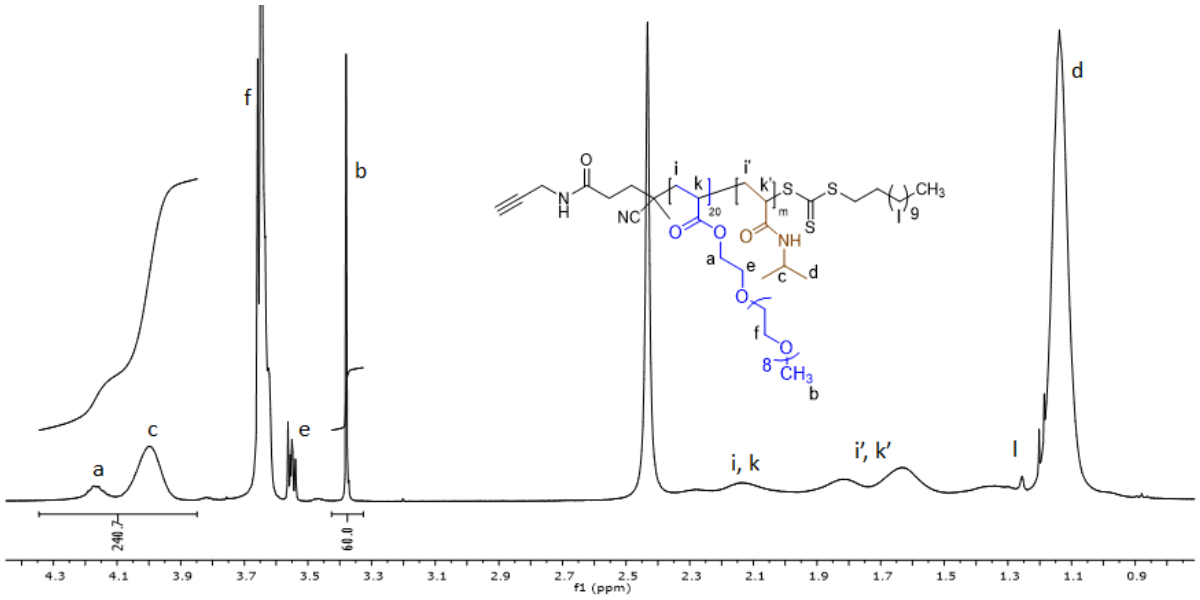


Figure II.14. $^{1}$H-NMR spectrum (400 MHz, $CDCl_3$) of purified Thermal-PPEGA$_{20}$-*b*-Thermal-PNIPAm$_{200}$ synthesized by thermally-initiated RAFT-PITSA of NIPAm using V50 and Thermal-PPEGA$_{20}$ ([PEGA]$_0$/[Thermal-PPEGA$_{20}$]$_0$/[V50]$_0$ = 204/1/0.3, solid content 2.4 wt.%) in water at 70°C after 6h of reaction.

The overlaid SEC traces of Thermal-PPEGA$_{20}$ and Thermal-PPEGA$_{20}$-*b*-Thermal-PNIPAm$_{200}$ block copolymer obtained using RI detection was illustrated in Figure II.15. The chain extension of Thermal-PPEGA$_{20}$ using NIPAm monomer by thermally-initiated RAFT-PITSA is quasi-quantitative but a bimodal and broad SEC signal was observed illustrating the presence of irreversible termination reactions ($\overline{M_{n,SEC}}$ = 41200 g.mol$^{-1}$, Đ = 1.56) at total NIPAm conversion.

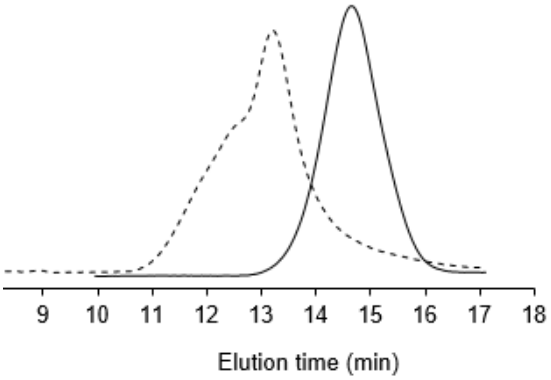


Figure II.15. Overlaid SEC (DMF, LiBr) traces using RI detection of the Thermal-PPEGA$_{20}$ (line) and of the Thermal-PPEGA$_{20}$-*b*-Thermal-PNIPAm (dash line) copolymer obtained after chain extension by thermally-initiated RAFT-PITSA of NIPAm in aqueous dispersion at 70°C (dash line).

In the following section, we perform UV-light initiated RAFT polymerizations of NIPAm in the presence of photo-I and a UV-PPEGA used as macro-CTA at different temperatures to figure out the impact of radical activation and polymerization temperature on the macromolecular structure of the resulting PPEGA-*b*-PNIPAm block copolymers.

#### 2.3.1.2 Synthesis of UV-PPEGA-b-UV-PNIPAm diblock copolymer by UV-light initiated RAFT polymerization of NIPAm in water from UV-PPEGA

The UV-PPEGA$_{18}$ previously synthesized (Table II.2, run 1) was used as macro-CTA in the UV-light initiated RAFT polymerization of NIPAm in water. For the synthesis of UV-PPEGA$_{18}$-*b*-UV-PNIPAm block copolymers, the initial molar ratio between UV-PPEGA$_{18}$, NIPAm and Photo-I ([NIPAm]$_0$/[UV-PPEGA$_{18}$]$_0$/[Photo-I]$_0$) was fixed at 204/1/0.3 with the solid content of 2.4 wt.% (similar experimental conditions as the chain extension initiated by the thermal activation). A first test was carried at 25 °C and so in an aqueous homogeneous medium (T < LCST of PNIPAm). As shown in Figure II.16A, a very fast initial rate of polymerization was observed which reached approximatively 100 % NIPAm conversion after 60 min (instead of 100 % NIPAm conversion after 360 min for the thermally-initiated RAFT-PITSA in aqueous dispersion). The conversion of NIPAm increases with the increase of polymerization time and a constant slope of ln([M]$_0$/[M]$_t$) *vs.* reaction time, relevant with a constant concentration of propagating radicals is observed. Figure II.16B illustrates the evolution of $\overline{M_{n,SEC}}$ and

*Đ versus* NIPAm conversion and Figure II.17 shows the overlaid SEC traces of resulting copolymers at different NIPAm conversions. The RAFT polymerization of NIPAm seems under a good control as *Đ* remains stable around 1.3-to-1.4. The discrepancy between $\overline{M_{n,SEC}}$ and $\overline{M_{n,theo}}$ can be attributed to the difference between the hydrodynamic volume of PMMA, used for SEC calibration, and the hydrodynamic volume of the copolymer in DMF. This conclusion is in agreement with the absence of high molecular weight shoulder in the SEC traces, even at full conversion of NIPAm (Figure II.17).

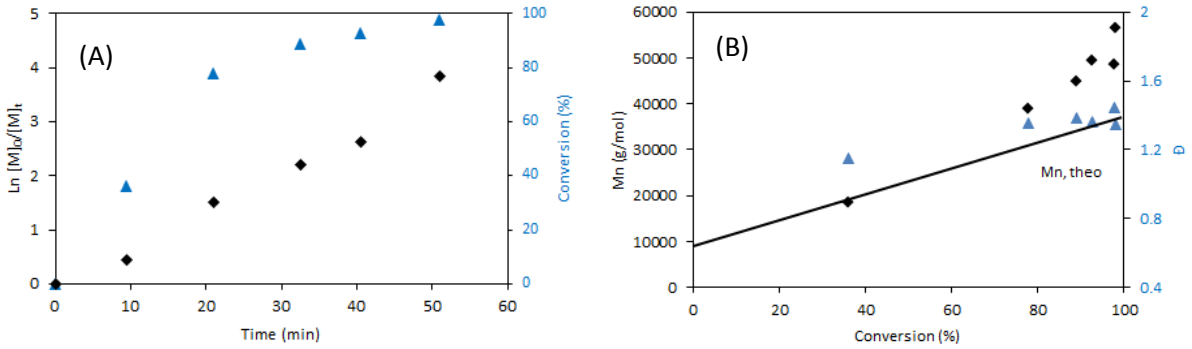


Figure II.16. Evolution of $\ln([M]_0/[M]_t)$ and conversion *vs.* time (A) and, evolution of $\overline{M_{n,SEC}}$ (symbol) and $\overline{M_{n,theo}}$ (line) and *Đ vs.* NIPAm (B) during the UV-light initiated RAFT polymerization of NIPAm using Photo-I as photoinitiator and UV-PPEGA$_{18}$ as macro-CTA in water at 25 °C.

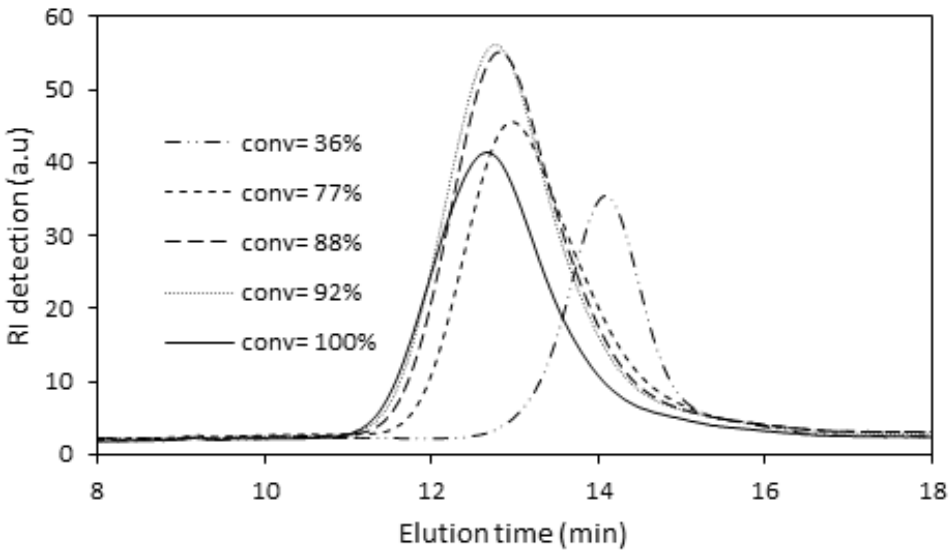


Figure II.17. Overlaid SEC (DMF, LiBr) traces of UV-PPEGA-*b*-UV-PNIPAm using RI detection obtained during the UV-light initiated RAFT polymerization of NIPAm using Photo-I as photoinitiator and UV-PPEGA$_{18}$ as macro-CTA in water at 25 °C.

The SEC analysis of the resulting copolymer showed a quantitative extension and a narrow monodal peak with $\overline{M_{n,SEC}}$ = 56 400 g.mol$^{-1}$ (PMMA equivalents) and $Đ$ = 1.34 (Figure II.18). The trithiocarbonate chain-end functionalization of the polymer was confirmed by overlaying RI and UV traces (Figure II.19).

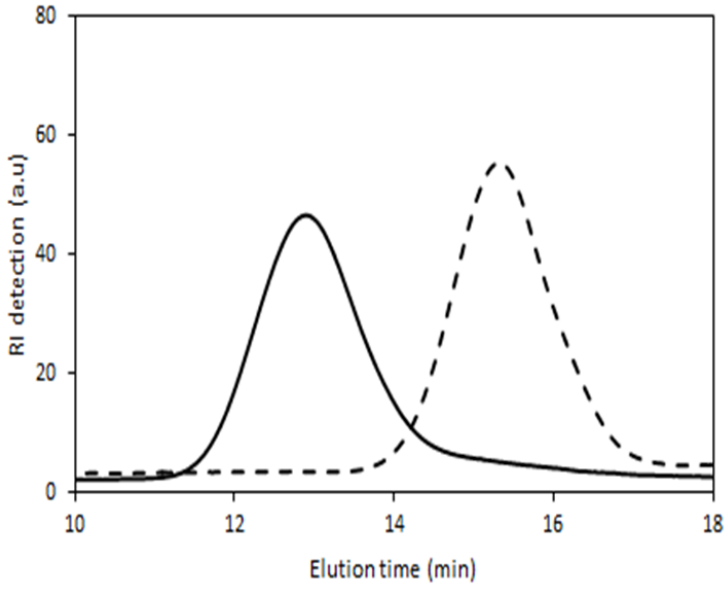


Figure II.18. Overlaid SEC (DMF, LiBr) traces using RI detection of UV-PPEGA$_{18}$ (dash line) and of UV-PPEGA$_{18}$-*b*-UV-PNIPAm copolymers (line) obtained after chain extension by the UV-light initiated RAFT polymerization of NIPAm using Photo-I as photoinitiator and UV-PPEGA$_{18}$ as macro-CTA in water at 25 °C.

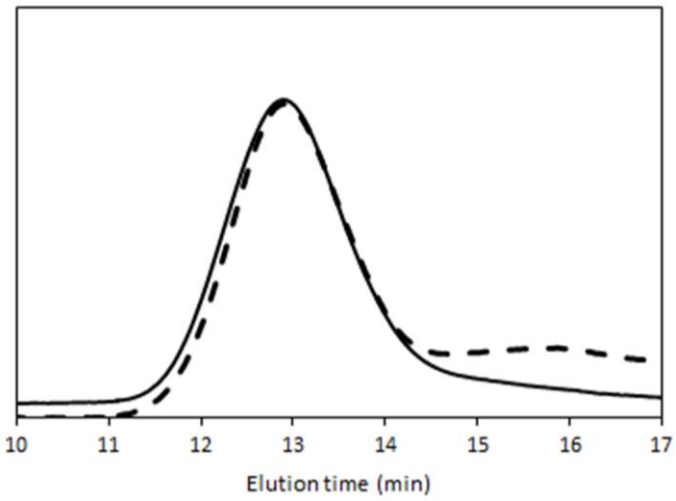


Figure II.19. Overlaid SEC (DMF) traces of purified UV-PPEGA$_{18}$-*b*-UV-PNIPAm using RI detection (line) and UV-vis detection (dash line) at 310 nm obtained after chain extension by UV-light initiated RAFT polymerization at 25 °C after 1h of reaction.

The efficient chain extension obtained by UV-light initiated RAFT polymerization in comparison with the one obtained through thermally-initiated RAFT-PITSA can be explained by either the initiating radical source or by the reactional medium temperature generating two different processes (PITSA at 70°C and homogeneous solution at 25°C). As the LCST of PNIPAm being 32°C, the UV-light initiated RAFT-PITSA of NIPAm at various temperatures (37°C, 50°C and 70°C) was studied and compared with the results of the UV-light initiated RAFT polymerization at 25°C (Table II.3, run 2) and thermally-initiated RAFT-PITSA polymerization at 70°C (Table II.3, run 1). The resulting UV-PPEGA$_{18}$-*b*-UV-PNIPAms obtained at 37, 50 and 70°C were analyzed by $^{1}$H NMR spectroscopy and SEC analysis to determine NIPAm conversion, $\overline{M_{n,SEC}}$ and Đ values (Table II.3, runs 3, 4 and 5).

Table II.3. Macromolecular characteristics of PPEGA-*b*-PNIPAm block copolymers synthesized by RAFT polymerization in water with initial molar ratio $[NIPAm]_0/[PPEGA]_0/[I]_0 = 204/1/0.3$ (2.4 wt.% solid content) at different temperatures using different activation modes.

| Run | Name | Initiator | T°C | Time (h) | Conv.[a] (%) | $\overline{DP_{n,\,PNIPAM}}$[b] | $\overline{M_{n,NMR}}$[c] (g.mol$^{-1}$) | $\overline{M_{n,SEC}}$[d] (g.mol$^{-1}$) | Đ[d] |
|---|---|---|---|---|---|---|---|---|---|
| 1 | Thermal-PPEGA$_{20}$-*b*-Thermal-PNIPAm | V50 | 70 | 6 | 100 | 200 | 32 600 | 41 200 | 1.56 |
| 2 | UV-PPEGA$_{18}$ *b*-UV-PNIPAm | Photo-I | 25 | 1 | 98 | 201 | 31800 | 56400 | 1.34 |
| 3 | UV-PPEGA$_{18}$ *b*-UV-PNIPAm | Photo-I | 37 | 1 | 94 | 190 | 30500 | 47200 | 1.32 |
| 4 | UV-PPEGA$_{18}$ *b*-UV-PNIPAm | Photo-I | 50 | 1 | 100 | 204 | 32100 | 42500 | 1.86 |
| 5 | UV-PPEGA$_{18}$ *b*-UV-PNIPAm | Photo-I | 70 | 1 | 100 | 204 | 32100 | 43600 | 2.01 |

[a] Determined by $^1$H-NMR spectroscopy (200 MHz, $CDCl_3$) by comparing the integration values of the formamide proton of DMF at 8.02 ppm and of the alkene protons of NIPAm between 5.7 and 6.5 ppm. [b] Determined by $^1$H-NMR spectroscopy (400 MHz, $CDCl_3$) by comparing the integration values of signals at 3.35 ppm ($(CH_2CH_2O)_8CH_3$,) and 4.15 ppm ($C(=O)OCH_2CH_2O$-$(CH_2CH_2O)_8$) characteristic of the PPEGA block and a signal at 3.95 ppm (-NH-$CH(CH_3)_2$) of the PNIPAm block. [c] $\overline{M_{n,NMR}} = \overline{DP_{n,\,PNIPAm}} \times M_{NIPAM} + \overline{M_{n,PPEGA}}$, where $\overline{M_{n,PPEGA}}$ is the number-average molar mass of PPEGA, $M_{NIPAM} = 113.16$ g.mol$^{-1}$. [d] Determined by SEC in DMF using PMMA equivalents.

At almost full NIPAm conversion (conv. ≥ 94 %), the dispersity values increase with reaction temperature using the UV-light initiated RAFT polymerization. Indeed, they increase from 1.3 at 25 °C and at 37 °C to 2.01 at higher temperature (70°C). The shoulders observed in SEC traces at short elution times (Figure II.20) for the block copolymers obtained by UV-light initiated RAFT-PITSA at 50°C and 70°C reflect the presence of irreversible termination reactions and/or irreversible transfer reactions predominant at higher temperature and in a confined space related to a reaction carried out at T ≥ LCST. However, the efficiency of RAFT-PITSA polymerization of NIPAm initiated by UV-light irradiation at low temperature (37 °C) makes possible to target well-defined UV-PPEGA-*b*-UV-PNIPAm block copolymers (run 3 in Table II.3 and Figure II.20).

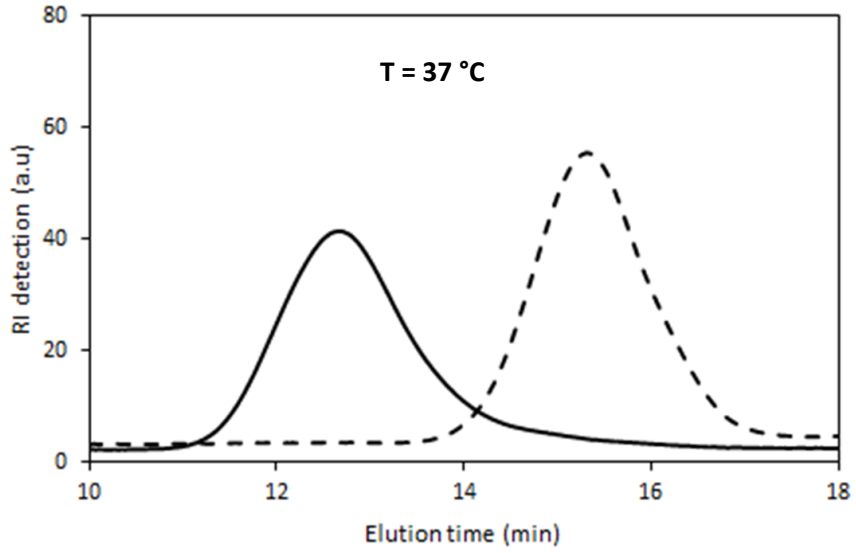
T = 37 °C
RI detection (a.u)
Elution time (min)
0
20
40
60
80
10
12
14
16
18

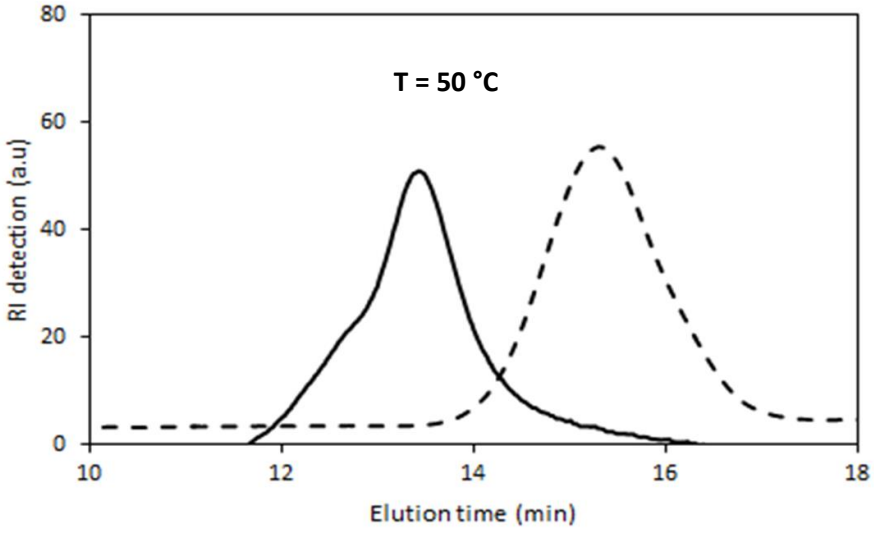
T = 50 °C
RI detection (a.u)
Elution time (min)
0
20
40
60
80
10
12
14
16
18

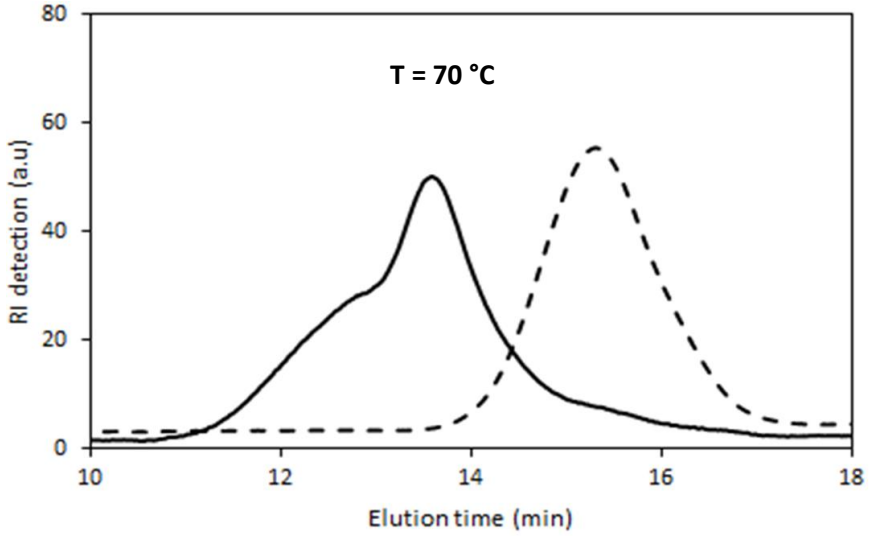
T = 70 °C
RI detection (a.u)
Elution time (min)
0
20
40
60
80
10
12
14
16
18

Figure II.20. Overlaid SEC (DMF, LiBr) traces using RI detection of UV-PPEGA$_{18}$ (dash line) and of UV-PPEGA$_{18}$-*b*-UV-PNIPAms copolymers (line) obtained after chain extension by UV-light initiated RAFT polymerization at various reaction temperatures.

In conclusion, well-defined PPEGA-*b*-PNIPAm diblock copolymers could be obtained by RAFT polymerization using UV-light activation at 25°C or 37 °C with a sufficient molar mass control and narrow molar masses distributions.

## 2.3.2 Extension with monomers precursors to UCST-type thermosensitive polymers

As mentioned in Chapter I, unlike LCST polymers, only a few polymer materials with UCST behavior in water are known. One of them is the poly(*N*-acryloyl glycinamide) (PNAGA). Due to the fact that many parameters can impact the UCST property of PNAGA, including monomer purity and the presence of ionic species, we first focused our study on other acrylamide monomers having chemical structures similar to that of NAGA to achieve potential UCST-type thermosensitive polymers from easily accessible monomers.

### 2.3.2.1 Synthesis of potential monomers precursors to UCST polymers, RAFT polymerization of these monomers and thermal properties of polymers

#### 2.3.2.1.1 Synthesis of VDM-derived acrylamide monomers

2-vinyl-4,4-dimethylazlactone (VDM) contains the azlactone ring which displays a high reactivity toward nucleophilic molecules such as primary amines, alcohol and thiols by means of a ring-opening addition reaction without the use of catalysts. In addition, there is no by-product eliminated from the ring-opening reaction between VDM and nucleophiles.[36,37] Moreover, the azlactone functionality shows a good resistance to hydrolysis at neutral pH: this is a considerable advantage compared to other activated acid forms.[38] Ammoniac and primary amines containing primary amid group(s) were chosen to react with VDM to prepare new VDM-derived acrylamide monomers with potential UCST-type thermosensitive property due to their ability to form hydrogen bonding (Scheme II.3).

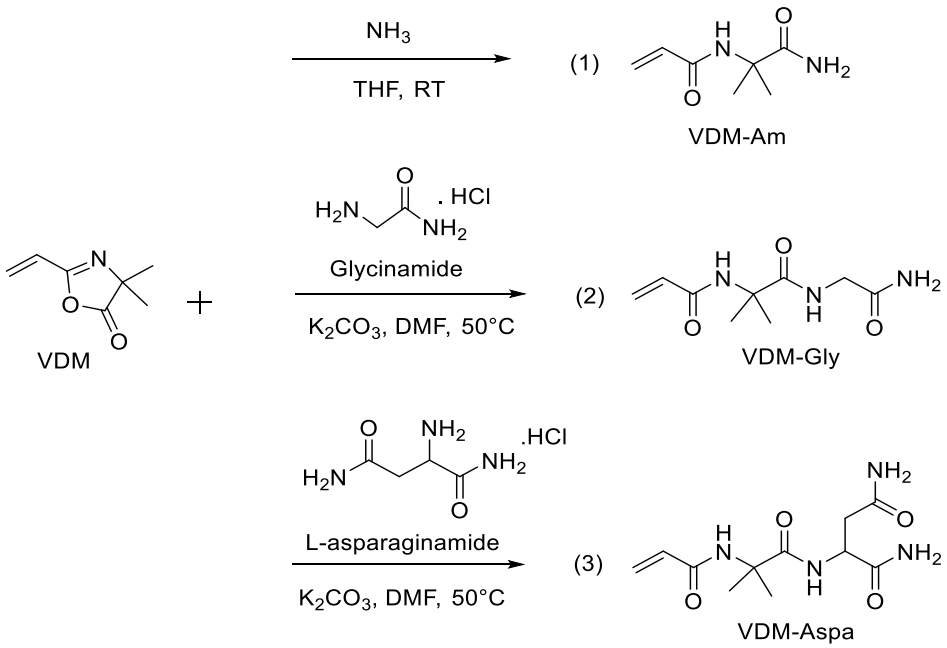


Scheme II.3. Synthesis of VDM-derived acrylamide monomers.

The experimental conditions of the synthesis of VDM-derived acrylamides and their characterization by $^{1}$H NMR analysis are summarized in Table II.4. Three different VDM-derived acrylamide monomers are successfully synthesized by the reaction of VDM with ammoniac and primary amines.

Table II.4. Experimental conditions of the synthesis of VDM-derived acrylamide monomers and their characterization by $^1$H NMR analysis.

| **Resulting monomer**[a] | **Reagents** | **Reaction conditions** | **Yield (%)** | **$^1$H-NMR signals attribution**[b] **$\delta$ (ppm)** |
|---|---|---|---|---|
| VDM-Am | VDM/$NH_3$ | stœchiometry, THF, RT, 1h | 100 | 5.78-6.36 (m, -C$H_2$C$H$-), 1.45 (s, -C$H_3$) |
| VDM-Gly | VDM/ glycinamide | stœchiometry, DMF, 50 °C, 12h | 70 | 5.78-6.36 (m, -C$H_2$C$H$-), 3.82 (s, NH-C$H_2$CO-) ,1.45 (s, -C$H_3$) |
| VDM-Aspa | VDM/ L-asparaginamide | stœchiometry, DMF, 50 °C, 12h | 63 | 5.78-6.36 (m, -C$H_2$C$H$-), 4.65 (m, -NHC$H$CH$_2$CO-),2.65 (m, CHC$H_2$CO-), 1.45 (s, -C$H_3$) |

[a] The resulting monomers with their chemical structures are illustrated in scheme II.3,
[b] Determined by $^1$H-NMR spectroscopy (400 MHz, $D_2O$).

#### 2.3.2.1.2 RAFT polymerization of the VDM-derived acrylamide monomers

UV-light initiated RAFT polymerization was employed for the synthesis of potential UCST-type thermosensitive polymer from precursor monomers based on VDM due to shorter time polymerization compared to thermal activation. The polymerizations were performed under UV-light irradiation using 4-cyano-4-(ethylsulfanylthiocarbonyl) sulfanylpentanoic acid (ECT) as CTA and photo-I as photoinitiator with a monomer content of 2.5 wt.% in water at 25°C, ECT was first dissolved in a minimum amount of DMF as co-solvent (Scheme II.4).

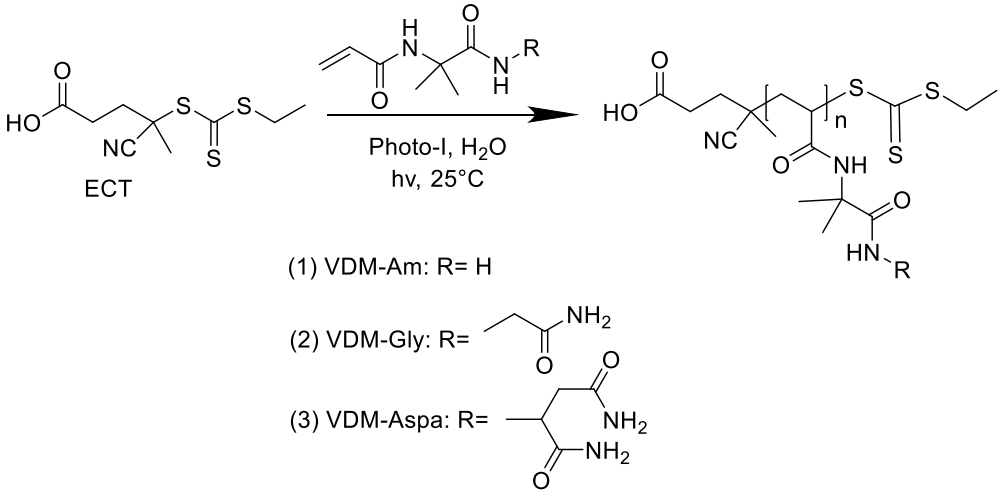


Scheme II.4. UV-light initiated RAFT polymerization of VDM-Am, VDM-Gly and VDM-Aspa monomers using ECT as chain transfer agent and photo-I as photoinitiator, in water at 25 °C.

UV-light initiated RAFT polymerization of VDM-Am, VDM-Gly and VDM-Aspa monomers was conducted at 25°C until complete conversion of the monomer as checked by $^1$H NMR spectroscopy. P(VDM-Am), P(VDM-Gly) and P(VDM-Aspa) were freeze dried without purification. The resulted polymers were characterized by $^1$H-NMR spectroscopy, SEC in water using PEO standards to determine $\overline{M_{n,SEC}}$ and Đ. The experimental synthesis conditions and macromolecular characteristics of polyacrylamides obtained through UV-light initiated RAFT polymerizations were shown in Table II.5. The three different polyacryamides were obtained through UV-light initiated RAFT polymerizations at 25 °C using the same initial molar ratio of $[M]_0/[ECT]_0/[photo\text{-}I]_0$ =200/1/0.3 with 100% conversion of monomers from 1.5 to 2h. The dispersity values are 1.20, 1.67 and 1.71 for P(VDM-Am), P(VDM-Gly) and P(VDM-Aspa), respectively.

Table II.5. Experimental synthesis conditions and macromolecular characteristics of polyacrylamides obtained through UV-light initiated RAFT polymerization of VDM-Am, VDM-Gly and VDM-Aspa monomers using ECT and photo-I, in water at 25 °C.[a]

| Run | Monomer (M) | $[M]_0/[ECT]_0/[photo\text{-}I]_0$ | Time (h) | $\overline{M_{n,theo}}$[b] (g.mol$^{-1}$) | $\overline{M_{n,SEC}}$[c] (g.mol$^{-1}$) | Đ[c] |
|---|---|---|---|---|---|---|
| 1 | VDM-Am | 200/1/0.3 | 2 | 31400 | 13900 | 1.20 |
| 2 | VDM-Gly | 200/1/0.3 | 1.5 | 33600 | 22300 | 1.67 |
| 3 | VDM-Aspa | 200/1/0.3 | 1.5 | 53900 | 25600 | 1.71 |

[a] Polymerizations were run at full monomer conversion. [b] $\overline{M_{n,theo}} = 200 \times M_{Monomer}$ + $M_{ECT}$ where $M_{VDM-Am}$ = 156 g.mol$^{-1}$, $M_{VDM-Gly}$ = 167 g.mol$^{-1}$, $M_{VDM-Aspa}$ = 268.5 g.mol$^{-1}$ and $M_{ECT}$ = 225 g.mol$^{-1}$ . [c] Determined by SEC in water using PEO standards.

The SEC traces of the so-obtained polyacrylamides show unimodal and narrow signals (Figure II.20). Overlaid RI SEC trace and UV SEC trace at 310 nm confirmed the chain-end functionalization of polymers P(VDM-Am), P(VDM-Gly) and P(VDM-Aspa) by a trithiocarbonate group (Figure II.20). Results reported in Table II.5 show a significant discrepancy between $\overline{M_{n,SEC}}$ and $\overline{M_{n,theo}}$. The reason is probably due to the SEC calibration as the hydrodynamic volume of PEO, used for SEC calibration in water, is different from the hydrodynamic volume of resulting polymers in water.

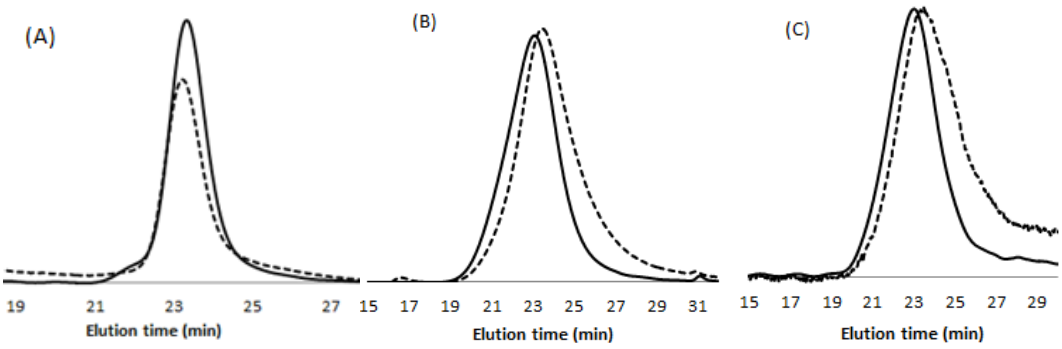


Figure II.21. Overlaid SEC (water, $NaNO_3$) traces using RI detection (line) and UV-vis detection (dash line) at 310 nm of different polyacrylamides obtained by UV-light initiated RAFT polymerization of VDM-Am (A), of VDM-Gly (B) and of VDM-Aspa (C).

#### 2.3.2.1.3 Thermal properties of polymers based on VDM-derived acrylamide monomers

Thermosensitive behaviors of P(VDM-Am), P(VDM-Gly) and P(VDM-Aspa) were studied by UV-Vis spectrophotometer by following turbidity of the samples to measure the cloud points (= UCST value) with the cooling/heating rate of 1°C.min$^{-1}$ from 5°C to 60°C. The polymer solutions were prepared in ultra-pure water with a concentration of 10 g.L$^{-1}$. No phase transition was observed for all polymers from the 5°C to 60°C. The reason is probably due to the presence of di-methyl groups in the pendant units preventing the formation of inter- and intramolecular hydrogen bonds within and between polymer chains, which are responsible for UCST phase transition behavior.

Well-defined P(VDM-Am), P(VDM-Gly) and P(VDM-Aspa) polymers are obtained by UV-light initiated RAFT polymerization of corresponding monomer precursors in water at 25 °C. However, the resulting polymers did not display UCST-type thermosensitive behavior. Therefore, NAGA monomer was selected as a well-known monomer precursor to UCST-polymer for further chain extension of PPEGA.

### 2.3.2.2 *N*-Acryloyl glycinamide (NAGA) monomer

PNAGA is a promising non-ionic polymer showing UCST behavior in water and saline solutions.[39–41] In the following part, the synthesis of NAGA monomer, the synthesis of PNAGA by thermal RAFT polymerization (Thermal-PNAGA, the synthesis of UCST-type thermosensitive block copolymers based on PNAGA by RAFT polymerization with different radical activation processes and their UCST thermosensitive behavior will be studied.

#### 2.3.2.2.1 *Synthesis of NAGA monomer*

NAGA was synthesized according to the previous reported procedure [40](Scheme II.5) with a yield of 28.8%. The purified compound was analyzed by $^{1}$H NMR spectroscopy.

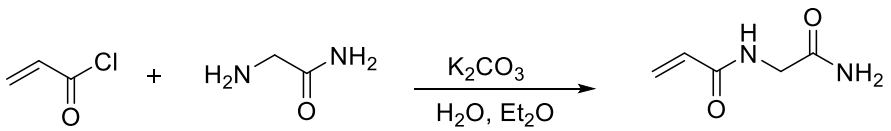


Scheme II.5. Synthesis of NAGA.

The $^{1}$H-NMR spectrum (Figure II.22) shows the characteristic signals of vinyl protons C*H*$_2$C*H* at 5.78-6.36 ppm (labeled a and b), a singlet at 3.82 ppm (labeled c) corresponding to the methylene protons HNC*H*$_2$CO.

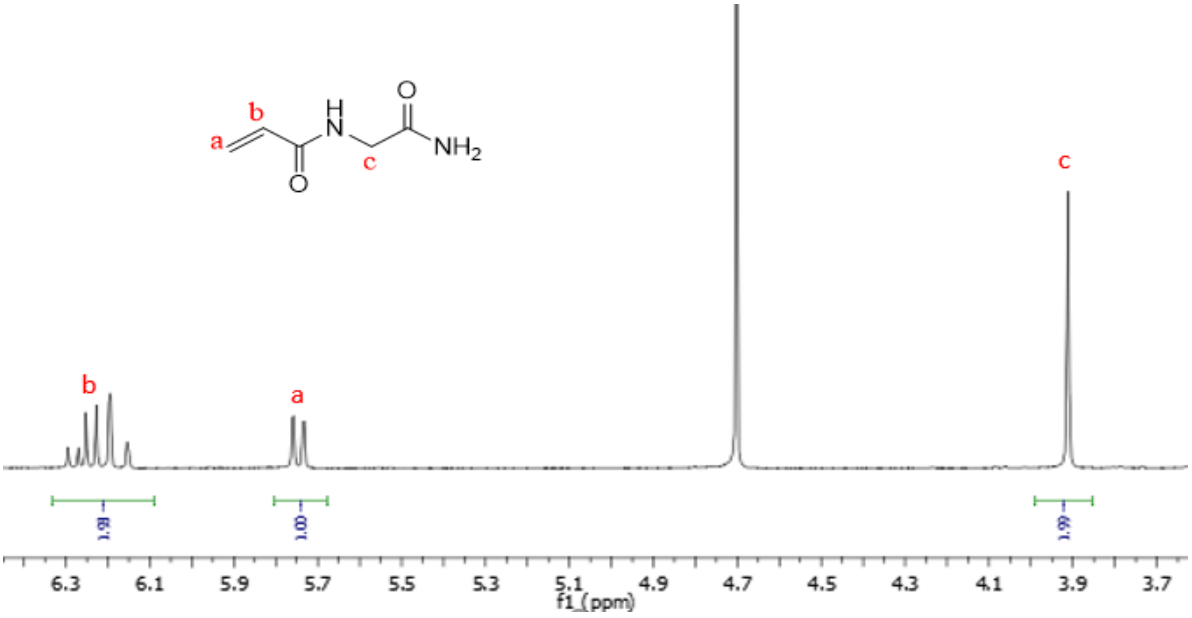


Figure II.22. $^{1}$H-NMR spectrum ($D_2O$, 400 MHz) of NAGA.

The high-resolution mass spectra (HR-MS) analysis also confirms the identity of NAGA monomer: calculated value for $[C_5H_8O_2N_2 + Na]^+$ = 151.0473 Da, experimental = 151.3568 Da. The differential scanning calorimetry (DSC) analysis was applied to confirm the purity of NAGA through the melting point measurement ($T_m$ = 140°C) which is close to the previously reported melting point [40]: 140-141 °C.

#### 2.3.2.2.2 PNAGA obtained by UV-light initiated RAFT polymerization (named UV-PNAGA) and thermal properties of UV-PNAGA

##### 2.3.2.2.2.1 PNAGA obtained by UV-light initiated RAFT polymerization

RAFT polymerization of NAGA was performed using same conditions that for the synthesis of polyacrylamides in part III.2.b.1, under UV-light irradiation with ECT used as CTA, photo-I as photoinitiator and a NAGA content of 2.5 wt.% in water at 25 °C with initial molar ratio $[NAGA]_0/[ECT]_0/[Photo\text{-}I]_0$ = 200/1/0.3 (Scheme II.6).

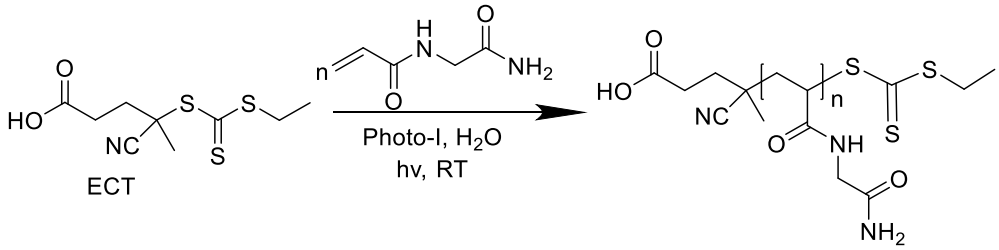


Scheme II.6. UV-light initiated RAFT polymerization of NAGA using ECT as CTA, photo-I as initiator in water at 25 °C.

NAGA conversion was determined by $^1$H-NMR spectroscopy by comparing the integration values of the formamide proton of DMF at 7.8 ppm and of the alkene protons of NAGA between 5.8 and 6.4 ppm at initial and final times of the polymerization. After 2h, 100% conversion of NAGA was observed. The resulting polymer was characterized by $^1$H NMR spectroscopy. The $^1$H NMR spectrum (Figure II.23) of the resulting UV-PNAGA shows signals between 3.6 to 4.1 ppm (NHC$H_2$CO, labeled c), 2.0 to 2.5 ppm and 1.3 to 1.8 ppm corresponding to the backbone protons (C$H_2$CH)$_n$ and (CH$_2$C$H$)$_n$ (labeled a and b, respectively). As a conversion of NAGA of 100% was confirmed by the absence of vinylic protons at final polymer, $\overline{DP_{n,\,PNAGA}}$ = 200.

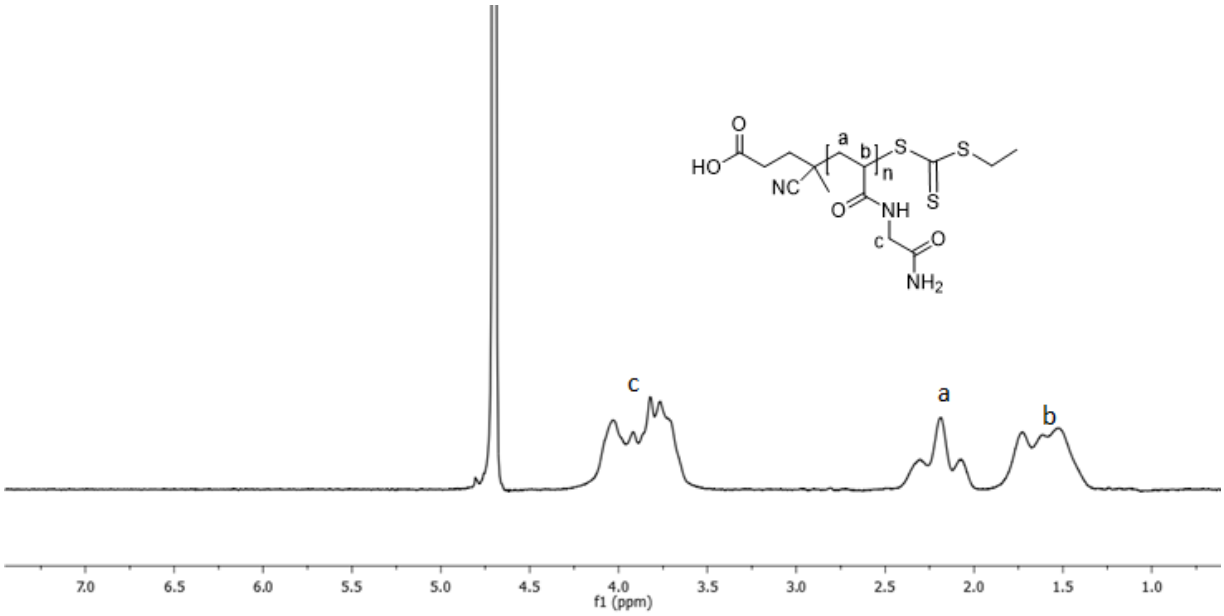


Figure II.23. $^{1}$H-NMR spectrum (400 MHz, $D_2O$) of UV-PNAGA synthesized by UV-light initated RAFT polymerization of NAGA mediated through Photo-I and ECT ($[NAGA]_0/[ECT]_0/[Photo\text{-}I]_0$ = 200/1/0.3, NAGA content 2.5 wt.%) in water at 25 °C after 2h of reaction.

The SEC trace of PNAGA using the RI detection shows an unimodal signal with $\overline{M_{n,SEC}}$ = 60 500 g.mol$^{-1}$ and $Đ$ = 1.84 (Figure II.24).

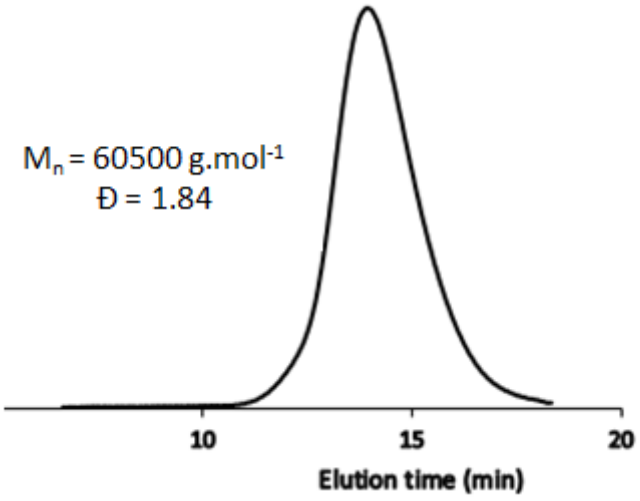


Figure II.24. SEC (DMSO, LiBr) traces using RI detection of UV-PNAGA obtained UV-light initiated RAFT polymerization of NAGA.

#### 2.3.2.2.2.2 Thermal properties of UV-PNAGA

The UCST-type thermosensitive behavior of UV-PNAGA$_{200}$ was studied by UV-vis spectrophotometry at a wavelength of 650 nm with a polymer concentration of 10 g.L$^{-1}$ in water (Figure II.25). The applied cooling/heating rate was 1 °C.min$^{-1}$. The transmittance increased gradually from 20 to 25°C, the solution became completely transparent at 25 °C, the UCST value of polymer was taken as mid-point of the curve at 22.5 °C upon heating. A significantly broad hysteresis of around 12 °C can be observed in the cooling process. The existence of a hysteresis in the cooling and heating of polymers in water was attributed to additional intra-chain or inter-chain H-bonds in the collapsed state. These intersegmental hydrogen bonds act as "the crosslinking" points among different chains so that each chain aggregate swells like a gel and the chain dissociation is delayed, which results in the observed hysteresis, which is already reported.[42]

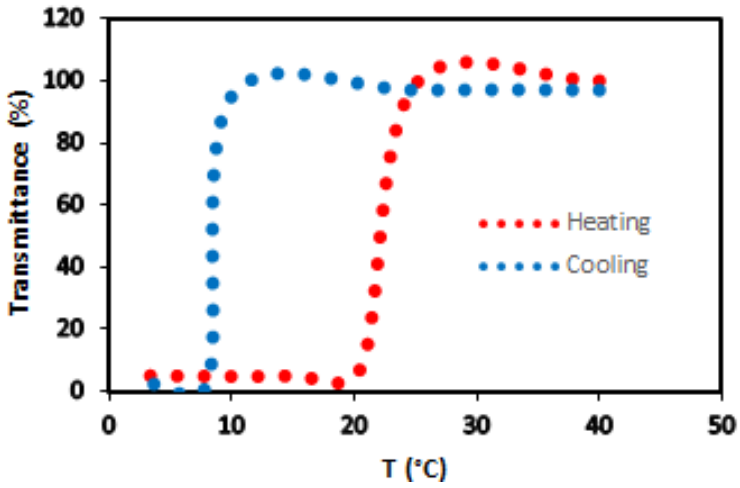


Figure II.25. Plots of transmittance as a function of temperature measured for aqueous solution (10 g.L$^{-1}$) of UV-PNAGA$_{200}$.

### 2.3.2.3 Synthesis of UCST-type thermosensitive block copolymers based on PNAGA(Thermal-PPEGA-b-PNAGA)

In this section UCST-type thermosensitive block copolymers based on PNAGA (Thermal-PPEGA-*b*-PNAGA) were targeted through thermally initiated and UV-light initiated RAFT polymerization in water. The impact of different radical activation processes on the polymerization of NAGA and thermosensitive behavior of resulting PPEGA-*b*-PNAGA block copolymers will be studied. The RAFT polymerization of NAGA by thermal activation and UV-light irradiation were conducted in water using a Thermal-PPEGA with a $\overline{DP_{n,PPEGA}}$ of 24 (Table II.1, run 4) as macro-CTA in the presence of V50 and photo-I as initiator (Scheme II.7).

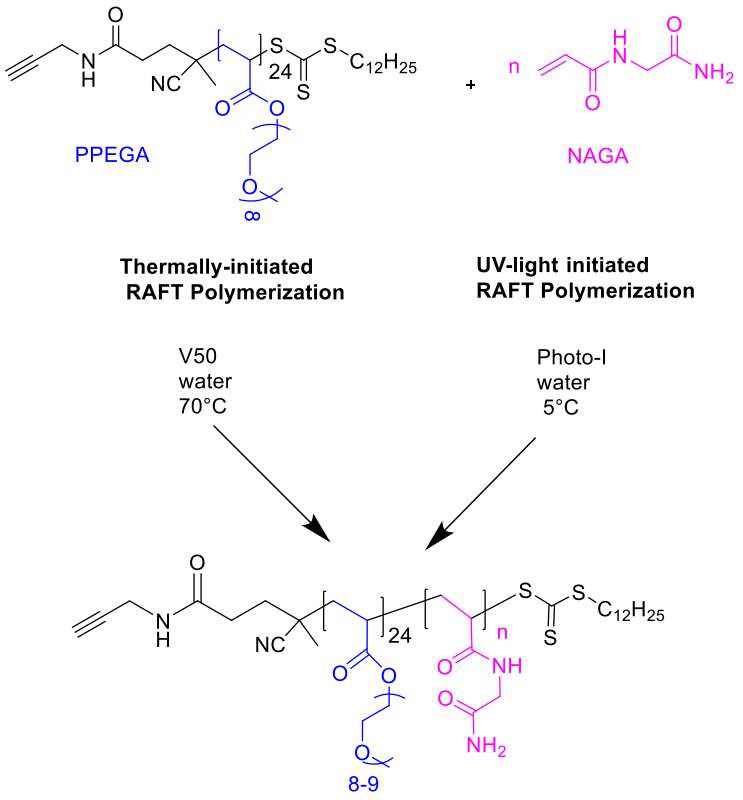


Scheme II.7. RAFT polymerization of NAGA using Thermal-PPEGA$_{24}$ as macro-CTA with various initiating radical sources (thermal and UV-light irradiation) and different temperatures.

#### 2.3.2.3.1 Synthesis and thermal properties of Thermal-PPEGA-b-Thermal-PNAGA diblock copolymers

##### 2.3.2.3.1.1 Synthesis of Thermal-PPEGA-b-Thermal-PNAGA diblock copolymers by thermally-initiated RAFT polymerization of NAGA in water

The thermally-initiated RAFT polymerization of NAGA was studied at 70 °C in water using Thermal-PPEGA$_{24}$ as macro-CTA and V50 as hydrosoluble initiator with the initial molar ratio of [NAGA]$_0$/[Thermal-PPEGA$_{24}$]$_0$/[V50]$_0$ equals to 200/1/0.3 and a solid content of 2.4 wt.%. A kinetic plot for the thermally initiated RAFT of NAGA was obtained by withdrawing samples at different time intervals (Figure II.26). Figure II.26A shows the evolution of ln([M]$_0$/[M]$_t$) and conversion *vs.* time. A constant slope of ln([M]$_0$/[M]$_t$) *vs.* reaction time, relevant with a constant concentration of propagating radicals is observed up to 80% NAGA conversion. The evolution of $\overline{M_{n,SEC}}$ *versus* NAGA conversion shows a slight increase during polymerization, as obtained for the trend of $\overline{M_{n,theo}}$ (Figure II.26B), which demonstrate that the polymerization is under a good control. The dispersity seems to remain stable around 1.4. The discrepancy between $\overline{M_{n,SEC}}$ and $\overline{M_{n,theo}}$ is attributed to the use of linear PMMA standards for the determination of $\overline{M_{n,SEC}}$ since the hydrodynamic volume of PMMA in DMSO differs from that of PNAGA, causing overestimation of the molar mass (Figure II.26B). At high NAGA conversion (> 80%), a decrease in the radical concentration would be expected due to a moderate proportion of dead chains with the appearance of high molar mass shoulders in the SEC traces at high NAGA conversions (Figure II.27).

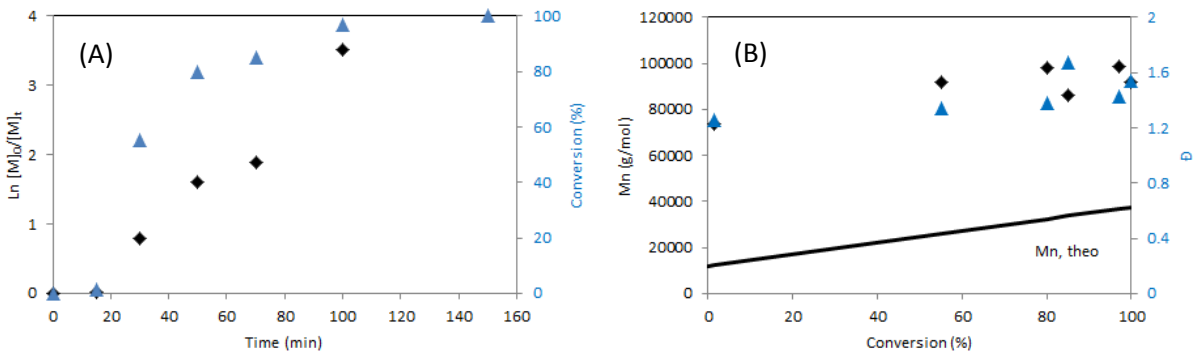


Figure II.26. Evolution of (A) ln([M]$_0$/[M]$_t$) (black square) and conversion (blue triangle) *vs.* time and (B) evolution of $\overline{M_{n,SEC}}$ (black square) and *Đ* (blue triangle*) vs.* NAGA conversion during the thermally-initiated RAFT polymerization of NAGA using V50 and Thermal-PPEGA$_{24}$ in water at 70°C with a solid content of 2.4 wt.%.

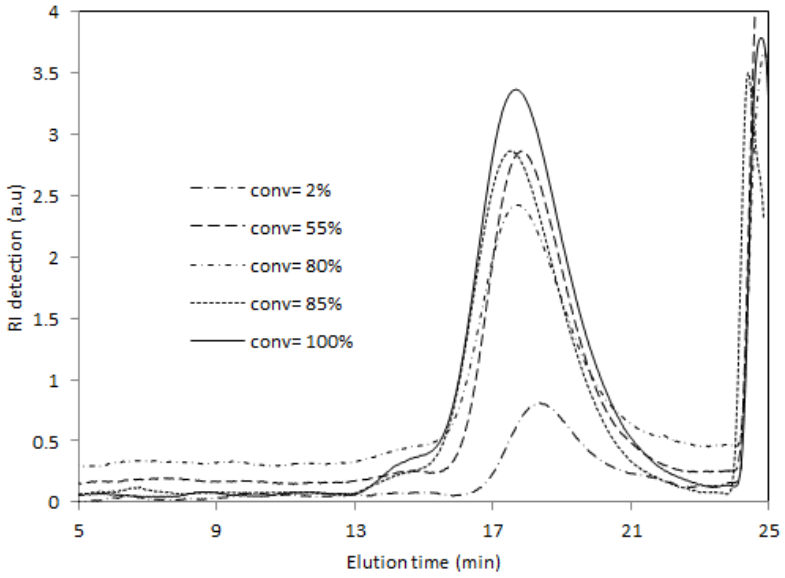


Figure II.27. Overlaid SEC (DMSO, LiBr) traces using RI detection of crude polymerization mixtures obtained during the thermally-initiated RAFT polymerization of NAGA using V50 and Thermal-PPEGA$_{24}$ in water at 70°C with a solid content of 2.4 wt.%.

The $^{1}$H-NMR spectrum (Figure II.28) of the final Thermal-PPEGA$_{24}$-*b*-Thermal-PNAGA shows signals at 3.35 ppm ((CH$_2$CH$_2$O)$_8$C*H$_3$*, labeled e) and 4.22 ppm (C(=O)OC*H$_2$*CH$_2$O-(CH$_2$CH$_2$O)$_8$, labeled d) characteristic of the PPEGA block. The signal from 1.3 to 2.5 ppm corresponds to the CH$_2$ and CH protons of PPEGA and PNAGA backbones. These signals were used to determine the molar composition of the resulting copolymer: $\overline{DP_{n,\,PPEGA}}$ = 24 and $\overline{DP_{n,\,PNAGA}}$ = 196.

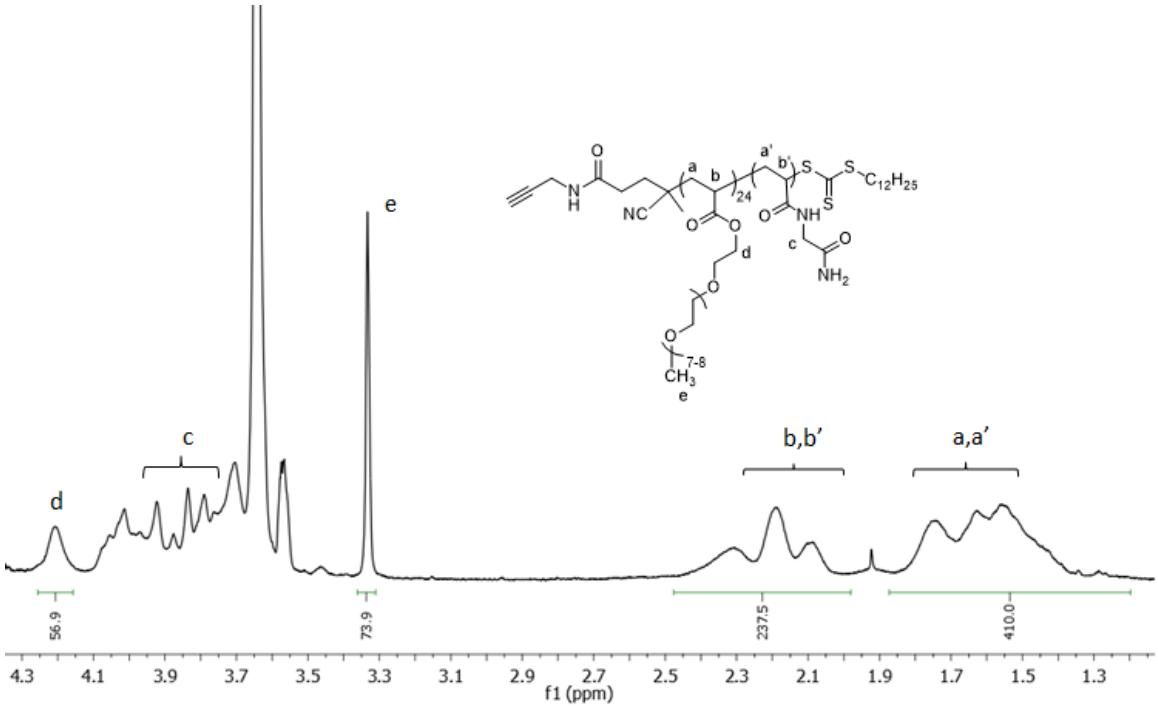


Figure II.28. $^{1}$H-NMR spectrum (400 MHz, $D_2O$) of Thermal-PPEGA$_{24}$-*b*-Thermal-PNAGA$_{196}$ synthesized by thermally-initiated RAFT polymerization of NAGA mediated through V50 and Thermal-PPEGA$_{24}$ ([NAGA]$_0$/[Thermal-PPEGA$_{24}$]$_0$/[V50]$_0$ = 200/1/0.3, solid content of 2.4 wt.%) in water at 70°C after 150 min of reaction.

The overlaid SEC traces of Thermal-PPEGA$_{24}$ and Thermal-PPEGA$_{24}$-*b*-Thermal-PNAGA$_{196}$ block copolymer obtained using RI detection was illustrated in Figure II.29. The chain extension of Thermal-PPEGA$_{24}$ using NAGA monomer by thermally-initiated RAFT polymerization at 70°C is nearly quantitative but a bimodal and broad SEC signal was observed illustrating the presence of side reactions including irreversible termination reactions at complete NAGA conversion. $\overline{M_{n,SEC}}$ = 91 700 g/mol and $Đ$ = 1.54 (SEC DMSO, PMMA standards).

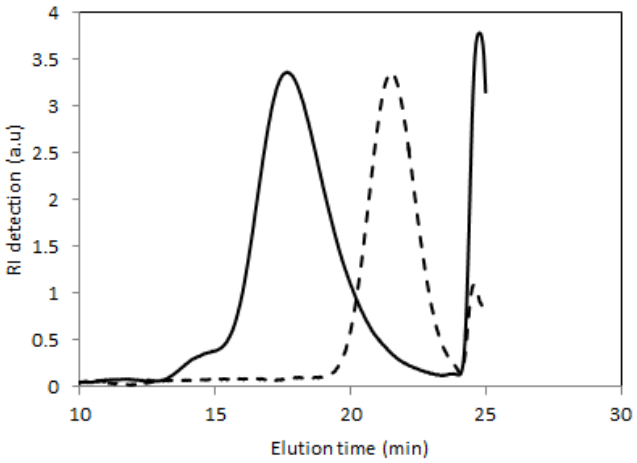


Figure II.29. Overlaid SEC (DMSO, LiBr) traces using RI detection of the Thermal-PPEGA$_{24}$ (dashed line) and of the Thermal-PPEGA$_{24}$-*b*-Thermal-PNAGA$_{196}$ copolymer (full line) obtained after chain extension through thermally-initiated RAFT polymerization of NAGA mediated through V50 and Thermal-PPEGA$_{24}$ ([NAGA]$_0$/[Thermal-PPEGA$_{24}$]$_0$/[V50]$_0$ = 200/1/0.3, solid content of 2.4 wt.% in water at 70°C.

#### 2.3.2.3.1.2 Thermal properties of Thermal-PPEGA$_{24}$-b-Thermal-PNAGA$_{196}$ diblock copolymers

The UCST-type thermosensitive behavior of Thermal-PPEGA$_{24}$-*b*-Thermal-PNAGA$_{196}$ block copolymer was studied by UV-vis spectrophotometry at a wavelength of 650 nm with a polymer concentration of 10 g.L$^{-1}$ in water. The applied cooling/heating rate was 1 °C.min$^{-1}$. There was a sharp phase transition of the sample upon heating (Figure II.30). The transmittance increased gradually from 15 to 22°C, the solution became completely transparent at 22 °C. The UCST value of copolymer was taken as mid-point of the curve at 18.5 °C upon heating. A hysteresis of 8 °C can be observed, the UCST value upon cooling of Thermal-PPEGA$_{24}$-*b*-Thermal-PNAGA$_{196}$ is 10°C. Compare to the UCST value of PNAGA$_{200}$ (22.5 °C upon heating and 10.5 °C upon cooling), when the PPEGA block was introduced, the UCST value of Thermal-PPEGA$_{24}$-*b*-Thermal-PNAGA$_{196}$ diblock copolymer is lower. This phenomenon is consistent with the literature[43] as incorporating the hydrophilic block into polymer results in the decrease of UCST value.

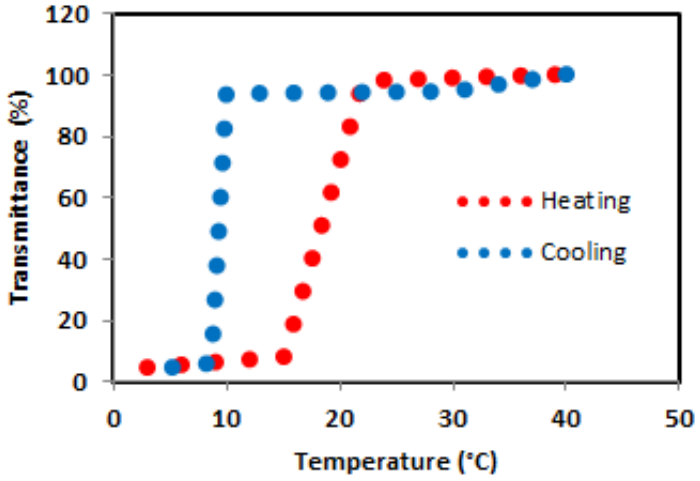


Figure II.30. Plots of transmittance as a function of temperature of a Thermal-PPEGA$_{24}$-*b*-Thermal-PNAGA$_{196}$ block copolymer aqueous solution at 10 g.L$^{-1}$.

#### 2.3.2.3.2 Synthesis and thermal properties of UV-PPEGA-b-UV-PNAGA diblock copolymers

##### 2.3.2.3.2.1 Synthesis of UV-PPEGA-b-UV-PNAGA diblock copolymers by UV-light initiated RAFT-PITSA of NAGA

In the following section, we perform UV light-initiated RAFT-PITSA of NAGA in the presence of photo-I at low temperature 5°C (T ≤ UCST of PNAGA) with a solid content of 2.4 wt.%. The initial molar ratio of [NAGA]$_0$/[Thermal-PPEGA$_{24}$]$_0$/[Photo-I]$_0$ equals to 200/1/0.3. A kinetic plot for the UV-light initiated RAFT of NAGA was obtained by withdrawing samples at different time intervals. As shown in Figure II.31A, a very fast initial rate of polymerization was observed which reached approximatively 90 % NAGA conversion after 20 min (instead of 80% NAGA conversion after 50 min for the thermally-initiated RAFT polymerization). A constant slope of ln([M]$_0$/[M]$_t$) *vs.* reaction time, relevant with a constant concentration of propagating radicals is observed until reaching 80% NAGA conversion. At high NAGA conversion, a decrease of the apparent propagation rate constant was observed, with a sharp increase in both $\overline{M_{n,SEC}}$ and *Đ*. In addition, broad SEC traces (Figure II.32) of block copolymers have been obtained by UV-light initiated RAFT-PITSA of NAGA at 5°C. The loss of control observed could be explained by the collapse of PNAGA at T ≤ UCST.

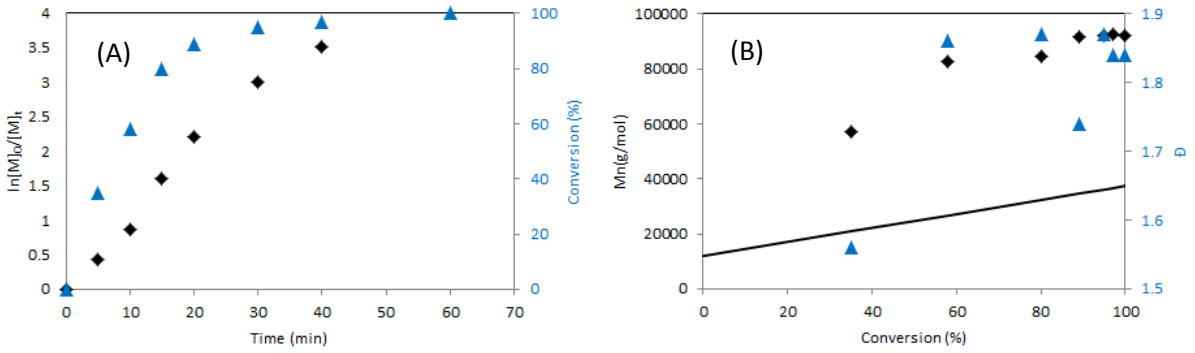


Figure II.31. Plots of (A) evolution of $\ln([M]_0/[M]_t)$ and conversion *vs.* time and (B) evolution of $\overline{M_{n,SEC}}$ (symbol) and $\overline{M_{n,theo}}$ (line) and *Đ vs.* NAGA conversion during the UV-light initiated RAFT-PITSA of NAGA using Photo-I as photoinitiator and Thermal-PPEGA$_{24}$ as macro-CTA in aqueous dispersion at 5 °C.

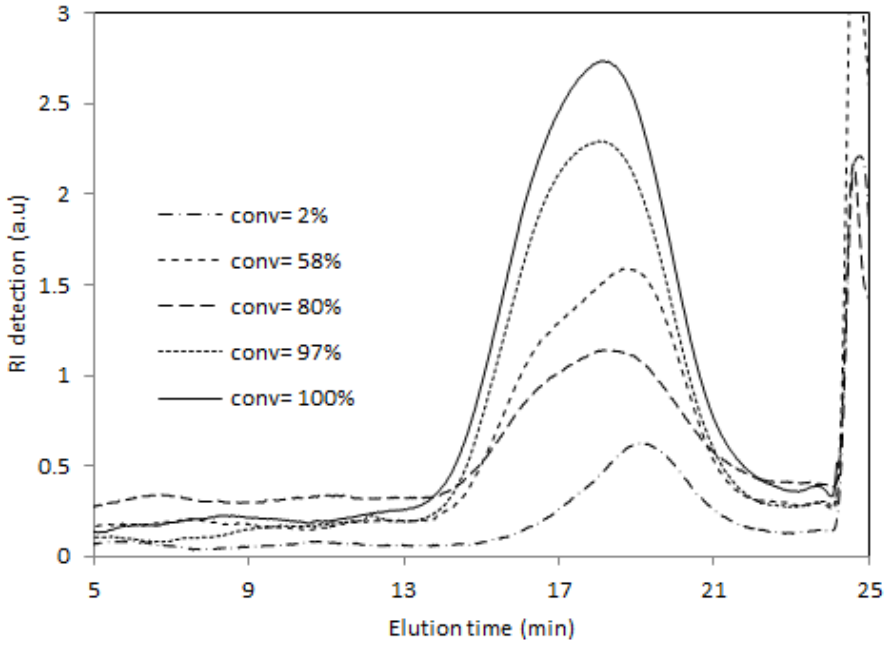


Figure II.32. Overlaid SEC (DMSO, LiBr) traces using RI detection of crude polymerization mixture obtained during the UV-light initiated RAFT-PITSA of NAGA using Photo-I as photoinitiator and Thermal-PPEGA$_{24}$ as macro-CTA in aqueous dispersion at 5 °C.

The final solution was opalescent due to the collapse of PNAGA block at low temperature (Figure II.33).

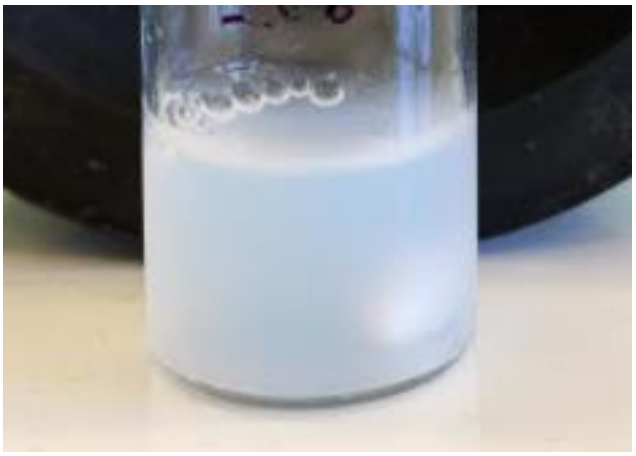

Figure II.33. The final solution picture resulting from UV-light initiated RAFT-PITSA of NAGA using Photo-I as photoinitiator and Thermal-PPEGA$_{24}$ as macro-CTA in aqueous dispersion at 5 °C.

The $^{1}$H NMR spectrum (Figure II.34) of the resulting Thermal-PPEGA$_{24}$-*b*-UV-PNAGA shows signals at 3.35 ppm ((CH$_2$CH$_2$O)$_8$C*H*$_3$, labeled e) and 4.22 ppm (C(=O)OC*H*$_2$CH$_2$O-(CH$_2$CH$_2$O)$_8$, labeled d) characteristic of the PPEGA block. The signal from 1.5 to 2.7 ppm corresponds to the CH$_2$ and CH protons of P(PEGA-*b*-NAGA) backbone. These signals were used to determine the molar composition of the resulting copolymer: $\overline{DP_{n,\,PPEGA}}$ = 24 and $\overline{DP_{n,\,PNAGA}}$ = 187.

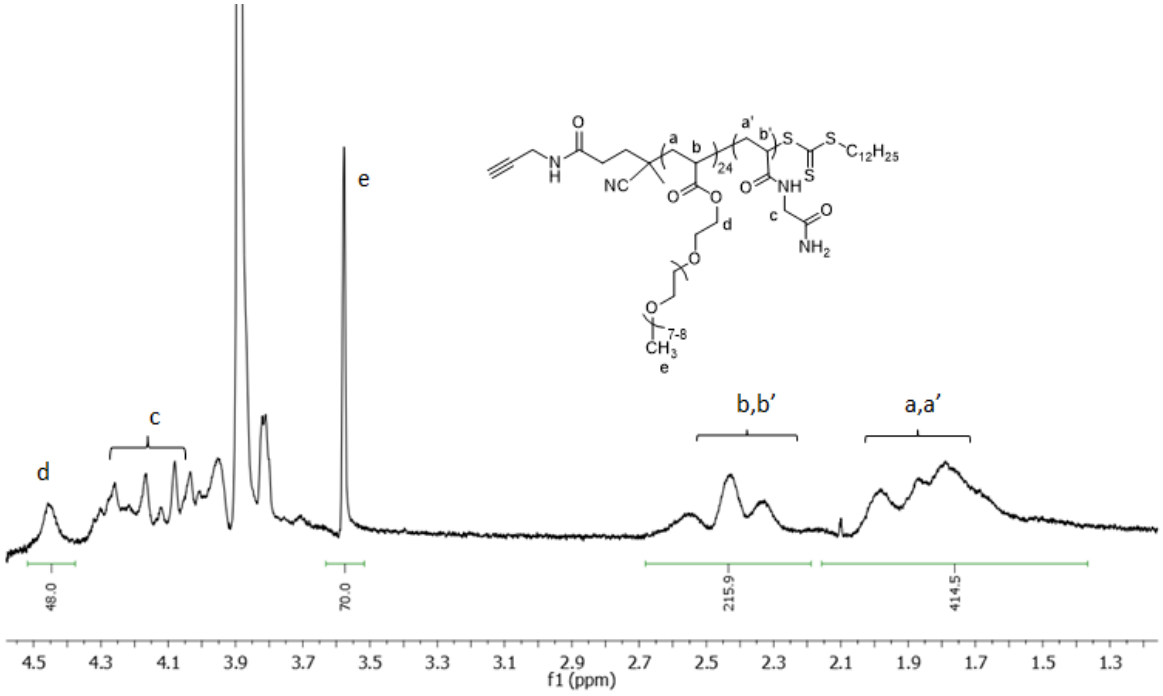


Figure II.34. $^{1}$H-NMR spectrum (400 MHz, D$_2$O) of Thermal-PPEGA$_{24}$-*b*-UV-PNAGA$_{187}$ synthesized by UV-light initiated RAFT-PITSA of NAGA using Photo-I and Thermal-PPEGA$_{24}$ ([NAGA]$_0$/[Thermal-PPEGA$_{24}$]$_0$/[Photo-I]$_0$ = 200/1/0.3) in aqueous dispersion at 5°C and a solid content of 2.4 %.

The SEC analysis of the resulting copolymer Thermal-PPEGA$_{24}$-*b*-UV-PNAGA$_{187}$ showed a quantitative extension of Thermal-PPEGA$_{24}$ resulting in a monodal chromatogram (Figure II.35) with $\overline{M_{n,SEC}}$ = 92 100 g.mol$^{-1}$ and Đ = 1.84 relative to PMMA standards.

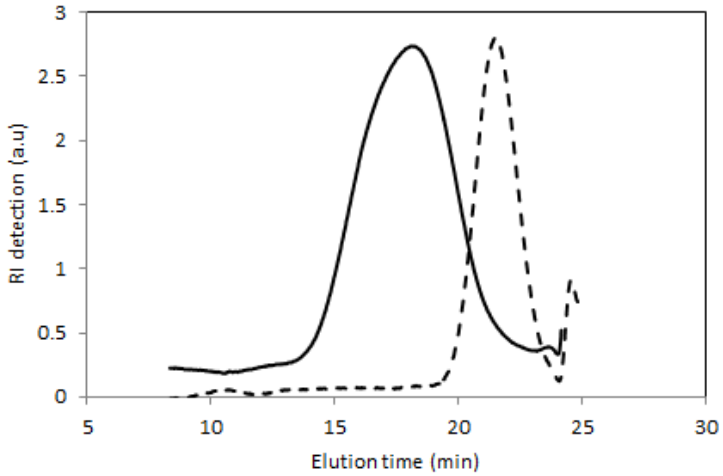


Figure II.35. Overlaid SEC (DMSO, LiBr) traces using RI detection of the Thermal-PPEGA$_{24}$ (dash line) and of the Thermal-PPEGA$_{24}$-*b*-UV-PNAGA$_{187}$ copolymer (line) obtained after chain extension of Thermal-PPEGA$_{24}$ through UV-light initiated RAFT-PITSA of NAGA using the [NAGA]$_0$/[Thermal-PPEGA$_{24}$]$_0$/[Photo-I]$_0$ initial molar ratio of 200/1/0.3, in aqueous dispersion at 5°C and a solid content of 2.4 wt.%.

The difference in chain extension efficiency using either UV-light initiated RAFT-PITSA at 5 °C or thermally-initiated RAFT polymerization at 70°C can be explained by either the initiating radical source and/or the polymerization process (homogeneous polymerization at 70°C or PITSA in aqueous dispersed medium at 5°C). Results show lower dispersity values through thermally-initiated homogeneous polymerization. However, the higher temperature employed in thermal activation process leads to the presence of a shoulder of high molecular weight, which is not observed using UV-light irradiation.

#### 2.3.2.3.2.2 Thermal properties of UV-PPEGA$_{24}$-b-UV-PNAGA$_{187}$ diblock copolymers

There was a sharp phase transition of Thermal-PPEGA$_{24}$-*b*-UV-PNAGA$_{187}$ diblock copolymer upon heating (Figure II.36). The transmittance of polymer solution increased gradually from 12 to 16°C and became completely transparent at 16 °C. The UCST value of copolymer was taken as mid-point of the curve at 14 °C upon heating. A hysteresis of 5 °C can be observed in the cooling process, results in the UCST upon cooling of 9 °C. Interestingly, there is a significant difference in the phase transition temperature of the Thermal-PPEGA$_{24}$-*b*-UV-PNAGA$_{187}$ obtained by UV-light initiated RAFT-PITSA and Thermal-PPEGA$_{24}$-*b*-Thermal-PNAGA$_{196}$ obtained by homogeneous thermally initiated RAFT polymerization. The cloud point of Thermal-PPEGA$_{24}$-*b*-UV-PNAGA$_{187}$ solution upon heating is 14 °C,

lower than that of Thermal-PPEGA$_{24}$-*b*-Thermal-PNAGA$_{196}$ (18.5°C). However, the Thermal-PPEGA$_{24}$-*b*-UV-PNAGA$_{187}$ represents a sharper phase transition temperature with narrower hysteresis of 5 °C between heating and cooling processes. This is probably due to the lower $\overline{DP_{n,\,PNAGA}}$ of the PNAGA block in the case of Thermal-PPEGA$_{24}$-*b*-UV-PNAGA$_{187}$, which leads to a lower UCST value of copolymer, as previously reported.[44]

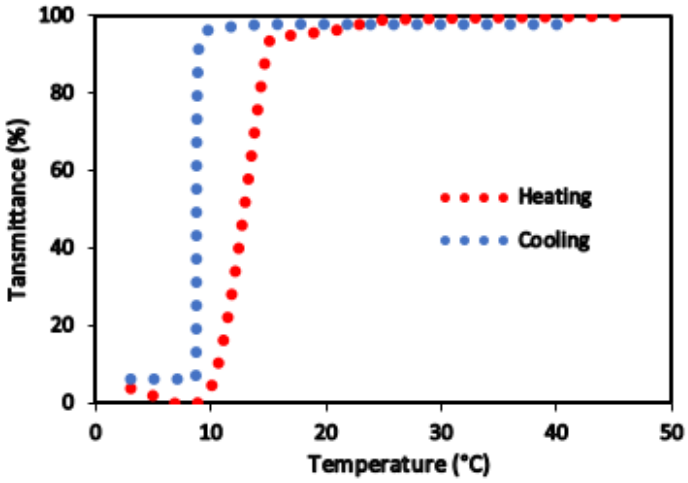


Figure II.36. Plots of transmittance as a function of temperature measured for an aqueous solution (10 g.L$^{-1}$) of Thermal-PPEGA$_{24}$-*b*-UV-PNAGA$_{187}$ block copolymer.

Therefore, the UV-light initiated RAFT-PITSA at low temperature (5°C) allows to target a well-defined block copolymer with UCST-type thermosensitive behavior and displaying a sharp phase transition temperature with a narrow hysteresis compared to thermal activation at high temperature.

## 2.4 Conclusions

PPEGAs were obtained by RAFT polymerization using either thermal activation or UV-light activation with a sufficient molar mass control and narrow molar masses distributions at low PEGA conversions. Despite a low temperature reaction, UV-light initiated RAFT polymerization did not afford an improved control compared to the thermally-initiated RAFT polymerization. However, employing a lower monomer concentration and stopping the reaction at low conversion results in a better control of PEGA polymerization. Such well-defined PPEGAs are able to be used as macro-CTA for further synthesis of thermosensitive diblock copolymers by RAFT polymerization in water.

Well-defined LCST-type thermosensitive PPEGA-*b*-PNIPAm diblock copolymers were obtained by RAFT polymerization using UV-light activation at 25 °C or 37 °C with a sufficient molar mass control and narrow molar masses distributions. Compare to thermal activation, UV-light activation offer a very fast initial rate of NIPAm polymerization, which reached 100% conversion after 1h (instead of 6h

for the thermally-initiated RAFT polymerization). However, the dispersity value is higher for PPEGA-*b*-PNIPAm diblock copolymers obtained by UV-light initiated RAFT polymerization at 70 °C

UCST-type thermosensitive PPEGA-*b*-PNAGA diblock copolymers were prepared using either UV-light initiated RAFT-PITSA at 5 °C or thermally-initiated RAFT polymerization at 70°C. Results show lower dispersity values through thermally-initiated homogeneous polymerization. However, the higher temperature employed in thermal activation process results in the presence of a high molar mass shoulder, which is not observed in the case of UV-light irradiation. In addition, compared to thermal activation at high temperature, UV-light initiated RAFT-PITSA at low temperature (5°C) allows targeting a block copolymer with UCST behavior displaying a sharper phase transition temperature with narrow hysteresis. The UCST value of Thermal-PPEGA$_{24}$-*b*-UV-PNAGA$_{187}$ solution upon heating is 14 °C, lower than that of Thermal-PPEGA$_{24}$-*b*-Thermal-PNAGA$_{196}$ (18.5°C)

## 2.5 Experimental section

### 2.5.1 Materials

All reagents were purchased from Sigma-Aldrich unless otherwise noted. *N*-isopropylacrylamide (NIPAm, >99%), 4,4'-azobis(4-cyanovaleric acid) (ACVA, 98%), 2,2'-azobis(2-methylpropionamidine) dihydrochloride (V50, 97%), 2-hydroxy-4'-(2-hydroxyethoxy)-2-methylpropiophenone (Photo-I, 98%), N,N-dimethylformamide (DMF, 99%), and aluminum oxide (basic activated), ammonia 0.5M (NH3, 98%), tetrahydrofuran (THF, 99%), potassium carbonate ($K_2CO_3$, 98%), L-asparaginamide hydrochloride (Aspa, 98%), glycinamide hydrochloride (98%), acryloyl chloride (98%), methanol (analytical use, 99%), dichloromethane ($CH_2Cl_2$, HPLC grade, Fisher Chemical), diethyl ether (99.8 %, Carlo Erba) and acetone (pure, Carlo Erba) were used without purification. All deuterated solvents were purchased from Euriso-top. Oligo(ethylene glycol) acrylate (PEGA of $M_n$ = 480 g.mol$^{-1}$, pure) was passed through a column of aluminum oxide prior to polymerization. The 2-cyano-5-oxo-5-(prop2-yn-1-ylamino)pentan-2yldodecyltrithiocarbonate (COPYDC) have been synthesized following reported procedures.[10] Ultra-pure water was obtained from a PureLab ELGA system and had a conductivity of 18.2 MΩm at 25°C.

### 2.5.2 Characterizations

**Nuclear magnetic resonance (NMR) spectroscopy.** Nuclear Magnetic Resonance (NMR) spectra were recorded on a Bruker AC-400 spectrometer for $^1$H-NMR (400 MHz and 200 MHz). Chemical shifts are reported in ppm relative to the deuterated solvent resonances.

**Size exclusion chromatography (SEC).** The average molar mass (number average molar mass $\overline{M_{n,SEC}}$ and dispersity (Đ = $\overline{M_{w,SEC}}$ / $\overline{M_{n,SEC}}$)) values of PPEGAs were measured by size exclusion chromatography (SEC) using THF as an eluent. Molar masses and dispersities were calculated using BREEZE 2 software. SEC was carried out using a system equipped with a pre-column (Waters, Styragel Guard column, 4.6 × 30 mm) followed by 2 columns (Waters, Styragel HR4 THF, 300 × 7.8 mm and Waters, Styragel HR2 THF, 300 × 7.8 mm) and with a Waters 2414 differential refractometer (RI) and a Waters 2998 UV-visible detector. The instrument was operated at a flow rate of 1.0 mL.min$^{-1}$, at a temperature of 30 °C, and was calibrated with narrow linear polystyrene (PS) standards ranging in molar mass from 580 g.mol$^{-1}$ to 483 000 g.mol$^{-1}$.

The average molar masses and dispersity values of PPEGA-*b*-PNIPAm diblock copolymers were measured by SEC using DMF-LiBr (1 g L$^{-1}$) as an eluent and using a system equipped with a guard column (Polymer Laboratories, PL Gel 5 µm), followed by two columns (Polymer Laboratories, 2 PL gel 5 µm MIXED-D columns) and equipped with a Waters 410 differential refractometer (RI) and a

Waters 481 UV-Visible detector. The instrument was operated at a flow rate of 1.0 mL.min$^{-1}$ at 60 °C and was calibrated with narrow linear poly(methyl methacrylate) (PMMA) standards ranging in molar mass from 904 g mol$^{-1}$ to 304 000 g mol$^{-1}$ . Molar masses and dispersities were calculated using Waters EMPOWER software.

The average molar masses (number-average molar mass $\overline{M_{n,SEC}}$, weight-average molar mass $\overline{M_{w,SEC}}$) and dispersity (Đ = $\overline{M_{w,SEC}}$ / $\overline{M_{n,SEC}}$)) of PPEGA-*b*-PNAGA diblock copolymer were measured by SEC using DMSO (LiBr 0.1M) as an eluent, and carried out using a system equipped with a pre-column and one PSS-GRAM analytical column. The instrument operated at a flow rate of 0.7 mL.min$^{-1}$ at 50°C and was calibrated with narrow linear PMMA standards ranging in molecular weight from 900 g.mol$^{-1}$ to 537 000 g.mol$^{-1}$.

The average molar masses and dispersity values of different polyacryamides P(VDM-Am), P(VDM-Gly) and P(VDM-Aspa) were measured by SEC in water with 0.1 M of $NaNO_3$ and carried out using a system equipped with a pre-column (Waters, Ultrahydrogel, 6 * 40 mm) followed by 3 columns (Waters, Ultrahydrogel 1000, 500, 120, 300 * 7.8 mm) and with a Waters 2998 UV detector and a Waters 2414 differential refractometer detector. The mobile phase is an aqueous solution (utra pure water from ELGA Lab Water system) of 0.1 M $NaNO_3$ at a flow rate of 1.0 mL.min$^{-1}$ and temperature of 35°C. Column calibration was provided by narrow poly(ethylene oxide) (PEO) standards with molar mass from 615 g.mol$^{-1}$ to 942 000 g.mol$^{-1}$.

**UV-Vis Spectrophotometry.** Turbidity measurements were carried out on a Aligent Cary 100 UV-Vis Spectrophotometer at wavelength of 650 nm. The phase transition temperatures were determined using polymer solution at a concentration of 10 g.L$^{-1}$ in water. The solution was cooled to 5°C overnight before UV measurement; a heating rate of 1 °C.min$^{-1}$ was employed to determine the phase transition temperature of the thermosensitive polymer.

**HR-MS.** High-resolution Mass Spectra (HR-MS) were recorded on a Bruker MicroTOF-QIII (ESI+) to determine the molar mass of NAGA monomer.

**Differential scanning calorimetry (DSC)**. Measurement was performed on a TA Instruments Q100 connected to a computer in aluminum pans under nitrogen. The DSC instrument was calibrated using an indium standard. Sample was heated from 25 to 200 °C at a heating rate of 10 °C.min$^{-1}$ and under a static nitrogen atmosphere.

**Thermally-initiated RAFT polymerization of PEGA in DMF using COPYDC as CTA (Thermal-PPEGA)**. In a round bottom flask, PEGA (1.364 g, 2.84 mmol, 50 equiv.) and COPYDC (0.025 g, 0.057 mmol, 1 equiv.) were dissolved in 1 mL DMF. Then 1 mL of ACVA (1.59 mg, 0.1 equiv.) solution (15.9 mg

ACVA/ 10 mL of DMF) was added ($[PEGA]_0$ = 1.45 mol.$L^{-1}$). The resulting solution was degassed for 30 min by bubbling with Argon. The flask was placed in a preheated oil bath of 70°C for 120 min. The reaction was stopped by cooling the round bottom flask in nitrogen liquid. PEGA conversion of 42 % was obtained by $^1$H-NMR spectroscopy. The polymer was purified by dialysis in water for 3 days and freeze-dried. A final yellow highly viscous liquid was obtained. $^1$H-NMR (400 MHz, $CDCl_3$) δ (ppm) = 3.65 (m, -C$H_2$C$H_2$O- from EO repeating units), 3.38 (s, -$(CH_2CH_2O)_9$C$H_3$- from repeating units of PPEGA), 0.88 (t, -C$H_3$ from dodecyl chain), 4.1-4.3 (from methylene protons C(=O)OC$H_2$$CH_2O(CH_2CH_2O)_9$ and HC≡CC$H_2$NH), $\overline{DP_{n,\,PPEGA}}$ = 20, $\overline{M_{n,NMR}} = 10\,840$ g.$mol^{-1}$; SEC (THF, PS standards), $\overline{M_{n,SEC}}$ = 10400 g.$mol^{-1}$ and $Đ$ = 1.18

**UV-light initiated RAFT polymerization of PEGA in DMF using COPYDC as CTA (UV-PPEGA)**. A photo-I solution was prepared by dissolving 50.9 mg of Photo-I in 10 g of DMF. PEGA (5.445 g, 11.3 mmol, 50 equiv.), COPYDC (0.1 g, 0.2 mmol, 1 equiv.) and 1 g of photo-I solution (0.02 mmol, 0.1 equiv.) were added to 26.2 mL DMF ($[PEGA]_0$ = 0.39 M). After purging with argon for 30 minutes, the mixture was placed in the middle of a UV lamp (λ = 365 nm, P = 34 mW/$cm^2$) under an argon atmosphere with stirring. The reaction was conducted for 1h45min and stopped by turning off the light and cooling the mixture in nitrogen liquid. PEGA conversion of 35 % was obtained by $^1$H-NMR spectroscopy. The polymer was purified by dialysis in water for 3 days and freeze-dried. A final yellow highly viscous liquid was obtained and the number-average polymerization degree was determined by $^1$H-NMR spectroscopy (400 MHz, $CDCl_3$): $\overline{DP_{n,\,PPEGA}}$ = 18, $\overline{M_{n,NMR}} = 9080$ g.$mol^{-1}$. The molar mass and dispersity were determined by SEC in THF (PS standards): $\overline{M_{n,SEC}}$ = 8500 g.$mol^{-1}$ and $Đ$ = 1.27.

**Synthesis of Thermal-PPEGA-*b*-Thermal-PNIPAm diblock copolymer by thermally-initiated RAFT-PITSA polymerization of NIPAm from Thermal-PPEGA**. In a round bottom flask, a Thermal-PPEGA (run 3, Table II.1) ($\overline{DP_{n,\,PPEGA}}$ = 20, 0.05 g, 0.005 mmol, 1 equiv.) was dissolved in 0.05 mL DMF. The NIPAm monomer (0.113 g, 1mmol, 204 equiv.) and 0.1 mL (0.0015 mmol, 0.3 equiv.) of V50 solution in water (containing 0.14 mg in 1 mL of water) was added. Total amount of water is 4.5 g. The final solid content is 2.4 wt.%. The solution was degassed by bubbling argon for 30 min. The flask was placed in a preheated oil bath of 70°C for 6h. A complete conversion of NIPAm was observed by $^1$H-NMR spectroscopy. The reaction was stopped by opening the flask to air. The copolymer was freeze-dried to obtain final product. $^1$H-NMR (400 MHz, $CDCl_3$) δ (ppm) = 3.35 ($(CH_2CH_2O)_{7-8}$C$H_3$) and 4.15 (C(=O)OC$H_2$$CH_2O$-$(CH_2CH_2O)_{7-8}$) from PPEGA block, 3.95 (−NH−C$H$$(CH_3)_2$) from PNIPAM block. $\overline{DP_{n,\,PNIPAM}}$ = 200, $\overline{M_{n,theo}} = 32\,640$ g.$mol^{-1}$; SEC (DMF, PMMA standards): $\overline{M_{n,SEC}}$ = 41200 g.$mol^{-1}$ and $Đ$ = 1.56.

**Synthesis of UV-PPEGA-*b*-UV-PNIPAm diblock copolymer by UV-light initiated RAFT polymerization of NIPAm from UV-PPEGA.** A photo-I solution was prepared by dissolving 1.86 mg Photo-I in 1 g water. UV-PPEGA (run 2, table II.2) ($\overline{DP_{n,\,PPEGA}}$ =18, 0.025 g, 0.0028 mmol, 1 equiv.), NIPAm (63.8 mg, 0.564 mmol, 204 equiv.) and 0.1 mL of photo-I solution (0.00084 mmol, 0.3 eq.) were added to 3.47 g of water to give a solid content of 2.4 wt%. 0.05 g of DMF was added in the mixture as an internal reference for $^1$H-NMR analysis to determine monomer conversion. Then, after purging with argon for 30 minutes, the mixture was placed in the middle of a UV lamp (λ = 365 nm, P = 34 mW/cm$^2$) under an argon atmosphere with stirring. The reaction was stopped by turning off the light and cooling the mixture in nitrogen liquid. NIPAm conversion of 100 % was obtained according to $^1$H-NMR spectroscopy after 1h at 25 °C. The copolymer was freeze-dried to obtain final product. The number-average polymerization degree was determined by $^1$H-NMR spectroscopy (400 MHz, $CDCl_3$): $\overline{DP_{n,\,PPEGA}}$ =18 $\overline{DP_{n,\,PNIPAM}}$ = 201, $\overline{M_{n,NMR}} = 31\,793$ g.mol$^{-1}$. The molar mass and dispersity were determined by SEC in DMF (PMMA standards): $\overline{M_{n,SEC}}$ = 56 400 g.mol$^{-1}$ and $Đ$ = 1.34.

**Synthesis of VDM-based acrylamide from VDM and $NH_3$ (VDM-Am).** To a solution of 0.5 g VDM (3.6 mmol) in THF (0.4 mL), a solution of ammonia (92 mg, 5.4 mmol) in THF (1.1 mL) with initial molar ratio of VDM/$NH_3$ equal to 1/1.5, was added dropwise. The reaction was conducted at soft condition as room temperature. After 1h, a white precipitate was observed and volatiles were removes under reduced pressure to give a white solid. The yield of reaction was 100%. $^1$H-NMR (400 MHz, $D_2O$) δ (ppm) = 5.78-6.36 (m, - C$H_2$C$H$ –vinyl protons), 1.45 (s, -C$H_3$).

**Synthesis of VDM-based acrylamide from VDM and glycinamide (VDM-Gly).** The synthesis of VDM-Gly was performed using VDM (1 g, 7.2 mmol) and glycinamide hydrochloride (0.8 g, 7.2 mmol) as reagents in 10 mL DMF at 50°C. The reaction was launched overnight in the oil bath. The final solution was passed through an aluminum oxide (base active) column, the solvent was removed by reduced pressure. The yield of reaction was 70%. $^1$H-NMR (400 MHz, $D_2O$) δ (ppm) = 5.78-6.36 (m, - C$H_2$C$H$ –vinylic protons), 1.45 (s, -C$H_3$), 3.82 (s, NHC$H_2$CO).

**Synthesis of VDM-based acrylamide from VDM and L-asparaginamide (VDM-Aspa).** VDM (1 g, 7.2 mmol) and L-asparaginamide hydrochloride(1.2 g, 7.2 mmol) were added in 10 of mL DMF. The reaction was launched overnight in the oil bath at 50°C. The final solution was passed through an aluminum oxide (base active) column, the solvent was removed by reduced pressure. The yield of reaction was 63 %. $^1$H-NMR (400 MHz, $D_2O$) δ (ppm) = 5.78-6.36 (m, - C$H_2$C$H$ –vinyl protons), 1.45 (s, -C$H_3$), 2.65 (m, CHC$H2$CO), 4.65 (m, NHC$H$(CO)($CH_2$)).

**Synthesis of P(VDM-Am).** In a 10 mL glass vial, 1 mg of ECT (0.003 mmol, 1eq) was dissolved by 0.05 mL DMF. Then, 93.6 mg VDM-Am (0.6 mmol, 200 eq) and 3.7 g water containing 0.2 mg photo-I

(0.001 mmol, 0.3 eq) were added to give a VDM-Am content of 2.5 wt.%, $[VDM\text{-}Am]_0$ = 0.18 M. The glass vial was bubbled with argon for 30 min, then the mixture solution was placed under an UV-light source (λ = 365 nm, P = 34 mW) with a stir bar. The polymerization was then stopped after 2h after checking a total conversion of monomer. $\overline{M_{n,SEC}}$ = 13900 g.mol$^{-1}$ (SEC in water, PEO equivalents) and *Đ* = 1.2.

**Synthesis of P(VDM-Gly).** In a 10 mL glass vial, 1 mg of ECT (0.003 mmol, 1eq) was dissolved by 0.05 mL DMF. Then, 100 mg VDM-Gly (0.6 mmol, 200 eq) and 4 g of water containing 0.2 mg photo-I (0.001 mmol, 0.3 eq) were added to give a final VDM-Gly content of 2.5 wt.%, $[VDM\text{-}Gly]_0$ = 0.18 M. The glass vial was bubbled with argon for 30 min then the mixture was placed under an UV-light source (λ = 365 nm, P = 34 mW/cm$^2$) with a stir bar. The polymerization was stopped after 1.5h after checking a total conversion of monomer. $\overline{M_{n,SEC}}$ = 22300 g.mol$^{-1}$ (SEC in water, PEO equivalents) and *Đ* = 1.67.

**Synthesis of P(VDM-Aspa).** In a 10 mL glass vial, 1 mg of ECT (0.003 mmol, 1eq) was dissolved by 0.05 mL DMF. Then, 161 mg VDM-Aspa (0.6 mmol, 200 eq) and 6.4 g of water containing 0.2 mg photo-I (0.001 mmol, 0.3 eq) were added to give a final VDM-Aspa content of 2.5 wt.%, $[VDM\text{-}Aspa]_0$ = 0.18 M. The glass vial was bubbled with argon for 30 min, then the mixture solution was placed under an UV-light source (λ = 365 nm, P = 34 mW/cm$^2$) with a stir bar. The polymerization was stopped after 1.5h after checking a total conversion of monomer. $\overline{M_{n,SEC}}$ = 25600 g.mol$^{-1}$ (SEC in water, PEO equivalents) and *Đ* = 1.71.

**Synthesis of *N*-acryloyl glycinamide (NAGA)**.NAGA was synthesized according to the previous reported procedure in literature.[43] Typically, glycinamide hydrochloride (3 g, 27.13 mmol) and $K_2CO_3$ (7.5 g, 54.27 mmol) were dissolved together in 50 mL of water and cooled using an ice bath. Acryloyl chloride (1.975 mL, 24.42 mmol) dissolved in 100 mL of diethyl ether was added dropwise to the cooled solution under vigorous stirring. The reaction was allowed to proceed at room temperature for 2h. Diethyl ether was removed and the remaining solution was freeze-dried. The crude solid product was extracted with acetone (5 times, 200 mL, 40 °C, 10 min). Insoluble potassium salt was filtered off and acetone was removed by rotary evaporation at 40 °C. The crude product obtained is dissolved in a methanol / dichloromethane mixture (1/4, $V_{total}$ = 240mL) and then purified using silica column (Rf NAGA =0.68 ; Rf acrylate de potassium =0.15). The solvents were removed by evaporator. The NAGA crystal was filtered, dissolved in deionized water and freeze-dried. The yield of the reaction is 64%. Melting point $T_m$ = 140 °C, $^1$H-NMR (400 MHz, $D_2O$) δ (ppm) = 5.78-6.36 ppm (C*H*$_2$C*H*), s, 3.82 ppm (HNC*H*$_2$CO), HR-MS: $C_5H_8O_2N_2$ + Na]$^+$ = 151.0473 Da.

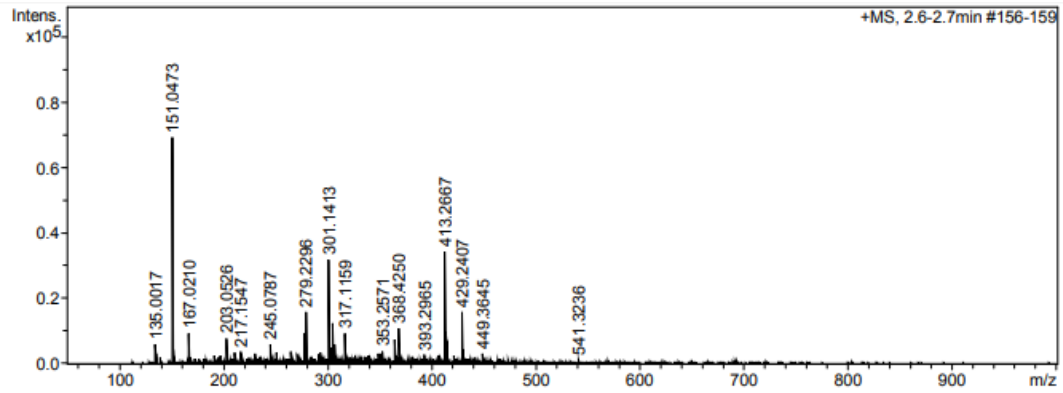


HR-MS of NAGA

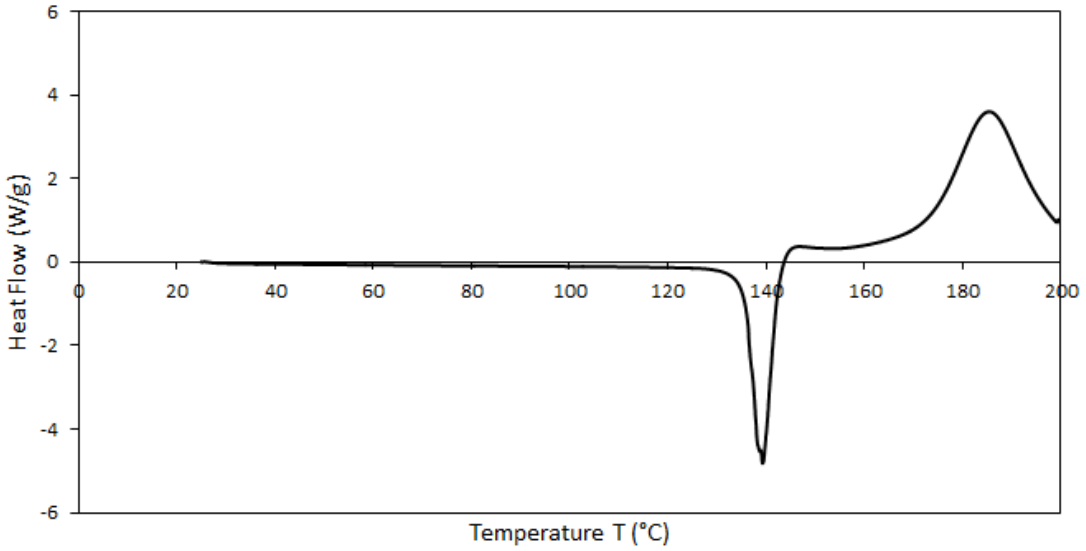


DSC thermogram of NAGA with heating ramp of 5 °C.min$^{-1}$.

**Synthesis of PNAGA by UV-light-initiated RAFT of NAGA from ECT.** In a 10 mL glass vial, 1 mg of ECT (0.003 mmol, 1 eq) was dissolved by 0.05 mL DMF. Then, 76.8 mg NAGA (0.6 mmol, 200 eq) and 3.1 g water containing 0.2 mg photo-I (0.001 mmol, 0.3eq) were added to give a NAGA content of 2.5 wt%, $[NAGA]_0$ = 0.18 M. The glass vial was bubbled with argon for 30 min, then the mixture solution was placed under an UV-light source (λ = 365 nm, P = 34 mW/cm$^2$) with a stir bar. The polymerization was stopped after 2h after checking a total conversion of NAGA by $^1$H NMR spectroscopy. $^1$H-NMR (400 MHz, $D_2O$) δ (ppm) = 3.6- 4.1 ppm (NHC$H_2$CO), 2.0- 2.5 ppm(C$H$CH$_2$)$_n$ and 1.3 -1.8 ppm (CHC$H_2$)$_n$. $\overline{M_{n,SEC}}$ = 60 500 g.mol$^{-1}$ (SEC in DMSO, PMMA equivalents) and $Đ$ = 1.84.

**Synthesis of Thermal-PPEGA-*b*-Thermal-PNAGA diblock copolymer by thermally-initiated RAFT polymerization of NAGA.** In a 10 mL round bottom flask, 107 mg of NAGA (0.84 mmol, 200 eq.) and 50 mg of Thermal-PPEGA$_{24}$ (run 4 Table II.1, 0.0042 mmol, 1 eq.) were dissolved in 6.4 g of water

containing 0.34 mg V50 (0.0013 mol, 0.3 eq.) to give a final solid content of 2.4 wt.% ([ThermalPPEGA$_{24}$]$_0$/[NAGA]$_0$/[V50]$_0$= 1/200/0.3; [NAGA]$_0$ = 0.13 M). The solution was bubbled with argon for 30 min in a preheated oil bath of 70°C. After checking a total conversion of NAGA by $^1$H NMR spectroscopy, the polymerization was stopped after 3h. $\overline{DP_{n,\,PPEGA}}$ = 24 and $\overline{DP_{n,\,PNAGA}}$ = 196 were determined by comparing the integration area values of the signals at 3.35 ppm ((CH$_2$CH$_2$O)$_8$C*H$_3$*), 4.22 ppm (C(=O)OC*H$_2$*CH$_2$O-(CH$_2$CH$_2$O)$_8$) and the signals from 1.5 to 2.7 ppm corresponds to the protons of extended alkane from $^1$H-NMR spectrum. $\overline{M_{n,SEC}}$ = 91 700 g/mol and *Đ* = 1.54 (SEC DMSO, PMMA standards).

**Synthesis of Thermal-PPEGA-*b*-UV-PNAGA diblock copolymer by UV-light initiated RAFT PITSA of NAGA from Thermal-PPEGA.** In a 10 mL glass vial, 107 mg of NAGA (0.84 mmol, 200 eq.) and 50 mg of Thermal-PPEGA$_{24}$ (run 2 Table II.2, 0.0042 mmol, 1 eq.) were dissolved in 6.4 g of water containing 0.28 mg photo-I to give a final solid content of 2.4 wt% ([Thermal-PPEGA$_{24}$]$_0$/[NAGA]$_0$/[Photo-I]$_0$= 1/200/0.3; [NAGA]$_0$ = 0.13 M). The glass vial was bubbled with argon for 30 min, then the mixture solution was placed in an ice-bath under an UV light source(λ = 365 nm, P = 34 mW/cm$^2$) with a stir bar. After checking a total conversion of NAGA by $^1$H NMR spectroscopy, the polymerization was stopped after 1h. $\overline{DP_{n,\,PPEGA}}$ = 24 and $\overline{DP_{n,\,PNAGA}}$ = 187 were determined by comparing the integration area values of the signals at 3.35 ppm ((CH$_2$CH$_2$O)$_8$C*H$_3$*), 4.22 ppm (C(=O)OC*H$_2$*CH$_2$O-(CH$_2$CH$_2$O)$_8$) and the signals from 1.5 to 2.7 ppm corresponding to the protons of extended alkane from $^1$H-NMR spectrum. SEC DMSO (0.1 M LiBr): $\overline{M_{n,SEC}}$ = 92 100 g.mol$^{-1}$ and Đ = 1.84 relative to PMMA standards.

## 2.6 References


(1) Molineux, G. Pegylation: Engineering Improved Biopharmaceuticals for Oncology. *Pharmacotherapy* **2003**, *23* (8 Part 2), 3S-8S. https://doi.org/10.1592/phco.23.9.3S.32886.

(2) Chen, B.; Jerger, K.; Fréchet, J. M. J.; Szoka, F. C. The Influence of Polymer Topology on Pharmacokinetics: Differences between Cyclic and Linear PEGylated Poly(Acrylic Acid) Comb Polymers. *JCR* **2009**, *140* (3), 203–209. https://doi.org/10.1016/j.jconrel.2009.05.021.

(3) Nauka, P. C.; Lee, J.; Maynard, H. D. Enhancing the Conjugation Yield of Brush Polymer–Protein Conjugates by Increasing the Linker Length at the Polymer End-Group. *Polym. Chem.* **2016**, *7* (13), 2352–2357. https://doi.org/10.1039/C6PY00080K.

(4) Yang, J.; Song, J.; Song, Q.; Rho, J. Y.; Mansfield, E. D. H.; Hall, S. C. L.; Sambrook, M.; Huang, F.; Perrier, S. Hierarchical Self-Assembled Photo-Responsive Tubisomes from a Cyclic Peptide-Bridged Amphiphilic Block Copolymer. *Angew. Chem. Int. Ed.* **2020**, *59* (23), 8860–8863. https://doi.org/10.1002/anie.201916111.

(5) Yu, L.; Zhang, Y.; Dai, X.; Zhang, L.; Tan, J. Monodisperse Poly(Methyl Methacrylate) Microspheres with Tunable Carboxyl Groups on the Surface Obtained by Photoinitiated RAFT Dispersion Polymerization. *Chem. Commun.* **2019**, *55* (54), 7848–7851. https://doi.org/10.1039/C9CC03452H.

(6) Johnson, R. P.; Uthaman, S.; John, J. V.; Lee, H. R.; Lee, S. J.; Park, H.; Park, I.-K.; Suh, H.; Kim, I. Poly(PEGA)- *b* -Poly( L -Lysine)- *b* -Poly( L -Histidine) Hybrid Vesicles for Tumoral PH-Triggered Intracellular Delivery of Doxorubicin Hydrochloride. *ACS Appl. Mater. Interfaces* **2015**, *7* (39), 21770–21779. https://doi.org/10.1021/acsami.5b05338.

(7) Eissa, A. M.; Wilson, P.; Chen, C.; Collins, J.; Walker, M.; Haddleton, D. M.; Cameron, N. R. Reversible Surface Functionalisation of Emulsion-Templated Porous Polymers Using Dithiophenol Maleimide Functional Macromolecules. *Chem. Commun.* **2017**, *53* (70), 9789–9792. https://doi.org/10.1039/C7CC03811A.

(8) Piogé, S.; Tran, T. N.; McKenzie, T. G.; Pascual, S.; Ashokkumar, M.; Fontaine, L.; Qiao, G. Sono-RAFT Polymerization-Induced Self-Assembly in Aqueous Dispersion: Synthesis of LCST-Type Thermosensitive Nanogels. *Macromolecules* **2018**, *51* (21), 8862–8869. https://doi.org/10.1021/acs.macromol.8b01606.

(9) Khomein, P.; Dutta, K.; Gnanasekaran, K.; Gianneschi, N. C.; Thayumanavan, S. Spatiotemporal Control over the Host–Guest Characteristics of a Stimulus-Triggerable Trifunctional Polymer Assembly. *Polym. Chem.* **2019**, *10* (12), 1423–1430. https://doi.org/10.1039/C8PY01788C.

(10) Le Bohec, M.; Piogé, S.; Pascual, S.; Fontaine, L. Heterofunctional RAFT-Derived PNIPAM via Cascade Trithiocarbonate Removal and Thiol-Yne Coupling Click Reaction. *J. Polym. Sci., Part A: Polym. Chem.* **2017**, *55* (21), 3597–3606. https://doi.org/10.1002/pola.28742.

(11) Heredia, K. L.; Nguyen, T. H.; Chang, C.-W.; Bulmus, V.; Davis, T. P.; Maynard, H. D. Reversible SiRNA–Polymer Conjugates by RAFT Polymerization. *Chem. Commun.* **2008**, No. 28, 3245. https://doi.org/10.1039/b804812f.

(12) Bays, E.; Tao, L.; Chang, C.-W.; Maynard, H. D. Synthesis of Semitelechelic Maleimide Poly(PEGA) for Protein Conjugation By RAFT Polymerization. *Biomacromolecules* **2009**, *10* (7), 1777–1781. https://doi.org/10.1021/bm9001987.

(13) Grover, G. N.; Alconcel, S. N. S.; Matsumoto, N. M.; Maynard, H. D. Trapping of Thiol-Terminated Acrylate Polymers with Divinyl Sulfone To Generate Well-Defined Semitelechelic Michael Acceptor Polymers. *Macromolecules* **2009**, *42* (20), 7657–7663. https://doi.org/10.1021/ma901036x.

(14) *Handbook of RAFT Polymerization*; Barner-Kowollik, C., Ed.; Wiley-VCH: Weinheim, 2008.

(15) Ahmad, N. M.; Charleux, B.; Farcet, C.; Ferguson, C. J.; Gaynor, S. G.; Hawkett, B. S.; Heatley, F.; Klumperman, B.; Konkolewicz, D.; Lovell, P. A.; Matyjaszewski, K.; Venkatesh, R. Chain Transfer to Polymer and Branching in Controlled Radical Polymerizations of *n* -Butyl Acrylate: Chain Transfer to Polymer and Branching in Controlled Radical Polymerizations …. *Macromol. Rapid Commun.* **2009**, *30* (23), 2002–2021. https://doi.org/10.1002/marc.200900450.

(16) Ballard, N.; Asua, J. M. Radical Polymerization of Acrylic Monomers: An Overview. *Prog. Polym. Sci.* **2018**, *79*, 40–60. https://doi.org/10.1016/j.progpolymsci.2017.11.002.

(17) Zhao, W.; Gody, G.; Dong, S.; Zetterlund, P. B.; Perrier, S. Optimization of the RAFT Polymerization Conditions for the in Situ Formation of Nano-Objects via Dispersion Polymerization in Alcoholic Medium. *Polym. Chem.* **2014**, *5* (24), 6990–7003. https://doi.org/10.1039/C4PY00855C.

(18) Le Bohec, M.; Bonchouo Kenzo, K.; Piogé, S.; Mura, S.; Nicolas, J.; Casse, N.; Forcher, G.; Fontaine, L.; Pascual, S. Structure-PDNA Complexation and Structure–Cytotoxicity Relationships of PEGylated, Cationic Aminoethyl-Based Polyacrylates with Tunable Topologies. *Polym. Chem.* **2019**, *10* (15), 1968–1977. https://doi.org/10.1039/C8PY01776J.

(19) Perrier, S.; Barner-Kowollik, C.; Quinn, J. F.; Vana, P.; Davis, T. P. Origin of Inhibition Effects in the Reversible Addition Fragmentation Chain Transfer (RAFT) Polymerization of Methyl Acrylate. *Macromolecules* **2002**, *35* (22), 8300–8306. https://doi.org/10.1021/ma0203445.

(20) Monteiro, M. J.; de Brouwer, H. Intermediate Radical Termination as the Mechanism for Retardation in Reversible Addition−Fragmentation Chain Transfer Polymerization. *Macromolecules* **2001**, *34* (3), 349–352. https://doi.org/10.1021/ma001484m.

(21) Wenn, B.; Reekmans, G.; Adriaensens, P.; Junkers, T. Photoinduced Acrylate Polymerization: Unexpected Reduction in Chain Branching. *Macromol. Rapid Commun.* **2015**, *36* (16), 1479–1485. https://doi.org/10.1002/marc.201500198.

(22) Wang, H.; Li, Q.; Dai, J.; Du, F.; Zheng, H.; Bai, R. Real-Time and in Situ Investigation of "Living"/Controlled Photopolymerization in the Presence of a Trithiocarbonate. *Macromolecules* **2013**, *46* (7), 2576–2582. https://doi.org/10.1021/ma400208j.

(23) Tian, X.; Ding, J.; Zhang, B.; Qiu, F.; Zhuang, X.; Chen, Y. Recent Advances in RAFT Polymerization: Novel Initiation Mechanisms and Optoelectronic Applications. *Polymers* **2018**, *10* (3), 318. https://doi.org/10.3390/polym10030318.

(24) Schultz, D. M.; Yoon, T. P. Solar Synthesis: Prospects in Visible Light Photocatalysis. *Science* **2014**, *343* (6174), 1239176–1239176. https://doi.org/10.1126/science.1239176.

(25) Bei, J.; He, W.; Hu, X.; Wang, S. Photodegradation Behavior and Mechanism of Block Copoly(Caprolactone-Ethylene Glycol). *Polym. Degrad. Stab.* **2000**, *67* (2), 375–380. https://doi.org/10.1016/S0141-3910(99)00139-1.

(26) Giroto, J. A.; Teixeira, A. C. S. C.; Nascimento, C. A. O.; Guardani, R. Degradation of Poly(Ethylene Glycol) in Aqueous Solution by Photo-Fenton and $H_2O_2$/UV Processes. *Ind. Eng. Chem. Res.* **2010**, *49* (7), 3200–3206. https://doi.org/10.1021/ie9015792.

(27) Sionkowska, A. The Influence of UV Light on Collagen/Poly(Ethylene Glycol) Blends. *Polym. Degrad. Stab.* **2006**, *91* (2), 305–312. https://doi.org/10.1016/j.polymdegradstab.2005.05.012.

(28) Skrabania, K.; Miasnikova, A.; Bivigou-Koumba, A. M.; Zehm, D.; Laschewsky, A. Examining the UV-Vis Absorption of RAFT Chain Transfer Agents and Their Use for Polymer Analysis. *Polym. Chem.* **2011**, *2* (9), 2074. https://doi.org/10.1039/c1py00173f.

(29) Aoshima, S.; Kanaoka, S. Synthesis of Stimuli-Responsive Polymers by Living Polymerization: Poly(N-Isopropylacrylamide) and Poly(Vinyl Ether)s. In *Wax Crystal Control · Nanocomposites · Stimuli-Responsive Polymers*; Advances in Polymer Science; Springer Berlin Heidelberg: Berlin, Heidelberg, **2007**; Vol. 210, pp 169–208. https://doi.org/10.1007/12_2007_120.

(30) Aseyev, V.; Tenhu, H.; Winnik, F. M. Non-Ionic Thermoresponsive Polymers in Water. *Self Organized Nanostructures of Amphiphilic Block Copolymers II*, **2011**, 29–89.

(31) Dimitrov, I.; Trzebicka, B.; Müller, A. H. E.; Dworak, A.; Tsvetanov, C. B. Thermosensitive Water-Soluble Copolymers with Doubly Responsive Reversibly Interacting Entities. *Prog. Polym. Sci.* **2007**, *32* (11), 1275–1343. https://doi.org/10.1016/j.progpolymsci.2007.07.001.

(32) Collins, J.; Kempe, K.; Wilson, P.; Blindauer, C. A.; McIntosh, M. P.; Davis, T. P.; Whittaker, M. R.; Haddleton, D. M. Stability Enhancing *N* -Terminal PEGylation of Oxytocin Exploiting Different Polymer Architectures and Conjugation Approaches. *Biomacromolecules* **2016**, *17* (8), 2755–2766. https://doi.org/10.1021/acs.biomac.6b00919.

(33) Figg, C. A.; Simula, A.; Gebre, K. A.; Tucker, B. S.; Haddleton, D. M.; Sumerlin, B. S. Polymerization-Induced Thermal Self-Assembly (PITSA). *Chem. Sci. J.* **2015**, *6* (2), 1230–1236. https://doi.org/10.1039/C4SC03334E.

(34) Li, Y.; Ye, Z.; Shen, L.; Xu, Y.; Zhu, A.; Wu, P.; An, Z. Formation of Multidomain Hydrogels via Thermally Induced Assembly of PISA-Generated Triblock Terpolymer Nanogels. *Macromolecules* **2016**, *49* (8), 3038–3048. https://doi.org/10.1021/acs.macromol.5b02538.

(35) Blackman, L. D.; Doncom, K. E. B.; Gibson, M. I.; O'Reilly, R. K. Comparison of Photo- and Thermally Initiated Polymerization-Induced Self-Assembly: A Lack of End Group Fidelity Drives the Formation of Higher Order Morphologies. *Polym. Chem.***2017**, *8* (18), 2860–2871. https://doi.org/10.1039/C7PY00407A.

(36) Heilmann, S. M.; Rasmussen, J. K.; Krepski, L. R. Chemistry and Technology of 2-Alkenyl Azlactones. *J. Polym. Sci. A Polym. Chem.* **2001**, *39* (21), 3655–3677. https://doi.org/10.1002/pola.10007.

(37) Guyomard, A.; Fournier, D.; Pascual, S.; Fontaine, L.; Bardeau, J.-F. Preparation and Characterization of Azlactone Functionalized Polymer Supports and Their Application as Scavengers. *Eur. Polym. J.* **2004**, *40* (10), 2343–2348. https://doi.org/10.1016/j.eurpolymj.2004.05.005.

(38) Messman, J. M.; Lokitz, B. S.; Pickel, J. M.; Kilbey, S. M. Highly Tailorable Materials Based on 2-Vinyl-4,4-Dimethyl Azlactone: (Co)Polymerization, Synthetic Manipulation and Characterization. *Macromolecules* **2009**, *42* (12), 3933–3941. https://doi.org/10.1021/ma900316t.

(39) Seuring, J.; Agarwal, S. Polymers with Upper Critical Solution Temperature in Aqueous Solution. *Macromol. Rapid Commun.* **2012**, *33* (22), 1898–1920. https://doi.org/10.1002/marc.201200433.

(40) Seuring, J.; Bayer, F. M.; Huber, K.; Agarwal, S. Upper Critical Solution Temperature of Poly( *N* -Acryloyl Glycinamide) in Water: A Concealed Property. *Macromolecules* **2012**, *45* (1), 374–384. https://doi.org/10.1021/ma202059t.

(41) Liu, F.; Agarwal, S. Thermoresponsive Gold Nanoparticles with Positive UCST-Type Thermoresponsivity. *Macromol. Chem. Phys.* **2015**, *216* (4), 460–465. https://doi.org/10.1002/macp.201400497.

(42) Lu, Y.; Zhou, K.; Ding, Y.; Zhang, G.; Wu, C. Origin of Hysteresis Observed in Association and Dissociation of Polymer Chains in Water. *Phys. Chem. Chem. Phys.* **2010**, *12* (13), 3188. https://doi.org/10.1039/b918969f.

(43) Mäkinen, L.; Varadharajan, D.; Tenhu, H.; Hietala, S. Triple Hydrophilic UCST–LCST Block Copolymers. *Macromolecules* **2016**, *49* (3), 986–993. https://doi.org/10.1021/acs.macromol.5b02543.

(44) Glatzel, S.; Badi, N.; Päch, M.; Laschewsky, A.; Lutz, J.-F. Well-Defined Synthetic Polymers with a Protein-like Gelation Behavior in Water. *Chem. Commun.* **2010**, *46* (25), 4517. https://doi.org/10.1039/c0cc00038h.

# CHAPTER III

# Elaboration of LCST-type thermosensitive and pH-degradable nanogels by RAFT-PITSA

## 3.1 Introduction

Nanogels, defined as chemically or physically crosslinked hydrogel particles with a nanoscale size, represent interesting soft nanomaterials as they are able to uptake a large amount of water with relatively low surface tension.[1,2] These nanomaterials can be designed to respond to a wide variety of stimuli, such as temperature.[3–6] As studied in chapter 1, thermosensitive nanogels were prepared *via* PITSA process by taking advantage of the copolymer precursor solubility change in water at LCST or at a UCST during the polymerization. In my work, LCST-type thermosensitive nanogels based on a crosslinked LCST-type thermosensitive polymer core were synthesized *via* direct RAFT-PITSA of a monomer precursor to LCST behavior and a crosslinker, using UV- and Thermal-PPEGA synthesized in chapter 2 as both macro-CTA and stabilizer, through both thermally and UV-light initiated systems in aqueous dispersion. PNIPAm-based nanogels containing a non-degradable MBA or a pH-degradable (ketal-derived) crosslinker will be synthesized and studied in order to extend their potential applications that require polymeric materials to be degraded into water-soluble products that can be cleared from the body for instance. In the first part of this chapter, the impact of radical activation process on the LCST-type thermosensitive nanogels synthesized by RAFT-PITSA in aqueous dispersion was studied. In the second part, we developed pH-degradable nanogels based on ketal-linked PNIPAm *via* UV-light initiated RAFT polymerization in aqueous dispersion. For this, a new hydrolyzable crosslinker containing an ketal group was first synthesized and then incorporated into the core of a LCST-type thermosensitive nanogel based on PNIPAm. Finally, the degradability of the so-obtained nanogels was studied at different pH.

## 3.2 Synthesis of LCST-type thermosensitive nanogels based on PPEGA-*b*-P(PNIPAm-*co*-MBA) copolymers through RAFT-PITSA

Several radical activation processes including thermal and UV-light ones, were first studied during the elaboration of LCST-type thermosensitive nanogels by RAFT-PITSA.

### 3.2.1 Study of the radical activation process

PNIPAm-based nanogels were synthesized through RAFT-PITSA in water using either a thermal initiator (V50) or a photo-initiator (Photo-I) (Scheme III.1).

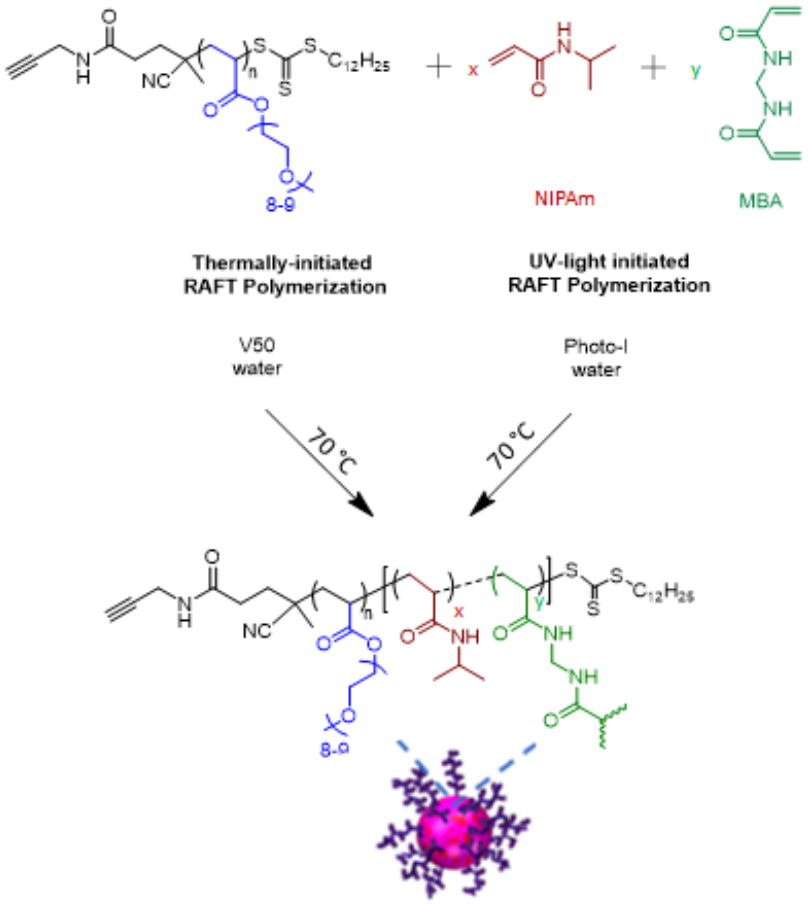


Scheme III.1. Synthesis of LCST-type thermosensitive nanogels based on PPEGA-*b*-P(NIPAm-*co*-MBA) through thermally and UV-light initiated RAFT PITSA in aqueous dispersion.

For the thermally-initiated RAFT-PITSA of NIPAm in aqueous dispersion at 70°C, V50 was used as initiator, a Thermal-PPEGA with $\overline{DP_{n,\,PPEGA}}$ of 20 (Table II.1 run 3 in chapter II) as macro-CTA and surfactant and MBA as crosslinker. The initial molar ratio of reactants employed was

$[NIPAm]_0/[MBA]_0/[Thermal\text{-}PPEGA_{20}]_0/[V50]_0$ = 204/8/1/0.3 with a solid content of 2.4 wt.% in water (Scheme III.1). After 6h, total conversions of NIPAm and MBA were observed (Figure III.1)

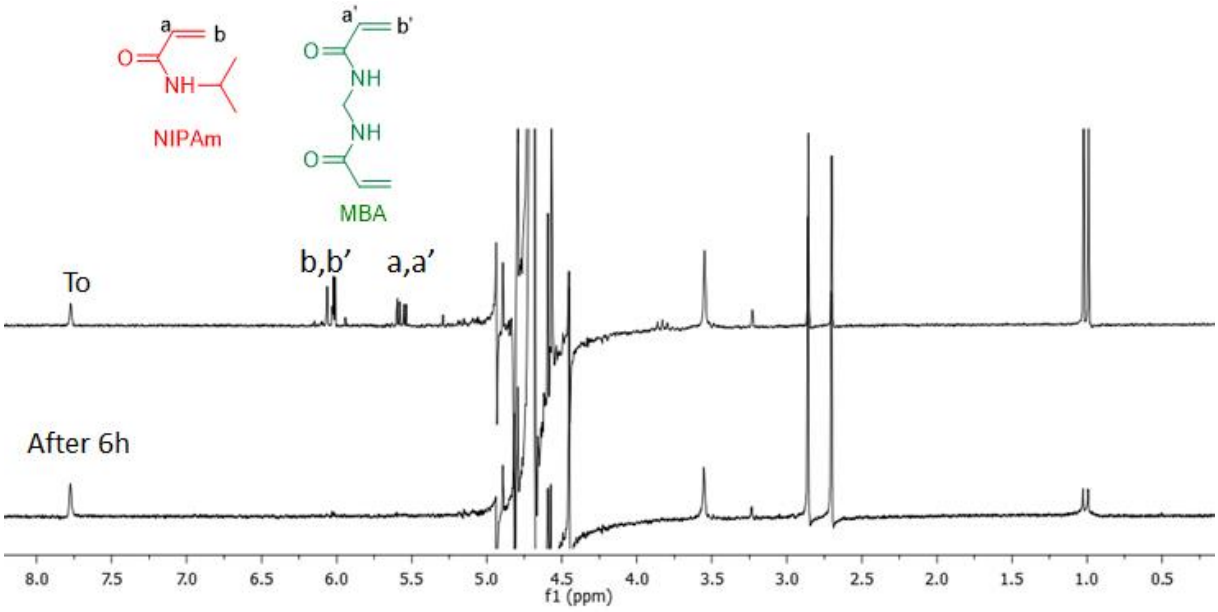


Figure III.1. Overlay $^1$H NMR spectra (200 MHz in $D_2O$) of polymerization medium at t = 0 and after 6h. The thermally-intiated RAFT-PITSA of NIPAm were conducted in aqueous dispersion and 70°C using a Thermal-$PPEGA_{20}$ and the MBA with the initial molar ratio of $[NIPAm]_0/[Thermal\text{-}PPEGA_{20}]_0/[MBA]_0/[V50]_0$ = 200/1/8/0.3 and 2.4 wt.% of solid content.

The final product was purified by dialysis and lyophilized to remove water for $^1$H NMR and DLS characterizations. The $^1$H NMR spectrum (Figure III.2) of the resulting purified nanogel shows signals at 3.35 ppm ($(CH_2CH_2O)_8CH_3$, labeled g) and 4.2 ppm ($C(=O)OCH_2CH_2O\text{-}(CH_2CH_2O)_8$, labeled a) characteristic of the PPEGA block; signals at 3.85 ppm (-NH-$CH(CH_3)_2$, labeled c) and 1.1 ppm (-NH-$CH(CH_3)_2$, labeled b) characteristic of the PNIPAm block. The signal from 1.3 to 2.2 ppm corresponds to the $CH_2$ and CH protons of the PPEGA, PNIPAm, PMBA backbone (labeled d, e, d', e', d'' and e''). The comparison of the integrations of signals g, c and d, e, d', e', d'' and e'' were employed to determine the molar composition of the resulting copolymer: $\overline{DP_{n,\,PPEGA}}$ = 20, $\overline{DP_{n,\,PNIPAM}}$ = 182 and $\overline{DP_{n,\,PMBA}}$ = 7.

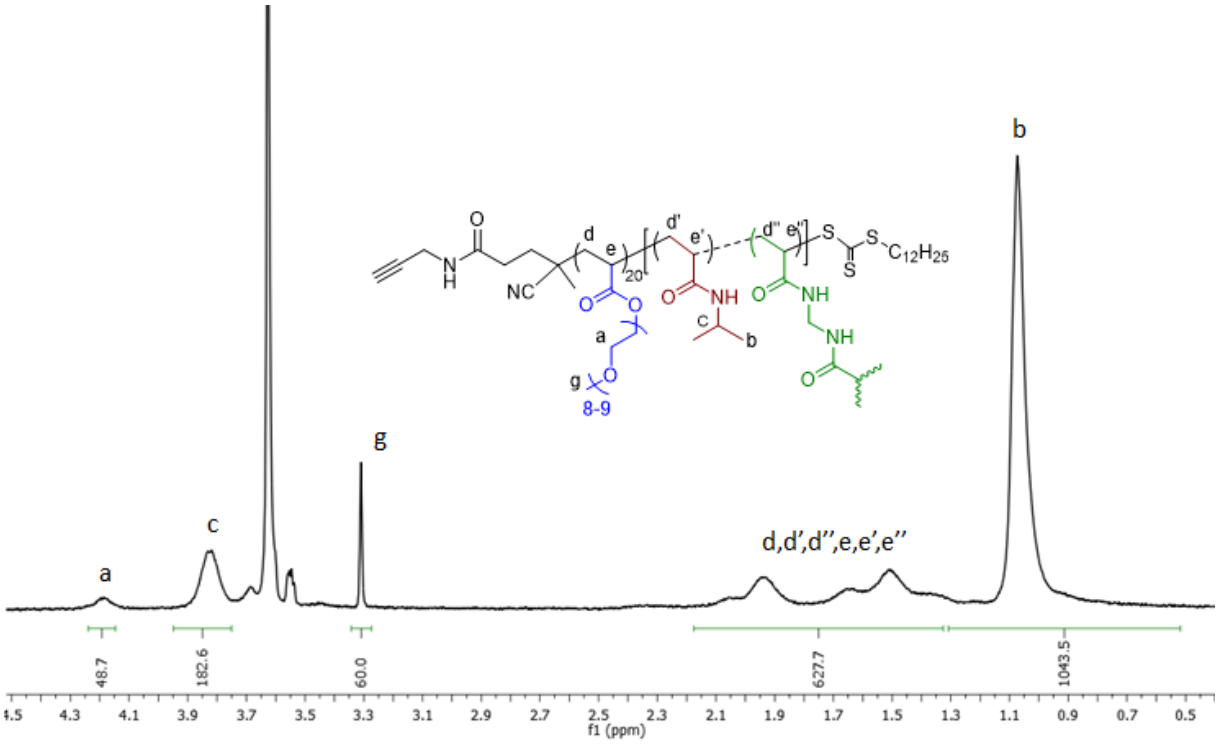


Figure III.2. $^{1}$H NMR spectrum (400 MHz, $D_2O$) of purified nanogel synthesized by thermally-initiated RAFT-PITSA of NIPAm/MBA mediated through V50 and Thermal-PPEGA$_{20}$ ([NIPAm]$_0$/[MBA]$_0$/[Thermal-PPEGA$_{20}$]$_0$/[V50]$_0$ = 204/8/1/0.3) with a solid content of 2.4 wt.% during 6h in water at 70°C.

The DLS study was performed on an aqueous solution of purified nanogel at a concentration of 5 g.L$^{-1}$ at different temperatures. At 20°C, the DLS number-average diameter distribution showed a single size distribution with the $D_h$ of 75 nm and a pdi of 0.081 (Figure III.3A). To study the thermosensitive behavior, the nanogel aqueous solution was analyzed by DLS at 45°C: the $D_h$ was 54 nm, and the pdi was 0.059 (Figure III.3A). The $D_h$ and pdi decreased upon heating related to the collapse of the crosslinked core based on P(NIPAm$_{182}$-*co*-MBA$_7$). This behavior was reversible and reproducible; the nanogel regained the same $D_h$ over successive shrink/swell cycles (heating 45°C / cooling 20°C) (Figure III.3B). This corresponds to a swelling volume ratio (f) of 2.68, which is determined by the equation $f = (D_{h,20°C}/D_{h,45°C})^3$.

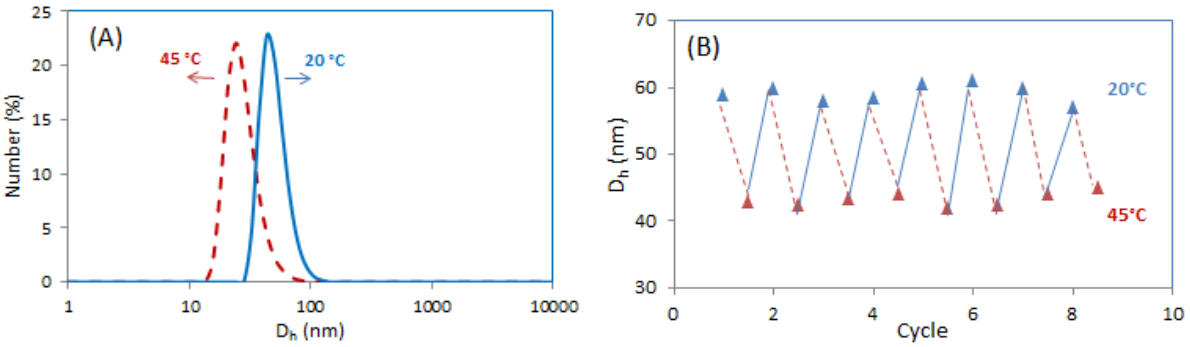


Figure III.3. (A) DLS number-average diameter distributions of the nanogel in water at 20°C (—) and at 45 °C (---). (B) The $D_h$ values of nanogel at 20°C and at 45°C from repeated heating and cooling experiments.

Transmission electronic microscopy (TEM) was used to characterize the morphology of the nanogel (Figure III.4). TEM images of the nanogel based on Thermal-PPEGA$_{20}$-*b*-P(NIPAm$_{182}$-*co*-MBA$_7$) indicated the formation of spherical nano-objects and size (40 nm) is consistent with the DLS study of the shrinked nanogel.

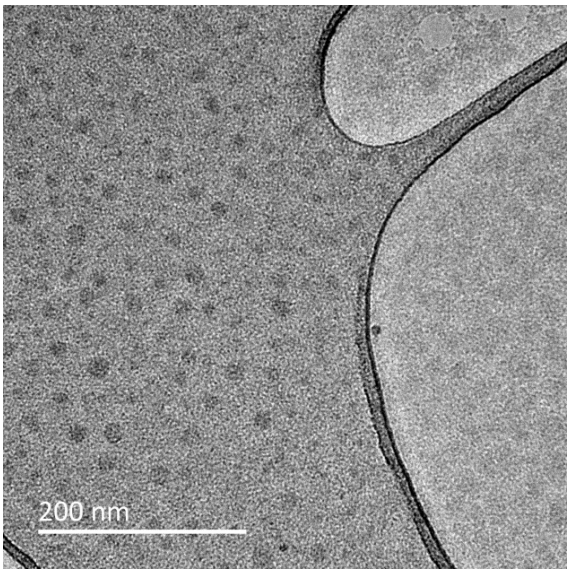


Figure III.4 TEM image of the purified Thermal-PPEGA$_{20}$-*b*-P(NIPAm$_{182}$-*co*-MBA$_7$) nanogel synthesized by thermally-initiated RAFT PITSA of NIPAm/MBA mediated through V50 and Thermal-PPEGA$_{20}$ ([NIPAm]$_0$/[MBA]$_0$/[Thermal-PPEGA$_{20}$]$_0$/[V50]$_0$ = 204/8/1/0.3) with a solid content of 2.4 wt.% during 6h in water at 70°C.

In order to compare with thermal activation process, a PNIPAm-based thermosensitive nanogel was targeted by UV-light initiated RAFT-PITSA in aqueous dispersion using UV-PPEGA with a $\overline{DP_{n,PPEGA}}$ of 18 (Table II.2 run 1, chapter II) as macro-CTA and surfactant (PPEGA with a similar $\overline{DP_{n,\,PPEGA}}$ as the one used for thermal activation process), photo-I as initiator and MBA as crosslinker, with the initial molar ratio [NIPAm]$_0$/[MBA]$_0$/[UV-PPEGA$_{18}$]$_0$/[photo-I]$_0$ = 204/8/1/0.3 and

a solid content of 2.4 wt.% in water at 70 °C in presence of UV-light source (λ = 365 nm, 34 mW/cm$^2$-Scheme III.1). After 30 min, a biphasic system appears under UV irradiation (Figure III.5).

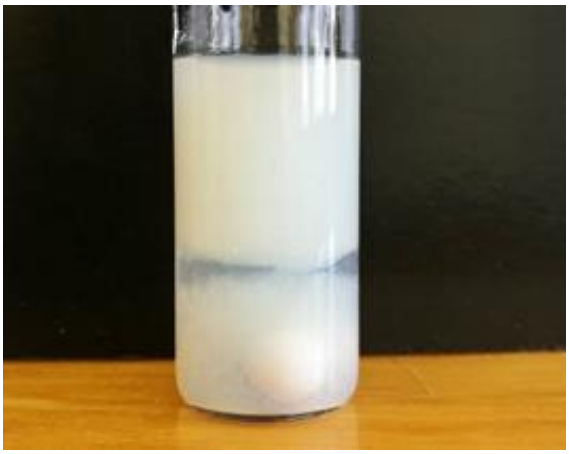

Figure III.5 Picture of the reaction medium obtained after 30 min of a UV-light initiated RAFT-PITSA of NIPAm/MBA mediated through photo-I and UV-PPEGA$_{18}$ ([NIPAm]$_0$/[MBA]$_0$/[UV-PPEGA$_{18}$]$_0$/[Photo-I]$_0$ = 204/8/1/0.3) with a solid content of 2.4 wt.% in water at 70°C.

In order to avoid the biphasic solution observed under UV-light irradiation, a second test was carried out using a PPEGA having a higher $\overline{DP_{n,\,PPEGA}}$ of 30 in order to improve the latex stability. Therefore, PNIPAm-based nanogels were targeted either through thermally-initiated and through UV-light initiated process using a PPEGA with $\overline{DP_{n,\,PPEGA}}$ of 30 as macro-CTA and surfactant, MBA as crosslinker and V50 or photo-I as initiators, respectively. The initial molar ratios of [NIPAm]$_0$/[MBA]$_0$/[PPEGA]$_0$/[initiator]$_0$ are 204/8/1/0.3 and the solid content is equal to 2.4 wt.%. Thermally-initiated RAFT-PITSA was conducted in aqueous dispersion at 70°C for 6h with complete NIPAm/MBA conversion whereas UV-light activated RAFT-PITSA was conducted under UV-light at 70°C for 30 min with 86% of NIPAm/MBA conversion. The Figure III.6 shows the $^1$H NMR spectrum of the resulting purified Thermal-PPEGA$_{30}$-*b*-Thermal-P(NIPAm-*co*-MBA) nanogel with: $\overline{DP_{n,\,PNIPAM}}$ = 188 and $\overline{DP_{n,\,PMBA}}$ = 7 and the Figure III.7 shows the $^1$H NMR spectrum of the resulting purified UV-PPEGA$_{30}$-*b*-UV-P(NIPAm-*co*-MBA) nanogel with $\overline{DP_{n,\,PNIPAM}}$ = 175 and $\overline{DP_{n,\,PMBA}}$ = 6. Apart from the kinetic, nanogels with similar $\overline{DP_n}$ of PNIPAm and PMBA blocks were obtained whatever the activation process.

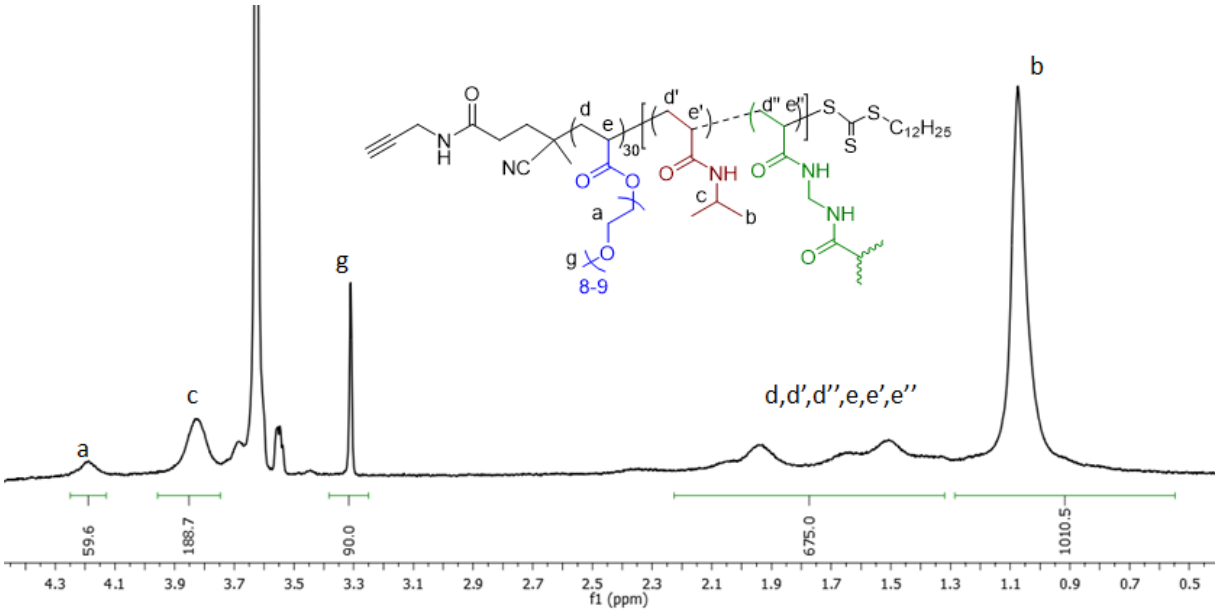


Figure III.6. $^{1}$H NMR spectrum (400 MHz, $D_2O$) of purified Thermal-PPEGA$_{30}$-*b*-Thermal-P(NIPAm$_{188}$-*co*-MBA$_7$) nanogel synthesized by thermally-initiated RAFT PITSA of NIPAm/MBA mediated through V50 and Thermal-PPEGA$_{30}$ (Table II.1 run 5, chapter II) ([NIPAm]$_0$/[MBA]$_0$/[Thermal-PPEGA$_{30}$]$_0$/[V50]$_0$ = 204/8/1/0.3) with a solid content of 2.4 wt.% in water at 70°C after 6h of reaction.

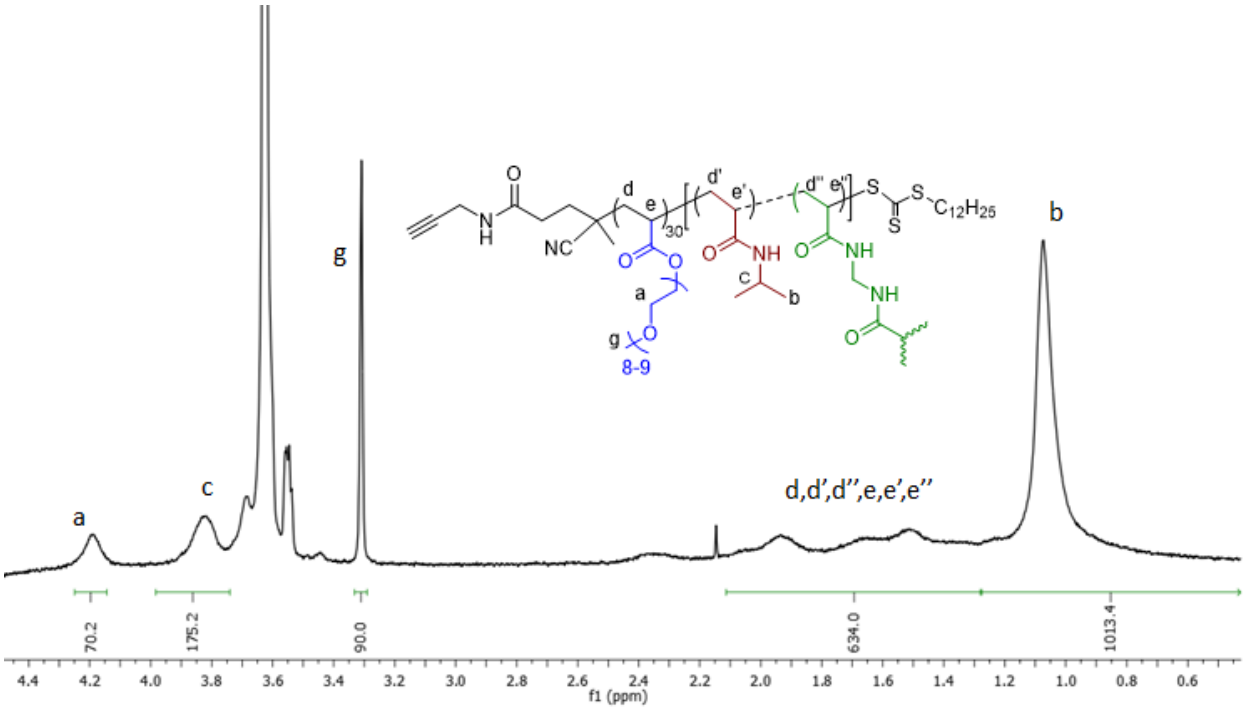


Figure III.7. $^{1}$H NMR spectrum (400 MHz, $D_2O$) of UV-PPEGA$_{30}$-*b*-UV-P(NIPAm$_{175}$-*co*-MBA$_6$) nanogel synthesized by UV light-initiated RAFT-PITSA of NIPAm/MBA mediated through UV-PPEGA$_{30}$ (Table II.2, run 3, chapter II) ([NIPAm]$_0$/[MBA]$_0$/[UV-PPEGA$_{30}$]$_0$/[Photo-I]$_0$ = 204/8/1/0.3) with a solid content of 2.4 wt.% in water at 70°C after 30 min of reaction.

The DLS study was performed on two different solutions containing the purified Thermal-PPEGA$_{30}$-*b*-Thermal-P(NIPAm$_{188}$-*co*-MBA$_7$) nanogel and UV-PPEGA$_{30}$-*b*-UV-P(NIPAm$_{175}$-*co*-MBA$_6$) nanogel respectively, at a concentration of 5 g.L$^{-1}$ at 20°C and at 45°C (Figure III.8). DLS analyses of the aqueous solutions of nanogels both showed a single size distribution at 20°C and at 45°C. In both cases, the $D_h$ decreased with the increase of temperature showing the LCST behavior of these nanogels. However, there is a significant difference in the $D_h$ of Thermal-PPEGA$_{30}$-*b*-Thermal-P(NIPAm$_{188}$-*co*-MBA$_7$) nanogel and UV-PPEGA$_{30}$-*b*-UV-P(NIPAm$_{175}$-*co*-MBA$_6$) nanogels in aqueous solutions at 20 and 45 °C. The Thermal-PPEGA$_{30}$-*b*-Thermal-P(NIPAm$_{188}$*co*-MBA$_7$) nanogel aqueous solution shows a $D_h$ of 75 nm with a pdi of 0.081 at 20 °C and at 45°C, where the P(NIPAm$_{188}$-*co*-MBA$_7$) block is insoluble, the $D_h$ decreases to 54 nm and the pdi was 0.059 (Figure III.8A). In comparison, the $D_h$ of UV-PPEGA$_{30}$-*b*-UV-P(NIPAm$_{175}$-*co*-MBA$_6$) nanogel aqueous solution increases to 122 nm with a pdi of 0.093 (Figure III.8B) and at 45 °C, the $D_h$ decreased to 76 nm and the pdi was equal to 0.065 corresponding to the collapse of crosslinked core based on P(NIPAm$_{175}$-*co*-MBA$_6$) block. The difference in the nanogels $D_h$ results in more opalescent color of the sample with bigger nanoparticle sizes obtained under UV-light initiated RAFT-PITSA activation (Figure III.9A *versus* Figure III.9B). The results demonstrate that thermal activation is more suitable to target LCST nanogels with lower pdi and smaller particles size in comparison with UV-light activation using comparable synthesis conditions. The reason is probably due to in the UV-light activation process, the rate of polymerization is very fast compared to thermal activation (as illustrated in the chapter II with the kinetics of RAFT polymerization of NIPAm from PPEGA as macro-CTA using both UV-light and thermal activation), which result in the higher consumption of NIPAm in a short time and produce bigger particles. However, for UV-light initiated polymerization, the biphasic system observed when a UV-PPEGA$_{18}$ was employed disappears with a UV-PPEGA with higher $\overline{DP_{n,\,PPEGA}}$ ($\overline{DP_{n,\,PPEGA}}$ = 30) and a monophasic system with a single size distribution of microgels was obtained. A minimum $\overline{DP_{n,\,PPEGA}}$ of the PPEGA block is thus necessary to reach effective stabilization of the nanogels formed *in-situ* during the PITSA process. Indeed for short macro-CTAs, the forming nanogels were not sterically stabilized enough and aggregation occurred during polymerization yielding in interparticle crosslinking and the formation of heterogeneous dispersions, as already observed before.[7–10]

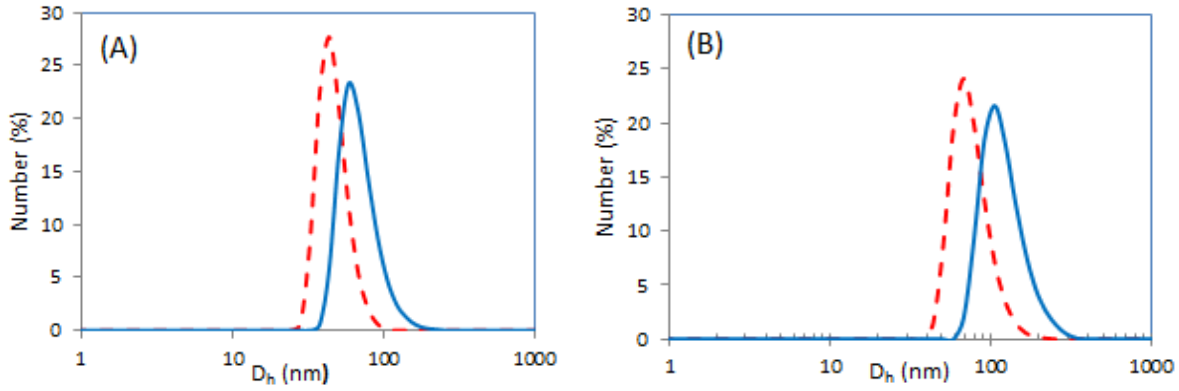


Figure III.8. DLS number-average diameter distributions of (A) the Thermal-PPEGA$_{30}$-*b*-Thermal-P(NIPAm$_{188}$-*co*-MBA$_7$) nanogel in water with a concentration of 5 g.L$^{-1}$ at 20°C (—) and at 45 °C (---) and of, (B) the UV-PPEGA$_{30}$-*b*-UV-P(NIPAm$_{175}$-*co*-MBA$_6$) nanogel in water with a concentration of 5 g.L$^{-1}$ at 20°C (—) and at 45 °C (---).

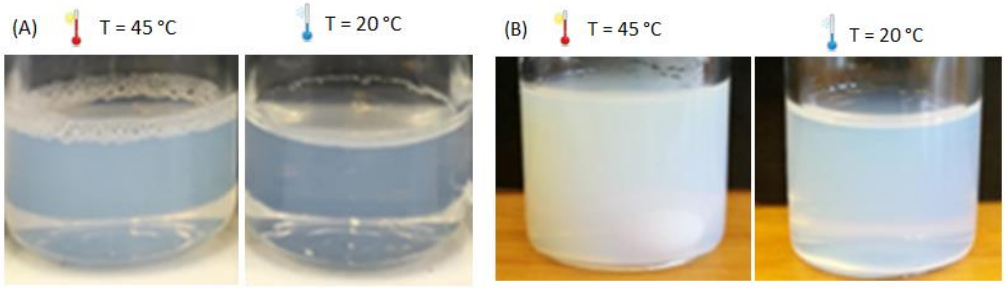


Figure III.9. Pictures of (A) Thermal-PPEGA$_{30}$-*b*-Thermal-P(NIPAm$_{188}$-*co*-MBA$_7$) nanogel aqueous solution and (B) UV-PPEGA$_{30}$-*b*-UV-P(NIPAm$_{175}$-*co*-MBA$_6$) nanogel aqueous solution at a concentration of 5 g.L$^{-1}$ at 20°C and 45 °C.

In conclusion, the thermally and UV-light initiated RAFT-PITSA were compared to target LCST-type thermosensitive nanogels based on PNIPAm by using PPEGAs with different $\overline{DP_{n,\,PPEGA}}$ as macro-CTA and surfactants. The results demonstrate that thermal activation is more suitable to target LCST nanogels with lower pdi and smaller particles size in comparison with UV-light activation using comparable synthesis conditions. After that, thermally-initiated RAFT PITSA will be employed to study the influence of $\overline{DP_{n,\,PPEGA}}$ and $\overline{DP_{n,\,PNIPAM}}$ on nanogel size, size distribution and swelling ratio.

## 3.2.2 Impact of $\overline{DP_{n,\,PPEGA}}$ on nanogel size, size distribution and swelling ratio

A range of PPEGA with different $\overline{DP_{n,\,PPEGA}}$ was employed to synthesize PNIPAm-based nanogels through thermally-initiated RAFT-PITSA. The experimental conditions to target Thermal-PPEGA-*b*-Thermal-P(NIPAm-*co*-MBA) nanogels and their characteristics including $D_h$, pdi and thermosensitive properties (f) are shown in Table III.1.

Table III.1. Synthesis conditions, $D_h$ and pdi at 20°C and at 45°C, swelling ratio of Thermal-PPEGA-*b*-Thermal-P(NIPAm-*co*-MBA)-based nanogels synthesized through thermally-initiated RAFT-PITSA in aqueous dispersion using PPEGAs with different $\overline{DP_{n,\,PPEGA}}$.[a]

| Run | $\overline{DP_{n,\,PPEGA}}$ (Thermal -PPEGA) | $D_h$[b] 20°C (nm) | $D_h$[b] 45°C (nm) | pdi[b] 20°C | pdi[b] 45°C | swelling ratio (f)[c] |
|---|---|---|---|---|---|---|
| 1 | 7 | [d] | [d] | [d] | [d] | [d] |
| 2 | 15 | 83 +/- 3 | 60+/- 2 | 0.089 | 0.069 | 2.65 |
| 3 | 20 | 75 +/- 3 | 54+/- 2 | 0.081 | 0.059 | 2.68 |
| 4 | 24 | 59 +/- 2 | 43+/- 2 | 0.102 | 0.050 | 2.58 |
| 5 | 30 | 46 +/- 2 | 34+/- 1 | 0.081 | 0.061 | 2.48 |
| 6 | 33 | 43 +/- 2 | 32+/- 2 | 0.082 | 0.055 | 2.43 |
| 7 | 49 | 39 +/- 2 | 30+/- 1 | 0.109 | 0.064 | 2.20 |

[a] Polymerization conditions: $[\text{Thermal-[PPEGA]}_0/[\text{NIPAm}]_0/[\text{MBA}]_0/[\text{V50}]_0 = 1/204/8/0.3$, solid content =2.4 wt.%, 70°C, 6h; NIPAm and MBA conversions were all quantitative as attested by $^1$H NMR spectroscopy with $\overline{DP_{n,\,PNIPAm}}$ *= 204 and* $\overline{DP_{n,\,PMBA}}$*= 8*. [b] Hydrodynamic diameters ($D_h$) and size distribution (pdi) of nanogels determined by DLS measurements conducted with 5 $g.L^{-1}$ water solutions at 20 and 45°C.d The volume swelling ratios $f = (D_{h,20°C}/D_{h,45°C})^3$. [c] Destabilization of the reactional medium during the polymerization with the formation of aggregates.

With the Thermal-PPEGA with $\overline{DP_{n,\,PPEGA}}$ equal and above to 15, stable LCST-type thermosensitive nanogels (runs -2, -3, -4, -5, -6 and -7, Table III.1.) were obtained. Moreover, the pdi and the volume swelling ratio were not affected significantly by the $\overline{DP_{n,PPEGA}}$ (Table III.1). At 20 °C, with increasing $\overline{DP_{n,PPEGA}}$, $D_h$ of the nanogels decreased from 83 to 39 nm (run 2 to run 7, Table III.1). However, with Thermal-$PPEGA_7$, a heterogeneous dispersion containing aggregates was obtained. A minimum $\overline{DP_{n,PPEGA}}$ is thus necessary to reach effective stabilization of the nanogels formed *in situ* during the PITSA process as observed before. To better understand this result, the self-assembly of amphiphilic PPEGAs containing the hydrophilic part based on the succession of PEGA units and the hydrophobic dodecyl chain is by steady state fluorescence spectroscopy analysis. The pyrene was used as fluorescence probe and aqueous solutions of Thermal-PPEGAs with $\overline{DP_{n,\,PPEGA}}$ of 7, 15 and 24 were employed for the study. Figure III.9 shows the pyrene excitation spectra of solutions containing pyrene at an initial concentration of $6.10^{-7}$ $mol.L^{-1}$ and PPEGA with various $\overline{DP_{n,\,PPEGA}}$ at an initial concentration of 8 $g.L^{-1}$, which corresponds to the initial concentration of PPEGA in the nanogel synthesis. The migration of the hydrophobic pyrene from the aqueous phase to the apolar micellar core is shown by a shift of the first vibronic band from 334 nm to 338 nm, which evidence the formation of micelles of PPEGA with $\overline{DP_{n,\,PPEGA}}$ = 15 and 24 in aqueous solution. Unlike the other PPEGAs, the one with a $\overline{DP_{n,\,PPEGA}}$ of 7 does not form micelles in aqueous solution.

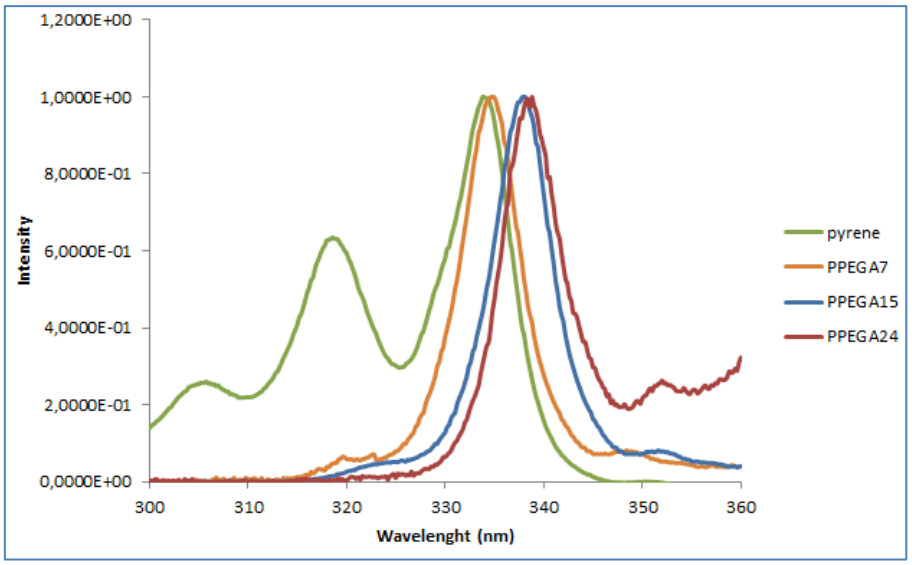


Figure III.10 Pyrene excitation spectra ($\lambda_{em}$ = 371 nm) in the presence of different Thermal-PPEGAs in water ([Thermal-PPEGA]$_0$ = 8 g.L$^{-1}$ and [pyrene]$_0$ = 6.10$^{-7}$ mol.L$^{-1}$).

The evolution of $D_h$ of the nanogel *vs.* $\overline{DP_{n,\,PPEGA}}$ at 20°C and 45 °C is shown in Figure III.11(a). The $D_h$ at 20 and 45 °C decreased with the increase of $\overline{DP_{n,\,PPEGA}}$ till 30 and then reached a plateau. Similar phenomenon was reported in the literature.[8] Indeed, for longer macro-CTAs, the forming nanogels were more sterically stabilized and aggregation of amphiphilic macro-CTAs occurred during polymerization resulting in the increase of intraparticle crosslinking and the formation of smaller particles. Figure III.11(b) shows the aqueous solutions containing Thermal-PPEGA-*b*-Thermal-P(NIPAm-*co*-MBA) nanogels with different $\overline{DP_{n,\,PPEGA}}$. These results confirm that higher $\overline{DP_{n,\,PPEGA}}$ of Thermal-PPEGA macro-CTAs lead to smaller particles and less opalescent sample solutions.

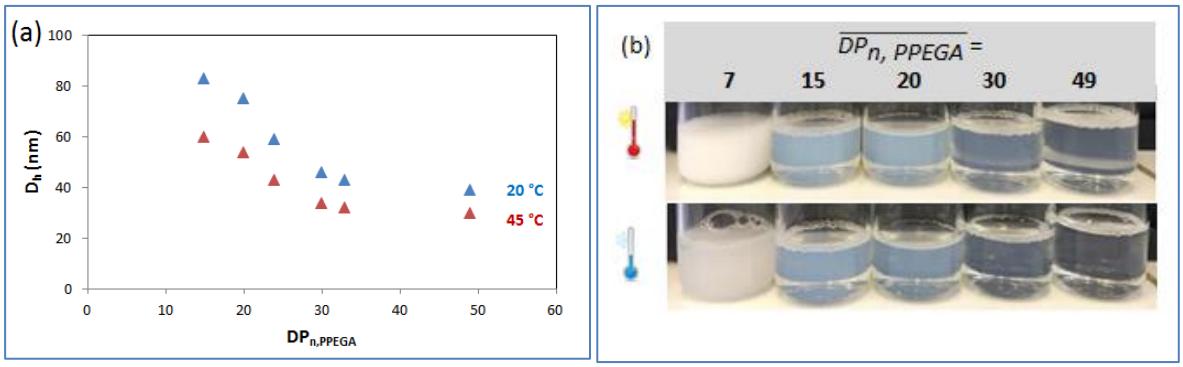


Figure III.11 (a) Evolution of the $D_h$ of the nanogel *vs.* $\overline{DP_{n,\,PPEGA}}$ at 20°C (blue) and 45 °C (red). (b) Pictures of aqueous solutions (5 g.L$^{-1}$) containing Thermal-PPEGA-*b*-Thermal-P(NIPAm-*co*-MBA) nanogel with different $\overline{DP_{n,\,PPEGA}}$ at 20°C and 45°C.

### 3.2.3 Impact of the $\overline{DP_{n,\,PNIPAM}}$ on nanogel size, size distribution and swelling ratio

We further investigated the effect of the $\overline{DP_{n,\,PNIPAM}}$ block on the size, size distribution, and volume swelling ratio of the nanogels. Using a PPEGA with a higher $\overline{DP_{n,\,PPEGA}}$ of 49 (Thermal-$PPEGA_{49}$) for targeting more stable nanogels, thermally-initiated RAFT-PITSAs were performed in the presence of [Thermal-$PPEGA_{49}$]$_0$/[NIPAm]$_0$ molar ratios ranging from 1/204 up to 1/600 and a constant [Thermal-$PPEGA_{49}$]$_0$/[MBA]$_0$ ratio (1/8) with a solid content of 2.4 % (Table III.2.).

Table III.2. Synthesis conditions, $D_h$ and pdi at 20°C and at 45°C, swelling ratio of Thermal-PPEGA$_{49}$-*b*-Thermal-P(NIPAm-*co*-MBA)-based nanogels synthesized through thermally-initiated RAFT-PITSA in aqueous dispersion using a Thermal-PPEGA of $\overline{DP_{n,\,PPEGA}}$ = 49 and different [Thermal-PPEGA$_{49}$]$_0$/[NIPAm]$_0$ initial molar ratios.[a]

| Run | [Thermal-PPEGA$_{49}$]$_0$/[NIPAm]$_0$/[MBA]$_0$/[V50]$_0$ | $\overline{DP_{n,\,PNIPAm}}$[b] | $\overline{DP_{n,\,PMBA}}$[b] | $D_h$[c] 20°C (nm) | $D_h$[c] 45°C (nm) | Pdi[c] 20°C | Pdi[c] 45°C | swelling ratio f[d] | LCST[e] (°C) |
|---|---|---|---|---|---|---|---|---|---|
| 1 | 1/204/8/0.3 | 204 | 8 | 39 +/- 2 | 30 +/- 1 | 0.109 | 0.064 | 2.20 | 33.5 |
| 2 | 1/400/8/0.3 | 400 | 8 | 82 +/- 4 | 50 +/- 4 | 0.075 | 0.028 | 4.41 | 34.5 |
| 3 | 1/600/8/0.3 | 600 | 8 | 212 +/- 5 | 102 +/- 4 | 0.286 | 0.191 | 8.98 | 34 |

[a] Polymerization conditions: solid content = 2.4 wt.%, 70°C, 6h; NIPAm and MBA conversions were all quantitative as attested by $^1$H NMR spectroscopy. [b] Number-average polymerization degree determined by $^1$H NMR spectroscopy. [c] Hydrodynamic diameters ($D_h$) and size distribution (pdi) of nanogels determined from DLS measurements conducted with 5 g.L$^{-1}$ water solutions at 20 and 45 °C. [d] Volume swelling ratio f = $(D_{h,20°C}/D_{h,45°C})^3$. [e]LCST values determined from DSC with polymer concentration of 0.8 g.mL$^-$

With a [Thermal-PPEGA$_{49}$]$_0$/[NIPAm]$_0$ molar ratio of 1 to 400, nanometric gel particles with single size distributions and low size distribution values at 20°C and at 45°C were obtained (run 2, Table III.2). With a molar ratio of 600 ([Thermal-PPEGA$_{49}$]$_0$/[NIPAm]$_0$= 1/600), the $D_h$ and pdi values obtained by DLS analysis revealed the formation of stabilized microgels (run 3, Table III.2). As shown in Table III.2., for run -1, -2, and -3, the volume swelling ratio increased from 2.20 to 4.41 and 8.98 upon heating from 20 to 45°C, with increasing the NIPAm molar equivalent with respect to Thermal-PPEGA$_{49}$ from 204 to 400 and to 600, respectively. This is due to a less compact core due to the lower quantity of MBA for the higher amount of NIPAm. Hence, higher $\overline{DP_{n,\,PNIPAM}}$ lead to bigger particles and higher volume swelling ratios. However, the LCST of nanogel remains stable around 34 °C whatever the $\overline{DP_{n,\,PNIPAM}}$ is.

In conclusion, the thermally-initiated RAFT-PITSA allows to obtain well-defined LCST-type thermosensitive nanogels with a wide range of PPEGA macro-CTAs with various lengths contrary to nanogels obtained by UV-light initiated RAFT-PITSA where a high $\overline{DP_{n,\,PPEGA}}$ is necessary to stabilize nanogel formed. However, the polymerization kinetics using thermal activation for the RAFT-PITSA is much lower than that obtained using UV-light activation. Therefore, UV-light activation will be used subsequently to target degradable and LCST-type thermosensitive nanogels in order to avoid the early degradation of the ketal-based crosslinker during the polymerization process

## 3.3 pH-degradable and LCST-type thermosensitive nanogels

The acid-labile ketal linkage has been widely introduced to fabricate pH-sensitive nanostructures and networks for intracellular drug delivery, in which the acetal/ketal groups are relatively stable under physiological conditions, while rapidly hydrolyzed at a mildly acidic pH to release the encapsulated cargo.[11–13] To target pH-degradable and LCST-type thermosensitive nanogels, a new hydrolyzable crosslinker containing a ketal group was first synthesized and then incorporated into the core of PNIPAm-based nanogels. Finally, the degradability of resulting nanogels was investigated.

### 3.3.1 Synthesis, characterization and stability of a ketal-based crosslinker

The ketal-containing crosslinker (named KB) acting as a divinyl comonomer suitable for one-pot procedure synthesis strategy and also bringing the pH-responsiveness to the nanogel due to the acid cleavage ketal group, was synthesized for the first time by a one-step process from 2,2'-[2,2-propanediylbis(oxy)]diethanamine (PDA) and VDM with an initial molar ratio [PDA]$_0$/[VDM]$_0$ of 1/2 at room temperature in THF (Scheme III.2). After 12 hours, a precipitate was formed and the THF was removed to obtain white product with a yield of 100 %. The final product was characterized by Fourier-transform infrared (FT-IR), $^1$H and $^{13}$C NMR spectroscopies.

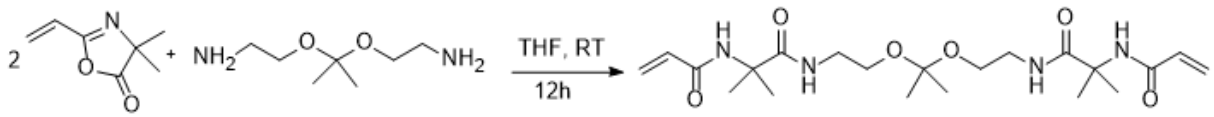


Scheme III.2. Synthesis of ketal-containing crosslinker (KB).

The comparison between the FT-IR spectra of VDM and KB shows the disappearance of signals at 1810 $cm^{-1}$ relative to C=O lactone stretching band. In addition, the signals at 1660 $cm^{-1}$ and 1529 $cm^{-1}$ appear which are relative to the C=O amide stretching band and N-H amide bending band, respectively (Figure III.11). This result therefore confirms the formation of KB.

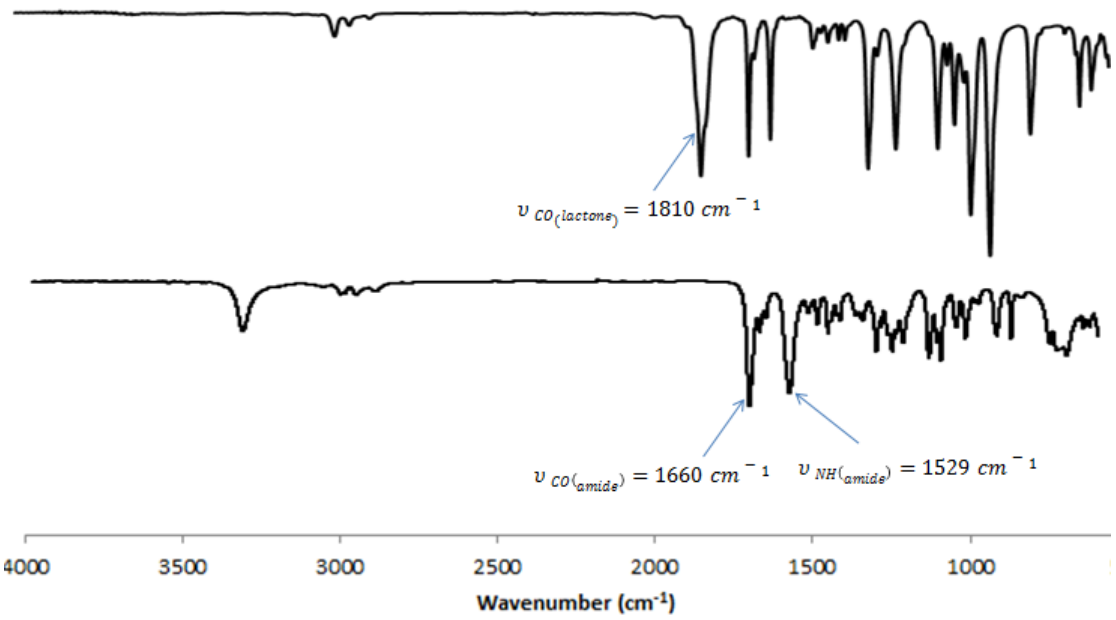


Figure III.12. Comparison of FT-IR spectra of VDM (top) and KB (bottom).

The $^{1}H$ NMR spectrum of KB (Figure III.13) shows two singlets at 1.25 and 1.38 ppm characteristics of the methyl protons of -OC($CH_3$)$_2$ (labelled f in Figure III.13) and of -NHC($CH_3$)$_2$ (labelled c in Figure III.13), respectively. The triplets at 3.25 and 3.47 ppm corresponds to methylene protons of -NC$H_2$CH$_2$ (labelled d in Figure III.13) and of CH$_2$C$H_2$O- (labelled e in Figure III.13), respectively. The characteristic signals of vinyl protons are present between 5.68 and 6.52 ppm (labelled a and b, Figure III.13).

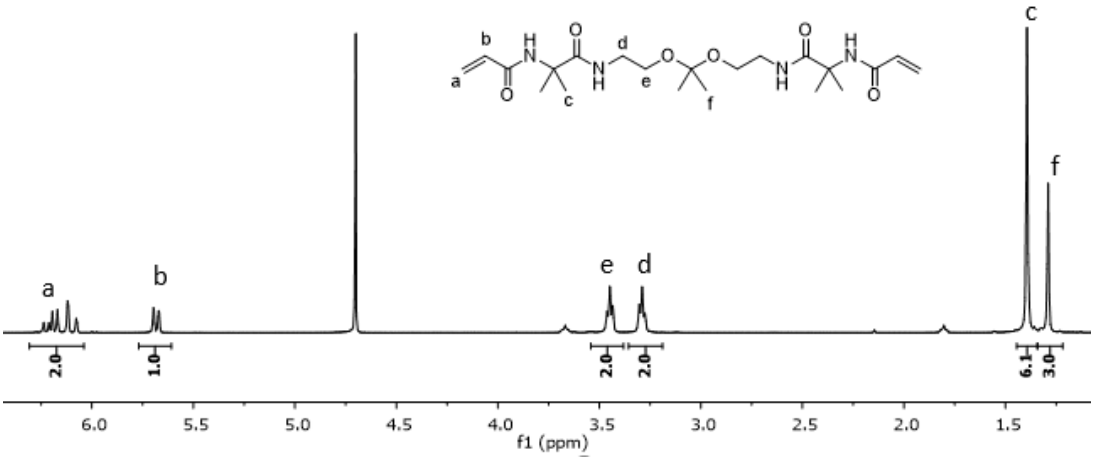


Figure III.13. $^{1}$H-NMR spectrum (400 MHz in $D_2O$) of KB.

The $^{13}$C NMR spectrum of KB (Figure III.14) shows two signals at 170 and 180 ppm corresponding to the carbon of two C=O amide groups (labelled 4 and 3, respectively) confirming the ring opening of VDM.

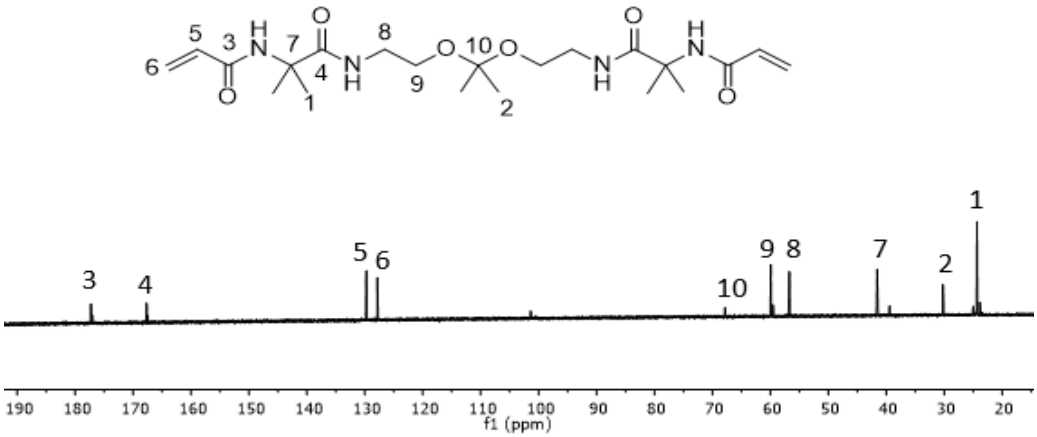


Figure III.14. $^{13}$C-NMR spectrum (400 MHz in $D_2O$) of KB.

The stability of KB was investigated at different pH, temperatures or under UV-light. It was first dissolved in buffer solutions with a range of pH from pH 4 to pH 9 with a concentration of 0.05 g.mL$^{-1}$ which corresponds to the concentration of KB in the polymerization medium to prepare nanogel. The degradability of KB was followed by $^{1}$H NMR spectroscopy in $D_2O$ at different times. The results are illustrated in Table III.3. An example of a $^{1}$H NMR spectra superposition before and after hydrolysis performed at pH 7 is shown in Figure III.15. During the hydrolysis process, the integration of methyl protons of -OC($CH_3$)$_2$ at 1.25 ppm (labeled a in Figure III.15) decreased and results in the formation of methyl protons of acetone at 2.15 ppm (labeled b in Figure III.15). The integration of methyl protons

of -NHC($CH_3$)$_2$ at 1.38 ppm was taken as reference to determine the degradation of KB *versus* time. Results are summarized in Table III.3.

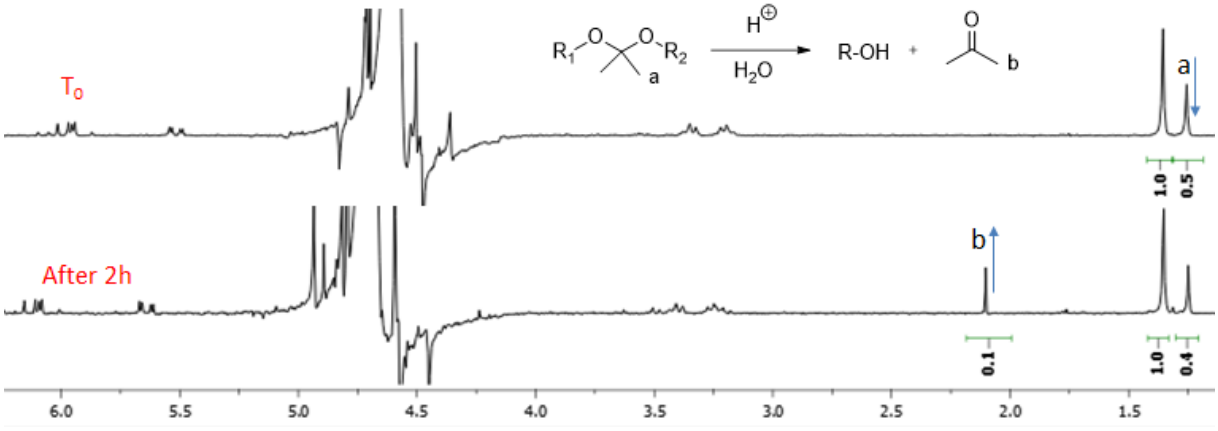


Figure III.15. Superposition of $^1$H NMR spectra (400 MHz, $D_2O$) of KB in solution pH 7 at the beginning and after 2h.

Table III.3. Results of the degradation study of KB under different conditions followed by $^1$H NMR spectroscopy.

| **Experimental Conditions** | **Time** | **Degradation[a] (%)** |
|---|---|---|
| Ultra-pure water (pH 5.5) at 25 °C | 30 min | 75 |
| | 2 h | 100 |
| pH 4, pH 5 or pH 6 at 25 °C | 2 h | 100 |
| pH 7 at 25°C | 2 h | 20 |
| pH 9 at 25°C | 8 days | 0 |
| pH 9 at 70 °C | 3 h | 40 |
| pH 9 at 70 °C under UV-light[b] | 1 h | 0 |

[a] Determined by $^1$H NMR spectroscopy in comparing the integration of methyl protons of -OC($CH_3$)$_2$ at 1.25 ppm or methyl protons of acetone at 2.15 ppm with the integration of methyl protons of -NHC($CH_3$)$_2$ at 1.38 ppm taken as reference. [b] UV-light source (λ = 365 nm, 34 mW.cm$^{-2}$).

Table III.3 shows that after 2h, at room temperature, the KB is completely degraded at acidic media (pH 4, pH 5 and pH 6), and partly degraded (20%) at neutral pH. With buffer solution pH 9, KB remains stable for a longer time at 25°C (1 week). However, KB in pH 9 solution was degraded 40 % after 3h when increasing the temperature to 70 °C. After 1h, at pH 9 under UV-light irradiation at 70

°C, the hydrolysis of KB was also not observed. Therefore, further synthesis of pH-degradable and LCST-type thermosensitive nanogel with KB used as crosslinker will be conducted in pH 9 solution under UV-light irradiation at 70°C for less than 1h.

### 3.3.2 Synthesis of pH-degradable and LCST-type thermosensitive nanogels using KB as crosslinker

As discussed previously, the UV-light activation was chosen to initiate the RAFT-PITSA to target both LCST-type thermosensitive and pH-degradable nanogels. To induce the collapse of PNIPAm into nanodomains, RAFT-PITSA will be conducted at a temperature above the LCST (70°C). Moreover, an alkaline solution at pH 9 was employed as continuous phase to avoid the hydrolysis of the ketal group. Therefore, UV-light initiated RAFT-PITSA of NIPAm were conducted in aqueous solutions at pH = 9 and 70°C using a UV-PPEGA of $\overline{DP_{n,\,PPEGA}}$ equal to 30 as macro-CTA and surfactant, KB as crosslinker and photo-I with the initial molar ratio of $[NIPAm]_0/[UV\text{-}PPEGA_{30}]_0/[KB]_0/[Photo\text{-}I]_0$ = 200/1/8/0.3 (Scheme III.3). The solid contents were varied from 2.4 wt.% to 10 wt.%.

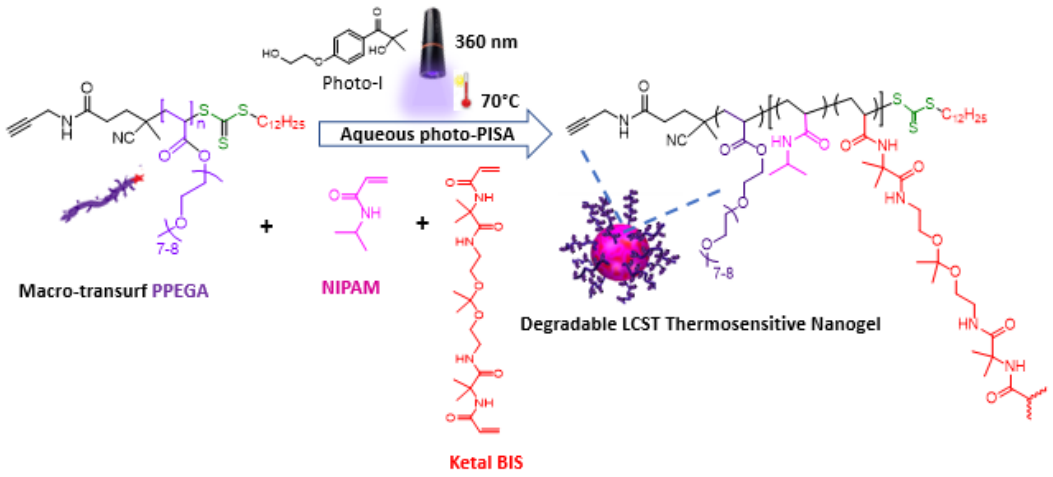


Scheme III.3. Synthesis of pH-degradable and LCST-type thermosensitive nanogels by UV-light initiated RAFT-PITSA in aqueous dispersion at pH 9 under UV-light irradiation at 70°C with an initial molar ratio of $[NIPAm]_0/[UV\text{-}PPEGA_{30}]_0/[KB]_0/[Photo\text{-}I]_0$ = 200/1/8/0.3.

The global conversion of NIPAm and KB monomers was calculated by $^1$H NMR analysis of crude mixtures. As an example, Figure III.16 shows the overlay of $^1$H NMR spectra at initial time (t = 0) and after 1h for a RAFT-PITSA of NIPAm using a solid content of 10 wt.%. The disappearance of vinyl protons between 5.62 ppm and 6.25 ppm is consistent with a full NIPAm and KB conversion.

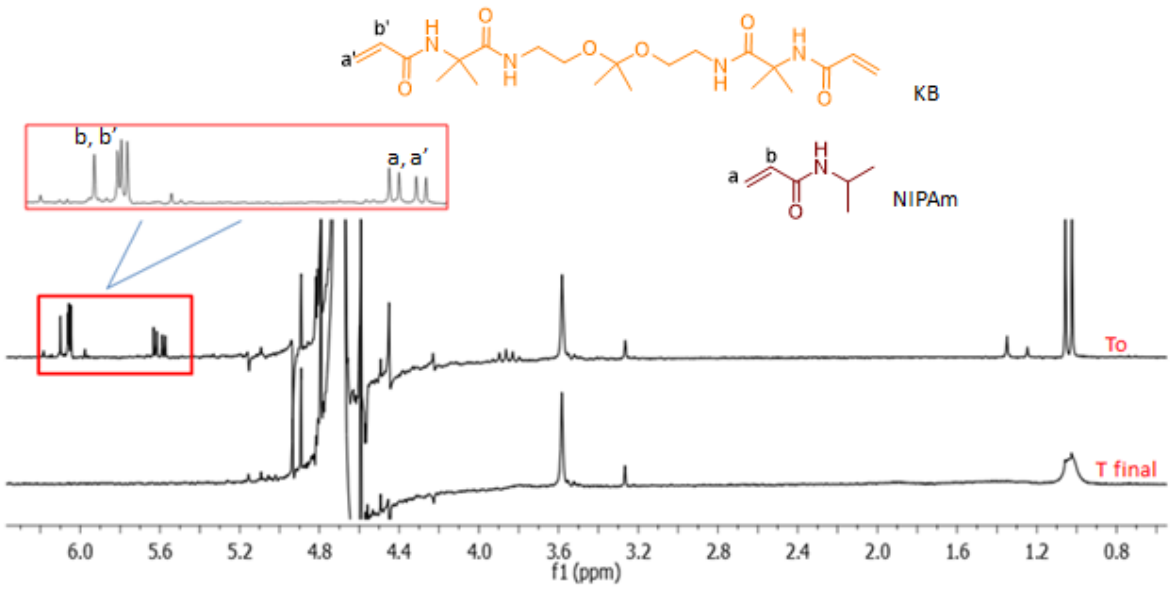


Figure III.16. Overlay $^{1}$H NMR spectra (200 MHz in $D_2O$) of polymerization medium at t = 0 and after 1h obtained through UV-light initiated RAFT-PITSA of NIPAm conducted in aqueous dispersion at pH 9 and 70°C using a UV-PPEGA$_{30}$ and the KB as crosslinker with the initial molar ratio of $[NIPAm]_0/[UV\text{-}PPEGA_{30}]_0/[KB]_0/[Photo\text{-}I]_0$ = 200/1/8/0.3 and 10 wt.% of solid content.

The final product was lyophilized to remove water for $^{1}$H NMR spectroscopy and DLS characterizations. The $^{1}$H NMR spectrum (Figure III.17) of the resulting nanogel shows signals at 3.35 ppm ($(CH_2CH_2O)_8CH_3$, labeled g) and 4.2 ppm ($C(=O)OCH_2CH_2O\text{-}(CH_2CH_2O)_8$, labeled a) characteristics of the PPEGA block; signals at 3.85 ppm (-NH-$CH(CH_3)_2$, labeled c) and 1.1 ppm (-NH-$CH(CH_3)_2$, labeled b) characteristics of the PNIPAm block. The signal from 0.6 to 2.5 ppm corresponds to the methyl protons from NIPAm and KB units, methylene and methine protons of the copolymer backbone (labeled b, b',b", d, e, d', e', d'' and e"). The comparison of these integrations were employed to determine the molar composition of the resulting copolymer UV-PPEGA$_{30}$-*b*-UV-P(NIPAm-*co*-KB) nanogel: $\overline{DP_{n,\,PPEGA}}$ = 30, $\overline{DP_{n,\,PNIPAM}}$ = 198 and $\overline{DP_{n,\,PKB}}$ = 7.

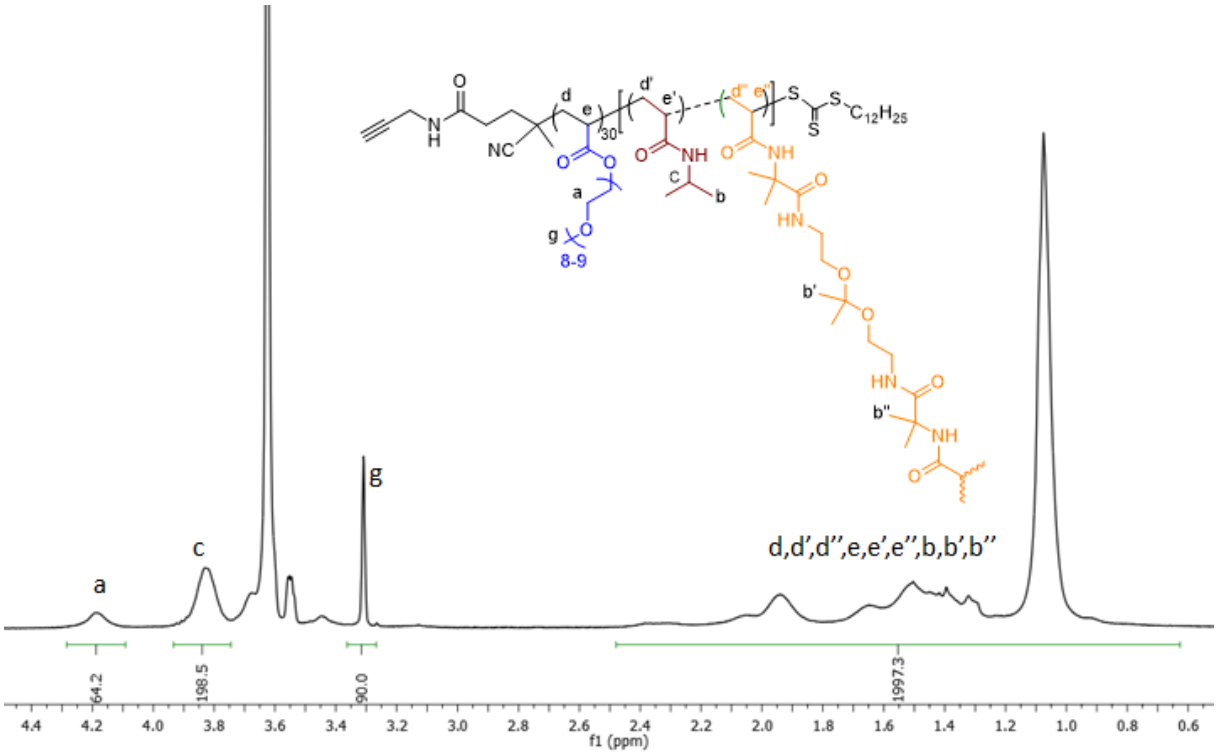


Figure III.17. $^{1}$H NMR spectrum (400 MHz, $D_2O$) of UV-PPEGA$_{30}$-*b*-UV-P(NIPAm-*co*-KB) nanogel synthesized by UV light-initiated RAFT-PITSA of NIPAm/KB mediated through UV-PPEGA$_{30}$ (Table II.2, run 3, chapter II) ([NIPAm]$_0$/[KB]$_0$/[UV-PPEGA$_{30}$]$_0$/[Photo-I]$_0$ = 204/8/1/0.3) with a solid content of 10 wt.% in water at 70°C after 1h of reaction.

Afterwards, final products obtained at different solid contents were freeze-dried and re-dispersed in buffer solution pH 9 with a concentration of 5 g.L$^{-1}$ for DLS characterization. The $D_h$ values and pdi of nanogels are shown in Figure III.18 and in Table III.4. The sample obtained using a solid content of 2.4 wt.% shows clearly two size distributions by number (Figure III.18A). When the solid content reaches 5 wt.%, the DLS analysis solution shows a single size distribution and similar $D_h$ at 20 and 45°C (Figure III.18B) which highlights the presence of not-defined nanogels based on PPEGA-*b*-P(NIPAm-*co*-KB) copolymers. With increasing the solid content to 7.5 wt.%, nanogels showing a LCST behavior were obtained with a decrease of $D_h$ from 112 nm at 20 °C to 80 nm at 45°C with a swelling ratio of 2.74 (run 3 in Table III.4, Figure III.18C) and pdi equal to 0.058 at 45°C, which is much smaller than the pdi at 20°C. The increase of the solid content from 7.5 to 10 wt% leads to an increase of the $D_h$ from 112 to 139 nm corresponding to a swelling ratio of 5.24. This is probably due to the higher solid content that promotes a higher density of intra-crosslink network in the nanoparticles and more polymer chains being incorporated into each nanogel which result into bigger particles.[14] The LCST value of PPEGA-*b*-P(NIPAm-*co*-KB) nanogel with 10 % solid content is 34 °C, which is slightly lower than that value of PPEGA-*b*-P(NIPAm-*co*-MBA) nanogels.

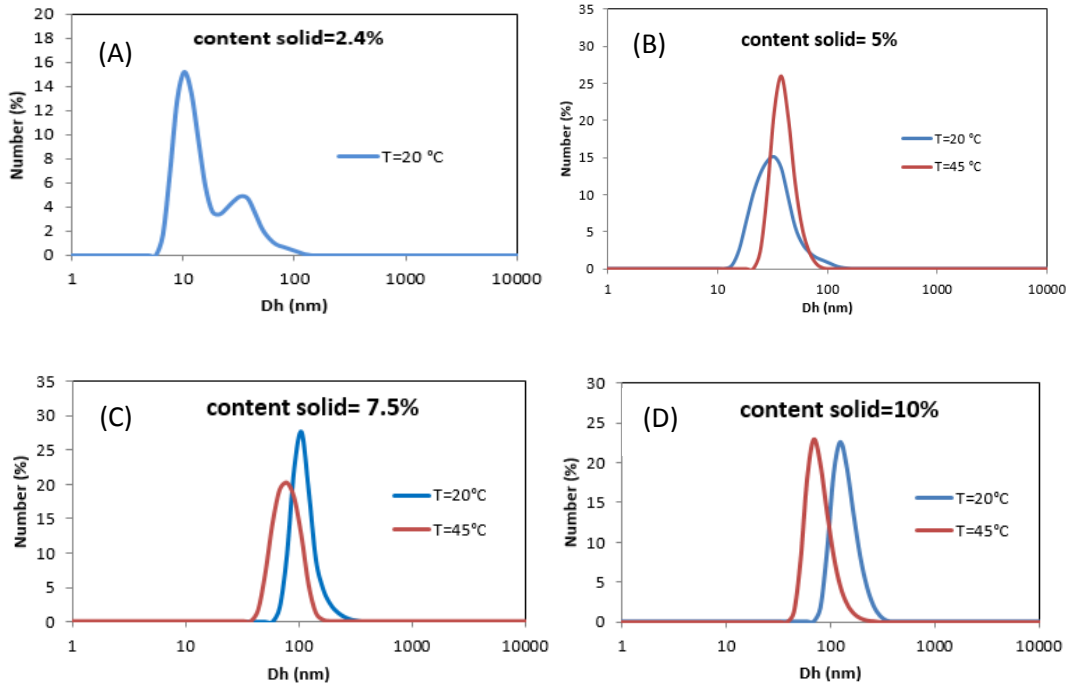


Figure III.18. DLS number-average diameter distributions of UV-PPEGA$_{30}$-*b*-UV-P(NIPAm-*co*-KB) nanogels solutions (5 g.L$^{-1}$) obtained from a DLS study at 20°C and 45°C using different solid contents during the UV-light initiated RAFT-PITSA in aqueous solution pH 9 under UV irradiation at 70°C with an initial molar ratio of [NIPAm]$_0$/[UV-PPEGA$_{30}$]$_0$/[KB]$_0$/[Photo-I]$_0$ = 200/1/8/0.3.

Table III.4. Polymerization conditions,[a] $D_h$ and pdi values at 20°C and at 45°C of UV-PPEGA-*b*-UV-P(NIPAm-*co*-KB) nanogels solutions obtained at 20°C and 45°C using different solid contents during the UV-light initiated RAFT-PITSA of NIPAm/KB in aqueous solution pH 9 at 70°C with an initial molar ratio of [NIPAm]$_0$/[UV-PPEGA$_{30}$]$_0$/[KB]$_0$/[Photo-I]$_0$ = 200/1/8/0.3.

| Run | Solid content (wt.%) | $D_h$ 20°C [b] (nm) | pdi[b] | $D_h$ 45°C [b] (nm) | pdi[b] | Swelling ratio | LCST (°C) |
|---|---|---|---|---|---|---|---|
| 1 | 2.4 | 2 size distributions | 0.255 | 41 | 0.032 | - | - |
| 2 | 5 | 38 +/- 2 | 0.253 | 41+/- 1 | 0.037 | - | - |
| 3 | 7.5 | 112 +/- 2 | 0.114 | 80 +/- 2 | 0.058 | 2.74 | - |
| 4 | 10 | 139 +/- 2 | 0.136 | 78 +/- 2 | 0.107 | 5.24 | 34 |

[a] Polymerization conditions: after 1h, complete NIPAm and KB conversions as determined by $^1$H NMR spectroscopy. [b] The hydrodynamic diameters ($D_h$) and size distribution (pdi) of nanogels were obtained from DLS measurements conducted with 5g.L$^{-1}$ in aqueous solution at pH9 at 20°C and 45°C.

### 3.3.3 Study of the degradability of nanogels based on UV-PPEGA-*b*-P(NIPAm-*co*-KB)

The ability of the UV-PPEGA$_{30}$-*b*-P(NIPAm$_{198}$-*co*-KB$_7$)-based nanogels to disassemble in aqueous medium by hydrolysis of ketal moieties was then studied. The dried nanogel (run 4, Table III.4) was dissolved at a concentration of 5 g.L$^{-1}$ in different pH buffer solutions. Since hydrolysis of the ketal group is possible under acidic conditions, we performed the experiments in solutions at pH 4, pH 5, pH 6 and pH 7 at 25 °C. The evolution of the $D_h$ *vs.* time was determined using DLS measurements (Figure III.19A for pH 4, pH 5 and pH 6 and Figure III.19B for pH 7).

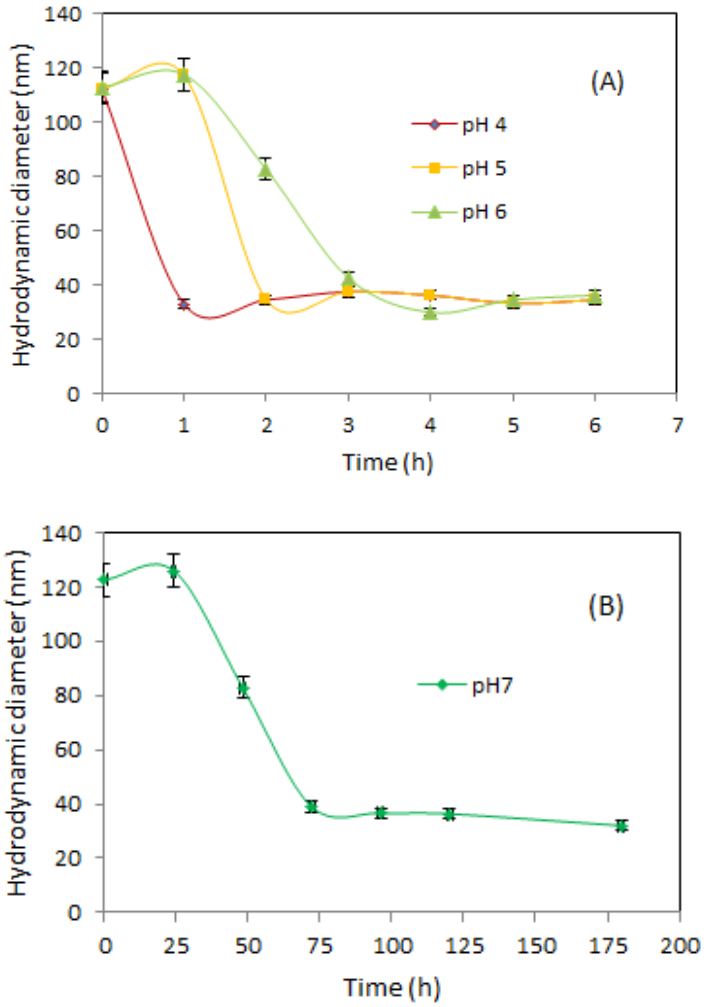


Figure III.19. Evolution of $D_h$ of the UV-PPEGA$_{30}$-*b*-UV-P(NIPAm$_{198}$-*co*-KB$_7$)-based nanogels solutions (5 g.L$^{-1}$) at 25 °C measured by DLS as a function of time in aqueous media at: (A) pH 4, pH 5 and pH 6, and (B) pH 7. The nanogels were obtained by UV-light initiated RAFT-PITSA of NIPAm/KB in aqueous solution pH 9 at 70°C with an initial molar ratio of $[NIPAm]_0/[UV\text{-}PPEGA_{30}]_0/[KB]_0/[Photo\text{-}I]_0$ = 200/1/8/0.3 with a solid content of 10 wt.%.

As shown in Figure III.19A, the degradation of UV-PPEGA$_{30}$-*b*-UV-P(NIPAm$_{197}$-*co*-KB$_7$)-based nanogel is rapid at pH 4.0, with a half-life of 30 min as the $D_h$ of particles drop dramatically at this time. The degradation rate dramatically decreased with increasing pH, from a calculated half-life of 60 min and 180 min for pH 5 and pH 6, respectively, while at pH 7, the hydrolysis is slow with a half-life of around 2 days (48h) (Figure III.19B). Such results are consistent with the degradability of KB at pH 4 and 5 solutions reported in Table III.3 in which a fully KB degradation was observed after 2h. When the pH 6 is considered, the ketal group in KB hydrolyzed faster than the ketal group in UV-PPEGA$_{30}$-*b*-UV-P(NIPAm$_{197}$-*co*-KB$_7$)-based nanogel as the KB is fully degraded after 2h and the nanogel is fully degraded at 3h at 25°C. The network polymer structure of the nanogel core seems to give somehow an additional protection of the ketal group.

To conclude, the nanogel is stable at pH = 7 during 24 h and can be degraded in short time (30 min) at pH = 4. Such behavior is of particular interest to control bio(macro)molecules delivery for instance.

## 3.4 Conclusions

Although the kinetic of thermal activation is much lower than that of UV-light activation for the RAFT-PITSA to target LCST-type thermosensitive PNIPAm-based nanogels, both activations allow to target nanogels with a single and low size distribution through RAFT-PITSA using a wide range of PPEGAs, with variable $\overline{DP_{n,\,PPEGA}}$, used as macro-CTA and surfactant. A minimum $\overline{DP_{n,\,PPEGA}}$ is necessary for the sterical stability of the nanogels formed *in situ* during the PITSA process and this value is dependent on activation process as UV-light activation required a higher $\overline{DP_{n,\,PPEGA}}$ to form stable nanogel.

Both $\overline{DP_{n,\,PPEGA}}$ and $\overline{DP_{n,\,PNIPAM}}$ of Thermal-PPEGA-*b*-Thermal-P(NIPAm-*co*-MBA) have a significant impact on size, pdi, and swelling ratio of the nanogels as the increase of $\overline{DP_{n,\,PPEGA}}$ up to 33 leads to smaller well-defined particles. By contrast, the increase of $\overline{DP_{n,\,PNIPAM}}$ results in particles having bigger size and higher swelling ratio. The LCST values of different nanogels remain stable around 33-34 °C whatever $\overline{DP_{n,\,PNIPAM}}$ is.

A new ketal-based crosslinker was synthesized in a simple and efficient way, and its degradability in different media was investigated. The UV-light initiated RAFT-PITSA of NIPAm were conducted in aqueous solutions at pH = 9 for 1h at 70°C using a UV-PPEGA of $\overline{DP_{n,\,PPEGA}}$ equal to 30 as macro-CTA and surfactant, KB as crosslinker and photo-I with the initial molar ratio of $[NIPAm]_0/[UV\text{-}PPEGA_{30}]_0/[KB]_0/[Photo\text{-}I]_0$ = 200/1/8/0.3 and the solid contents were varied from 2.4 wt.% to 10 wt.%. With higher solid content (7.5 wt.% and 10 wt.%), more defined dual LCST and pH-sensitive nanogels were obtained. These nanogels with LCST of 34 °C are stable at pH 7 during 24 hours and

can be fully degraded in a short time: 1h at pH 4 and 2h at pH 5. Such characteristics makes these “smart” nanogels excellent candidates in the controlled delivery of bio(macro)molecules.

## 3.5 Experimental section

### 3.5.1 Materials

All reagents were purchased from Sigma-Aldrich unless otherwise noted. 2-Hydroxy-4'-(2-hydroxyethoxy)-2-methylpropiophenone (photo-I, 98%), 2,2'-azobis(2-methylpropionamidine) dihydrochloride (V50, 97%), *N,N*-dimethylformamide (DMF, 99%), tetrahydrofuran (THF, 99%), *N*,*N*'-methylenebis(acrylamide) (MBA, 99%), *N*-isopropylacrylamide (NIPAm, >99%), 2,2'-[2,2-propanediylbis(oxy)]diethanamine (PDA, 99%). Different PPEGA-macro CTAs were synthesized in Chapter II. Vinylazlactone (VDM) was according to previously reported procedure.[15] All deuterated solvents were purchased from Euriso-top. All buffer solution with different pH were purchased from Merck KGaA. Ultra-pure water used for RAFT polymerization and preparation of nanogel solutions was obtained from a PureLab ELGA system and had a conductivity of 18.2 MΩm at 25°C.

### 3.5.2 Characterizations

**Nuclear magnetic resonance (NMR) spectroscopy.** Nuclear Magnetic Resonance (NMR) spectra were recorded on a Bruker AC-400 spectrometer for $^{1}$H-NMR and $^{13}$C-NMR (400 MHz and 200 MHz). Chemical shifts are reported in ppm relative to the deuterated solvent resonances.

**Dynamic light scattering (DLS).** DLS measurements were performed on a Malvern Instruments Zetasizer Nano (ZS) fitted with a Helium-Neon laser operating at 633 nm with an angle detection (173°). Different samples were prepared by dissolving nanogels in aqueous solutions at different pH (5 g.L$^{-1}$) and the nanogel solution was filtered using nylon membrane filter of 0.45 µm porosity. The hydrodynamic diameter ($D_h$) of nanogels and size distribution pdi were recorded at 20°C and 45°C. The aqueous solutions of nanogels were first equilibrated at 20°C and 45°C for 10 min before recording. Each measurement was repeated 5 times and hydrodynamic diameter of nanogel was taken as the average size number distribution. The degradation of nanogel at different pH was follow by the evolution of the hydrodynamic diameter of nanogel as a function of time at 25 °C.

**Transmission electronic microscopy (TEM)**. TEM analysis was carried out using a JEOL2100 at an accelerating voltage of 120 kV. To prepare the TEM samples, a dilute aqueous solution (5 g.L$^{-1}$) of nanogels was dropped onto a carbon-coated copper grid. The sample was left to gently dry 24h at room temperature.

**FT-IR** spectra were recorded using a Nicolet iS5 FT-IR spectrometer operating with an attenuated total reflection (iD5 ATR Diamond) gate. Spectra were analyzed with OMNIC software.

**Fluorescence Measurements.** Fluorescence spectra were recorded with a Horiba-Jobin Yvon fluorescence spectrophotometer in the right-angle geometry. For the fluorescence measurements, 3 mL of each sample were placed in a 1.0 cm square quartz cell. The emission spectra, were recorded using the excitation wavelength at 329 nm and the excitation spectra, were recorded using the emission wavelength at 371 nm. The widths of slits were set at 2 nm for both excitation and emission fluorescent measurements.

**Differential scanning calorimetry (DSC).** DSC measurement was performed on a TA Instruments Q100 connected to a computer in aluminum pans under nitrogen otherwise noted. The DSC instrument was calibrated using an indium standard. Sample was heated from 15 °C to 50 °C at a heating rate of 10 °C.min$^{-1}$ and under a static nitrogen atmosphere, followed by cooling to 15°C at the same rate after an isotherm at 50°C during 2 minutes. Thermal transitions was obtained from the maximum of the endotherm (heating scan).

**Elaboration LCST-type thermosensitive nanogel based on PPEGA-*b*-P(NIPAm-*co*-MBA) by thermally initiated RAFT-PITSA** A typical procedure: In a 10 mL round bottom flask was added 97 mg of NIPAm (0.86 mmol, 204 eq.), 54.4 mg of Thermal-PPEGA$_{20}$ ($\overline{DP_{n,\,PPEGA}}$ = 20, run 3 Table II.1, 4.2x 10$^{-3}$ mmol, 1 eq.) and 50 µL of V50 solution (71.2 mg of V50 in 10 mL of water, (1.26x 10$^{-3}$ mmol, 0.3 eq.)) in 5.24 g of water to give a solid content of 2.4 wt.%. The flask was spared with argon for 30 min then placed in a preheated oil bath of 70°C for 6h. After checking the total monomers conversion by $^{1}$H NMR spectroscopy, the reaction was stopped by opening the flask to air. The reaction medium was freeze-dried and characterized by $^{1}$H NMR spectroscopy, DSC and DLS.

**Elaboration LCST-type thermosensitive nanogel based on PPEGA-*b*-P(NIPAm-*co*-MBA) by UV-light initiated RAFT-PITSA** A typical procedure: In a 10 mL glass vial was added UV-PPEGA$_{18}$ ($\overline{DP_{n,\,PPEGA}}$ = 18, run 1 Table II.2, 25 mg, 2.76x 10$^{-3}$ mmol, 1 eq.), NIPAm (63.8 mg, 0.564 mmol, 204 eq.), MBA crosslinker (3.24 mg, 0.021 mmol, 8 eq.), 0.1 mL of photo-I solution (1.86 mg of photo-I in 1 mL of water) (8.3x 10$^{-4}$ mmol, 0.3 eq) and 3.84 g water to give a solid content of 2.4 wt.%. 0.05g of DMF was added as reference in $^{1}$H NMR spectroscopy. After purging with argon for 30 minutes, the mixture was placed in the middle of a UV lamp (λ = 365 nm, 34 mW.cm$^{-2}$) an argon atmosphere with stirring. The system was placed in an oven to keep the reaction at certain temperature for 1h. The reaction was stopped by turning off the light and cooling the mixture in nitrogen liquid. NIPAm conversion of 86 % was obtained by $^{1}$H NMR spectroscopy. The final product was obtained by freeze-drying and characterized by $^{1}$H NMR spectroscopy, DSC and DLS.

**Synthesis of ketal-containing crosslinker** The ketal-containing crosslinker (KB) was synthesized by a one-step process from 2,2'-[2,2-propanediylbis(oxy)] diethanamine (PDA) and vinyldimethylazlactone

(VDM) with an initial molar ratio $[PDA]_0/[VDM]_0$ of ½. In a 100 mL round bottom flask was added 0.5 g of PDA (3.08 mmol, 1 equiv.), 0.858 g VDM (6.16 mmol, 2 equiv.) and 30 mL of THF. The mixture was mixed by a stirring bar at room temperature. After 12 hours, a precipitate was formed. THF was removed under reduced pressure to obtain KB as a white product with a yield of 100 %. FT-IR ($\upsilon$ in $cm^{-1}$): 3306 (C-H), 2981 (C=C), 1660 (C=O, amide), 1529 (N-H, amide) $^1$H NMR (400 MHz, $D_2O$), $\delta$ (ppm): 1.24 (s, OC($CH_3$)$_2$, 6 H), 1.38 (s, NHC($CH_3$)$_2$, 12 H), 3.25 (t, $NCH_2CH_2$, 4 H), 3.47 (t, $CH_2CH_2O$, 4 H), 5.68 (d, $CH_2CHCO$, 2 H), 6.52 (m, $CH_2CHCO$, 4 H) $^{13}$C NMR (100 MHz, $D_2O$), $\delta$ (ppm) : 17 (NH*C*-$CH_3$), 30 (O*C*-$CH_3$), 42 (NH*C*-CO), 58 (NH*C*$H_2$-$CH_2$), 60 (*C*$H_2$-$CH_2O$), 68 (O-*C*$CH_3$), 128 (*C*$H_2$=CH), 130 (CH=*C*$H_2$), 166 (C(*C*=O)NH-$CH_3$), 176 ($CH_2CH$(*C*=O)NH).

**Elaboration of pH-degradable and LCST-type thermosensitive nanogel based on PPEGA-*b*-P(NIPAm-*co*-KB) by UV-light initiated RAFT-PITSA.** A typical procedure: In a 10 mL glass vial was added UV-$PPEGA_{30}$ ($\overline{DP_{n,\,PPEGA}}$ =30, run 3 Table II.2, 42 mg, 2.76x $10^{-3}$ mmol, 1 eq.), NIPAm (63.8 mg, 0.564 mmol, 204 eq.), KB crosslinker (9.37 mg, 0.021 mmol, 8 eq.), 0.1 mL of photo-I solution (1.86 mg of photo-I in 1 mL of buffer solution pH 9) (8.3x $10^{-4}$ mmol, 0.3 eq) and 4.67g of buffer solution pH9 to give a solid content of 2.4 wt%. 0.05g of DMF was added as reference in $^1$H NMR spectroscopy. Then, after purging with argon for 30 minutes, the mixture was placed in the middle of a UV lamp (λ = 365 nm, 34 $mW.cm^{-2}$) under an argon atmosphere with stirring for 1 hour. The reaction was stopped by turning off the light and cooling the mixture in liquid nitrogen. NIPAm and KB conversions of 100 % were obtained by $^1$H NMR spectroscopy. The final product was obtained by freeze-drying and characterized by $^1$H NMR spectroscopy, DSC and DLS.

## 3.6 References


(1) Chacko, R. T.; Ventura, J.; Zhuang, J.; Thayumanavan, S. Polymer Nanogels: A Versatile Nanoscopic Drug Delivery Platform. *Adv. Drug Deliv. Rev.***2012**, *64* (9), 836–851. https://doi.org/10.1016/j.addr.2012.02.002.

(2) Cheng, G.; Mi, L.; Cao, Z.; Xue, H.; Yu, Q.; Carr, L.; Jiang, S. Functionalizable and Ultrastable Zwitterionic Nanogels. *Langmuir* **2010**, *26* (10), 6883–6886. https://doi.org/10.1021/la100664g.

(3) Molina, M.; Asadian-Birjand, M.; Balach, J.; Bergueiro, J.; Miceli, E.; Calderón, M. Stimuli-Responsive Nanogel Composites and Their Application in Nanomedicine. *Chem. Soc. Rev.* **2015**, *44* (17), 6161–6186. https://doi.org/10.1039/C5CS00199D.

(4) Zhang, X.; Malhotra, S.; Molina, M.; Haag, R. Micro- and Nanogels with Labile Crosslinks – from Synthesis to Biomedical Applications. *Chem. Soc. Rev.* **2015**, *44* (7), 1948–1973. https://doi.org/10.1039/C4CS00341A.

(5) Li, Y.; Maciel, D.; Rodrigues, J.; Shi, X.; Tomás, H. Biodegradable Polymer Nanogels for Drug/Nucleic Acid Delivery. *Chem. Rev.* **2015**, *115* (16), 8564–8608. https://doi.org/10.1021/cr500131f.

(6) Zhuang, J.; Gordon, M. R.; Ventura, J.; Li, L.; Thayumanavan, S. Multi-Stimuli Responsive Macromolecules and Their Assemblies. *Chem. Soc. Rev.* **2013**, *42* (17), 7421. https://doi.org/10.1039/c3cs60094g.

(7) Sanson, N.; Rieger, J. Synthesis of Nanogels/Microgels by Conventional and Controlled Radical Crosslinking Copolymerization. *Polym. Chem.* **2010**, *1* (7), 965. https://doi.org/10.1039/c0py00010h.

(8) An, Z.; Shi, Q.; Tang, W.; Tsung, C.-K.; Hawker, C. J.; Stucky, G. D. Facile RAFT Precipitation Polymerization for the Microwave-Assisted Synthesis of Well-Defined, Double Hydrophilic Block Copolymers and Nanostructured Hydrogels. *J. Am. Chem. Soc* **2007**, *129* (46), 14493–14499. https://doi.org/10.1021/ja0756974.

(9) Rieger, J.; Grazon, C.; Charleux, B.; Alaimo, D.; Jérôme, C. Pegylated Thermally Responsive Block Copolymer Micelles and Nanogels via *in Situ* RAFT Aqueous Dispersion Polymerization. *Journal of Polymer Science Part A: Polym. Chem.* **2009**, *47* (9), 2373–2390. https://doi.org/10.1002/pola.23329.

(10) Grazon, C.; Rieger, J.; Sanson, N.; Charleux, B. Study of Poly(N,N-Diethylacrylamide) Nanogel Formation by Aqueous Dispersion Polymerization of N,N-Diethylacrylamide in the Presence of Poly(Ethylene Oxide)-b-Poly(N,N-Dimethylacrylamide) Amphiphilic Macromolecular RAFT Agents. *Soft Matter* **2011**, *7* (7), 3482. https://doi.org/10.1039/c0sm01181a.

(11) Bachelder, E. M.; Beaudette, T. T.; Broaders, K. E.; Dashe, J.; Fréchet, J. M. J. Acetal-Derivatized Dextran: An Acid-Responsive Biodegradable Material for Therapeutic Applications. *J. Am. Chem. Soc.* **2008**, *130* (32), 10494–10495. https://doi.org/10.1021/ja803947s.

(12) Chen, W.; Meng, F.; Li, F.; Ji, S.-J.; Zhong, Z. PH-Responsive Biodegradable Micelles Based on Acid-Labile Polycarbonate Hydrophobe: Synthesis and Triggered Drug Release. *Biomacromolecules* **2009**, *10* (7), 1727–1735. https://doi.org/10.1021/bm900074d.

(13) Steinhilber, D.; Witting, M.; Zhang, X.; Staegemann, M.; Paulus, F.; Friess, W.; Küchler, S.; Haag, R. Surfactant Free Preparation of Biodegradable Dendritic Polyglycerol Nanogels by Inverse Nanoprecipitation for Encapsulation and Release of Pharmaceutical Biomacromolecules. *JCR* **2013**, *169* (3), 289–295. https://doi.org/10.1016/j.jconrel.2012.12.008.

(14) Xu, Y.; Li, Y.; Cao, X.; Chen, Q.; An, Z. Versatile RAFT Dispersion Polymerization in Cononsolvents for the Synthesis of Thermoresponsive Nanogels with Controlled Composition, Functionality and Architecture. *Polym. Chem.* **2014**, *5* (21), 6244–6255. https://doi.org/10.1039/C4PY00867G.

(15) Levere, M. E.; Ho, H. T.; Pascual, S.; Fontaine, L. Stable Azlactone-Functionalized Nanoparticles Prepared from Thermoresponsive Copolymers Synthesized by RAFT Polymerization. *Polym. Chem.* **2011**, *2* (12), 2878. https://doi.org/10.1039/c1py00320h.

# Chapter IV

# Elaboration of UCST-type thermosensitive and pH-degradable nanogels by RAFT-PITSA

## 4.1 Introduction

Unlike LCST-type thermosensitive nanogels, the use of the PITSA process to achieve UCST-type nanogels is comparatively underdeveloped. This is probably due to the behavior of UCST-type thermosensitive polymers[1] that show a precipitation in water at low temperature (lower than UCST for the polymer to collapse into nanodomains) and limits radical activation methods for the RAFT-PITSA. Starting from a hydrophilic polymer acting as macro-CTA and surfactant, either a two steps procedure or either a direct procedure has been reported to synthesize UCST-type thermosensitive nanogels. The two steps procedure involves the polymer self-assembly and the crosslinking micelles[2] and the direct procedure based on RAFT-PITSA.[3,4] Among the hydrogen-bonding UCST-type thermosensitive polymers, the poly(*N*-acryloyl glycinamide) (PNAGA),[4,5] known since 1964, presents tunable UCST-thermosensitive properties which make it useful in applications such as controlled drug release,[6] cell culture[7] or catalysis.[8] It is thus of great interest to develop a simple and robust process to elaborate this type of nanoparticles in an environmentally friendly aqueous dispersed media and to study their UCST behavior. In the present chapter, we report for the first time the synthesis of hydrogen-bonding UCST-type thermosensitive nanogels using the direct RAFT-PITSA protocol. In the first part of this chapter, the synthesis of hydrogen-bonding UCST-type thermosensitive nanogels based on PNAGA using the direct RAFT-PITSA process in aqueous dispersion is presented.[**] PNAGA-based nanogels containing a non-degradable crosslinker MBA are synthesized and the influence of various synthesis parameters on nanogels stability, size, polydispersity in size, swelling ratio and thermosensitive properties, *i.e.,* value of UCST, will also be investigated.

[**] This study has been published in *Macromolecular Rapid Communications* (T.N. Tran *et al. Macromol. Rapid Commun.* **2020**, *41*, 2000203).

A significant disadvantage of up-to-now reported UCST-type thermosensitive nanogels is, their inherent non-degradability while controlled degradation of polymer materials is more and more necessary for environmental issues and also for biomedical applications. Whereas gelatin is a good example of a degradable natural macromolecular UCST system,[6,9] degradable synthetic UCST-type thermosensitive polymers are extremely rare. Only a few recent studies have been reported. Pineda-Contreras *et al*. [10] reported the pH-dependent UCST-transitions of diblock of statistical copolymers of Am and AN. Loss and regeneration of the phase transition temperature of these copolymers was achieved by changing the pH from basic to acidic. Wolf *et al*. introduced interesting class of copolymers containing pendant double bonds with well-defined degradable and adjustable UCST value.[11] By changing the pH value, a reduction of the UCST phase transition temperature and broadening of the transition range were observed under basic conditions, the polymeric system can degraded completely. However, due to the presence of ionizable groups these polymers cannot exhibit UCST behavior at physiological pH. Sponchioni *et al*.[12] developed a new class of degradable zwitterionic UCST-type thermosensitive polymer nanoparticles and found out that the degradation rate of the nanoparticles at pH 14 is dependent on the length of the oligoester grafts. Roth *et al*.[13] described the synthesis of thioester-based statistical UCST-type thermoensitive copolymers and the degradation of such UCST-type thermosenstive polymers was investigated through aminolysis. De Geest and co-workers [14] synthesized an amide-functional homopolymer which showed the aqueous UCST behavior and its hydrolytic degradation within a physiologically relevant window. Boustta *et al*. [15] studied the synthesis and the degradation of UCST-type thermosensitive hydrogels based on hyaluronic-PNAGA copolymers through enzymatic degradation. Even if just very recent few studies have been reported on degradable synthetic UCST-type thermosensitive polymers, to the best of our knowledge, no study has been reported on degradable synthetic UCST-type thermosensitive nanogel. In our work, the ketal hydrolyzable crosslinker (KB, synthesized in chapter III) will be incorporated into the core of UCST-type thermosensitive nanogels based on PNAGA. Therefore, in the second part of this chapter, we report the synthesis of pH-degradable and UCST-type thermosensitive nanogels by using the KB and the pH-degradability of the so-obtained nanogels.

## 4.2 UCST-type thermosensitive nanogels synthesized through UV-light initiated RAFT-PITSA

To target hydrogen-bonding UCST-type thermosensitive nanogels based on a PPEGA-*b*-P(PNAGA-*co*-MBA) copolymers using the direct RAFT-PITSA process, a Thermal-PPEGA$_{30}$ (run 5, Table II.1) was used as both stabilizer and macro-CTA for the UV-light initiated RAFT-PITSA of NAGA and MBA in aqueous dispersion in order to get a crosslinked P(NAGA-*co*-MBA) core and a PPEGA shell.

### 4.2.1 PPEGA-b-P(PNAGA-co-MBA)-based UCST-type thermosensitive nanogels: synthesis, macromolecular characterizations and thermosensitive properties

In order to reach UCST-type thermosensitive nanogel at low temperature, the UV-light initiated RAFT-PITSA was initiated by photo-I under UV irradiation (λ = 365 nm, P = 34 mW.cm$^2$) at 3 °C leading to the self-assembly of PPEGA-*b*-P(NAGA-*co*-MBA) copolymers into nanogels (Scheme IV.1).

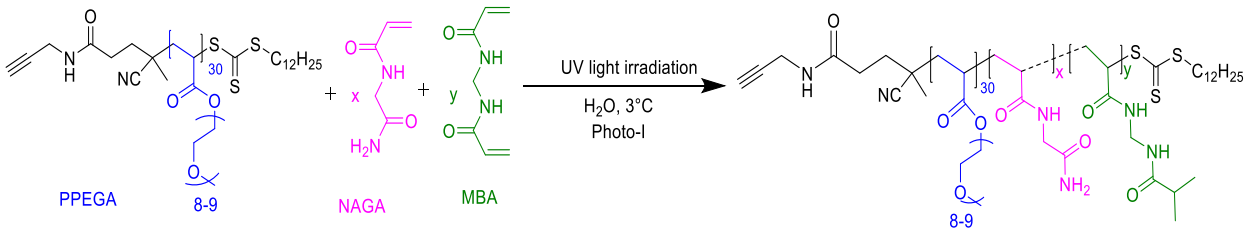


Scheme IV.1. Synthesis of H-bond UCST-type thermosensitive nanogels by UV-light initiated RAFT-PITSA in aqueous dispersion.

A UCST-type thermosensitive nanogel (UCST-1) was prepared using the Thermal-PPEGA$_{30}$ and an initial molar ratio [NAGA]$_0$/[Thermal-PPEGA$_{30}$]$_0$/[MBA]$_0$/[photo-I]$_0$ = 400/1/16/0.3 with a solid content of 2.4 wt.%. After 1 h of irradiation, complete monomers conversion was observed by $^1$H-NMR spectroscopy (Figure IV.1) and the opalescent reaction medium was stable (Figure IV.2).

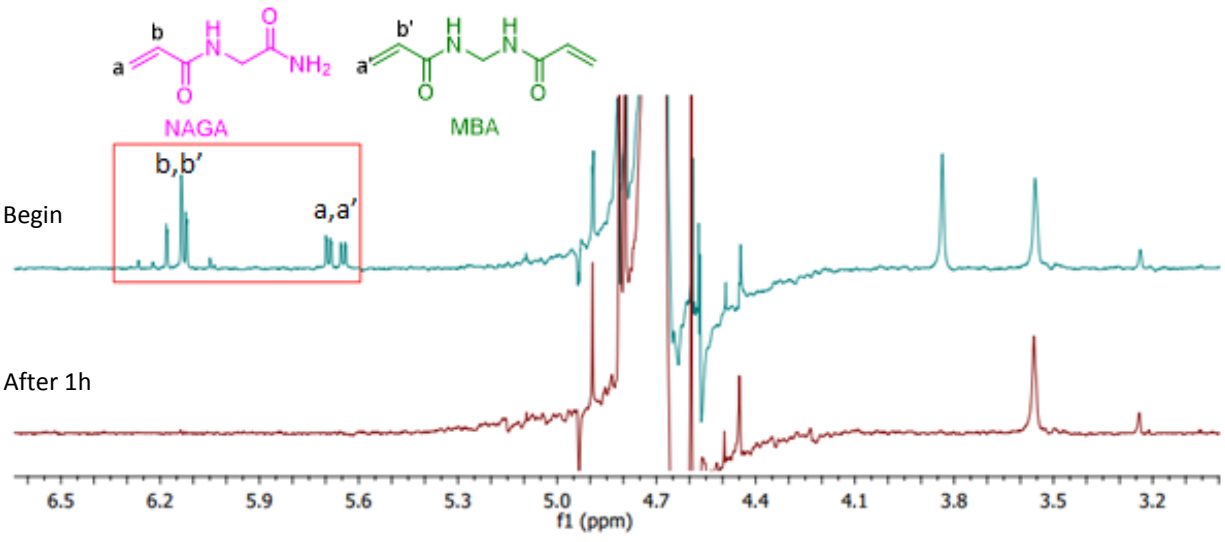


Figure IV.1. Overlaid $^1$H-NMR spectra recorded at room temperature (200 MHz, $D_2O$) of UCST-1 sample at the beginning and after 1h of UV-light initiated RAFT-PITSA of NAGA/MBA using Thermal-PPEGA$_{30}$ in water at 3°C. Initial molar ratio: [Thermal-PPEGA$_{30}$]$_0$/[NAGA]$_0$/[MBA]$_0$/[Photo-I]$_0$ =1/400/16/0.3 with a solid content of 2.4 wt.%.

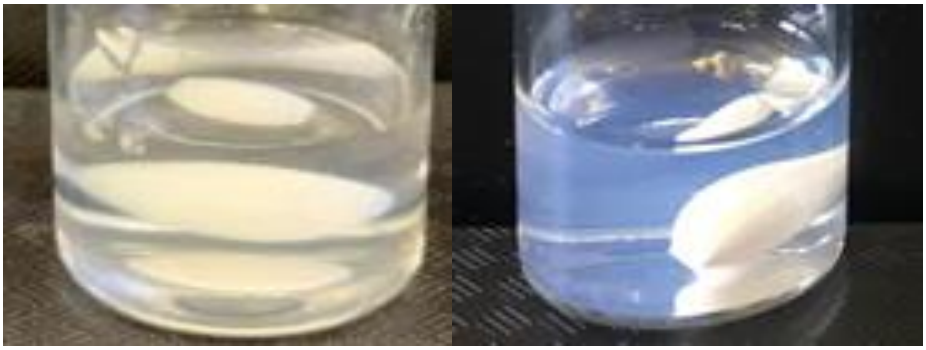

Figure IV.2. Picture of the reactional medium of UCST-1 before and after 1h of UV-light initiated RAFT PITSA of NAGA/MBA using Thermal-$PPEGA_{30}$ in water at 3°C. Initial molar ratio: [Thermal-$PPEGA_{30}]_0$/$[NAGA]_0$/$[MBA]_0$/$[Photo\text{-}I]_0$ =1/400/16/0.3 with a solid content of 2.4 wt.%.

The nanogel then was freeze-dried and characterized by $^1H$ NMR spectroscopy and DSC. The $^1H$ NMR spectrum of UCST-1 in $D_2O$ showed the characteristic peaks of PPEGA shell and P(NAGA-*co*-MBA) core (Figure IV.3). The signals of vinylic protons were not observed in the range of 5.56 to 6.48 ppm illustrating 100 % monomers (NAGA and MBA) consumptions. The global $\overline{DP_n}$ of P(NAGA-*co*-MBA) = 390.

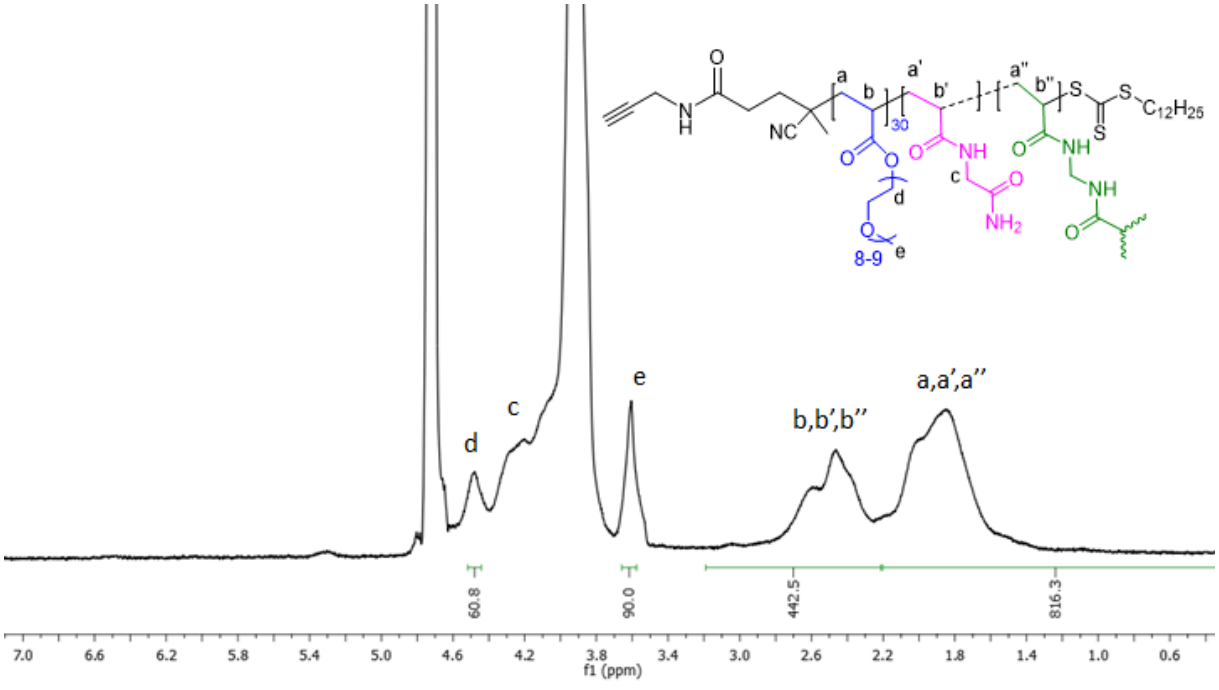


Figure IV.3. $^1H$-NMR spectrum (400 MHz, $D_2O$, 70°C) of UCST-1 nanogel synthesized by UV-light RAFT-PITSA of NAGA/MBA using Thermal-$PPEGA_{30}$ in water at 3°C. Initial molar ratio: [Thermal-$PPEGA_{30}]_0$/$[NAGA]_0$/$[MBA]_0$/$[Photo\text{-}I]_0$ =1/400/16/0.3, with a solid content of 2.4 wt.%.

DSC analysis further confirms the absence of unreacted NAGA and MBA monomers in the final nanogel, and the glass transition temperature of nanogel UCST-1 was found to be 160 °C (Figure IV.4), a value consistent with the literature[16] where a glass transition temperature between 125 to 186 °C was observed depending on the NAGA molar fraction in the copolymer.

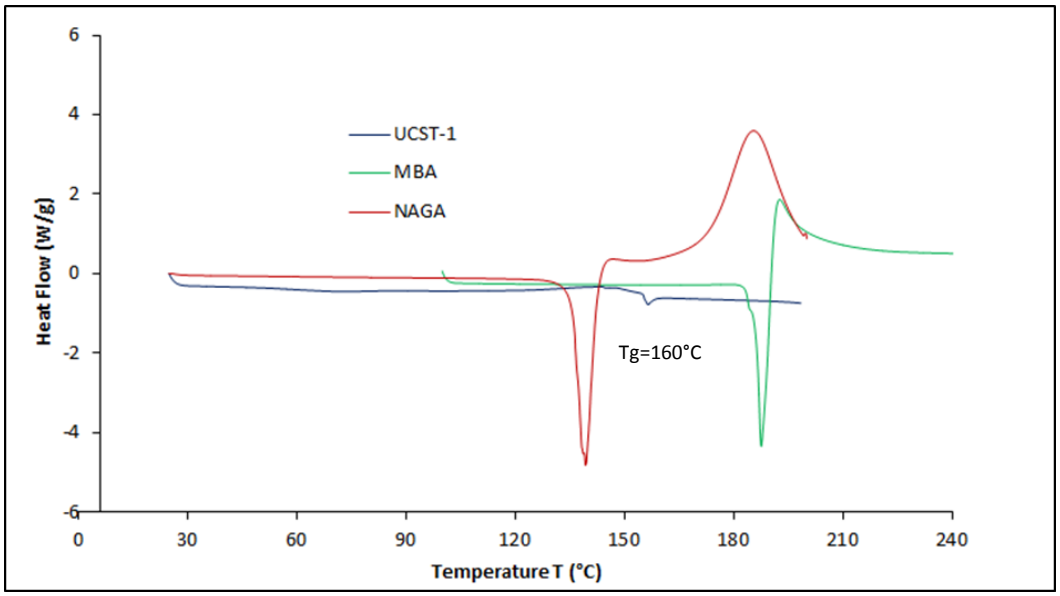


Figure IV.4. Overlaid DSC thermograms of NAGA, MBA and UCST-1 nanogel with heating ramp of 5 °C.min$^{-1}$.

The nanogel was then re-dispersed in ultrapure water for further DLS and TEM characterizations (Figure IV.5). DLS study of UCST-1 showed a single size distribution at 25 °C, a $D_h$ of 58 nm and a pdi of 0.18 were observed (Figure IV.5.a). The same solution was employed to characterize the morphology of the nanogel by TEM. Spherical nano-objects were observed by TEM (Figure IV.5.b) and the size was in the range of 45-50 nm, consistent with a nanogel shrunk in the dry state.

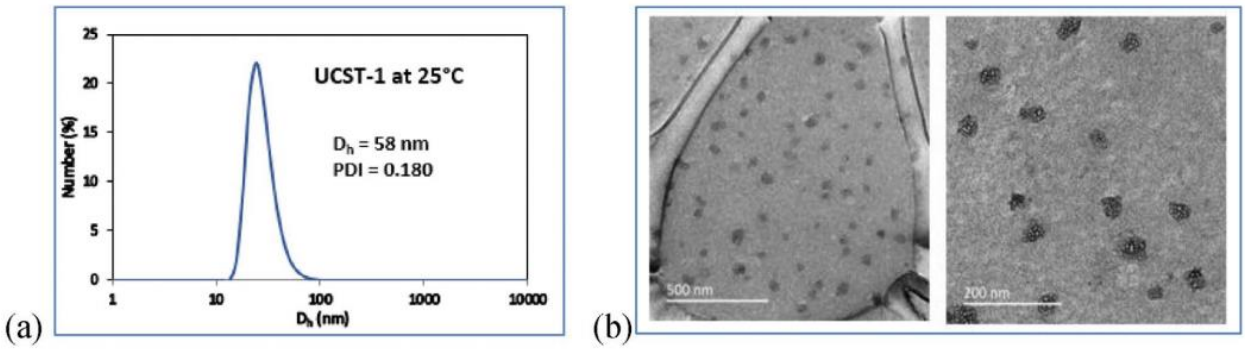


Figure IV.5. (a) Hydrodynamic diameter ($D_h$) distribution obtained from a DLS study at 25 °C. (b) TEM images of UCST-1 from a 5 g.L$^{-1}$ aqueous solution.

The UCST-thermosensitive behavior in aqueous solution of UCST-1 was further studied by DLS and UV-Vis spectrophotometry (Figure IV.6). An aqueous solution of UCST-1 (5 $g.L^{-1}$) was first equilibrated at 55 °C for 10 min, and the $D_h$ of nanogel was 65 nm with a pdi of 0.19. Then, the UCST-1 solution was cooled to 5 °C for 10 min, and the $D_h$ of nanogel and the pdi decreased to 52 nm and 0.15, respectively (Figure IV.6A). The $D_h$ and pdi decrease upon cooling is related to the collapse of the crosslinked core based on P(NAGA-*co*-MBA) that led to the opalescence of the solution at 5 °C (Figure IV.6B). This behavior was reversible and reproducible, the transparent-cloudy transitions were observed and the nanogels regained the same $D_h$ over successive shrink/swell cycles (Figure IV.6C) corresponding to a volume swelling ratio of 1.95. We also further investigated the UCST transition of a 10 $g.L^{-1}$ UCST-1 solution in water by UV–Vis spectrophotometry at a wavelength of 650 nm. In the cooling process, there was a gradual decrease of the transmittance in function of temperature, however, the transmittance of the sample increased gradually upon heating from 5 to 40 °C and then remained relatively constant until 70 °C (Figure IV.6D). The solution started becoming transparent from 40 °C, which was taken as the UCST transition temperature of UCST-1 nanogel solution upon heating.

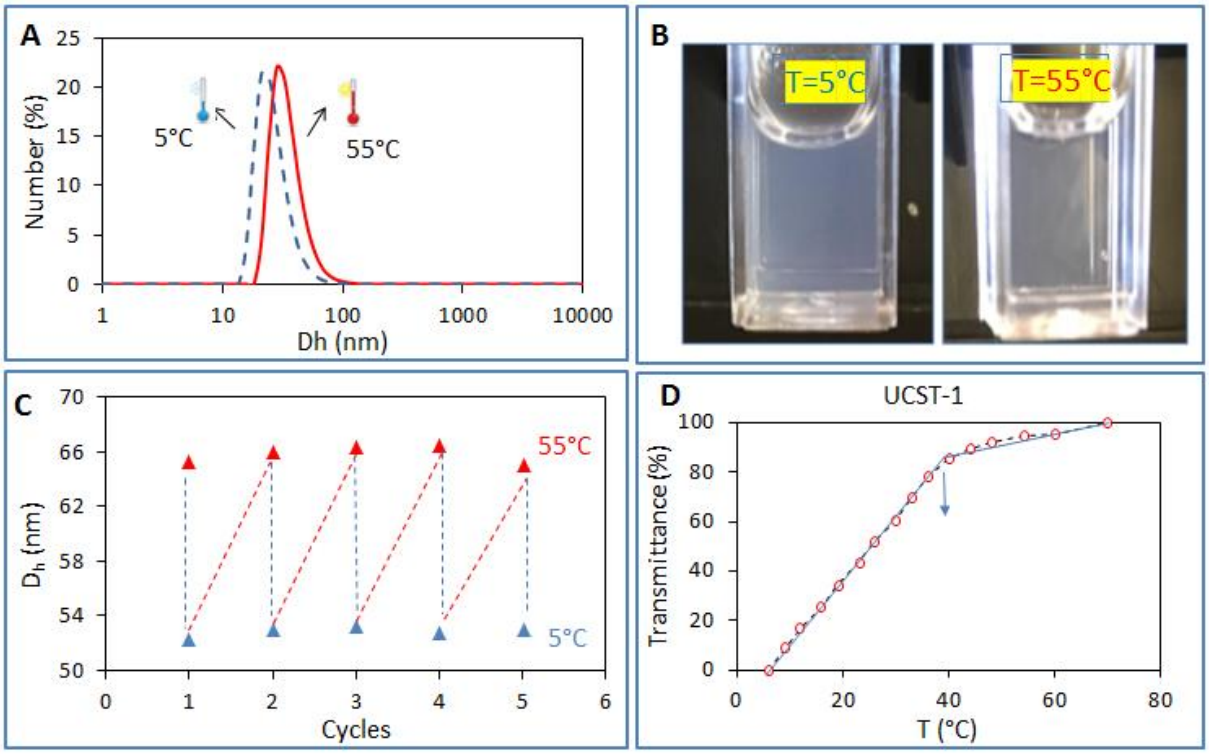


Figure IV.6. (A) DLS number-average diameter distributions. (B) Pictures of 5 $g.L^{-1}$ solution nanogel UCST-1 in water at 5 and at 55 °C. (C) $D_h$ values of UCST-1 solution at 55 and 5 °C from repeated heating and cooling cycles. (D) Determination of phase transition temperature for 10 $g.L^{-1}$ UCST-1 solution in water.

We also confirmed the PNAGA chain extension from Thermal-PPEGA$_{30}$ by performing a control experiment in the absence of MBA crosslinker. The polymerization of NAGA was conducted using Thermal-PPEGA$_{30}$ as macro-CTA and an initial molar ratio [NAGA]$_0$/[PPEGA$_{30}$]$_0$/[photo-I]$_0$ = 400/1/0.3 in aqueous dispersion at 3 °C with a solid content of 2.4 wt.%. The polymerization went to completion after 1 h. The SEC analysis of crude diblock copolymer showed that the peak of Thermal-PPEGA$_{30}$ shifted to high molar mass side and remained monomodal, testifying the successful chain extension of Thermal-PPEGA$_{30}$ to form a Thermal-PPEGA$_{30}$-*b*-UV-PNAGA diblock copolymer (Figure IV.7).

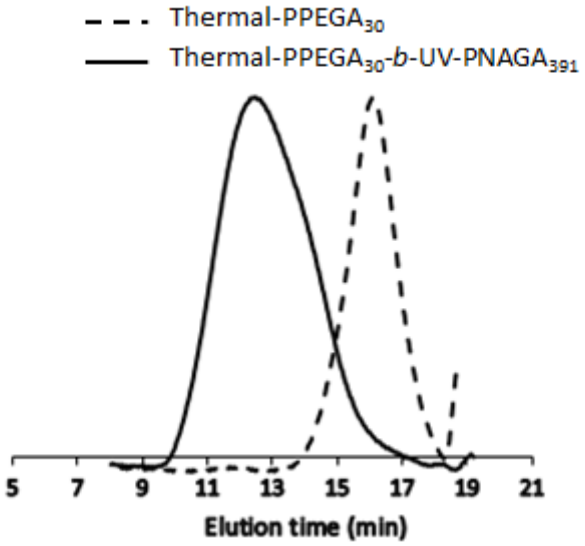


Figure IV.7. Overlaid SEC chromatograms (DMSO, LiBr) of Thermal-PPEGA$_{30}$ macro-CTA and Thermal-PPEGA$_{30}$-*b*-UV-PNAGA$_{391}$ diblock copolymer.

The $^1$H NMR spectrum (Figure IV.8) of the resulting Thermal-PPEGA$_{30}$-*b*-UV-PNAGA shows signals at 3.6 ppm ((CH$_2$CH$_2$O)$_8$C*H$_3$*, labeled e) and 4.45 ppm (C(=O)OC*H$_2$*CH$_2$O-(CH$_2$CH$_2$O)$_8$, labeled d) characteristic of the PPEGA block. The signal from 1.2 to 2.2 ppm corresponds to the CH and CH$_2$ protons of the copolymer backbone from both PPEGA and PNAGA blocks. These signals were used to determine the molar composition of the resulting copolymer: $\overline{DP_{n,PPEGA}}$ = 30 and $\overline{DP_{n,PNAGA}}$ = 391.

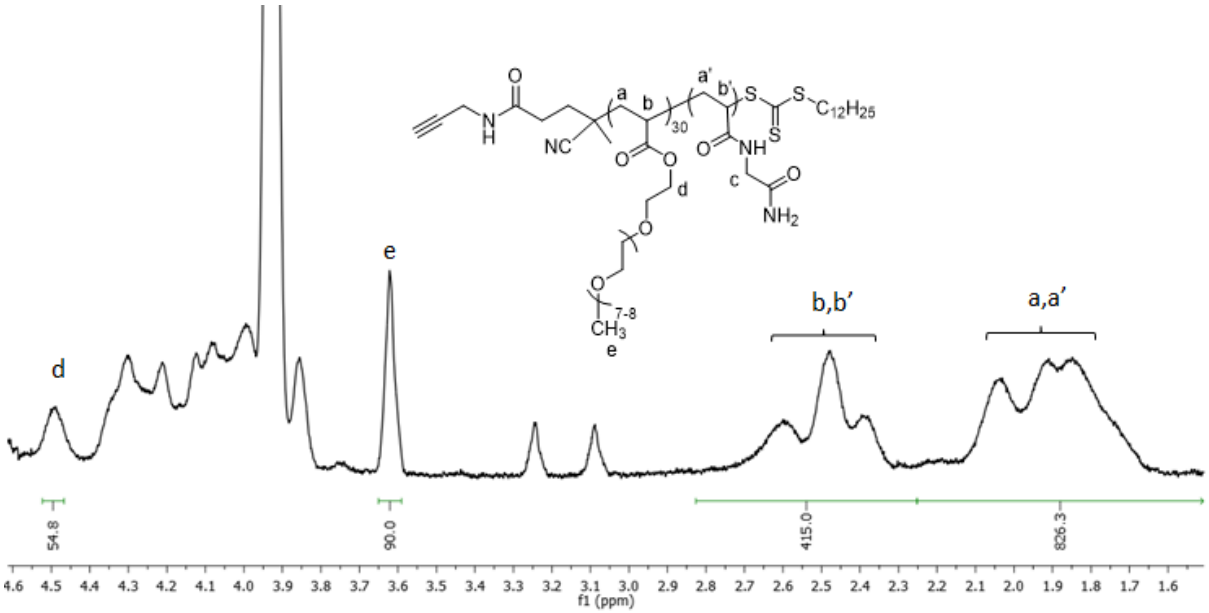


Figure IV.8. $^{1}$H-NMR spectrum (400 MHz, $D_2O$) of Thermal-PPEGA$_{30}$-*b*-PNAGA$_{391}$ synthesized by UV-light initiated RAFT-PITSA of NAGA mediated through Photo-I and Thermal-PPEGA$_{30}$ ([NAGA]$_0$/[Thermal-PPEGA$_{30}$]$_0$/[Photo-I]$_0$ = 400/1/0.3) in aqueous dispersion at 3°C.

Taken together, these results demonstrate for the first time that a H-bond UCST-type thermosensitive nanogel can be successfully synthesized at low temperature using the RAFT-PITSA process in aqueous dispersion under UV-light irradiation at low temperature.

## 4.2.2 Influence of synthesis parameters on nanogels size, polydispersity in size and UCST value

In order to deeper understand the influence of synthesis parameters on PPEGA-*b*-P(PNAGA-*co*-MBA)-based UCST-type thermosensitive nanogels physicochemical characteristics and properties, we systematically changed the molar ratio of NAGA-to-Thermal-PPEGA macro-CTA and the amount of the crosslinker MBA in the UV-light initiated RAFT-PITSA of NAGA. The $D_h$, pdi values, volume swelling ratios and UCST values of resultant nanogels were characterized by DLS and by UV-Vis spectrophotometry. The results are shown in Table IV.1.

Table IV.1. Experimental conditions, $D_h$, pdi, volume swelling ratio and UCST value of PPEGA-*b*-P(NAGA-*co*-MBA) nanogels in aqueous solution[a]

| Run | $\overline{DP_{n,\,PPEGA}}$ | [Thermal-PPEGA]$_0$/[NAGA]$_0$/[MBA]$_0$ | $D_h$ (nm)[b] T = 55°C | $D_h$ (nm)[b] T = 5°C | pdi[b] T = 55°C | pdi[b] T = 5°C | Volume swelling ratio[c] (f) | UCST[d] (°C) |
|---|---|---|---|---|---|---|---|---|
| UCST-1 | 30 | 1/400/16 | 65 +/-5 | 52 +/-3 | 0.192 | 0.153 | 1.95 | 40 |
| UCST-2 | 30 | 1/300/16 | 63 +/-4 | 51 +/-3 | 0.203 | 0.195 | 1.91 | 36 |
| UCST-3 | 30 | 1/200/16 | 58 +/-3 | 49 +/-2 | 0.174 | 0.168 | 1.62 | no UCST |
| UCST-4 | 30 | 1/100/16 | 46 +/-1 | 44 +/-1 | 0.380 | 0.339 | 1.12 | no UCST |
| UCST-5 | 30 | 1/400/8 | 83 +/-4 | 61 +/-3 | 0.223 | 0.191 | 2.47 | 43 |
| UCST-6 | 30 | 1/400/32 | 59 +/-2 | 51 +/-2 | 0.220 | 0.181 | 1.52 | no UCST |
| UCST-7 | 14 | 1/400/16 | 74 +/-3 | 53 +/-2 | 0.235 | 0.185 | 2.67 | 43-44 |
| UCST-8 | 20 | 1/400/16 | 68 +/-3 | 52 +/-2 | 0.235 | 0.181 | 2.30 | 43 |
| UCST-9 | 40 | 1/400/16 | 61 +/-2 | 49 +/-2 | 0.240 | 0.189 | 1.86 | no UCST |

[a] Polymerization conditions: 3°C, 1h, [Thermal-PPEGA]$_0$/[photo-I]$_0$ = 1/0.3, content solid = 2.4 wt.%, complete monomers conversion. [b] The hydrodynamic diameters ($D_h$) and polydispersities in size (pdi) of nanogels were obtained from DLS measurements conducted with 5 g.L$^{-1}$ nanogel aqueous solutions at 5°C and 55°C. [c] The volume swelling ratio f = ($D_h$,55°C / $D_h$,5°C)$^3$. [d] UCST transition temperature of 10 g.L$^{-1}$ nanogel aqueous solution upon heating by UV-Vis spectrophotometry.

#### 4.2.2.1 Impact of the $\overline{DP_{n,PPEGA}}$ of the Thermal-PPEGA *macro-CTA*

A series of nanogels were synthesized using the same initial molar ratio of PPEGA-to-MBA crosslinker (1/16) and the same NAGA-to-PPEGA initial molar ratio (400/1) while varying the $\overline{DP_{n,PPEGA}}$ (14, 20, 30, and 40) (UCST-1, UCST-7, UCST-8 and UCST-9, Table IV.1). At 55°C, $D_h$ of resulting nanogels decreased from 74 to 68, 65 and 61 nm corresponding to $\overline{DP_{n,PPEGA}}$ of PPEGA of 14, 20, 30, and 40, respectively (Figure IV.9(a)), and the volume swelling ratio dropped sharply from 2.67 to 2.3, 1.95 and 1.86 for UCST-7, UCST-8, UCST-1 and UCST-9 nanogels, respectively (Table IV.1). For longer macro-CTAs, the formed nanogels were higher sterically stabilized and aggregation occurred during polymerization yielding smaller particles. This phenomenon was previously observed in the case of LCST-type thermosensitive PNIPAm nanogels in chapter 3. The UCST transition upon heating of UCST-7 and UCST-8 solutions ($\overline{DP_{n,PPEGA}}$ equal to 14 and 20, respectively) were around 43°C. This value decreased to 40 °C for UCST-6 ($\overline{DP_{n,PPEGA}}$ = 30) with the same aqueous solution concentration 10 $g.L^{-1}$. When the $\overline{DP_{n,PPEGA}}$ reached 40 (UCST-9), the nanogel did not show UCST transition (Figures IV.9(b) and IV.9(c)). Such depression of the phase transition temperature can be ascribed to the increased hydrophilicity of the copolymer having higher $\overline{DP_{n,PPEGA}}$ slowing down the hydrogen bonds formation driving the phase transition. Similar observation was previously made during Mäkinen's study for diblock copolymer PEO-*b*-PNAGA which showed a lower UCST value (15.8 °C) compare to the PNAGA (22 °C) with the same $\overline{DP_n}$ of 220.

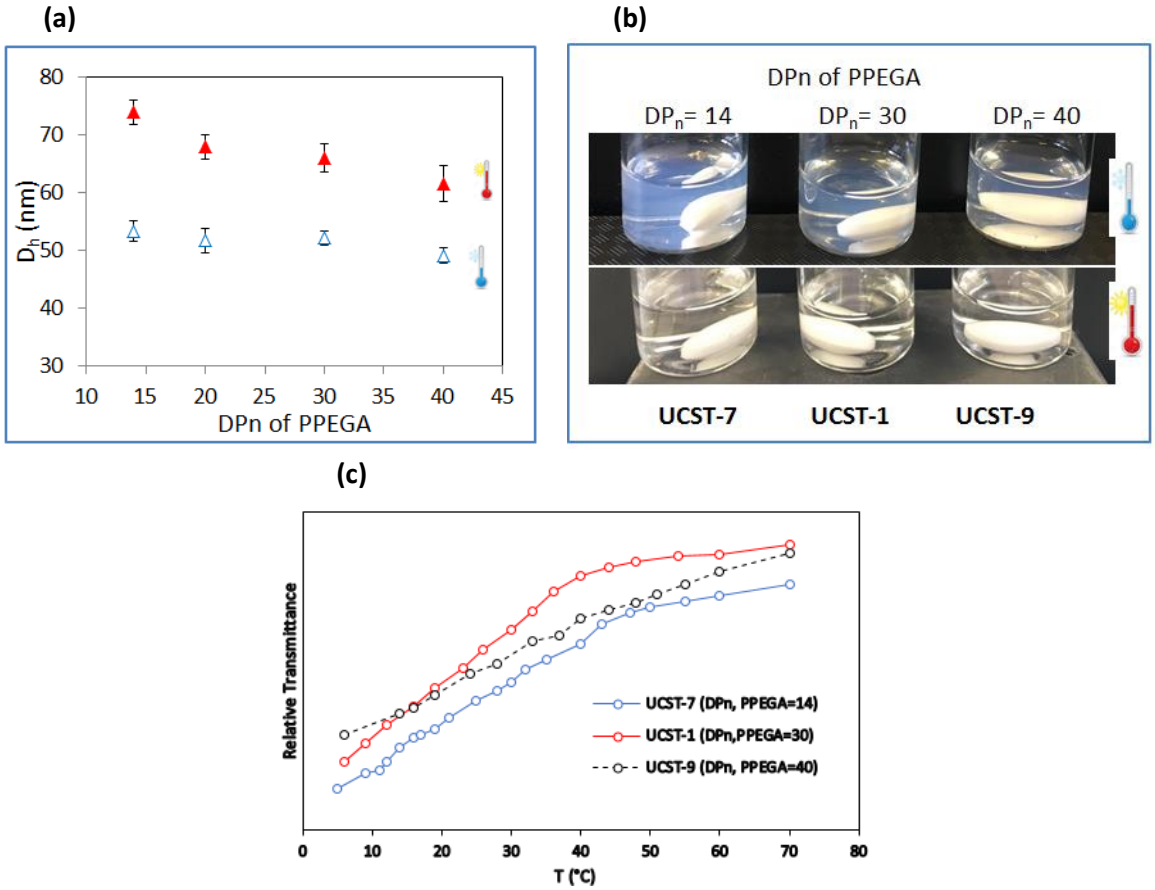


Figure IV.9. (a) Evolution of $D_h$ of UCST-7, -8, -1 and -9 nanogels with the increase of $\overline{DP_{n,PPEGA}}$ from 14 to 20, 30 and 40, respectively at 5°C and 55°C; (b) pictures of UCST-7, -1 and -9 nanogel solutions after stopping the polymerization; (c) turbidity curves of 10 $g.L^{-1}$ UCST-7, -1 and -9 solutions in water, obtained from UV-Vis spectrophotometry.

### 4.2.2.2 Impact of NAGA monomer-to-Thermal-PPEGA macro-CTA molar ratio

A series of four nanogels using the same molar ratio of Thermal-PPEGA macro-CTA-to-MBA crosslinker (1/16) with different monomer-to-macro-CTA molar ratios (UCST-1, UCST-2, UCST-3, and UCST-4) were synthesized. Increasing NAGA from 100 (UCST-4) to 200 (UCST-3), 300 (UCST-2), and 400 equiv. (UCST-1) while keeping the $\overline{DP_{n,PPEGA}}$ equal to 30, increased the $D_h$ of nanogels from 46 to 58, 63, and 65 nm, respectively at 55 °C (UCST-1, UCST-2, UCST-3 and UCST-4, Table IV.1). A similar trend was observed for the $D_h$ of nanogels at 5 °C (UCST-1, UCST-2, UCST-3 and UCST-4, Table IV.1; Figure IV.10.a). The phase transition temperature was not observed neither by visualization (Figure IV.10.b) nor by turbidity measurements (Figure IV.10.c) for samples UCST-3 and UCST-4. This is likely due to the lower targeted $\overline{DP_{n,PNAGA}}$ responsible for the UCST property. Lutz's team[17] made a similar observation: PNAGA homopolymer with short polymer chains ($\overline{DP_{n,PNAGA}}$ = 100-200) did not form gels at a concentration of less than 10 wt.%. The absence of UCST property can also be associated to a higher degree of crosslinking in those samples resulting in a lower swelling capability as shown by

the low volume swelling ratios (UCST-3 and UCST-4, Table IV.1). The UCST transitions of nanogels UCST-1 and UCST-2 upon heating were 40 and 36 °C, respectively (Figure IV.10.c). The decrease of PNAGA length in the nanogel leads to lower transition temperature, as previously reported.[18] Furthermore, the volume swelling ratios of these nanogels increased from 1.12 to 1.62, 1.91, and 1.95, with increasing NAGA equivalents from 100, 200, 300, and 400 in respect to Thermal-PPEGA$_{30}$ macro-CTA and keeping constant the macro-CTA-to-MBA crosslinker initial ratio (UCST-4, UCST-3, UCST-2 and UCST-1, Table IV.1). This is consistent with a lower degree of crosslinking for higher amounts of NAGA monomer.

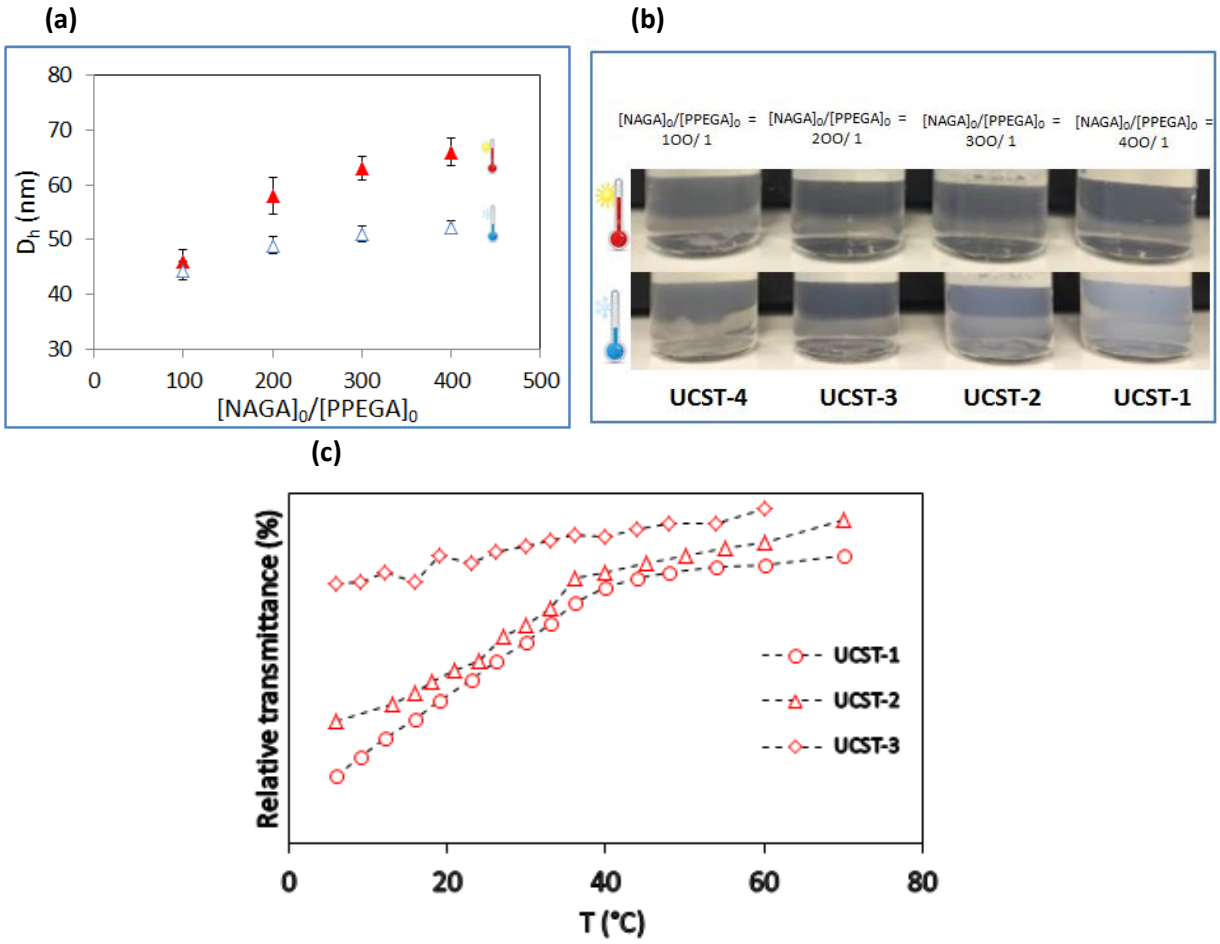


Figure IV.10. (a) Evolution of $D_h$ of UCST-1, UCST-2, UCST-3 and UCST-4 with the increase of initial molar ratio $[NAGA]_0/[Thermal\text{-}PPEGA_{30}]_0$ at 5°C and 55°C; (b) pictures of UCST-1, UCST-2, UCST-3 and UCST-4 aqueous solution with a concentration of 10 g.L$^{-1}$ at 5°C and 55°C; (c) turbidity curves of 10 g.L$^{-1}$ UCST-1, UCST-2 and UCST-3 aqueous solutions, obtained from UV-Vis spectrophotometry.

#### 4.2.2.3 Impact of MBA crosslinker-to- Thermal -PPEGA macro-CTA molar ratio

Nanogels UCST-1, UCST-5, and UCST-6 have been prepared using the same synthesis conditions with various amounts of MBA crosslinker. Decreasing the molar ratio of MBA-to-Thermal-PPEGA$_{30}$ macro-CTA from 32/1 to 16/1 and to 8/1 increases $D_h$ at 55 °C from 59 to 65 and 83 nm, respectively

(UCST-6, UCST-1 and UCST-5, Figure IV.11.a). The volume-swelling ratio increased from 1.52 to 1.95 and to 2.47 with the decrease of crosslinker amount. The higher swelling capacity, consistent with a lower crosslinking degree due to a reduced amount of MBA is probably due to a less dense network core. Moreover, the increase of $D_h$ is explained by the increase of volume swelling ratio leading to a higher mobility of the P(NAGA-*co*-MBA) chains susceptible to form hydrogen bonding with water. In addition, two aqueous solutions of UCST-1 and UCST-5 nanogels (10 $g.L^{-1}$) showed turbidity upon heating (Figure IV.10.b) with phase transition temperature of 40 and 43 °C, respectively (UCST-1 and UCST-5 in Table IV.1 and Figure IV.11.c). A lower amount of MBA crosslinker leads to a higher UCST value due to the fact that hydrogen bondings are more susceptible to occur within P(NAGA-*co*-MBA) core. Moreover, when the initial molar ratio of MBA crosslinker to Thermal-$PPEGA_{30}$ macro-CTA increased to 32/1 in UCST-6 nanogel, UCST behavior was not observed for 10 $g.L^{-1}$ aqueous solution. This result can be attributed to a compact core limiting the hydrogen bonding responsible for the UCST phenomenon.

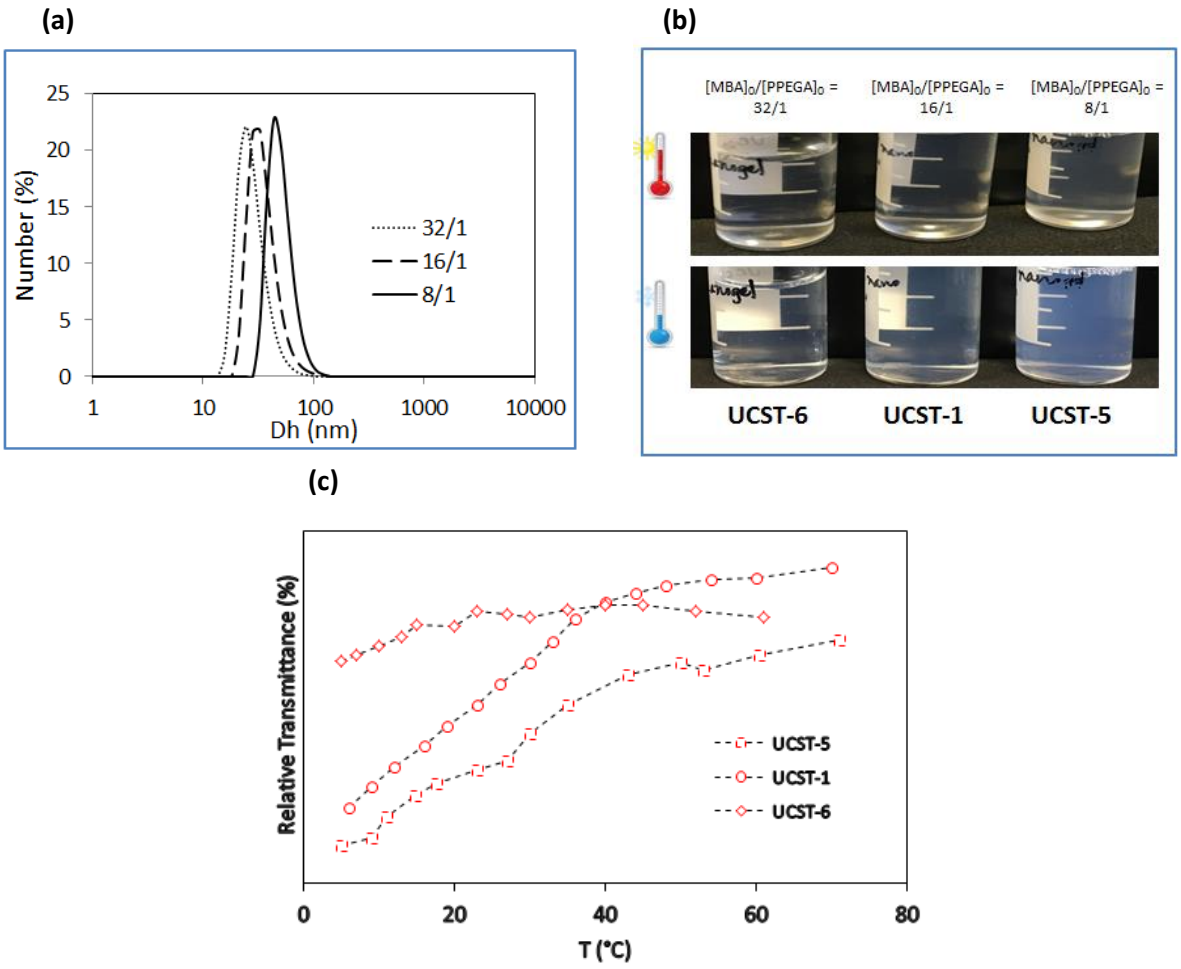


Figure IV.11. (a) Evolution of $D_h$ of UCST-5, UCST-1 and UCST-6 nanogels with the increase of initial molar ratio $[MBA]_0/[thermal\text{-}PPEGA_{30}]_0$ from 8/1 to 16/1 and 32/1 at 55°C; (b) pictures of UCST-5, UCST-1 and UCST-6

nanogels solutions with concentration of 5 g.L$^{-1}$ at 5°C and 55°C; (c) turbidity curves of 10 g.L$^{-1}$ UCST-5, UCST-1 and UCST-6 solutions in water, obtained from UV-Vis spectrophotometry.

## 4.3 UCST-type thermosensitive and pH-degradable nanogels by UV-light initiated RAFT-PITSA

In this study, the UCST-thermo-sensitivity and the pH-degradability will be brought by the PNAGA and the KB crosslinker described in chapter III to target dual UCST-type thermosensitive and pH-degradable nanogels. The synthesis of such dual-responsive nanogels will be conducted by RAFT-PITSA in aqueous dispersion at a pH 9 to avoid premature hydrolysis of the ketal group of KB crosslinker. The physicochemical characteristics, thermosensitive properties and degradability of resulting nanogels will be studied by $^{1}$H NMR spectroscopy, DLS, UV-Vis spectrophotometry and TEM.

### 4.3.1 PEGA-b-P(NAGA-co-KB)-based UCST-type thermosensitive and pH-degradable nanogels: synthesis, macromolecular characterizations and thermosensitive properties

In order to reach pH-degradable and UCST-type thermosensitive nanogels by self-assembly of PPEGA-*b*-P(NAGA-*co*-KB) copolymers, RAFT-PITSA of NAGA were conducted in aqueous solutions pH 9 at low temperature (3°C) using a UV-PPEGA of $\overline{DP_{n,PPEGA}}$ equal to 30 as macro-CTA and surfactant, KB as crosslinker and photo-I as photo-initiator under UV-light irradiation (λ = 365 nm, 34 mW/cm$^2$) (Scheme IV.2).

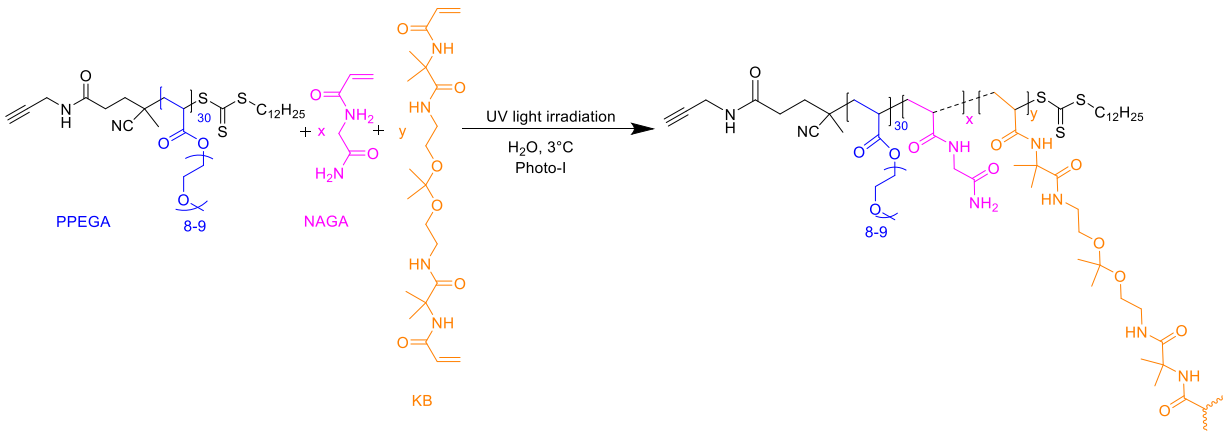


Scheme IV.2. Synthesis of pH-degradable and UCST-type thermosensitive nanogels by UV-light initiated RAFT-PITSA in aqueous dispersion at pH 9 and at 3°C in presence of UV-PPEGA$_{30}$ and photo-I.

The initial molar ratio of $[NAGA]_0/[UV\text{-}PPEGA_{30}]_0/[KB]_0/[Photo\text{-}I]_0$ = 400/1/16/0.3 was employed with a solid content of 2.4 wt.%. The NAGA and KB conversions were determined by $^1H$ NMR spectroscopy of the crude mixture after 1h of polymerization (Figure IV.12). The disappearance of vinyl protons between 5.68 ppm and 6.45 ppm is consistent with a full NAGA and KB conversions.

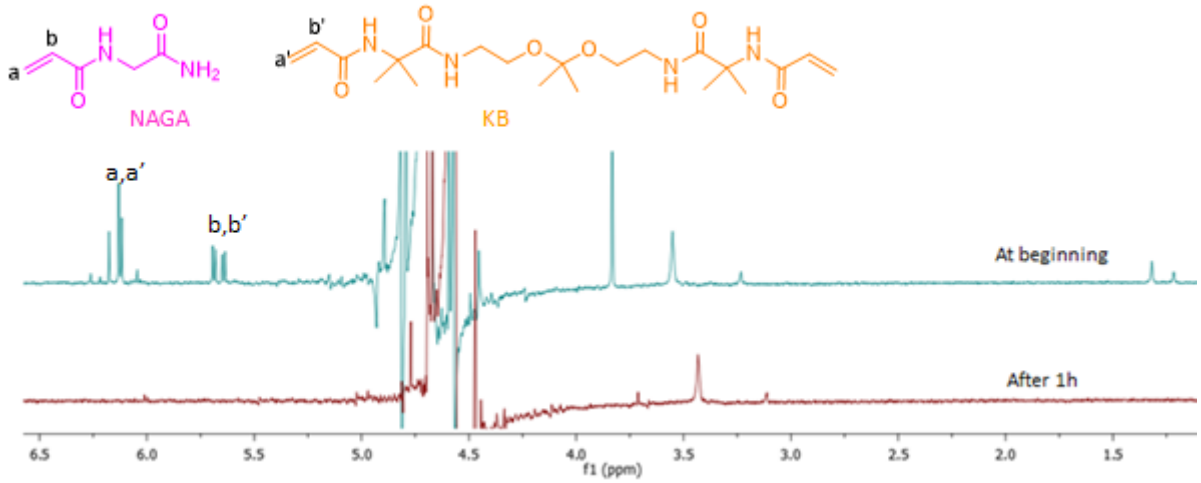


Figure IV.12. Overlaid $^1H$-NMR spectra recorded at room temperature (200 MHz, $D_2O$) of polymerization solution samples at t = 0 and after 1h obtained through UV-light initiated RAFT-PITSA of NAGA/KB using UV-$PPEGA_{30}$ as macro-CTA in buffer solution pH 9 at 3°C. Initial molar ratio: $[UV\text{-}PPEGA_{30}]_0/[NAGA]_0/[KB]_0/[Photo\text{-}I]_0$ =1/400/16/0.3 with a solid content of 2.4 wt.%.

The polymerization medium after 1h was also opalescent (Figure IV.13) due to the aggregation of resulting PNAGA at temperature lower that its UCST value.

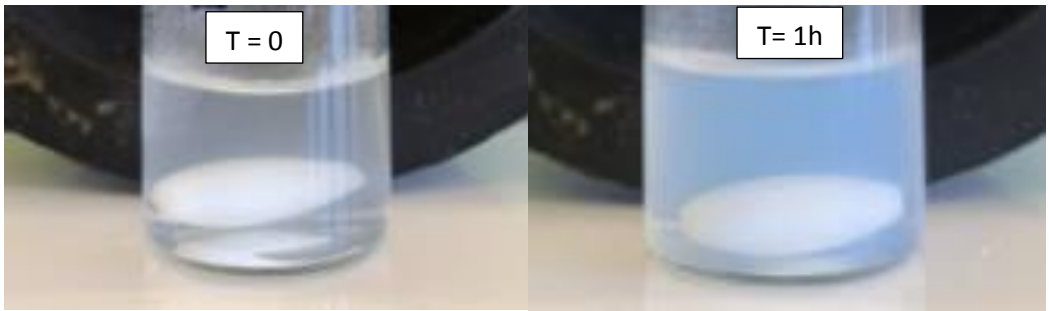


Figure IV.13. Picture of the reactional medium before and after 1h of UV-light initiated RAFT-PITSA of NAGA/KB using UV-$PPEGA_{30}$ in buffer solution pH 9 at 3°C. Initial molar ratio: $[UV\text{-}PPEGA_{30}]_0/[NAGA]_0/[KB]_0/[Photo\text{-}I]_0$ =1/400/16/0.3 with a solid content of 2.4 wt.%.

As complete NAGA and KB conversions were observed, the nanogel was directly freeze-dried for further characterizations. The $^1H$ NMR spectrum of sample in $D_2O$ (Figure IV.14). showed the

characteristic peaks of PPEGA shell at 3.8 ppm $(CH_2CH_2O)_8CH_3$, labeled e) the signal from 2.4 to 3.1 ppm corresponds to the C*H* protons of the PPEGA, PNAGA, PKB backbone (labeled a, a',a''). The comparison of the integrations of these signals e, a, a', a'' were employed to determine the molar composition of the resulting copolymer: $\overline{DP_{n,\,PPEGA}}$ = 30, $\overline{DP_{n,\,PNAGA}}$ + $\overline{DP_{n,\,PKB}}$ = 413.

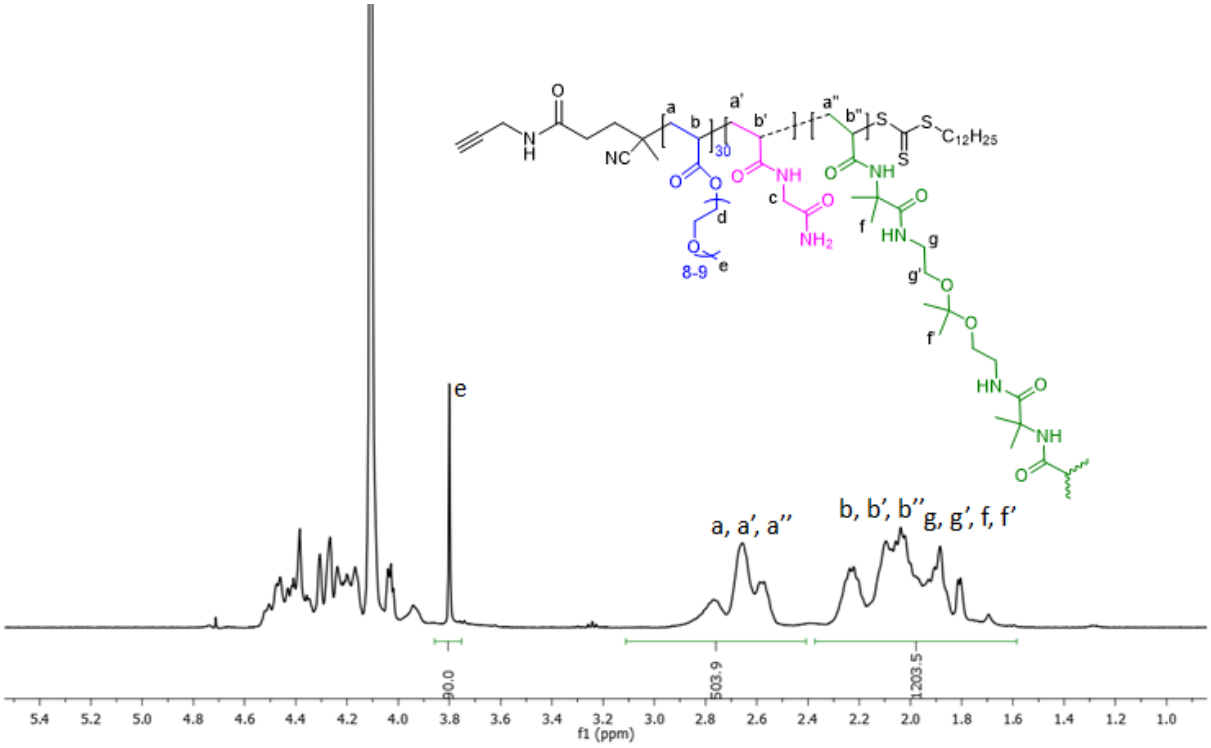


Figure IV.14. $^1$H-NMR spectrum (400 MHz, $D_2O$, 70°C) of nanogel synthesized by UV-light initiated RAFT-PITSA of NAGA/KB using UV-$PPEGA_{30}$ in buffer solution pH 9 at 3°C. Initial molar ratio: [UV-$PPEGA_{30}]_0$/$[NAGA]_0$/$[KB]_0$/$[Photo\text{-}I]_0$ =1/400/16/0.3, with a solid content of 2.4 wt.%.

The UV-$PPEGA_{30}$-*b*-P(NAGA-*co*-$KB)_{413}$-based nanogel was then re-dispersed in buffer solution pH 9 for further DLS, TEM and UV-Vis characterizations. DLS study of nanogel at a concentration of 5 $g.L^{-1}$ showed a single size distribution at 25 °C. Moreover, a $D_h$ of 64 nm and a pdi of 0.21 were observed.The same solution was employed to characterize the morphology of the nanogel by TEM (Figure IV.15). Spherical nano-objects were observed and the size was in the range of 40-45 nm, consistent with a nanogel shrunk in the dry state.

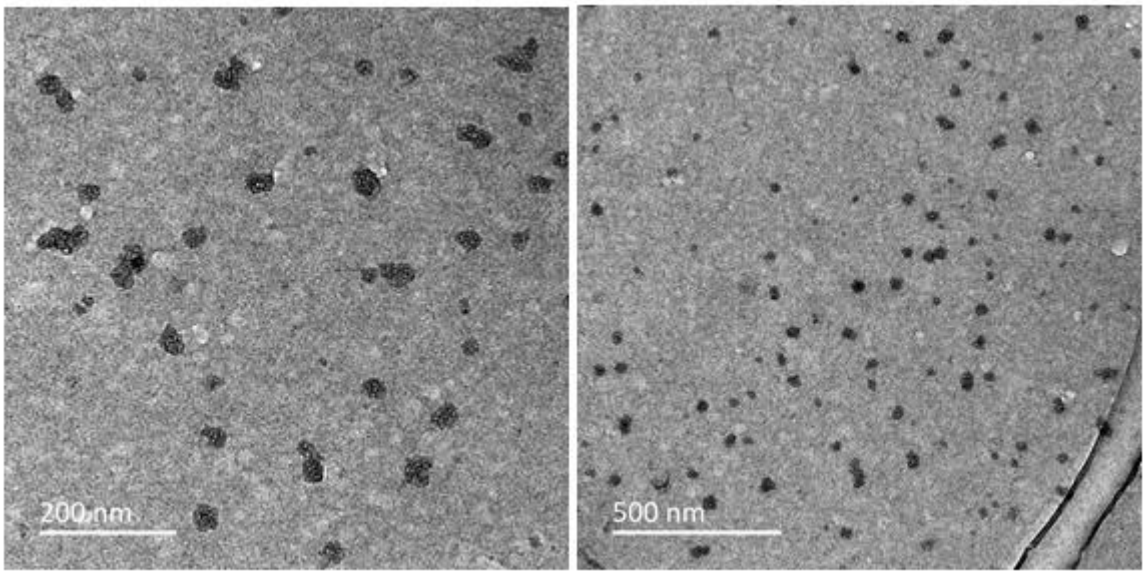


Figure IV.15. TEM images of UV-PPEGA$_{30}$-*b*-P(NAGA-*co*-KB)$_{413}$-based nanogel from a 5 g.L$^{-1}$ aqueous solution.

The UCST-thermosensitive behavior in pH 9 aqueous solution of nanogel was further studied by DLS and UV-Vis spectrophotometry. An aqueous solution of nanogel (5 g.L$^{-1}$) was first equilibrated at 55 °C for 10 min, and the $D_h$ of nanogel was 72 nm with a pdi of 0.26. Then, the solution was cooled to 5 °C for 10 min, and the $D_h$ of nanogel and the pdi decreased to 58 nm and 0.19, respectively (Figure IV.16A). These $D_h$ of nanogel crosslinked with KB are slightly higher than that of the nanogel using MBA crosslinker (65 nm, run1 Table IV.1), however, the pdi for KB-nanogel are lower (0.15) The decrease of $D_h$ and pdi upon cooling observed with KB-based nanogels is related to the collapse of the crosslinked core based on P(NAGA-*co*-KB) that led to the opalescence of the solution at 5 °C (Figure IV.16B). This behavior was reversible and reproducible until two successive shrink/swell cycles: the transparent-cloudy transitions were observed and the nanogels regained the same $D_h$ over (Figure IV.16C) corresponding to a volume swelling ratio of 1.91, similar to that of MBA-nanogel (f= 1,95, run 1, Table IV.1). Further heating from 5 to 55 °C in the third cycle results in the sharp drop of the $D_h$ to 20 nm. This result could be explained by the degradation of the nanogel to become polymer unimers due to the hydrolysis of the ketal group within the crosslinked core during successive shrink/swell cycles which led to increase the nanogel solution at 55°C twice. As discussed in chapter III, the ketal group hydrolysis is favored at high temperature even at pH 9 (Table III.3). After nanogel degradation, the cooling from 55 to 5 °C leads to the aggregation of unimers with aggregates formation with a $D_h$ of 66 nm and pdi of 0.22 (Figure IV.16.C).

We also further investigated the UCST transition of a 10 g.L$^{-1}$ nanogel solution in water by UV-Vis spectrophotometry at a wavelength of 650 nm. The transmittance of the sample increased gradually upon heating from 5 to 41 °C and then remained relatively constant (Figure IV.16.D). The solution

started becoming transparent from 41 °C, which was taken as the UCST transition temperature of polymer nanogel solution upon heating. The UCST values of nanogel based on UV-PPEGA$_{30}$-*b*-P(NAGA-*co*-KB)$_{413}$ is slightly higher with sharper phase separation transition comparing to UCST of nanogel based on Thermal-PPEGA$_{30}$-*b*-P(NAGA-*co*-MBA)$_{390}$ (40 °C, run 1 Table IV.1, Figure IV.6).

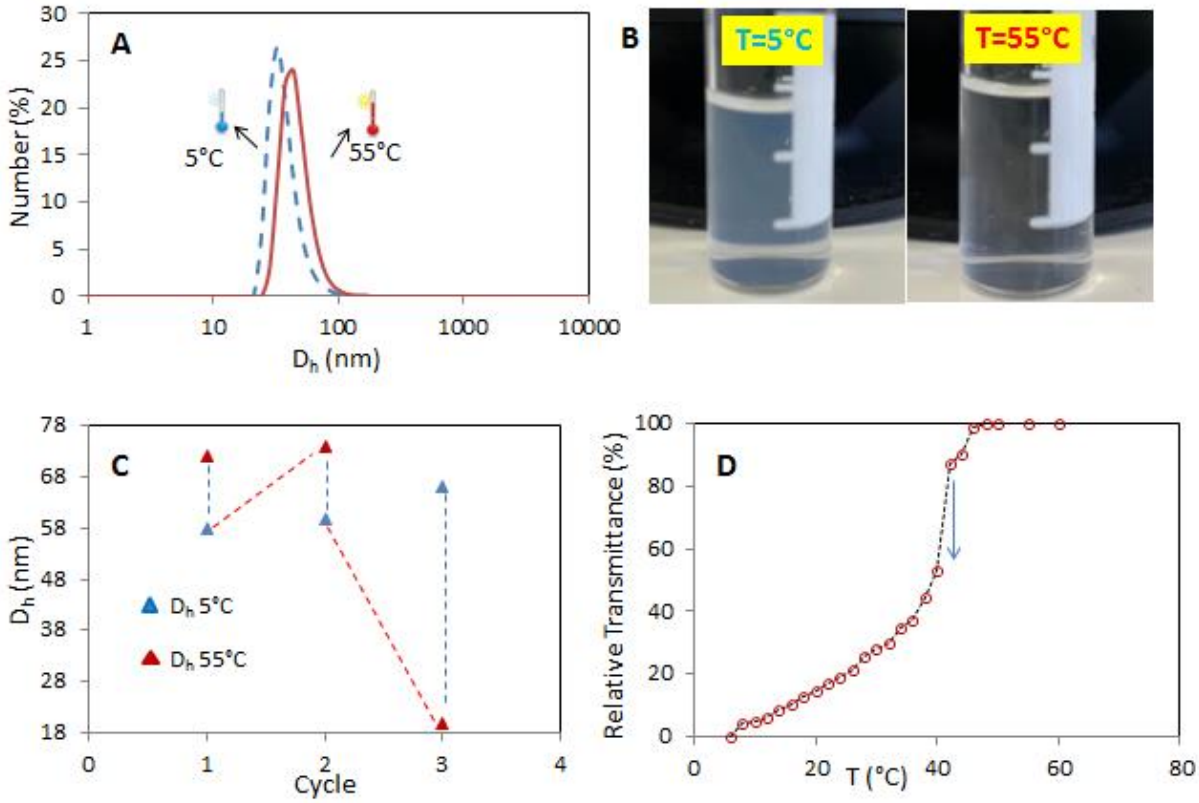


Figure IV.16. (A) Number-average diameter distributions of UV-PPEGA$_{30}$-*b*-P(NAGA-*co*-KB)$_{413}$ nanogel solutions (5 g.L$^{-1}$ in buffer solution at pH 9) at 5°C and at 55°C. (B) Pictures of 5 g.L$^{-1}$ solution of UV-PPEGA$_{30}$-*b*-P(NAGA-*co*-KB)$_{413}$ nanogel in buffer solution pH 9 at 5 and at 55 °C. (C) $D_h$ values of nanogel solution at 5 and 55 °C from repeated heating/cooling cycles. (D) Determination of phase transition temperature for 10 g.L$^{-1}$ nanogel solution in buffer solution pH 9. Initial molar ratio: [UV-PPEGA$_{30}$]$_0$/[NAGA]$_0$/[KB]$_0$/[Photo-I]$_0$ =1/400/16/0.3, with a solid content of 2.4 wt.%.

We also made an effort to target more stable PPEGA-*b*-P(PNAGA-*co*-KB)-based nanogels by changing the amount of solid content and the initial KB crosslinker to PPEGA macro-CTA molar ratio. Unfortunately, we were unsuccessful with either increasing the solid content to 5 wt.% or either increasing KB to PPEGA macro-CTA initial molar ratio to 32/1 as the gel formation was observed in both cases (Figures IV.17A and B, respectively). Increasing the solid content or amount of crosslinker decreases the distance between propagating chains, which enhances the probability of intermolecular crosslinking, consequently macroscopic gelation will be obtained.[19]

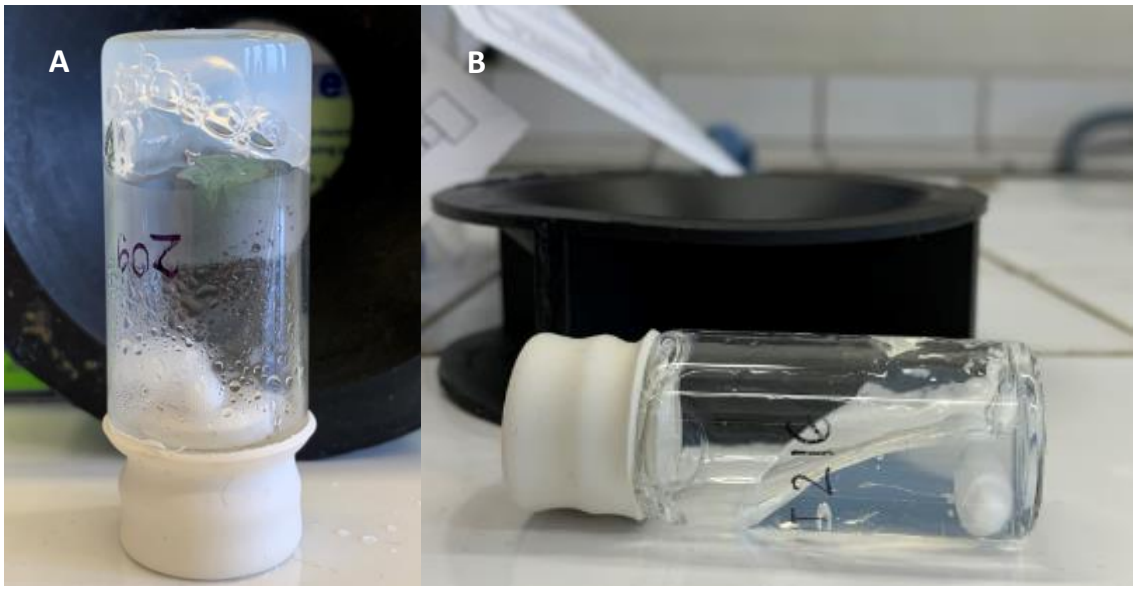


Figure IV.17. Pictures of the reactional media of after 1h of UV-light initiated RAFT-PITSA of NAGA/KB using UV-PPEGA$_{30}$ in buffer solution pH 9 at 3°C using (A) an [UV-PPEGA$_{30}$]$_0$/[NAGA]$_0$/[KB]$_0$/[Photo-I]$_0$ initial molar ratio of 1/400/16/0.3 and a solid content of 5 wt.% and (B) an [UV-PPEGA$_{30}$]$_0$/[NAGA]$_0$/[KB]$_0$/[Photo-I]$_0$ initial ratio of 1/400/32/0.3 and a solid content of 2.4 wt.%.

Even if we previously confirmed the successful extension of UV-PPEGA$_{30}$ with PNAGA by performing a control experiment with an initial molar ratio [NAGA]$_0$/[UV-PPEGA$_{30}$]$_0$/[photo-I]$_0$ = 400/1/0.3 in aqueous dispersion at 3 °C with a solid content of 2.4 wt.%. (in §II.1 of this chapter), we need to study this reaction in aqueous dispersion at pH 9 at 3 °C. Therefore, a polymerization of NAGA was conducted using UV-PPEGA$_{30}$ as macro-CTA and an initial molar ratio [NAGA]$_0$/[UV-PPEGA$_{30}$]$_0$/[photo-I]$_0$ = 400/1/0.3 in aqueous dispersion pH 9 at 3 °C with a solid content of 2.4 wt.%. As show in Figure IV.18.A, a very fast initial rate of polymerization was observed which reached approximatively 93 % NAGA conversion after 30 min. The conversion of NAGA increases with the increase of polymerization time and a constant slope of ln([M]$_0$/[M]$_t$) *vs.* reaction time, relevant with a constant concentration of propagating radicals is observed. Figure IV.18B illustrates the evolution of $\overline{M_{n,SEC}}$ and *Đ versus* NAGA conversion and Figure IV.19 shows the overlaid SEC traces of resulting copolymers at different NAGA conversions. The dispersity is quite high, however, the RAFT polymerization of NAGA seems under a good control as *Đ* remains stable around 2.2-to-2.4. The discrepancy between $\overline{M_{n,SEC}}$ and $\overline{M_{n,theo}}$ can be attributed to the difference between the hydrodynamic volume of PMMA, used for SEC calibration, and the hydrodynamic volume of the copolymer in DMSO. This conclusion is in agreement with the absence of high molar mass shoulder in the SEC traces, even at full conversion of NAGA (Figure IV.19).

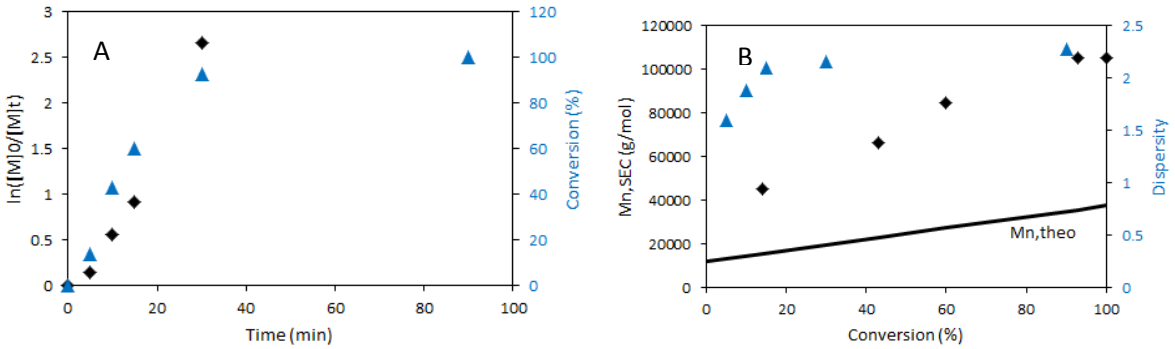


Figure IV.18. Plots of (A) evolution of $\ln([M]_0/[M]_t)$ and conversion *vs.* time and (B) evolution of $\overline{M_{n,SEC}}$ (symbol) and $\overline{M_{n,theo}}$ (line) and *Đ vs.* NAGA conversion during the UV-light initiated RAFT-PITSA of NAGA using photo-I and UV-PPEGA$_{30}$ in aqueous dispersion at pH 9, at 5 °C using the initial $[NAGA]_0/[UV\text{-}PPEGA_{30}]_0/[photo\text{-}I]_0$ molar ratio of 400/1/0.3 with a solid content of 2.4 wt.%.

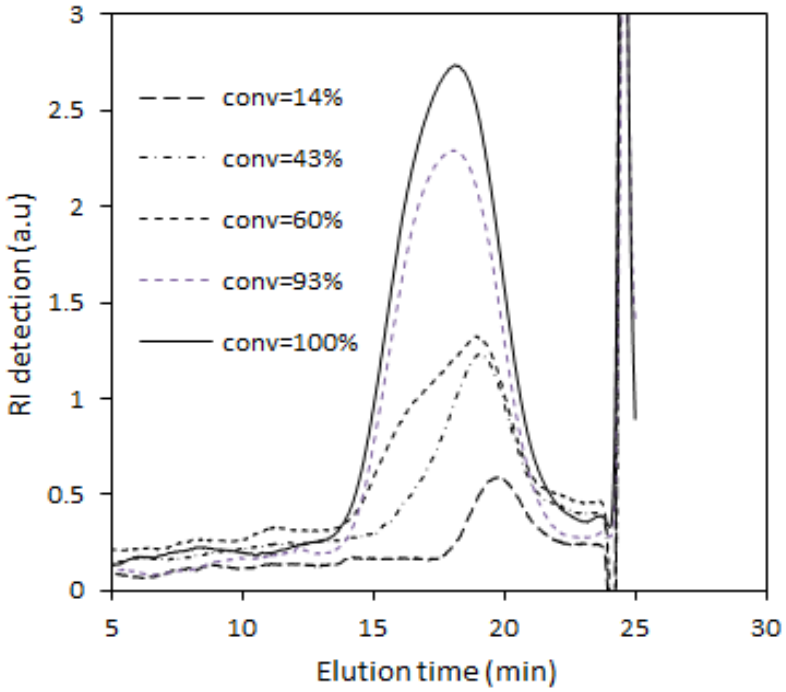


Figure IV.19. Overlaid SEC (DMSO, LiBr) traces of UV-PPEGA$_{30}$-*b*-PNAGA using RI detection obtained during the UV-light initiated RAFT-PITSA of NAGA using photo-I and UV-PPEGA$_{30}$ in aqueous dispersion at pH 9, at 5 °C using the initial $[NAGA]_0/[UV\text{-}PPEGA_{30}]_0/[photo\text{-}I]_0$ molar ratio of 400/1/0.3 with a solid content of 2.4 wt.%.

The $^1$H NMR spectrum (Figure IV.20) of the resulting UV-PPEGA$_{30}$-*b*-UV-PNAGA shows a signal at 3.6 ppm ($(CH_2CH_2O)_8CH_3$, labeled e) characteristic of the PPEGA block and broad signals from 1.6 to 2.9 ppm corresponding to methylene and methine protons of PPEGA and PNAGA polymers backbones. These signals were used to determine the molar composition of the resulting copolymer: $\overline{DP_{n,PPEGA}}$ = 30 and $\overline{DP_{n,\ PNAGA}}$ = 397.

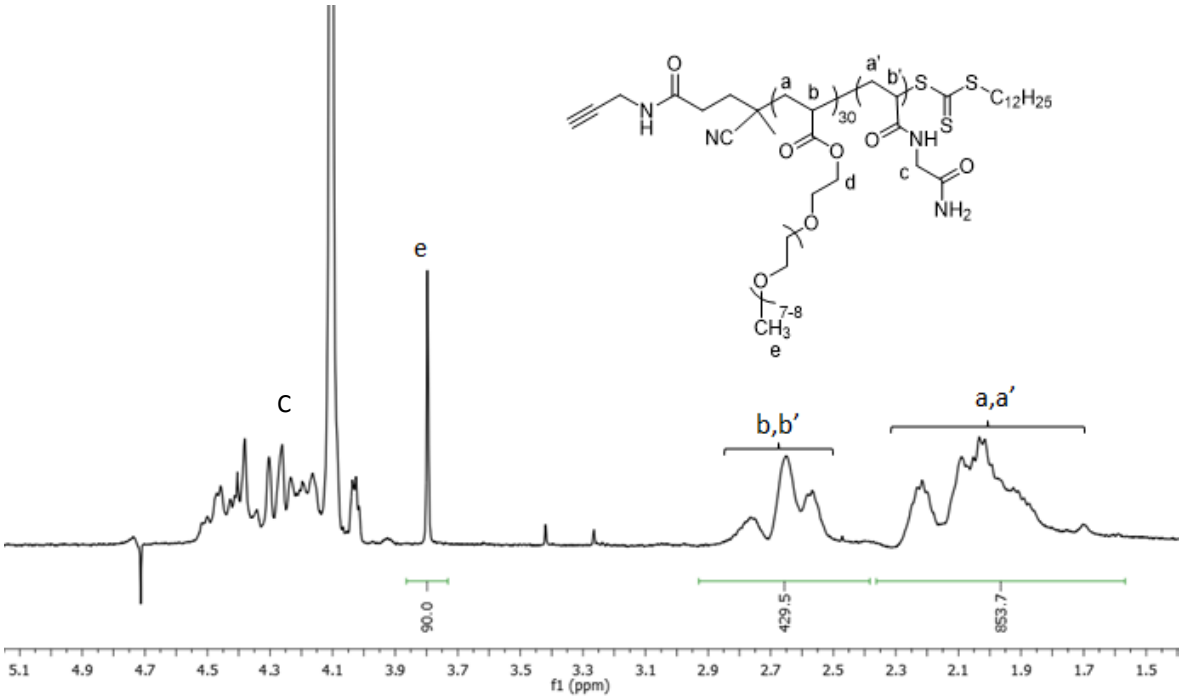


Figure IV.20. $^{1}$H-NMR spectrum (400 MHz, $D_2O$) of UV-PPEGA$_{30}$-*b*-PNAGA$_{397}$ synthesized by UV-light initiated RAFT-PITSA of NAGA mediated through photo-I and UV-PPEGA$_{30}$ ([NAGA]$_0$/[UV-PPEGA$_{30}$]$_0$/[photo-I]$_0$ = 400/1/0.3) in aqueous dispersion at pH 9 and at 5 °C.

The SEC analysis showed that the chromtagram of UV-PPEGA$_{30}$ shifted to high molar mass side and remained monomodal, testifying the successful chain extension of UV-PPEGA$_{30}$ to form a UV-PPEGA$_{30}$-*b*-PNAGA$_{397}$ diblock copolymer in buffer solution pH 9 at 3 °C (Figure IV.21).

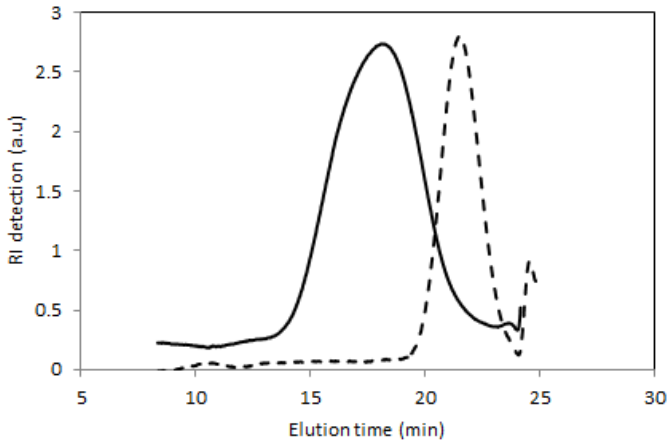


Figure IV.21. Overlaid SEC chromatograms (DMSO, PMMA standard) of UV-PPEGA$_{30}$ macro-CTA and UV-PPEGA$_{30}$-*b*-PNAGA$_{397}$ diblock copolymer obtained during the UV-light initiated RAFT-PITSA of NAGA using photo-I and UV-PPEGA$_{30}$ in aqueous dispersion pH 9 at 3 °C.

### 4.3.2 Study of the degradability of nanogels based on PPEGA-b-P(NAGA-co-KB)

The ability of the UCST-type thermosensitive UV-PPEGA$_{30}$-*b*-P(NAGA-*co*-KB)$_{413}$-based nanogels to disassemble in aqueous medium by hydrolysis of ketal moieties was then studied. Freeze-dried nanogels were dissolved at a concentration of 5 g.L$^{-1}$ in different pH buffer solutions. Since hydrolysis of the ketal group is possible under acidic conditions, we performed the experiments in solutions at pH 4, pH 6 at 25 °C. The evolution of the $D_h$ *vs.* time was determined using DLS measurements (Figure IV.22).

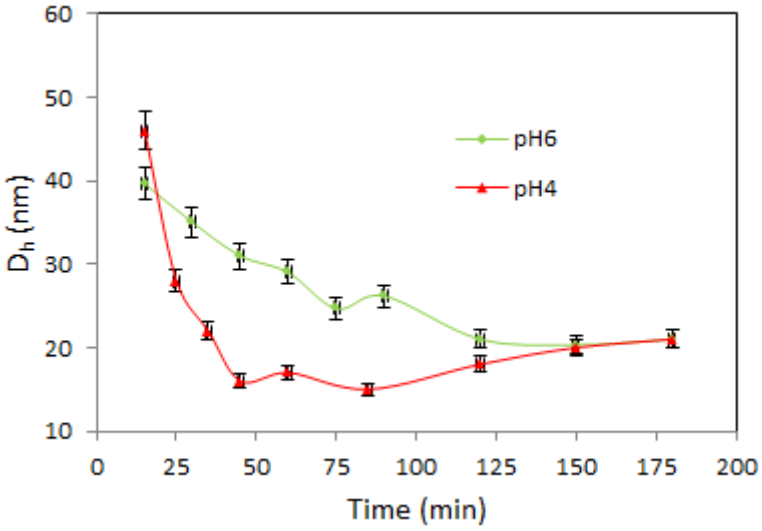


Figure IV.22. Evolution of $D_h$ of the UV-PPEGA$_{30}$-*b*-P(NAGA-*co*-KB)$_{413}$-based nanogels solutions (5 g.L$^{-1}$) at 25 °C measured by DLS as a function of time in aqueous media at pH 4 and pH 6. Nanogels were obtained by UV-light initiated RAFT-PITSA of NAGA/KB in aqueous solution pH 9 at 3°C with an initial $[NAGA]_0/[UV\text{-}PPEGA_{30}]_0/[KB]_0/[Photo\text{-}I]_0$ molar ratio of 400/1/16/0.3.

As shown in Figure IV.22, the degradation of PPEGA-*b*-P(NAGA-*co*-KB)-based nanogel is rapid in acidic media, with a half-life of 25 and 45 min for aqueous solutions at pH 4 and pH 6, respectively. The degradation rate decreased with increasing pH from 4 to 6. A similar trend of the degradability was observed in the case of dual LCST-thermosensitive and pH degradable nanogel based on PPEGA-*b*-P(NIPAm-*co*-KB). These results are consistent with the degradability of KB in different pH solutions as reported in Table III.3.

Taken together, these results demonstrate for the first time that a dual UCST-type thermosensitive and pH-degradable nanogel can be successfully synthesized using the RAFT-PITSA process in aqueous dispersion under UV-light irradiation at low temperature (T < UCST).

## 4.4 Conclusions

In conclusion, we have shown that UV-light initiated RAFT-PITSA process is an efficient strategy to obtain well-defined hydrogen-bonding UCST-type thermosensitive nanogels in aqueous dispersion at low temperature. The morphology, physico-chemical characteristics ($D_h$, pdi, f) and UCST thermosensitive properties of the so-obtained nanogels were confirmed by TEM, DLS, and UV–Vis spectrophotometry. The hydrodynamic diameter, volume swelling ratio, and UCST transition temperature of resulting nanogels can be tuned by modifying the polymerization parameters such as $\overline{DP_{n,PPEGA}}$, the initial molar ratio of NAGA monomer-to-PPEGA macro-CTA and the amount of MBA crosslinker. The increase of $\overline{DP_{n,PPEGA}}$ results in the decreased of $D_h$ and volume swelling ratio. Higher $\overline{DP_{n,PNAGA}}$ block lead to bigger particles, higher volume swelling ratios and UCST values. The volume swelling ratio increased with the decrease of MBA crosslinker, which also corresponds for the increase of UCST values.

Dual UCST-type thermosensitive and pH-sensitive nanogel has been targeted using the same synthesized strategy above and a KB crosslinker containing a ketal cleavage groups. The morphology, hydrodynamic diameter and thermosensitive properties of the so-obtained nanogels were confirmed by TEM, DLS, and UV-Vis spectrophotometry. The nanogel ($D_{h,25°C}$ = 64 nm, $pdi_{,25°C}$ = 0.21 and f = 1.35) illustrated a reversible UCST phase transition with UCST value of 41 °C and can be degraded in short time in acidic pH.

We can envision that these novel UCST-thermosensitive nanogels based on PPEGA-*b*-P(NAGA-*co*-MBA) and dual UCST-type thermosensitive and pH-sensitive nanogels based on PPEGA-*b*-P(NAGA-*co*-KB) might open new opportunities for the application of polymer nanogels as “smart” drug delivery systems and for imaging and sensing.

## 4.5 Experimental section

### 4.5.1 Materials

All reagents were purchased from Sigma-Aldrich unless otherwise noted. 2-Hydroxy-4′-(2-hydroxyethoxy)-2-methylpropiophenone (photo-I, 98%), *N,N*-dimethylformamide (DMF, 99%), tetrahydrofuran (THF, 99%), *N*,*N*′-methylenebis(acrylamide) (MBA, 99%), 2,2'-[2,2-propanediylbis(oxy)]diethanamine (PDA, 99%), different UV-PPEGA-macro-CTAs were synthesized in chapter II. *N*-Acryloyl glycinamide (NAGA) was synthesized according to the reported procedure in Chapter III and inspired by the litterature.[18] Vinylazlactone (VDM) was synthesized according to previously reported procedure.[20]All deuterated solvents were purchased from Euriso-top. All buffer solution with different pH were purchased from Merck KGaA. Ultra-pure water used for RAFT polymerization and preparation of nanogel solutions was obtained from a PureLab ELGA system and had a conductivity of 18.2 MΩm at 25°C.

### 4.5.2 Characterizations

**Nuclear magnetic resonance (NMR) spectroscopy.** Nuclear Magnetic Resonance (NMR) spectra were recorded on a Bruker AC-400 spectrometer for $^{1}$H-NMR (400 MHz and 200 MHz). Chemical shifts are reported in ppm relative to the deuterated solvent resonances.

**Size exclusion chromatography (SEC).** The average molar masses (number-average molar mass $M_n$, weight-average molar mass $M_w$) and dispersity ($Đ = M_w/ M_n$) of diblock copolymer PPEGA-*b*-PNAGA were measured by SEC using DMSO (with 0.1 M LiBr) as an eluent, and carried out using a system equipped with a pre-column and one PSS-GRAM analytical column. The instrument operated at a flow rate of 0.7 mL.min$^{-1}$ at 50°C and was calibrated with narrow linear poly(methyl methacrylate) (PMMA) standards ranging in molecular weight from 900 g.mol$^{-1}$ to 537000 g.mol$^{-1}$.

**Dynamic light scattering (DLS).** DLS measurements were performed on a Malvern Instruments Zetasizer Nano (ZS) fitted with a Helium–Neon laser operating at 633 nm with an angle detection (173°). The sample was prepared by dissolving nanogels in pure water (5 g.L$^{-1}$) then the solution was filtered using nylon membrane filter to 0.45 µm porosity. The hydrodynamic diameter ($D_h$) of nanogels and polydispersity index (pdi) were recorded at 5°C and 55°C. The aqueous solutions of nanogels were first equilibrated at 55°C and 5°C for 10 min before recording. Each measurement was repeated 5 times and hydrodynamic diameter of nanogel was taken as the average of these values. Different sequent heating (from 5 to 55 °C) /cooling (from 55 to 5 °C) cycles were preformed to confirm the reversible swelling/shrinking bahavior of nanogels. The degradability of nanogel was

following by the evolution of $D_h$ at different times. Each measurement was repeated 3 times and Dh of nanogel was taken as the average of these values.

**UV-Vis Spectrophotometry**. Turbidity measurements were carried out on a Aligent Cary 100 UV-Vis spectrophotometer at wavelength of 650 nm. The phase transition temperatures were determined using nanogel solution at a concentration of 10 $g.L^{-1}$ in water. The solution was cooled to 5°C overnight before UV measurement; a heating rate of 1 $°C.min^{-1}$ was employed to determine the phase transition temperature of the nanogel.

**Transmission electronic microscopy (TEM).** TEM analysis was carried out using a JEOL2100 at an accelerating voltage of 120 kV. To prepare the TEM samples, a dilute aqueous solution (5 $g.L^{-1}$) of nanogels was dropped onto a carbon-coated copper grid. The sample was left to gently dry 24h at room temperature.

**UV-light initiated RAFT-PITSA in aqueous dispersion for synthesis of UCST-type thermosensitive nanogels based on PPEGA-*b*-P(NAGA-*co*-MBA).** The following description relates to the synthesis of nanogel UCST-1. In a 10 mL glass vial, 51.8 mg of NAGA (0.4 mmol, 400 eq.) and 15.0 mg of UV-$PPEGA_{30}$ (rune 3, Table II.2, 0.001 mmol, 1 eq.) were dissolved in 2.8 g of water containing 2.5 mg MBA crosslinker monomer (0.016 mmol, 16 eq.) and 0.068 mg of photo-I initiator (0.0003 mmol, 0.3 eq.) to give a solid content of 2.4 wt.% ($[UV\text{-}PPEGA_{30}]_0/[NAGA]_0/[MBA]_0/[photo\text{-}I]_0$= 1/400/16/0.3, $[NAGA]_0$ = 0.145M). The glass vial was bubbled with argon for 30 min, then the mixture solution was placed in an ice-bath under an UV-light source (λ = 365 nm, 34 $mW/cm^2$) with a stir bar for an hour. After complete monomer conversion checked by $^1$H-NMR spectroscopy, the polymerization was stopped and the reactional medium was freeze dried.

**UV-light initiated RAFT-PITSA in aqueous dispersion for synthesis of UCST UV-$PPEGA_{30}$-b-PNAGA diblock copolymer.** In a 10 mL glass vial, 51.8 mg of NAGA (0.4 mmol, 400 eq.) and 15.0 mg of UV-$PPEGA_{30}$ (0.001 mmol, 1 eq.) were dissolved in 2.8 g of water to give a solid content of 2.4 wt.% ($[UV\text{-}PPEGA_{30}]_0/[NAGA]_0$= 1/400; $[NAGA]_0$=0.145M). The glass vial was bubbled with argon for 30 min, then the mixture solution was placed in an ice-bath under an UV-light source (λ = 365 nm, 34 $mW/cm^2$) with a stir bar for one hour. After checking the total conversion of NAGA by $^1$H-NMR, the polymerization was stopped. The diblock copolymer was then freeze-dried for further characterizations.$^1$H-NMR(400 MHz, $D_2O$): $\overline{DP_{n,\,PPEGA}}$ = 30 and $\overline{DP_{n,\,PNAGA}}$ = 391. SEC (DMSO, PMMA standards): $\overline{M_{n,SEC}}$ = 11.45 x $10^4$ $g.mol^{-1}$, Đ = 2.12.

**UV-light initiated RAFT-PITSA in aqueous dispersion for synthesis of dual UCST-type thermosensitive and pH-sensitive nanogels based on PPEGA-*b*-P(NAGA-*co*-KB).** In a 10 mL glass vial,

69 mg of NAGA (0.54 mmol, 400 eq.) and 20 mg of UV-PPEGA$_{30}$ (0.0013 mol, 1 eq.) were dissolved in 4.1 g of buffer solution pH 9 containing 9.5 mg KB crosslinker monomer (0.022 mmol, 16 eq.) and 0.0027 mg of photo-I initiator (0.0004 mmol, 0.3 eq.) to give a solid content of 2.4 wt.% ([UV-PPEGA$_{30}$]$_0$/[NAGA]$_0$/[KB]$_0$/[photo-I]$_0$= 1/400/16/0.3, [NAGA]$_0$ = 0.135 M). The glass vial was bubbled with argon for 30 min, then the mixture solution was placed in an ice-bath under an UV-light source (λ = 365 nm, 34 mW/cm$^2$) with a stir bar for an hour. After complete monomer conversion checked by $^1$H-NMR spectroscopy, the polymerization was stopped and the reactional medium was freeze dried.

**UV-light initiated RAFT-PITSA in aqueous dispersion pH 9 for synthesis of UCST-type thermosensitive PPEGA$_{30}$-*b*-PNAGA diblock copolymer.** In a 10 mL glass vial, 51.8 mg of NAGA (0.4 mmol, 400 eq.) and 15.0 mg of UV-PPEGA$_{30}$ (0.001 mmol, 1 eq.) were dissolved in 2.8 g of water to give a solid content of 2.4 wt% ([UV-PPEGA$_{30}$]$_0$/[NAGA]$_0$= 1/400; [NAGA]$_0$=0.145M). The glass vial was bubbled with argon for 30 min, then the mixture solution was placed in an ice-bath under an UV-light source (λ = 365 nm, 34 mW/cm$^2$) with a stir bar for one hour. After checking the conversion of NAGA by $^1$H NMR, the polymerization was stopped. The diblock copolymer was then freeze-dried for further characterizations.$^1$H-NMR(400 MHz, $D_2O$): $\overline{DP_{n,PPEGA}}$ = 30 and $\overline{DP_{n\ PNAGA}}$ = 397. SEC (DMSO, PMMA standards): $\overline{M_{n,SEC}}$ = 10.5 x 10$^4$ g.mol$^{-1}$, $Đ$ = 2.28.

## 4.6 References


(1) Bansal, K. K.; Upadhyay, P. K.; Saraogi, G. K.; Rosling, A.; Rosenholm, J. M. Advances in Thermo-Responsive Polymers Exhibiting Upper Critical Solution Temperature (UCST). *Express Polym. Lett.* **2019**, *13* (11), 974–992. https://doi.org/10.3144/expresspolymlett.2019.85.

(2) Ohshio, M.; Ishihara, K.; Maruyama, A.; Shimada, N.; Yusa, S. Synthesis and Properties of Upper Critical Solution Temperature Responsive Nanogels. *Langmuir* **2019**, *35* (22), 7261–7267. https://doi.org/10.1021/acs.langmuir.9b00849.

(3) Fu, W.; Luo, C.; Morin, E. A.; He, W.; Li, Z.; Zhao, B. UCST-Type Thermosensitive Hairy Nanogels Synthesized by RAFT Polymerization-Induced Self-Assembly. *ACS Macro Letters* **2017**, *6* (2), 127–133. https://doi.org/10.1021/acsmacrolett.6b00888.

(4) Seuring, J.; Bayer, F. M.; Huber, K.; Agarwal, S. Upper Critical Solution Temperature of Poly( *N* -Acryloyl Glycinamide) in Water: A Concealed Property. *Macromolecules* **2012**, *45* (1), 374–384. https://doi.org/10.1021/ma202059t.

(5) Xu, Z.; Liu, W. Poly( *N* -Acryloyl Glycinamide): A Fascinating Polymer That Exhibits a Range of Properties from UCST to High-Strength Hydrogels. *Chem. Commun.* **2018**, *54* (75), 10540–10553. https://doi.org/10.1039/C8CC04614J.

(6) Boustta, M.; Colombo, P.-E.; Lenglet, S.; Poujol, S.; Vert, M. Versatile UCST-Based Thermoresponsive Hydrogels for Loco-Regional Sustained Drug Delivery. *JCR.* **2014**, *174*, 1–6. https://doi.org/10.1016/j.jconrel.2013.10.040.

(7) Xue, X.; Thiagarajan, L.; Braim, S.; Saunders, B. R.; Shakesheff, K. M.; Alexander, C. Upper Critical Solution Temperature Thermo-Responsive Polymer Brushes and a Mechanism for Controlled Cell Attachment. *J. Mater. Chem. B* **2017**, *5* (25), 4926–4933. https://doi.org/10.1039/C7TB00052A.

(8) Yang, D.; Viitasuo, M.; Pooch, F.; Tenhu, H.; Hietala, S. Poly( *N* -Acryloylglycinamide) Microgels as Nanocatalyst Platform. *Polym. Chem.* **2018**, *9* (4), 517–524. https://doi.org/10.1039/C7PY01950E.

(9) Gupta, A.; Mohanty, B.; Bohidar, H. B. Flory Temperature and Upper Critical Solution Temperature of Gelatin Solutions. *Biomacromolecules* **2005**, *6* (3), 1623–1627. https://doi.org/10.1021/bm0492430.

(10) Pineda-Contreras, B. A.; Schmalz, H.; Agarwal, S. PH Dependent Thermoresponsive Behavior of Acrylamide–Acrylonitrile UCST-Type Copolymers in Aqueous Media. *Polym. Chem.* **2016**, *7* (10), 1979–1986. https://doi.org/10.1039/C6PY00162A.

(11) Wolf, T.; Rheinberger, T.; Simon, J.; Wurm, F. R. Reversible Self-Assembly of Degradable Polymersomes with Upper Critical Solution Temperature in Water. *J. Am. Chem. Soc.* **2017**, *139* (32), 11064–11072. https://doi.org/10.1021/jacs.7b02723.

(12) Sponchioni, M.; Rodrigues Bassam, P.; Moscatelli, D.; Arosio, P.; Capasso Palmiero, U. Biodegradable Zwitterionic Nanoparticles with Tunable UCST-Type Phase Separation under Physiological Conditions. *Nanoscale* **2019**, *11* (35), 16582–16591. https://doi.org/10.1039/C9NR04311J.

(13) Bingham, N. M.; Nisa, Q. un; Chua, S. H. L.; Fontugne, L.; Spick, M. P.; Roth, P. J. Thioester-Functional Polyacrylamides: Rapid Selective Backbone Degradation Triggers Solubility Switch Based on Aqueous Lower Critical Solution Temperature/Upper Critical Solution Temperature. *ACS Appl. Polym. Mater.* **2020**, *2* (8), 3440–3449. https://doi.org/10.1021/acsapm.0c00503.

(14) Zhang, Z.; Li, H.; Kasmi, S.; Van Herck, S.; Deswarte, K.; Lambrecht, B. N.; Hoogenboom, R.; Nuhn, L.; De Geest, B. G. A Synthetic, Transiently Thermoresponsive Homopolymer with UCST Behaviour within a Physiologically Relevant Window. *Angew. Chem. Int. Ed.* **2019**, *58* (23), 7866–7872. https://doi.org/10.1002/anie.201900224.

(15) Boustta, M.; Vert, M. Hyaluronic Acid-Poly(N-Acryloyl Glycinamide) Copolymers as Sources of Degradable Thermoresponsive Hydrogels for Therapy. *Gels* **2020**, *6* (4), 42. https://doi.org/10.3390/gels6040042.

(16) Seuring, J.; Agarwal, S. Non-Ionic Homo- and Copolymers with H-Donor and H-Acceptor Units with an UCST in Water. *Macromol. Chem. Phys.* **2010**, *211* (19), 2109–2117. https://doi.org/10.1002/macp.201000147.

(17) Glatzel, S.; Badi, N.; Päch, M.; Laschewsky, A.; Lutz, J.-F. Well-Defined Synthetic Polymers with a Protein-like Gelation Behavior in Water. *Chem. Commun.* **2010**, *46* (25), 4517. https://doi.org/10.1039/c0cc00038h.

(18) Mäkinen, L.; Varadharajan, D.; Tenhu, H.; Hietala, S. Triple Hydrophilic UCST–LCST Block Copolymers. *Macromolecules* **2016**, *49* (3), 986–993. https://doi.org/10.1021/acs.macromol.5b02543.

(19) Sanson, N.; Rieger, J. Synthesis of Nanogels/Microgels by Conventional and Controlled Radical Crosslinking Copolymerization. *Polym. Chem.* **2010**, *1* (7), 965. https://doi.org/10.1039/c0py00010h.

(20) Levere, M. E.; Ho, H. T.; Pascual, S.; Fontaine, L. Stable Azlactone-Functionalized Nanoparticles Prepared from Thermoresponsive Copolymers Synthesized by RAFT Polymerization. *Polym. Chem.* **2011**, *2* (12), 2878. https://doi.org/10.1039/c1py00320h.

# General Conclusions

During my PhD work, the procedure to target thermosensitive and pH-degradable nanogels was controlled step by step. To produce PPEGA macro-CTAs (also being the shell of the nanogel), RAFT polymerization in solution (DMF) at 70°C from COPYDC, a hydrophobic CTA , was employed using either thermal activation or UV-light activation with a sufficient molar mass control and narrow molar masses distributions at low PEGA conversions (60 %). Despite a low temperature reaction, UV-light initiated RAFT polymerization did not afford an improved control compared to the thermally-initiated RAFT polymerization. However, employing a lower monomer concentration results in a better control of PEGA polymerization at 76 % monomer conversion ([PEGA] = 039 mol.$L^{-1}$, $[PEGA]_0/[COPYDC]_0/[photo\text{-}I]_0$ = 50/ 1/ 0.1). Such well-defined PPEGAs were able to be used as amphiphilic macro-CTA for further synthesis of LCST- and UCST-type thermosensitive diblock copolymers based on PNIPAm and PNAGA, respectively, through RAFT polymerization in water. Well-defined LCST-type thermosensitive PPEGA-*b*-PNIPAm diblock copolymers were obtained by homogeneous RAFT polymerization in water using UV-light activation at 25°C with a sufficient molar mass control and narrow molar masses distributions. Compare to thermal activation, UV-light activation offers a very fast initial rate of NIPAm polymerization, which reached full conversion after 1h (instead of 6h for the thermally-initiated RAFT polymerization). UCST-type thermosensitive PPEGA-*b*-PNAGA diblock copolymers were prepared using either UV-light initiated RAFT-PITSA at 5°C or thermally-initiated RAFT polymerization at 70°C in water. Results show lower dispersity values through thermally-initiated homogeneous RAFT polymerization. However, the higher temperature employed in thermal activation process results in the presence of a high molar mass shoulder, which is not observed in the case of UV-light irradiation. PNIPAm-based nanogels were targeted either through thermally-initiated or through UV-light initiated process using a PPEGA with $\overline{DP_{n,\,PPEGA}}$ of 30 as macro-CTA and surfactant, MBA as crosslinker and V50 or photo-I as initiators, respectively. The initial molar ratios of $[NIPAm]_0/[MBA]_0/[PPEGA]_0/[initiator]_0$ are 204/8/1/0.3 and the solid content is equal to 2.4 wt.%. Although the kinetic of thermal activation is much lower than that of UV-light activation during the RAFT-PITSA to target LCST-type thermosensitive PNIPAm-based nanogels, both activations allow to target nanogels with a single and low size distribution through RAFT-PITSA using a wide range PPEGAs, with variable $\overline{DP_{n,PPEGA}}$, used as macro-CTA and surfactant. A minimum $\overline{DP_{n,PPEGA}}$ is necessary for the steric stability of the nanogels formed *in situ* during the PITSA process and this value is dependent on activation process: the UV-light activation required a higher $\overline{DP_{n,PPEGA}}$ to form stable nanogel. A range of spherical, well-defined LCST-type thermosensitive nanogels based of Thermal-PPEGA-*b*-P(NIPAm-*co*-MBA) was thus obtained and characterized by $^1$H-NMR

spectroscopy, DLS, TEM and UV-Vis spectrophotometry. The size of obtained nanogels can be finely tuned (40 ≤$D_h$≤ 210 nm at 20 °C) by changing $\overline{DP_{n,PPEGA}}$ or $\overline{DP_{n,PNIPAm}}$ of PPEGA-*b*-P(NIPAm-*co*-MBA). The size of nanogel increases with the rise in $\overline{DP_{n,PNIPAm}}$ and decreases with the increase of $\overline{DP_{n,PPEGA}}$. The LCST of nanogel remains stable around 33-34 °C and did not be impacted by block polymer chain length.

Dual LCST-type thermosensitive and pH-degradable nanogels have been targeted using a new ketal crosslinker, through UV-light initiated RAFT-PITSA in aqueous dispersion at 70°C and at pH = 9. These spherical nanogels ($D_h$= 139nm, pdi = 0.13 at 25°C) with LCST of 34°C (reversible swelling/shrinking transition for at least 8 cycles) are stable at pH = 9 during several days, at pH 7 during 24 hours and can be degraded in a short time: 30 min at pH 4 and 1h at pH 5, which is suitable for potential bioapplications.

Finally, we have shown that one-pot UV-light initiated RAFT-PITSA process is an efficient strategy to obtain well-defined hydrogen-bonding UCST-type thermosensitive nanogels in aqueous dispersion at low temperature. The first UCST-type thermosensitive nanogel based on PNAGA have been obtained. The morphology, physicochemical characteristics ($D_h$, pdi, f) and UCST thermosensitive properties of the so-obtained nanogels were confirmed by TEM, DLS, and UV-Vis spectrophotometry. The hydrodynamic diameter, volume swelling ratio, and UCST transition temperature of resulting nanogels can be tuned by modifying the polymerization parameters such as $\overline{DP_{n,PPEGA}}$, the initial molar ratio of NAGA monomer-to-PPEGA macro-CTA and the amount of MBA crosslinker. Obtained nanogels show a single size distribution with a pdi in the range of 0.15 to 0.19 and the UCST value can be tuned betwwen 39 and 43 °C. The increase of $\overline{DP_{n,PPEGA}}$ results in the decreased of $D_h$ and volume swelling ratio. Higher $\overline{DP_{n,PNAGA}}$ block lead to bigger particles, higher volume swelling ratios and UCST values. The volume swelling ratio increased with the decrease of MBA crosslinker, which also corresponds for the increase of UCST values.

Dual UCST-type thermosensitive and pH-degradable nanogel has been targeted using the same synthesized strategy above and a ketal-based crosslinker with initial molar ratio of $[NAGA]_0/[UV\text{-}PPEGA_{30}]_0/[KB]_0/[Photo\text{-}I]_0$ = 400/1/16/0.3 and a solid content of 2.4 wt.%. for 1h of polymerization in pH 9 buffer solution. The morphology, hydrodynamic diameter and thermosensitive properties of the so-obtained nanogels were confirmed by TEM, DLS, and UV-Vis spectrophotometry. The spherical nanogel ($D_{h,25°C}$ = 64 nm, $pdi_{,25°C}$ = 0.21 and f = 1.35) illustrated a reversible UCST phase transition (two swelling/shrinking transition cycles) with UCST value of 41 °C, was stable at pH 9 at room temperature during a week, and can be degraded in short time in acidic pH (p = 5 after 25 min ).

In conclusion, the research conducted in my PhD thesis made two notable contributions to the field of stimuli-sensitive core-shell nanogel design. Our first contribution is the demonstration of a facile approach for targeting hydrogen-bonding UCST-type thermosensitive nanogels. The one-pot method reported the RAFT-PITSA of a precursor monomer of UCST-type thermosensitive polymer at low temperature using a water-soluble photo-initiator, a crosslinker and an amphiphilic macro-CTA under UV-light irradiation in aqueous dispersion. Well-defined UCST-type thermosensitive nanogels are obtained with full monomers consumptions in a very short time. Moreover, from this strategy dual UCST-type thermosensitive and pH-degradable nanogels could be prepared for the first time by incorporating a ketal-based linker into the core of nanogel. That brings a new door to design "smart" nanogels for required applications. We can envision that these novel UCST-thermosensitive nanogels based on PPEGA-*b*-P(NAGA-*co*-MBA) and dual UCST-type thermosensitive and pH-degradable nanogels based on PPEGA-*b*-P(NAGA-*co*-KB) might open new opportunities for the application of polymer nanogels as "smart" drug delivery systems and for imaging and sensing. The powerful reported one-pot RAFT-PITSA can be employed to design different multi stimuli-sensitive nanogels by incorporating a redox or light-sensitive groups, for examples, with a crosslink agent.